Title
Design and Transient Analysis of Passive Safety Cooling Systems for Advanced Nuclear Reactors

Author
Galvez, Cristhian

Publication Date
2011

Peer reviewed|Thesis/dissertation

Design and Transient Analysis of Passive Safety Cooling Systems for Advanced Nuclear Reactors

By

Cristhian Galvez

A dissertation submitted in partial satisfaction of the

requirements for the degree of

Doctor of Philosophy

in

Engineering – Nuclear Engineering

in the

Graduate Division

of the

University of California, Berkeley

Committee in charge:

Professor Per F. Peterson, Chair
Professor Van P. Carey
Professor Ehud Greenspan
Professor Brian D. Wirth

Spring 2011

ABSTRACT

Design and Transient Analysis of Passive Safety Cooling Systems for Advanced Nuclear Reactors

Cristhian Galvez

Doctor of Philosophy in Engineering - Nuclear Engineering

University of California, Berkeley

Professor Per F. Peterson, Chair

The Pebble Bed Advanced High Temperature Reactor (PB-AHTR) is a pebble fueled, liquid salt cooled, high temperature nuclear reactor design that can be used for electricity generation or other applications requiring the availability of heat at elevated temperatures. A stage in the design evolution of this plant requires the analysis of the plant during a variety of potential transients to understand the primary and safety cooling system response. This study focuses on the performance of the passive safety cooling system with a dual purpose, to assess the capacity to maintain the core at safe temperatures and to assist the design process of this system to achieve this objective. The analysis requires the use of complex computational tools for simulation and verification using analytical solutions and comparisons with experimental data.

This investigation builds upon previous detailed design work for the PB-AHTR components, including the core, reactivity control mechanisms and the intermediate heat exchanger, developed in 2008. In addition the study of this reference plant design employs a wealth of auxiliary information including thermal-hydraulic physical phenomena correlations for multiple geometries and thermophysical properties for the constituents of the plant. Finally, the set of performance requirements and limitations imposed from physical constrains and safety considerations provide with a criteria and metrics for acceptability of the design. The passive safety cooling system concept is turned into a detailed design as a result from this study.

A methodology for the design of air-cooled passive safety systems was developed and a transient analysis of the plant, evaluating a scrammed loss of forced cooling event was performed. Furthermore, a design optimization study of the passive safety system and an approach for the validation and verification of the analysis is presented. This study demonstrates that the resulting point design responds properly to the transient event and maintains the core and reactor components at acceptable temperatures within allowable safety margins. It is also demonstrated that the transition from steady full-power, forced-cooling mode to steady decay-heat, natural-circulation mode is stable, predictable and well characterized.

CONTENTS

ACKNOWLEDGEMENTS

The work presented here was performed under the overall guidance from Nuclear Engineering Professor and Chair, Per F. Peterson in relation to plant design and molten salt pebble bed reactor technology. Valuable insight was obtained from Mechanical Engineering Professor Van P. Carey in the subject of natural circulation in communicating channels. Useful comments in the preparation of this document were also provided by Professors Brian D. Wirth and Ehud Greenspan in their role of members as the dissertation committee.

It is also necessary to acknowledge the input from Dr. Cliff Davis from Idaho National Laboratory and Dr. Richard Wagner from Innovative Systems Solutions. Both of these researches contributed immensely to the understanding and correct usage of the thermal-hydraulic analysis tools.

The author also acknowledges the input from fellow graduate students at the Nuclear Thermal Hydraulics Laboratory within the NE Dept. and the numerous undergraduate students who contributed with their diligence documenting model input decks.

LIST OF FIGURES

LIST OF TABLES

NOMENCLATURE

Variables

∇	del operator
A	area
AL	arc length
a	pipe radius
B	friction factor formula coefficient
Bi	Non-dimensional Biot number
C	flow thermal capacity
c	friction factor formula exponent
C_p	heat capacity
D	diameter
e	emissivity
E	energy
EF	Enhancement Factor
efs	effectiveness
f	friction factor
g	gravitational constant
G	mass flux rate
Gr	Grashoff non-dimensional number
h	heat transfer coefficient
H	height
HTA	heat transfer area
K	form loss coefficient
k	heat conduction coefficient

L	Length
m	mass flow rate
M	moderator density
n	n_{th} time step
N	number of restrictions
NTU	Number of Thermal Units
Nu	Non-dimensional Nusselt number
Q	Thermal power
P	pressure
Pit	Pitch
Ph	Heated perimeter
PoD	Pitch to Diameter ratio
Pr	Prandtl non-dimensional number
q	heat transfer rate
r	radial coordinate distance from center
R	Radius
$\overline{R}$	Universal gas constant
Rc	Radius of curvature
Ra	Raleigh non-dimensional number
Re	Reynolds non-dimensional number
s	source
T	temperature
t	time
tr	transport mechanisms
U	internal energy

UA overall heat transfer coefficient

V average velocity

v velocity

VF View factor

w wall

x Cartesian axial direction

Greek symbols

α tube horizontal angle

α_v void fraction

α_f void fraction

β_T total delayed neutron fraction

β volumetric thermal expansion

γ decay constant for delayed neutrons

Δ change

ε porosity

ε_R surface roughness

κ thermal diffusivity

η transformation factor

θ angle between direction of flow and gravity

ι prompt neutron lifetime

λ reactivity feedback coefficient

μ kinematic viscosity

ρ density

ρ_R reactivity insertion

σ Stefan-Boltzman constant

φ Neutron flux

Φ Tangential spherical angle

χ restrictions multiplier

ψ neutron angular flux

Ω solid spherical angle

τ wall shear

Subscripts

$_{=}$ tensor

b bulk

c cross section

cp center pi

C cold

char Characteristic

D Diameter used for length scale

e effective hydraulic

eq equivalent

f fluid phase

g gas phase

H hot

h hydraulic

in inner

i+1/2 upstream control volume

i-1/2 downstream control volume

i	surface number i
j	surface number j
j+1/2	upstream volume junction
j-1/2	downstream volume junction
L	length scale
lm	log mean
m	mean
M	moderator temperature
o	initial
ou	outer
cp	center pipe
p	pebble
r	ratio
ref	reference
sc	scattering
s	surface
T	fuel temperature
to	total
t	tube
thick	thickness

Superscripts

-	mean value
¯	vector quantity
·	per unit of time

’	alternate value for variable
’’	per unit of area
’’’	per unit of volume
^{o}	degree

1. INTRODUCTION

The current concerns about carbon emissions worldwide have created a revived interest in the design of advanced nuclear reactors to meet a strict set of requirements in order to further improve reliability and safety. An international response was led by the Gen IV International Forum (GIF) organizing international cooperation, performing research and development needed for the next generation nuclear systems [1]. In the U.S., this effort is coordinated by the Department of Energy (DOE). The Gen IV coordinated research roadmap [2] recommends research work towards the development of these systems focused on the following areas: 1) sustainability 2) economics 3) safety and reliability and 4) proliferation resistance and physical protection. The ultimate goal is to develop technologies that excel in these four areas.

As a result of the multi-party GIF discussions, six specific nuclear system concepts were chosen to be further investigated. They are 1) gas cooled fast reactors (GFR), 2) very high temperature reactors (VHTR), 3) supercritical water cooled reactors (SCWR), 4) sodium cooled fast reactors (SCFR), 5) lead cooled fast reactors (LFR) and 6) molten salt reactors (MSR). Each of these concepts offers the desired features in the four areas. Current research is focused on understanding the physical processes that are required in order to make these reactor designs work. Much of the technology is in a developmental phase, however, there is knowledge dispersed among member countries of this forum, which also seeks to promote research collaboration.

One particular design is the fluid-fueled Molten Salt Reactor (MSR), a design that has been investigated in substantial detail in the United States in the past. In 1965, an experimental MSR was built at Oak Ridge National Laboratory (ORNL) [3] and was run for five years, where a wealth of information was acquired on a variety of subjects including liquid fuel manipulation, breeding systems and on-site reprocessing. The large number of technical publications resulting from this experimental period is the basis for the continuation of research on MSR technology. This experimental facility is formally referred to as the Molten Salt Reactor Experiment (MSRE).

Currently a number of institutions research key technological aspects of the MSR. In the United States, DOE has supported work to investigate a new class of reactors that use molten fluoride salts as coolants but use solid fuels, referred to as Advanced High Temperature Reactors (AHTRs). This U.S. research has focused on several technical aspects of the AHTR such as neutronics, thermal hydraulics, fuel development and characterization, chemistry and corrosion of molten salts, and high efficiency power conversion systems among many other aspects. One of said institutions is the University of California at Berkeley, where research focuses on the design, performance and characterization of a specific design of an AHTR.

1.1 OVERVIEW

There are various areas of research in support of the technology development of AHTRs at UC Berkeley. Work at UC Berkeley in nuclear applications of salts started in 1990 as molten salts were considered as coolants for fusion energy systems. In 2002, molten salts were recommended for the use on AHTRs given their excellent properties in reactor environments [4]. Since 2003, active research work has taken place at UC Berkeley and elsewhere on design, neutronics, and safety of AHTRs.

The base design for the AHTR in current development at the university was similar to the MSRE experiment, with the exception that the fuel is in solid form and therefore did not mix with the liquid coolant. A number of variations have occurred since and each of these designs for the MSR is optimized for certain application. All design variations however include the following basic characteristics: a) solid fuel in pebble form and assembled together forming a bed of spheres b) liquid salt coolant as the working fluid for heat transport and moderation and c) graphite moderation. Given these general features, the overall design was named the Pebble Bed Advanced High Temperature Reactor and the acronym PB-AHTR was adopted as well.

The PB-AHTR is currently represented by two design alternatives. Both designs use buoyant pebbles that re-circulate slowly into the bottom and out of the top of the core. In the earlier design variant, the pebbles are contained within pebble channels where the flow of coolant can be set to give a desired temperature rise. The flow of the coolant is upwards and is axial along the channel in the same direction as the pebbles circulate as figure 1-1 shows. This pebble-channel design considers the usage of low enriched uranium fuel. A second annular core design considers a variation of the baseline core design allowing and the use of thorium blanket fuels with LEU seed has been studied as well. In the annular core design, coolant flows multi-directionally and is engineered specifically to reduce pumping power and therefore reduce the auxiliary system's energy consumption and enhance passive safety. This design is not only optimized for energy generation but also for increased conversion ratio. All other features of the reactors, besides the core configuration are identical between the channel and annular core designs. Figure 1-2 shows a detail flow diagram with the annular core.

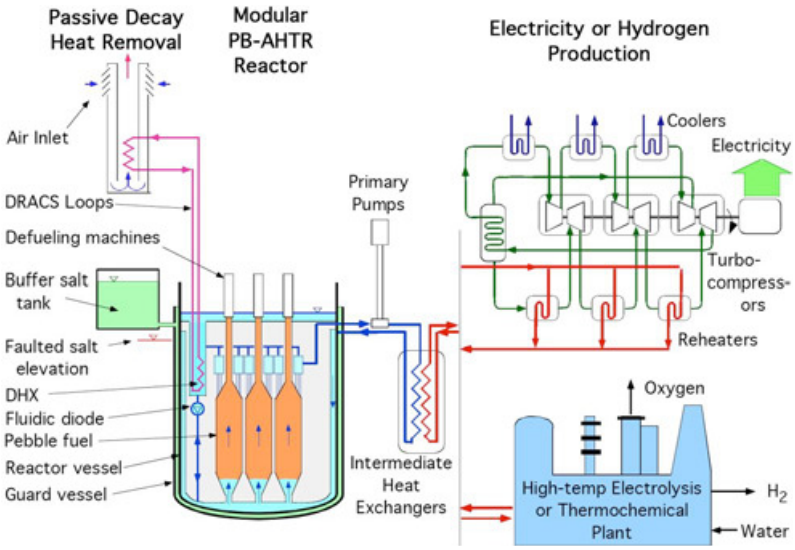

Fig. 1-1 Channel-type pebble bed reactor

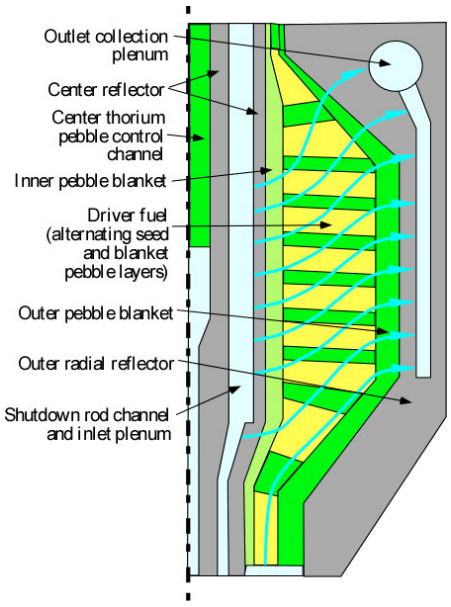

Fig. 1-2 Annular-type pebble bed reactor detail flow diagram

One of the key technical areas that has been evaluated extensively at UCB is the design of safety systems to ensure that the reactor design can operate within set margins of safety, during both anticipated operational occurrences, design basis events, and beyond design basis events. These safety margins must be demonstrated to obtain a license from the U.S. Nuclear Regulatory Commission. Currently these requirements are well defined only for Light Water Reactors (LWR), since the entire fleet of nuclear power reactors correspond to this category, and proper regulation is absent for Gen IV reactors. There is certain information regarding safety margins for the case of advanced high temperature reactors such as the PB-AHTR. There are other sources of safety margins that arise from physical limitations, material lifetime and engineering

design uncertainty that are further discussed in detail in later chapters. In this context, the subject of this study is on the evaluation of the safety systems for the PB-AHTR, in particular, the performance of the *passive* safety systems.

1.2 PREVIOUS WORK

Previous work in the area of design, performance and safety comes from several sources. One group includes early work from ORNL related to the engineering design of the Molten Salt Breeder Reactor (MSBR). Additionally, there is work done at UC Berkeley on various components of the reactor. Finally, the work that is relevant to specific components of the plant, but may not hold relation with molten salt reactor technology that was conducted in many other institutions was also employed in this study. Every report is referenced when appropriate.

Information originating from ORNL includes thermophysical properties of salts [5], salt heat exchanger analysis methodology [6] and design of heat removal plant equipment [7]. Work originating from previous researchers at UC Berkeley includes the analysis of the baseline integral pebble bed reactor [11] and work on the transient analysis on the modular pebble bed reactor [12], although both researchers limited their study to analysis of the core, excluding other important plant components. Also, work on the design of salt heat exchangers [13] and passive shutdown rod insertion [14] in case of transients was performed at UC Berkeley and contributed to the present study.

The most important contribution pertaining to this study stemming from the previous work at UC Berkeley consists of identifying the appropriate computational tools for plant component analysis [11], [13]. Other important results consist of the detailed technical design of the reactor core [12],[18], the envisioned transients of interest [15], core neutron-kinetics parameters and control systems reactivity worth [16], normalized core power density [11] and safety limits for transients [18]. This report builds upon detailed designed achieved in the past by these referenced researchers and these previously studied design parameters are considered fixed and are used here as well. The parameters which are subject to investigation correspond to the passive safety cooling system and its components. Previous work regarding this system has been limited to conceptual design and qualitative assessment [17], although the information provided by reference [18] is sufficient to begin the design and assessment of the design, which is the subject of this study. Both the advanced and detailed aspects of the design as well as the conceptual and general aspects of the design are reviewed in detail in chapters 3 and 4 of this dissertation respectively.

Another group of documents that are relevant to MSR safety research is the methodology for safety analysis using computational tools relevant to LWR technology. A large majority of existing tools and methods are designed for this industry. General methodology on safety analysis [8] along with a description of the current computational tools [9] and current standards

for analysis modeling practices [10] are all general references that also contribute to the basis of this study.

1.3 MOTIVATIONS OF THE STUDY

The primary motivation of this study is to generate a method to perform transient analysis of AHTR designs at the plant level, particularly including the safety systems for passive decay heat removal using a Direct Reactor Auxiliary Cooling System (DRACS). Work previous to this study was limited to the analysis of the core of the reactor isolated and subject to very simplified boundary conditions. These studies provide preliminary insights on core behavior under idealized conditions, such as the effectiveness of inherent reactivity control mechanisms and the performance of the passive cooling loop. In order to establish a timescale for the transient, taking into consideration the thermal inertia of the solid plant components, the coolant dispersed throughout pipes and components and the travel time around the primary system it is necessary to perform the analysis at the plant level. These considerations are important as they directly impact the maximum temperatures the system reaches during a transient event and the available time for operator response, thus impacting on the safety of the reactor design.

Additional motivation to this study is to develop an understanding of the reactor safety system and the how the envisioned limitations and advantages have an effect in the overall nuclear reactor performance. The reactor safety system can be designed to remove the excess heat in case of transients, however, it is not clear if this design can be achieved while meeting existing design constraints, such as available vertical height in the building for the DRACS salt loops and the air cooled, passive heat exchangers with their associated air inlet and outlet ducts.

1.4 OBJECTIVES

- To investigate, implement and demonstrate that a methodology exists for the analysis of a nuclear reactor plant employing molten salt coolant and pebble bed fuel under steady and transient operation.
- To investigate, implement and report on a suitable design for the passive decay heat removal system that serves as an alternate heat sink in case of primary heat sink failure caused by a series of plausible, low probability events.
- To investigate, implement and report an approach to verify the results presented in this study by providing alternate methods of calculation, especially those regarding the design of the passive safety cooling systems.
- To develop an understanding of the fundamental phenomena which affect the performance of the passive safety cooling system and recommend an approach for the subsequent design optimization.

1.5 REFERENCES

[1] OECD Nuclear Energy Agency *The Generation IV International Forum.* http://www.gen-4.org/ August (2010)

[2] U.S. DOE Nuclear Energy Research Advisory Committee and Generation IV International Forum. *A Technology Roadmap for Generation IV Nuclear Energy Systems.* December (2002)

[3] H. G. MacPherson *The molten salt adventure* Nuclear Science and Engineering 90 (1985) 374-380

[4] C.W. Forsberg, P. Pickard, and P.F. Peterson, *Molten-Salt-Cooled Advanced High-Temperature Reactor for Production of Hydrogen and Electricity*. Nuclear Technology 144 (2003) 289-302

[5] D. F. Williams, L. M. Toth, K. T. Clarno *Assessment of candidate molten salt coolants for the advanced high temperature reactor (AHTR)* Oak Ridge National Laboratory ORNL/TM-2006/12, March (2006)

[6] C. E. Bettis et. al., *Computer programs for MSBR heat exchangers.* Oak Ridge National Laboratory ORNL/TM-2815, June (1971)

[7] J. R. McWherter *Molten salt breeder experiment design basis.* Oak Ridge National Laboratory ORNL/TM-3177, November (1970)

[8] International Atomic Energy Agency *Incorporation of advanced accident analysis methodology into safety analysis reports.* IAEA-TECDOC-1351, May (2003)

[9] Idaho National Laboratory *Relap5-3D* INL Presentation http://www.inel.gov/relap5/relap5-3.htm (2005)

[10] International Atomic Energy Agency *Approaches and tools for severe accident analysis for nuclear power plants* IAEA Safety Report Series No. 56. December (2008)

[11] A. Griveau *Modeling and Transient Analysis for the Pebble Bed Advanced High Temperature Reactor (PB-AHTR)* M.S. Project Report UCBTH-07-001 (2007)

[12] A. Niquille *Modeling and Transient Analysis for the Modular Pebble Bed Advanced High Temperature Reactor (PB-AHTR)* M.S. Project Report UCBTH-07-002 (2007)

[13] H. J. Lim, P. F. Peterson *Conceptual design of the intermediate heat exchanger (IHX) for the PB-AHTR* UC Berkeley Report UCBTH-09-005, May 20 (2009)

[14] E. D. Blandford, P. F. Peterson *A novel buoyantly-driven shutdown rod design for passive reactivity control of the PB-AHTR.* 4th International Topical Meeting on High Temperature Reactor Technology (HTR-2008), Washington, DC (2008)

[15] F. P. Fardin, F. Koenig *Preliminary study of the pebble bed advanced high temperature reactor.* M.S. Project Report UCBTH-06-001 (2006)

[16] M. Fratoni *Development and applications of methodologies for the neutronic design of the pebble bed advanced high temperature reactor (PB-AHTR)* Ph.D. Dissertation, UC Berkeley (2008)

[17] P. F. Peterson, H. Zhao, *Passive decay heat removal for the advanced high temperature reactor.* UCBTH-03-005, February (2004)

[18] P. F. Peterson, *Design, analysis and development of the modular PB-AHTR.* Proceedings of ICAPP '08, Anaheim, CA, June (2008)

2 LITERATURE REVIEW

The analysis performed in this study consists of the construction of computer-solved numerical models which represent the physical phenomena occurring in the problem in addition to the construction of analytical models and solved employing calculation worksheets. Both of these approaches are used, often complementarily. The following section establishes the mathematical expressions for the physical relations that occur in the systems subject in this study.

The PB-AHTR is composed of multiple systems for heat generation and removal. These different systems employ components in different geometries for fluid flow and heat transfer. Some of the components include tube and shell heat exchangers, air coolers and pebble bed cooling channels among many others. It is necessary to present the expressions for the governing processes to set a standard for calculations that are required for prediction and benchmarking of simulations.

This chapter has three separate sections dealing with the thermal, hydraulic and coupled multi-physics processes.

THERMAL PROCESSES

2.1 CONDUCTION HEAT TRANSPORT INSIDE PEBBLE FUEL

The PB-AHTR uses pebble fuel that has a low-density center graphite kernel, an annulcar layer of fuel, and an outside shell of graphite that protects the fuel layer. The density of the center kernel is adjusted to assure that the total mass of the pebble provides the desired buoyancy. Conduction in the pebble fuel can be modeled using the transient energy conservation equation in spherical coordinates,

$$\frac{1}{r^2}\frac{\partial}{\partial r}\left(kr^2\frac{\partial T}{\partial r}\right)+\frac{1}{r^2\sin^2\theta}\frac{\partial}{\partial \Phi}k\left(\frac{\partial T}{\partial \Phi}\right)+\frac{1}{r^2\sin\theta}\frac{\partial}{\partial \theta}\left(k\sin\theta\frac{\partial T}{\partial \theta}\right)+\dot{q}'''=\rho C_p\frac{\partial T}{\partial t} \qquad (2.1)$$

Given that the distribution of fuel materials inside the pebble can be assumed to be uniform in the directions of the spherical angles Φ and θ then Eq. 2.1 can be further simplified to the radial distribution of the temperature.

$$\frac{1}{r^2}\frac{\partial}{\partial r}\left(kr^2\frac{\partial T}{\partial r}\right)+\dot{q}'''=\rho C_p\frac{\partial T}{\partial t} \qquad (2.2)$$

The equation above can be solved for the independent variable of temperature as a function of radial location. The following picture shows the radial coordinate system and boundaries used for the solution.

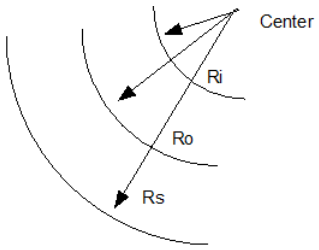

Fig. 2-1 Pebble geometry and radial locations

During steady state heat generation, the equilibrium temperature distribution is expressed by the following relation as a function of radius, assuming homogeneous energy generation in the entire pebble. The solutions presented in the next set of equations assume pebble geometry where heat generation occurs uniformly in the annular region between R_i and R_o only. R_s is the surface of the pebble

$$T(r) = \frac{\dot{q}''' R_i^3}{3k}\left(\frac{1}{R_o} - \frac{1}{r}\right) + \frac{\dot{q}'''}{6k}\left(R_o^2 - r^2\right) \tag{2.3}$$

for $R_i<r<R_o$

In the regions of the pebble where there is no heat generation, then the temperature distribution of the pebble is as follows:

$$T(r) = T_{Ro} - \left(T_{Ro} - T_s\right)\frac{1 - \frac{R_o}{r}}{1 - \frac{R_o}{R_s}} \tag{2.4}$$

for $R_o<r<R_s$

If a sphere is composed of a combination of heat generating and non heat generating layers, then the temperature difference between the center and the surface of the sphere are approximated by the following equation, which is derived from Eq. 2.2

$$\Delta T_{cent-surf} = \frac{\dot{q}'''}{3k_{fuel-eff}}\left(R_i^3\left(\frac{1}{R_o} - \frac{1}{R_i}\right) + 2\left(R_o^2 - R_i^2\right)\right) + \dot{q}\frac{\left(\frac{1}{R_o} - \frac{1}{R_s}\right)}{4\pi k_{graphite}} \tag{2.5}$$

In general, one can express the temperature drop and the flow of heat impeded by thermally conductivity similarly to the voltage drop and the flow of electric current impeded by resistance in the following manner

$$i = \Delta V \cdot R_{electric}$$
$$q = \Delta T \cdot R_{thermal} \tag{2.6}$$

where i is the electric current, ΔV is the voltage drop and $R_{electric}$ is the electric resistance. Similarly, q is the heat flux, ΔT is the temperature drop and $R_{thermal}$ is the thermal resistance. In the case of composite spheres, the thermal resistance can be represented by:

$$R_{thermal} = \frac{\frac{1}{r_0} - \frac{1}{r_1}}{4\pi k_{r_0 \to r_1}} + \frac{\frac{1}{r_1} - \frac{1}{r_2}}{4\pi k_{r_1 \to r_2}} + \frac{\frac{1}{r_2} - \frac{1}{r_3}}{4\pi k_{r_2 \to r_3}} \ldots N_{layer} \tag{2.7}$$

The equation above assumes multi-layered spherical geometry without heat generation; thus heat travels due to conduction alone.

2.2 CONDUCTION HEAT TRANSPORT THROUGH HEAT EXCHANGER TUBE WALLS

Similarly to spherical geometries, the conduction of heat through cylindrical walls is represented as a function of the axial and radial location.

$$\frac{1}{r}\frac{\partial}{\partial r}\left(kr\frac{\partial T}{\partial r}\right) + \frac{\partial}{\partial z}k\left(\frac{\partial T}{\partial z}\right) + \dot{q} = \rho C_p \frac{\partial T}{\partial t} \tag{2.8}$$

Neglecting axial conduction of heat this equation becomes

$$\frac{1}{r}\frac{\partial}{\partial r}\left(kr\frac{\partial T}{\partial r}\right) + \dot{q} = \rho C_p \frac{\partial T}{\partial t} \tag{2.9}$$

Solving for temperature as a function of radial location, for the case of pure conduction through a tube of inner radius R_o and outer radius R_s

$$T(r) = T_{Ro} + (T_{Ro} - T_s)\frac{\ln\frac{r}{R_o}}{\ln\frac{R_s}{R_o}} \tag{2.10}$$

For cylindrical geometries, the thermal resistance can be represented by

$$R_{thermal} = \frac{\ln \frac{r_0}{r_s}}{2\pi k_{r_0 \to r_s} w_{thick}} \tag{2.11}$$

2.3 FORCED CONVECTION HEAT TRANSPORT INSIDE PEBBLE BEDS

Forced convection inside pebble beds results in high heat transfer coefficients since flows around spheres involve tortuous paths and new boundary layers form on each pebble. At low flow velocity, the flow develops smoothly around the pebbles. In this section, a few correlations are presented, along with the methodology for its evaluation. A primary difference occurs based on how the fluid flow is characterized and at what temperature the properties are evaluated at as recommended. Essentially, if the correlation indicates evaluation based on superficial velocity, then the mean velocity is calculated by assuming that the volume of the bed is entirely occupied by the fluid, as opposed to real velocity where the flow velocity is higher due to a constrained flow that occurs in fraction of the total cross sectional area of the volume of the pebble bed. Based on a literature review, the heat transfer coefficient is best approximated by the following relation suggested by Wakao [1].

$$h = \frac{k}{D_p}\left(2 + 1.1\,\mathrm{Re}^{0.62}\,\mathrm{Pr}^{0.33}\right) \tag{2.12}$$

for 5<Re<100,000 where the Reynolds number Re is based on superficial velocity and thermophysical properties are calculated at the mean fluid temperature. The pebble diameter is used as the length scale.

The equation shown above includes two terms. The first constant term represents the heat conduction from a single pebble submerged in stagnant fluid. The second term is a function of the fluid flow through the pebble bed, thus indicating a dependence on the conditions of the flow.

Another useful correlation was obtained by Whittaker [7] primarily by performing experiments with gases in a packed beds, however, the data also applies for fluids with similar thermophysical characteristics as liquid salts in the range of interest for the PB-AHTR.

$$h = \frac{k}{D_h}\left(0.5\,\mathrm{Re}^{1/2} + 0.2\,\mathrm{Re}^{2/3}\right)\mathrm{Pr}^{1/3}\left(\frac{\mu_b}{\mu_s}\right)^{0.14} \tag{2.13}$$

for 20<Re<10,000 where Re is based on real velocity and thermophysical properties are evaluated at the bulk fluid temperature except for the correction factor which is evaluated at the mean surface temperature. The characteristic hydraulic diameter is used as the length scale.

Finally, another equation that is employed in the prediction of pebble bed to fluid heat transfer as reported by Gnielinski [8].

$$h = \frac{k}{D_h}\left(1+1.5(1-\varepsilon)\right)\left(2+\sqrt{\left[0.664\,\mathrm{Re}^{1/2}\,\mathrm{Pr}^{1/3}\right]^2+\left[\frac{0.037\,\mathrm{Re}^{0.8}\,\mathrm{Pr}}{1+2.443\,\mathrm{Re}^{-1/10}(\mathrm{Pr}^{2/3}-1)}\right]^2}\right) \tag{2.14}$$

for Re<20,000 where Re is based on real velocity and thermophysical properties are calculated at the mean fluid temperature. The characteristic hydraulic diameter is used as the length scale.

2.4 FORCED CONVECTION HEAT TRANSPORT INSIDE AND OUTSIDE TUBES

Forced convection assumes the absence of free convection effects. When heat transfer occurs strictly in the turbulent regime, free convection effects can be neglected even in vertical orientations, however in the laminar and the laminar-turbulent transitional regimes, free convection effects may have significant contribution in the overall convective heat transfer. In this section, convective heat transfer strictly due to forced flow is discussed.

2.4.1 Single straight tube

Internal laminar flow

In the case of internal laminar flow, the heat transfer coefficient with a constant wall heat flux boundary condition and assuming developed hydraulic flow profile, then the heat transfer coefficient is:

$$h = \frac{k}{D_h}\left(\frac{48}{11}\right) \tag{2.15}$$

If one assumes a constant wall temperature boundary condition, then the heat transfer coefficient becomes

$$h = \frac{k}{D_h}\left(3.657\right) \tag{2.16}$$

It is important to notice that the heat transfer coefficient is independent of location along the pipe. Derivation details are included in Incropera and Dewitt [2] and can easily be found in other heat transfer texts. Both of these relations are valid for laminar (Re<2300) flows.

Internal turbulent flow

Because fluoride salts have relatively high Prandtl numbers, turbulent flow and even the use of heat transfer enhancement such as knurled tubes can play an important role in increasing heat transfer. Fluids flowing in the turbulent flow regime can be much more effective removing heat from the wall as opposed to fluids in the laminar regime. In the case of turbulent flows, there is no distinction if the boundary condition is a constant heat flux or constant temperature, since the heat removal rate is very high already. Incropera and Dewitt [2] present the classical correlation known as the Dittus-Boelter relation for convective heat transfer in smooth-walled tubes,

$$h = \frac{k}{D_h}\left(0.023\,\mathrm{Re}^{0.8}\,\mathrm{Pr}^{n}\right) \tag{2.17}$$

for Re>10,000, and 0.7<Pr<100

Where the power coefficient n takes the value of $n=0.3$ when the fluid is being cooled and $n=0.4$ when the fluid is being heated. In order to better take into account the variations the fluid viscosity as it is being heated or cooled, especially if the fluid experiments large temperature variations, a better approximation is offered by the Sieder and Tate relation discussed in Incropera and Dewitt [2].

$$h = \frac{k}{D_h}\left(0.027\,\mathrm{Re}^{0.8}\,\mathrm{Pr}^{1/3}\right)\left(\frac{\mu_b}{\mu_s}\right)^{0.14} \tag{2.18}$$

for Re>10,000, 0.7<Pr<120

where the viscosity of the fluid is evaluated at two different reference temperatures, the subscript *s* refers to surface temperature and the *b* refers to the temperature of the bulk of the fluid. Finally, another recent correlation, which offers precision for fully developed turbulent heat transfer at low Reynolds number is the Gnielinski correlation [18].

$$h = \frac{k}{D_h}\frac{\frac{f}{8}\left(\mathrm{Re}-1000\right)\mathrm{Pr}}{1+12.7\left(\frac{f}{8}\right)^{\frac{1}{2}}\left(\mathrm{Pr}^{\frac{2}{3}}-1\right)} \tag{2.19}$$

for 3,000<Re<5x10^6, 0.5<Pr<2000

The correlation above requires the evaluation of the friction factor coefficient, which is a function of the Reynolds number. The calculation of this factor is discussed in section 2.10.

Internal transitional flow

The validity of the heat transfer relations presented in equations (2.14) – (2.19) are limited to the flow regime where experimental data appear to validate the mathematical expression. In the flow

regimes in between however, the initial formation of turbulent eddies is highly dependent upon inlet conditions and for this reason, it is difficult to characterize the heat transfer in the transition region, however Gnielinski [3] offers the following empirical relation

$$h = \frac{k}{D_h}\left(0.012(\mathrm{Re}^{0.87} - 280)\,\mathrm{Pr}^{0.4}\left(\frac{\mathrm{Pr}_b}{\mathrm{Pr}_w}\right)^{0.11}\right) \tag{2.20}$$

for 2300>Re>10,000, 0.6<Pr<105

The relation shown above assumes a large tube aspect ratio (L/d>30) and includes a temperature correction factor in terms of Pr number, which reduces to unity with small fluid temperature differences between the bulk and the wall.

2.4.2 Bank of straight tubes

Heat transfer external to a bank of tubes is less sensitive to the flow regime since the geometry is complex unlike flow inside a pipe, therefore transition effects between laminar and turbulent flow can be neglected based on experimental work on heat exchangers by Donohue [4]. For this reason, the following correlations can be applied in both turbulent and transition regimes.

External laminar and turbulent flow parallel to tubes

$$h = \frac{k}{D_o}\left(0.128\,\mathrm{Re}^{0.6}\,\mathrm{Pr}^{1/3}\right)\left(\frac{\mu_b}{\mu_s}\right)^{0.14} \tag{2.21}$$

External laminar and turbulent flow perpendicular to tubes

$$h = \frac{k}{D_o}\left(0.346\,\mathrm{Re}^{0.618}\,\mathrm{Pr}^{1/3}\right)\left(\frac{\mu_b}{\mu_s}\right)^{0.14} \tag{2.22}$$

Both of the correlations shown above are applicable for 1<Pr<500 and are best suited for fluids in the liquid phase. In order to characterize heat transfer for gases, Grimson [15] offers the following expression, applicable for aligned tube banks with equal longitudinal and transverse pitch, within $1.5<P_oD<4.0$ ratio.

$$h = \frac{k}{D_o} c\,\mathrm{Re}_{\max}^{m} \tag{2.23}$$

where both c and m factors are dependent of the tube arrangement. The following expression is a quadratic interpolation from tabulated data from Incropera [2].

$$c = 0.13P_oD^2 - 0.58P_oD + 0.85 \tag{2.24a}$$

$$m = -0.049P_oD^2 + 0.22P_oD + 0.41 \tag{2.24b}$$

The correlations above employ the outer tube diameter as the length scale of the problem. Reynolds is calculated using the velocity which results from the smallest area of flow between adjacent tubes. Thermo physical properties are evaluated at mean temperatures.

2.4.3 Single curved tube

The physical process of forced convection on curved tubes is similar to that of straight tubes; however the centrifugal acceleration produces a transverse pressure gradient within the tube, thus causing a secondary flow perpendicular to the direction of the primary flow. This secondary flow results in an enhancement of the heat transfer when compared to straight tubes. The following relations are obtained from Mori [5], [6] based on experimental and theoretical analysis.

Internal laminar flow

$$h = \frac{k}{D_{in}} \frac{0.1979\left(\frac{a}{Rc}\right)^{0.25}\mathrm{Re}^{0.5}}{\varsigma\left(1+\frac{37.05}{\varsigma}\left(\frac{1}{40}-\frac{17}{120}\varsigma+\left(\frac{1}{10\varsigma}+\frac{13}{30}\right)\frac{1}{10\,\mathrm{Pr}}\right)\left(\mathrm{Re}\left(\frac{a}{Rc}\right)^{0.5}\right)^{-0.5}\right)} \tag{2.25a}$$

$$\varsigma = \frac{2}{11}\left(1+\left(1+\frac{77}{4}\frac{1}{\mathrm{Pr}^2}\right)\right) \tag{2.25b}$$

$0.7<\mathrm{Pr}<400$ and $40<\mathrm{Re}\cdot(a/Rc)^{0.5}<1000$

Internal turbulent flow

$$h = \frac{k}{D_{in}}\frac{1}{41}\mathrm{Re}^{\frac{5}{6}}\left(\frac{a}{Rc}\right)^{\frac{1}{12}}\left(1+\frac{0.061}{\left(\mathrm{Re}\left(\frac{a}{Rc}\right)^{2.5}\right)^{\frac{1}{6}}}\right)\mathrm{Pr}^{0.4} \tag{2.26}$$

This is applicable for $0.7<\mathrm{Pr}<400$ and $8000<\mathrm{Re}<10^5$

In the calculations above, the ratio *a/Rc* refers to the ratio of coil tube inner radius to the radius of curvature of the coil. Reynolds number is calculated using the inner diameter as the length scale, and the thermophysical properties of the fluid are evaluated at mean fluid temperatures.

Internal transitional flow

Given the formation of secondary flow in curved pipes, the transitional flow is included in the empirical correlations shown above, given that the experimental data which supports these correlations was obtained experimenting with coils oriented with the cylindrical axis parallel and perpendicular with the direction of gravity. Orientation does not have a significant effect on the overall heat transfer coefficient; however there is an effect due to the surface temperature of the coils.

2.4.4 Bank of curved tubes

External forced convection heat transfer coefficients for a bank of curved tubes can be approximated to a bank of straight tubes in order to calculate heat transfer coefficients on external cross flow calculations. Given that the correlations for external straight pipe flow have already being introduced, it is suggested that these correlations are employed however keeping in consideration the following limiting conditions.

In the case of pure cross flow heat transfer, common in shell and tube heat exchangers, the correlations are constructed usually with experiments where the fluid inside the tubes flows with the same temperature variation axially, and the external fluid encounters internal fluid at even temperatures on that same axial location common to all straight tubes set in parallel. In the case of curved tubes, the internal fluid is always increasing in its temperature, thus the external fluid encounters fluids at different temperatures as it flows across the bank of tubes. This idealization is known as the 1 stream mixed 1 stream unmixed idealization.

2.5 CONVECTIVE HEAT TRANSPORT DUE TO SURFACE ENHANCEMENT

Convection heat transfer can be enhanced if the surface of interface is treated with certain characteristics. Enhancement is achieved by introducing features which elevate the heat transfer coefficient, or which increase the surface area. The most common method to accomplish convection enhancement is by introducing surface roughness and thus enhance turbulence. H.J. Lim [9] reports the following empirical relation which applies to surface knurled tubes internally and externally on pipes.

$$EF_{tube-side} = 1 + \left(\frac{\mathrm{Re} - 1000}{9000} \right)^{\frac{1}{2}} \tag{2.27}$$

$$EF_{shell-side} = 1 + \frac{1}{3}\left(\frac{\mathrm{Re} - 1000}{9000} \right)^{\frac{1}{2}} \tag{2.28}$$

for1,000<Re<10,000

$$EF_{tube-side} = \begin{cases} 1 \rightarrow \mathrm{Re} < 1,000 \\ 2 \rightarrow \mathrm{Re} > 10,000 \end{cases} \tag{2.29}$$

$$EF_{shell-side} = \begin{cases} 1 \rightarrow \mathrm{Re} < 1,000 \\ \frac{4}{3} \rightarrow \mathrm{Re} > 10,000 \end{cases} \tag{2.30}$$

for Re<1000 and Re >10,000

These factors multiply the heat transfer coefficient obtained with the appropriate correlations directly.

2.6 RADIATIVE HEAT TRANSPORT

In the case of high temperature reactors radiation heat transfer is an important phenomenon. Bardet [17] discusses that in the case of flow of transparent fluid inside heat transfer channels, it is common that the surfaces that view each other have similar temperature, so the net radiation heat transfer is small compared to convective heat transfer. Based on this principle, it can be assumed that radiation heat transfer inside the PB-AHTR core can be neglected compared to convective heat transfer, as it is cooled by flibe, a transparent fluid. In the case however of the passive safety cooling system, where high temperature pipes carrying liquid salt is exposed to ambient temperatures, radiation heat transfer is expected to be significant. The subject of radiation heat transfer is ample, and this section will present relations applicable to cylinders radiating to a wall as shown in the figure below. The relations presented in this section correspond to the exchange of heat between two surfaces as discussed by Incropera and Dewitt [2].

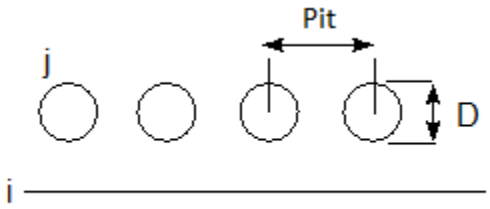

Fig. 2-2 Thermal radiation from an infinite row of cylinders to an infinite plane

Figure 2 shows an infinite number of cylinders of infinite length next to an infinite plane. The view factor of surface *i* with respect to surface *j* become:

$$VF_{ij} = 1 - \left[1 - \left(\frac{D}{Pit}\right)^2\right]^{\frac{1}{2}} + \left(\frac{D}{Pit}\right)\tan^{-1}\left(\frac{Pit^2 - D^2}{D^2}\right)^{\frac{1}{2}} \tag{2.31}$$

Employing the reciprocal relationship, the inverse view factor can be obtained based on the total area A_i and A_j of surfaces i and j respectively as follows:

$$VF_{ji} = VF_{ij}\frac{A_i}{A_j} \tag{2.32}$$

Assuming surface j is at higher temperature than surface i, then the net amount of heat being transferred through radiation is:

$$\dot{q} = \frac{\sigma\left(T_j^4 - T_i^4\right)}{\frac{1-e_j}{e_j A_j} + \frac{1}{VF_{ij}A_i} + \frac{1-e_i}{e_i A_i}} \tag{2.33}$$

Where e_i and e_j are emissivities of surfaces i and j respectively. σ is the Stefan-Boltzmann constant and it takes the value of $5.670\text{x}10^{-8}$ W/m^{2}K^4.

In the case of complex geometries, it is convenient to express the heat transfer similarly as a convective process as the equation below:

$$\dot{q} = h_{eq}A_j\left(T_j - T_i\right) \tag{2.34}$$

$$h_{eq} = \frac{\sigma\left(T_j + T_i\right)\left(T_j^2 + T_i^2\right)}{\frac{1-e_j}{e_j} + \frac{1}{VF_{ij}A_i}\frac{A_j}{A_i} + \frac{1-e_i}{e_i}\frac{A_j}{A_i}} \tag{2.35}$$

The effective heat transfer coefficient h_{eq} can become important at higher temperatures because it depends upon the cube of the absolute temperature.

HYDRAULIC PROCESSES

2.7 FLOW PRESSURE DROP INSIDE PEBBLE BEDS

Flow losses inside pebble beds can result in relatively large pressure drops due to the tortuous paths the fluid is forced to travel. At low flow velocity, the flow develops smoothly around the spheres, but it always breaks at the point of contact between spheres. The following relations discussed by Mills [10] can be integrated along the length of the pebble bed to determine the overall pressure drop.

2.7.1 Due to Friction losses

$$\left.\frac{dP}{dx}\right|_{friction} = \frac{150\mu V}{L_{char}{}^2} \tag{2.36}$$

2.7.2 Due to Form Drag losses

$$\left.\frac{dP}{dx}\right|_{form} = \frac{1.75\rho V^2}{L_{char}} \tag{2.37}$$

The losses in a pebble bed occur simultaneously due to friction and due to form drag, for this reason, the overall pressure drop calculation must be included the addition of both contributing factors. The coefficients 150 and 1.75 were obtained empirically and Bardet [14] suggest the values of 180 and 1.8 can also be used respectively; however this study employs the former values for the both relations, also known as the Ergun correlation for pebble beds.

The pebble bed hydraulic or characteristic diameter, along with the real velocity is calculated as follows:

$$L_{char} = D_{pebble}\frac{\varepsilon}{1-\varepsilon} \tag{2.38}$$

$$V = \frac{\dot{m}}{\rho A_{no-pebbles}\varepsilon} \tag{2.39}$$

where ε is the porosity of the pebble bed and $A_{no\text{-}pebbles}$ is the area of flow of the channels which contain the pebble bed assuming there aren't any pebbles present in the bed.

2.8 INTERNAL PRESSURE DROPS INSIDE TUBES

2.8.1 Single Straight tube – Friction losses

Primarily, the wall friction coefficient is a function of the Re number, which is the ratio of the fluid inertia forces to the viscous dissipation forces.

$$\mathrm{Re} = \frac{\rho VD}{\mu} \tag{2.40}$$

Thus, the relations to predict the pressure drop due to wall friction can be estimated based on the friction factor.

$$\Delta P = f \frac{L}{D_h} \rho \frac{V^2}{2} \tag{2.41}$$

The equation above can be used to predict the pressure drop ΔP for fluid flowing a distance L through a pipe whose hydraulic diameter is D_h and the fluid is characterized to have a density ρ and flow at a mean velocity V. Below is the methodology to calculate the friction factor.

Laminar

Under laminar regime, the friction losses are calculated through the Darcy friction factor

$$\mathrm{Re} < 2200$$
$$f = \frac{64}{\mathrm{Re}} \tag{2.42}$$

Turbulent

In the turbulent regime, several relations exists for the calculation of the friction factor, however for completion, the Zigrang-Sylvester equation is presented

$$\mathrm{Re} > 3000$$
$$\frac{1}{f} = -2\log\left\{\frac{\varepsilon_R}{3.7D} + \frac{2.51}{\mathrm{Re}}\left[1.14 - 2\log\left(\frac{\varepsilon_R}{D} + \frac{21.25}{\mathrm{Re}^{0.9}}\right)\right]\right\} \tag{2.43}$$

Transitional

For the case of flows characterized by Re numbers that lie in between 2200 and 3000, a linear interpolation is employed between those two points.

$$f = \left(3.75 - \frac{8,250}{\mathrm{Re}}\right)\left(f_{\mathrm{Re}=3000} - f_{\mathrm{Re}=2200}\right) + f_{\mathrm{Re}=2200} \tag{2.44}$$

2.8.2 Form losses

Form losses occur in flows due to obstructions, changes in flow area, or any other anomaly. This is usually taken into account by multiplying the dynamic pressure by a loss coefficient K to estimate the pressure drop due to the anomaly in the flow.

$$\Delta P = K \rho \frac{V^2}{2} \tag{2.45}$$

The factor *K* is pre-determined given the obstruction, such as flow areas, elbows, u-bends, etc. These factors can be found in standard fluid mechanics handbooks, such as Crane [16].

2.8.3 Single Curved tube – Friction and Form losses

The pressure drop of flows inside curved circular tubes is similar to the flows occurring inside straight tubes; however, a secondary flow field is formed arising from the centrifugal acceleration and thus causing a pressure differential. Form losses are treated in equal manner to the those occurring in straight tubes, but the friction losses are accounted from empirical correlations provided by Mori [5],[6].

$$\Delta P = f_{curved} \frac{L}{D_h} \rho \frac{V^2}{2} \tag{2.46}$$

In the case of laminar flows

$$\frac{f_{curved}}{f_{straight}} = 0.108 \left(\mathrm{Re} \sqrt{\frac{a}{Rc}} \right)^{0.5} \tag{2.47}$$

For turbulent flows

$$\frac{f_{curved}}{f_{straight}} = \frac{0.029 + 0.304 \left(\mathrm{Re} \left(\frac{a}{Rc} \right)^2 \right)^{-0.25}}{0.184 \, \mathrm{Re}^{-0.2}} \tag{2.48}$$

where *a* is the tube radius and *Rc* is the radius of curvature of the tube. Once these friction factors are obtained, they are used to adjust the friction factor calculated assuming straight pipe geometry.

2.9 EXTERNAL FLOW PRESSURE DROP OUTSIDE TUBES

The friction drop on flows that is parallel or perpendicular through a bank of tubes of diameter *D* and separated by the tube center-to-center distance of a pitch *Pit* have been studied empirically by Todreas and Kazimi [13]. The relations are included below.

2.9.1 Parallel flow on bank of straight tubes

$$\Delta P = f_{bundle} \frac{L}{D} \rho \frac{V^2}{2} \tag{2.49}$$

The equation above yields the wall friction pressure drop for a bundle of tubes of length *L* with fluid of density ρ flowing at mean velocity *V*. The friction factor is calculated as follows:

$$\frac{f_{bundle}}{f_{tube}} = \begin{Bmatrix} 1.045 + 0.071\left(\frac{Pit}{D} - 1\right) \rightarrow 10^4 < \mathrm{Re} < 10^5 \\ 1.036 + 0.054\left(\frac{Pit}{D} - 1\right) \rightarrow \mathrm{Re} > 10^5 \end{Bmatrix} \tag{2.50}$$

where f_{tube} is the usual friction factor that can be calculated from the Zigrang-Sylvester relation presented for wall friction tube-side for turbulent flows. In the case of the laminar pressure drop, the relation is much more complex and is very sensitive to the pitch and the tube lattice. Todreas and Kazimi [13] contain detailed relations in the case of laminar flows for this geometry.

2.9.2 Perpendicular flow through a bank of straight or curved tubes

$$\Delta P = \frac{f}{2}\frac{G_{\max}{}^2 L}{D_h \rho} \tag{2.51}$$

In the equation above, f is the friction factor. For external cross flow through a bank of aligned tubes, the factor f is the following as recommended by Emerson [19].

$$f = 4\left[0.044 + 0.08\left(\frac{S_L}{D_{to}}\right)\left(\frac{S_T}{D_{to}} - 1\right)^{-0.43 - 1.13\frac{S_L}{D_{to}}}\right]\left(\mathrm{Re}_{D_h}\right)^{-0.15} \tag{2.52}$$

Equation (2.52) requires that the maximum mass flux, the hydraulic diameter and Reynolds number are calculated as follows

$$G_{\max} = \frac{\dot{m}}{A_{flow}\left(1 - \frac{1}{P_o D}\right)} \tag{2.53}$$

$$\mathrm{Re}_{D_h} = \frac{G_{\max} D_h}{\mu} \tag{2.54}$$

$$D_h = L_{bank}\frac{A_{flow}\left(1 - \frac{1}{P_o D}\right)}{\pi D_{to} L_{tube}^{total}} \tag{2.55}$$

The parameters S_L and S_T represent the spacing between tubes in the longitudinal (parallel) and transversal (perpendicular) direction relative to the flow respectively.

The length of the bank, L_{bank} is defined as the overall distance of the tube bank which fluid travels through.

2.10 PRESSURE DROP DUE TO SURFACE ENHANCEMENT

Pressure drop due to surface enhancement for improved convective heat transfer also causes increased pressure drop, both for internal and external flow in heat exchangers. H.J. Lim [9] reports the following correlations.

$$EF_{tube-side} = 1.3 \tag{2.56}$$

for $0<\mathrm{Re}10^6$

$$EF_{shell-side} = \begin{cases} 1 \rightarrow \mathrm{Re} < 1{,}000 \\ 2 \rightarrow \mathrm{Re} > 10{,}000 \end{cases} \tag{2.57}$$

for Re<1,000 and Re>10,000

$$EF_{shell-side} = 1 + \left(\frac{\mathrm{Re} - 1000}{9000} \right)^{\frac{1}{2}} \tag{2.58}$$

for 1,000<Re<10,000

These factors affect the wall friction as follows:

$$\Delta P_{enhanced} = \Delta P_{smooth} EF \tag{2.59}$$

COUPLED THERMAL-HYDRAULIC PROCESSES

2.11 NATURAL CIRCULATION ANALYSIS

Natural circulation consists on fluid flow in a loop which absorbs heat at a lower elevation of the loop and rejects heat at a higher elevation of the loop, thus enabling a steady flow on a loop balancing the buoyant-induced flow with the friction dissipation. In order to establish the equilibrium mass flow rate, the equations for conservation of momentum and energy are integrated along the flow loop, and combined to determine the equilibrium flow rate which balances heat transfer through the loop.

$$\oint \rho g \cos\theta = \oint f \frac{G|G|}{2 D_h \rho} \tag{2.60}$$

The recommended technique is to break down the flow loop into several segments which can be integrated separately and summed together afterwards. After some manipulation

$$\left(\rho_C - \rho_H \right) L_{thermal} g = \sum_{k=1}^{loop-segments} f_k \frac{L_k}{D_{h,k}} \rho \frac{V_k^{\,2}}{2} \tag{2.61}$$

where ρ_c and ρ_h refers to the hot and cold density of the fluid and $L_{thermal}$ is the vertical distance between the thermal centers of the hot and cold segments of the loop. L_k is the length of k_{th} segment of the loop. Applying the Bousinesq approximation and solving for the velocity, expressed as the mass flow rate in a constant flow area loop.

$$\dot{m} = \sqrt[2-c]{\frac{gL_{thermal}\beta\Delta T g\rho^2}{B\left(\frac{D_h}{A\mu}\right)^{-c}\frac{L}{2A^2D_h}}} \tag{2.62}$$

where L is the total loop length, and B and c result from assuming that the friction coefficient can be expressed as follows

$$f = B\,\mathrm{Re}^{-c} \tag{2.63}$$

The set of equations shown above assume that the fluid flow is in equilibrium with the heat flow through the loop. The relations from above can be applied to study transient response when disturbances are applied, such as applying a sudden increase in temperature difference ΔT between the hot and cold sides of the loop. Todreas and Kazimi [12] explain these processes in detail.

2.12 HEAT EXCHANGER ANALYSIS

The analysis of heat exchangers can be performed based on the required heat load and determine the heat exchanger size from the required minimum heat transfer area, assuming fixed mass flow rates for the heating and cooling fluids through the heat exchanger.

However, in certain problems, the size of the heat exchanger is not only a function of the heat load, but also of the allowable fluid pressure drop across one or both of the fluids through the heat exchanger. This problem is known as the thermal-hydraulic exchanger design process, where fluid and thermal considerations must be taken simultaneously.

Applying the number of thermal units (NTU) methodology as detailed by Mills [10], the required heat load along with the mass flow rates and the fluid heat capacity yield the effectiveness, which then can be used to calculate the *NTU* number, based on charts or calculated with relations specific to the heat exchanger type. Once the *NTU* is calculated, the overall heat transfer coefficient U can be calculated based on the appropriate heat transfer correlations using the heated perimeter P_h, the following relations determine the heat exchanger sizing problem.

$$NTU = \frac{UP_hL}{C_{\min}} \tag{2.64}$$

where L is the length of the heat exchanger. Another relation which depends on the heat exchanger sizing

$$\Delta P = f \frac{L}{D_h} \frac{1}{2} \rho V^2 \tag{2.65}$$

Both relations above depend on the tube length *L*, which is the common factor for both equations. In the case of a maximum allowed pressure drop, an iterative process is necessary to meet both requirements while varying the geometric parameters.

COUPLED THERMAL-HYDRAULIC-NEUTRONIC PROCESSES

2.13 POINT KINETICS WITH FUEL AND MODERATOR TEMPERATURE REACTIVITY FEEDBACK

Heat generation rate within a reactor core varies when reactivity changes occur. A reactivity change is a perturbation in the steady conditions of the nuclear core, which causes a perturbation in the overall rate of fission nuclear reactions. Negative reactivity insertion, typically caused be increased neutron absorption, causes the heat generation rate drop, and positive reactivity insertion, typically caused by the removal of neutron highly-absorbent material causes heat generation rates to increase. The following equation as discussed by Duderstadt [11] illustrates the variation of heat generation rate *Q* as a function of time *t*.

$$Q(t) = Q_o \left[\frac{\beta_T}{\beta_T - \rho_R} e^{\frac{(\gamma \rho_R)}{\beta_T - \rho_R} t} - \frac{\rho_R}{\beta_T - \rho_R} e^{-\frac{(\beta_T - \rho_R)}{l} t} \right] \tag{2.66}$$

The parameter ρ represents the reactivity insertion into the core, as a consequence of a perturbation. These perturbations can be small or large, for instance, insertion or removal of a control rod would represent a large perturbation whereas changes in temperature or density of the fuel and neutron moderator would represent small perturbations. The point kinetics equation shown above still holds for both types of perturbations.

The transient analysis of nuclear reactors is focused with the behavior subsequent to small perturbations in the reactor core. In order to estimate the insertion of reactivity from a temperature *T* or moderator density *M* perturbation, it is necessary to know the temperature and moderator density reactivity feedback coefficient, denoted λ_T and λ_M below.

$$\lambda_T = \frac{\partial \rho_R}{\partial T} \rightarrow \partial \rho_R = \lambda_T \partial T \rightarrow \Delta \rho_R = \lambda_T \Delta T \tag{2.67}$$

$$\lambda_M = \frac{\partial \rho_R}{\partial M} \rightarrow \partial \rho_R = \lambda_M \partial M \rightarrow \Delta \rho_R = \lambda_M \Delta M \tag{2.68}$$

As it can be inferred from the relations above, the insertion of reactivity $\Delta \rho_R$ resulting from perturbations can be estimated from the magnitude of the perturbation itself and the knowledge

of these feedback coefficients, which are determined in the nuclear reactor core design. The linear relation shown is only valid for small perturbations, usually within the same range of validity as the feedback coefficients themselves, as these coefficients are functions of temperature and moderator density as well, but for small perturbations the relations above hold valid as explained in Duderstadt [11].

The temperature and moderator perturbations denoted ΔT and ΔM are a function of the thermal-hydraulic plant behavior. A decrease in the forced cooling capacity or an increase in coolant pressure would result in these perturbations. The result does not only affect the heat transfer rate or the pressure drop across the core, but the heat generation rate as well. For this reason, the coupled problem of multiple phenomena in nuclear reactors is particularly difficult.

2.14 REFERENCES

[1] N. Wakao, S. Kaguei *Heat and Mass transfer in Packed Beds*. Gordon and Breach Science Publishers, New York (1982)

[2] F. P. Incropera, D. P. Dewitt *Fundamentals of Heat and Mass Transfer 5th edition.* John Wiley and Sons, New York (2001)

[3] V. Gnielinski *New Equations for heat and mass transfer in turbulent pipe and channel flow.* Int. Chem. Eng. 16(2) (1976) 359-367

[4]D. A. Donohue *Heat transfer and pressure drop in heat exchangers* Ind. Eng. Chem., 41(1949) 2499-2511

[5] Y. Mori, W. Nakayama *Study on forced convective heat transfer in curved pipes (1st report laminar region).* Int. J. Heat Mass Transfer. 8 (1965) 67-82

[6] Y. Mori, W. Nakayama *Study on forced convective heat transfer in curved pipes (2nd report turbulent region).* Int. J. Heat Mass Transfer. 10 (1967) 37-59

[7] Whittaker, S., "Forced convection heat transfer correlations for flow in pipes, past flat plates, single cylinders, single spheres, and for flow in packed beds and tube bundles," AlChE Journal, 18 (1972) 361–371

[8] V. Gnielinski, *Gleichungen zur Berechnung des Wärme- und Stoffaustausches in durchströmten ruhenden Kugelschütten bei mittleren und großen Peclet-Zahlen.* Verfahrenstechnik. 12 (6) (1978) 363-366

[9] H. J. Lim, P. F. Peterson *Conceptual design of the intermediate heat exchanger (IHX) for the PB-AHTR* UC Berkeley Report UCBTH-09-005, May 20. (2009)

[10] A. F. Mills *Basic Heat & Mass Transfer 2nd edition*. Prentice-Hall, Upper Saddle River, New Jersey (1999)

[11] J. J. Duderstadt, L. J. Hamilton *Nuclear Reactor Analysis* John Wiley and Sons, New York (1976)

[12] N. E. Todreas, M. S. Kazimi *Nuclear Systems II Elements of Thermal Hydraulic Design.* Hemisphere Publishing Corporation (1990)

[13] N. E. Todreas, M. S. Kazimi *Nuclear Systems I Thermal Hydraulic Fundamentals.* Taylor & Francis (1993)

[14] P. Bardet et al., *The pebble recirculation experiment (PREX) for the AHTR.* Global 2007, Boise, Idaho, September 9-13, 2007.

[15] E. D. Grimson, *Trans. ASME,* 59,583,(1937)

[16] Crane Company. *Flow of Fluids Through Valves, Fittings, and Pipe; Technical Paper No. 410*. Crane Company, New York. (1986)

[17] P. Bardet, P. F. Peterson *Options for scaled experiments for high temperature liquid salt and helium fluid mechanics and convective heat transfer.* Nuclear Technology 163 (2008) 344-357

[18] V. Gnielinski, *Int. Chem. Eng.,* 16, 359, 1976

[19] W. H. Emmerson *Shell side pressure drop and Heat transfer with Turbulent flow in segmentally baffled shell-and-tube heat exchangers* Int. J. Heat Mass Transfer Vol. 6, (1963) 649-668

3. DESCRIPTION OF THE PB-AHTR PLANT PRIMARY SYSTEM DESIGN

The methodology developed through this study is applied to the transient analysis of the Pebble Bed Advanced High Temperature Reactor (PB-AHTR). The history and evolution of the PB-AHTR design is discussed in detail in the introduction. In this section, the technical details of the reactor design studied are specified.

The design aspects of the PB-AHTR presented in this chapter include features already developed by other researchers in substantial detail. There are other design details however that are omitted in this section since this study focuses on the fundamental phenomena which occur at the plant level of the reactor design. Design details of the plant such as external heat loss to surrounding air, thermal inertia of piping connecting main components, safety valves and pump manufacturing details are examples of many design details which may exist but are not included in this section for simplicity.

Primary System Design Basis

The design basis of the primary system is to represent a high energy density system that is efficient in the usage of space and materials, thus making an economic design. Another criteria for the design of the primary system, is the usage of systems compatible with liquid salt coolants and high temperature environments. Finally, the primary system is required to have a high thermodynamic efficiency based on the use of a coolant with excellent high-temperature thermophysical properties.

The design of the reactor pebble core [1] and the direct and intermediate heat exchanger [2] were performed independently by researchers at UC Berkeley. This report offers an overview of the design of these components with limited and condensed information from the references. For more details, the reader is directed to the source reports.

3.1 CORE

3.1.1 Fuel: Geometry, Materials, Thermal Performance

Pebble fuel is made from various materials. The center region of the pebble is made from low-density graphite, the TRISO fuel annular region is made from TRISO particles imbedded into the graphite matrix material. Finally, the outer layer is purely made from full density graphite. Figure 3-1 depicts the configuration of a fuel pebble.

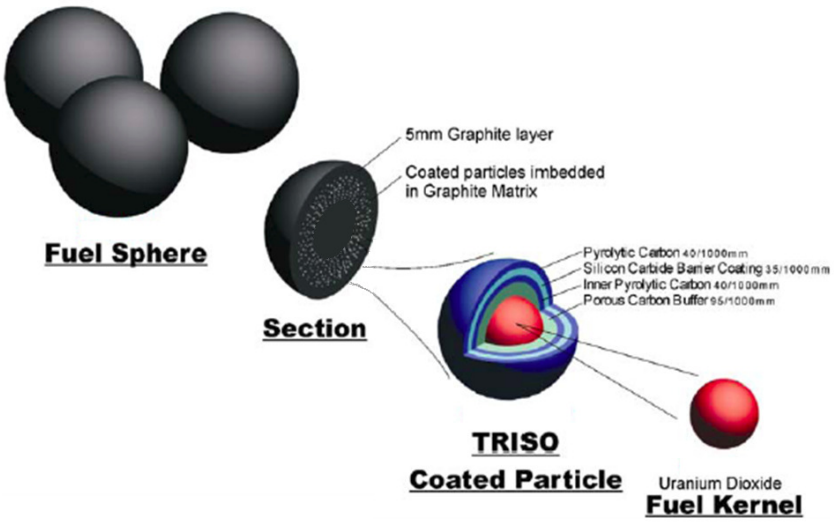

Fig. 3-1 Pebble fuel composition

The PB-AHTR employs fuel pebbles that are 3.0 cm in diameter. The size and density of the center graphite kernel are adjusted to give the desired pebble buoyancy, with a typical diameter of 1.98 cm. The TRISO outer annulus region is 2.5 cm in diameter. The composition of the each TRISO coated particle is shown in Figure 3-1, and includes pyrolitic carbon, silicon carbide, and a porous carbon buffer. Sterbentz et. al. [3] include more details on TRISO fuel design. The fuel kernels are made from Low Enriched Uranium (LEU) in the form of uranium oxi-carbide.

The fuel design of the PB-AHTR is in an advanced stage of analysis and methodology for the fuel performance was developed by Fratoni [5] and has been proven effective for the study of the neutronics of fuel pebbles and cores, however the design varies depending on the fuel burn-up requirements, allowable thermal gradients, reliability and reactivity feedback limitations. The standard point design is assumed in this study. Table 3-1 displays the assumed thermophysical properties for the fuel pebble constituents.

	ρC_p [J/m^{3}K]	k [W/mK]
Graphite	3.0×10^6	80
Fuel composite	3.0×10^6	15

Table 3-1 Pebble fuel constituents thermophysical properties

Holcomb [8] suggested the usage of the reported value for the pebble TRISO fuel layer. This recommendation is also suggested by Kohtz [9] as the steady state burn-up value experimentally determined for similar fuel design as the current pebble fuel. The assumed conduction coefficient for the graphite center core and outer layer are determined from a report originating from Idaho National Laboratory [10] where graphite type S2020 is suggested as a candidate material for NGNP reactor design applications.

The expected temperature profile inside the average fuel pebble can be obtained analytically from the conduction equation for annular spheres with partial heat generation and the appropriate boundary conditions as shown in Equations (2-3) and (2-4), in addition to the thermophysical properties for the fuel pebble shown in table 3-1. Figure 3-2 shows the results.

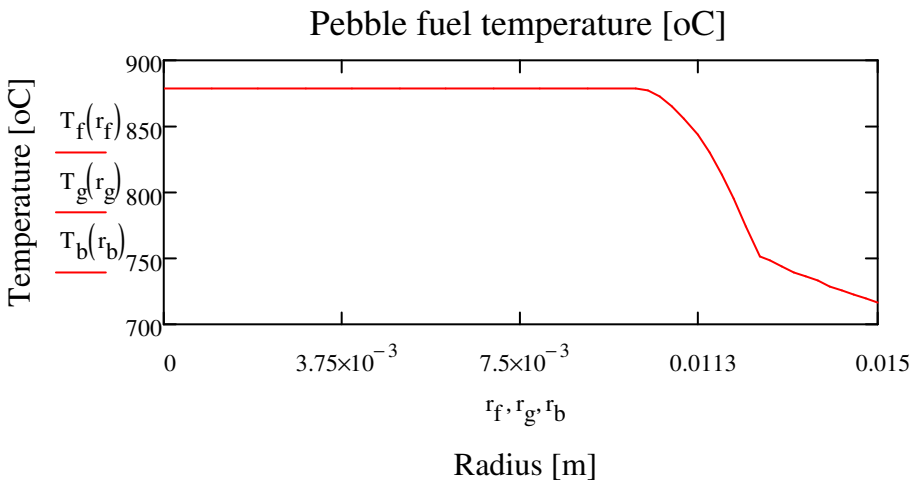

Fig. 3-2 Temperature profile of the average fuel pebble at full power. The average power per pebble is 2.67 kW_{th}

The fuel pebble generates heat only in the TRISO fuel layer region. In this present analysis, the assumption is that the normalized power generation is homogeneous everywhere in the TRISO fuel region. In reality, the heat generation is not homogeneous and will be a function of the local burn up and neutron flux. In addition, at the scale of individual fuel particles conduction must occur through the kernel and coating materials, so that the actual fuel kernels will be at a higher temperature than the temperature of the graphite binder material around the particles. These differences will impact in the predictions for the hottest regions within the pebble fuel, however, for the purposes of this study, the assumption of homogeneous power generation is reasonable.

3.1.2 Fuel conveyance: Geometry, Materials, Mechanical Performance

Fueling of the PB-AHTR is a complex process. Fuel pebbles are designed to float in liquid salt, and this is the guiding principle in the design of the pebble channels. The design basis is to allow the online refueling of the pebble bed reactor.

The core of the reactor consists of many vertically oriented solid structures, referred to as Pebble Channel Assemblies (PCAs), that are primarily constructed from graphite blocks shaped in hexagonal form and elongated from the lower coolant inlet region and stretching into the upper plenum of the reactor. These graphite blocks contain 18 channels which are cylinders arranged in hexagonal lattice structure and are located equidistant from each channel. These channels contain the pebble fuel and coolant and allow for the displacement of both, in this case, upwards as this

is the direction of flow through the fuel channels. The specific geometry of the channel was designed and optimized for pebble fuel insertion, displacement and removal through the defueling chutes above the core taking pebble dynamic considerations into account as discussed by Peterson [1].

Each PCA consists of a stack of hexagonal blocks of graphite. These assemblies are maintained together in the vessel by mechanical means; however, there is a gap in between these PCA's to allow for thermal expansion and swelling of the graphite as a function of varying thermal and radiation environments. A small core bypass flow channel exists in the spaces in between graphite blocks. The structural material envisioned for the PCA is Graphite H-451 or equivalent material for the convenient neutron radiation response, neutron moderation characteristics and available thermal inertia for excess heat generation.

The PCA channels, the top and bottom plenum, the upper and outer reflectors are graphite materials as well. Liquid salt shows no chemical reaction with graphite material. Although significant work has been performed in the characterization of graphite fabrication as well as abrasion processes for HTGRs, investigation is underway in the case of liquid salt interaction with graphite.

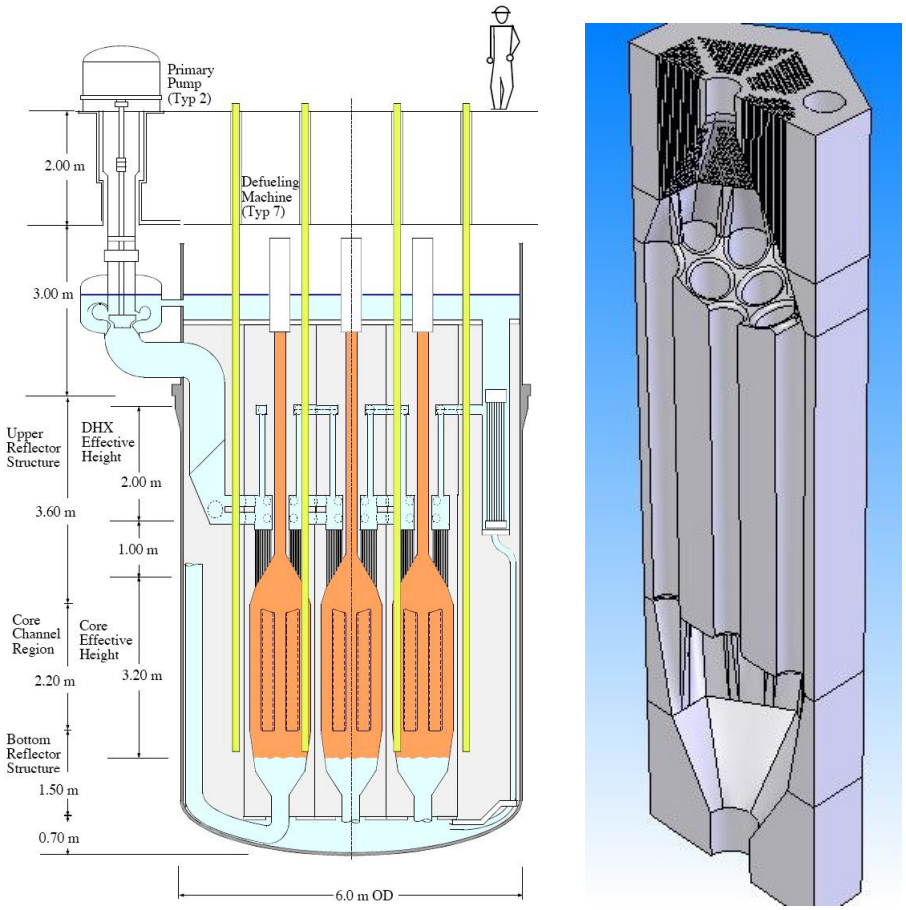

Fig. 3-3 Channel-type core vertical cross section. Red areas indicate regions where pebble fuel is circulated (left) and 3D view of a single pebble channel assembly (right)

The fuel channels have a carefully selected entrance and exit geometry, to allow for pebble entrance, displacement and exit in the channels. The graphite material which stands in between the pebble channels also acts as a moderating material which is designed to produce adequate neutron moderation for the targeted fuel utilization and burn-up.

3.1.3 Neutron reflectors: Geometry, Material, Neutronic and Thermal Performance

Surrounding the hexagonal pebble channel assembly blocks, the outer graphite reflector serves as the outer core boundary, neutron reflector and as housing for part of the Direct Reactor Auxiliary Cooling System (DRACS) systems. The diverted flow from the lower core plenum crosses the outer reflector and is forced to flow upwards through the fluidic diode and shell side of the DRACS Heat Exchanger (DHX). Both of these components sit inside cavitities in the outer reflector. There are 8 cavities overall, to accommodate 8 DRACS loops.

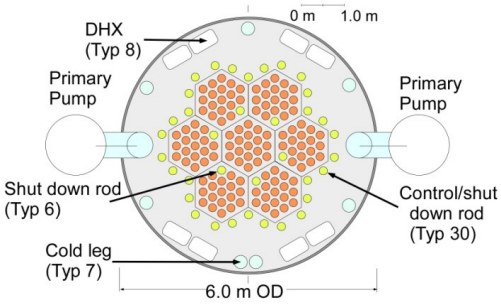

Fig. 3-4 Core outer neutron reflector and adjacent components

Above the PCA's is the upper reflector. The upper reflector, in addition to reflecting neutrons back from the top of the core, provides additional thermal inertia and acts as a fuel conveyor component. The geometry of this component is designed to guide pebbles exiting the PCA's into the defueling chute, where pebble fuel can be removed by a defueling machine for inspection and processing for later re-insertion. The upper plenum is also designed to have numerous but narrow coolant channels, where a large surface area of contact between liquid salt and the graphite reflector exists, such that in case of a sudden PCA outlet coolant temperature increase, the voluminous upper reflector absorbs the additional heat, therefore effectively using the large thermal inertia to reduce the rate of increase of the overall core coolant outlet temperature.

Reflectors used in the reactor core are considered to be composed of graphite H-451 or equivalent. Levels of irradiation of graphite will be different for the various core components. The design of the PB-AHTR considers permanent and replaceable graphite core components depending on the irradiation and the neutron dose.

3.1.4 Cooling channels: Geometry, Material, Thermal-hydraulic Performance

The coolant employed in the PB-AHTR primary loop is $^{7}Li_2BeF_4$, also referred as flibe. The intermediate loop coolant is assumed here is a mixture of LiF-NaK-KF, also referred as flinak. Williams [4] reports that in general, liquid salts are excellent nuclear reactor primary heat transfer fluids because of their high volumetric heat capacity, low vapor pressure, low parasitic neutron capture and sufficient moderating capability to allow the design of cores with negative void reactivity coefficients. This study does not evaluate cooling voiding accidents as these family of events are assumed unfeasible due to the high boiling point of liquid salts.

Flibe has excellent material compatibility and very low corrosion rates with high nickel alloys, when proper chemistry control is used. The activation products resulting from irradiation on flibe are short lived, thus causing low radiation levels associated with the coolant.

The cost of flibe is high due to the cost of beryllium and enriched lithium, therefore the PB-AHTR is designed to minimize the primary salt inventory in the primary cooling loops, once again, following the ideology of high energy-density components.

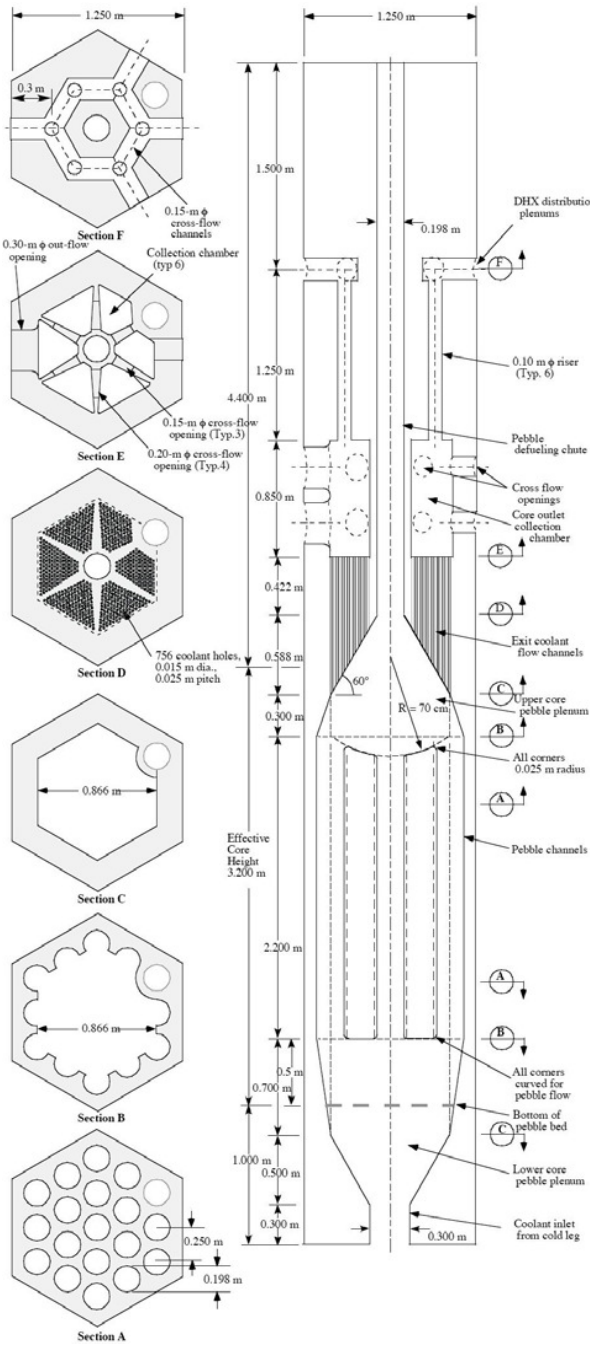

Fig. 3-5 Various horizontal cross section cuts of the core fuel and coolant channel (left) and the corresponding vertical cross section (right)

The lower plenum is located below the PCA's. Similarly to all core components, this graphite plenum has a carefully chosen geometry to allow homogeneous flow of coolant into the core and allow for the bypass of certain amount of coolant into the DRACS. The cavities in the lower plenum are designed to distribute the flow from two cold legs into seven PCA's and into 8

DRACS bypass channels, in addition, there are cavities which guide the insertion of pebble fuel into the PCA's. The DRACS system is described in detail in section 4.2.

Finally, the upper plenum is designed to collect coolant exiting the upper reflector and returning from the DRACS system and enhance the mixture based on a careful geometric design to obtain homogeneous thermal equilibrium of the outlet core coolant. The lower plenum also supports the core internal mechanism for refueling and the shutdown rod control mechanism. In addition, the upper plenum also serves as the outlet cavity that collects hot salt to flow to the primary pumps which pressurize the coolant and drive the flow into hot leg and the intermediate heat exchangers as it is further explained in the next section.

3.1.5 Assembled Core: Assembled Geometry, Power Distribution, Neutron flux

To analyze the reactor core thermal hydraulics it is necessary to assume a normalized power density function. It is well understood that power will vary locally inside the core, causing local temperature variations. In general, it is important to quantify the amount of variation, for example in LWRs where local power peaking must be predicted to avoid critical heat flux that may cause local boiling of the coolant. In the case of the PB-AHTR, the liquid salt boiling point is far from the operating average coolant temperature (boiling point of ~1500 °C vs. 650 °C average temperature). Therefore the power peaking factors can be reasonably assumed to be a factor of second order importance. For the purposes of this analysis, the methodology employed by Griveau [6] which assumes an analytically-derived cosine power density function across the core is employed to model the power distribution axially, but invariant radially. This is a reasonable assumption, and essentially neglects the neutron flux variations effect of the upper and outer reflectors, in addition to other mechanisms that affect the power distribution inside the core.

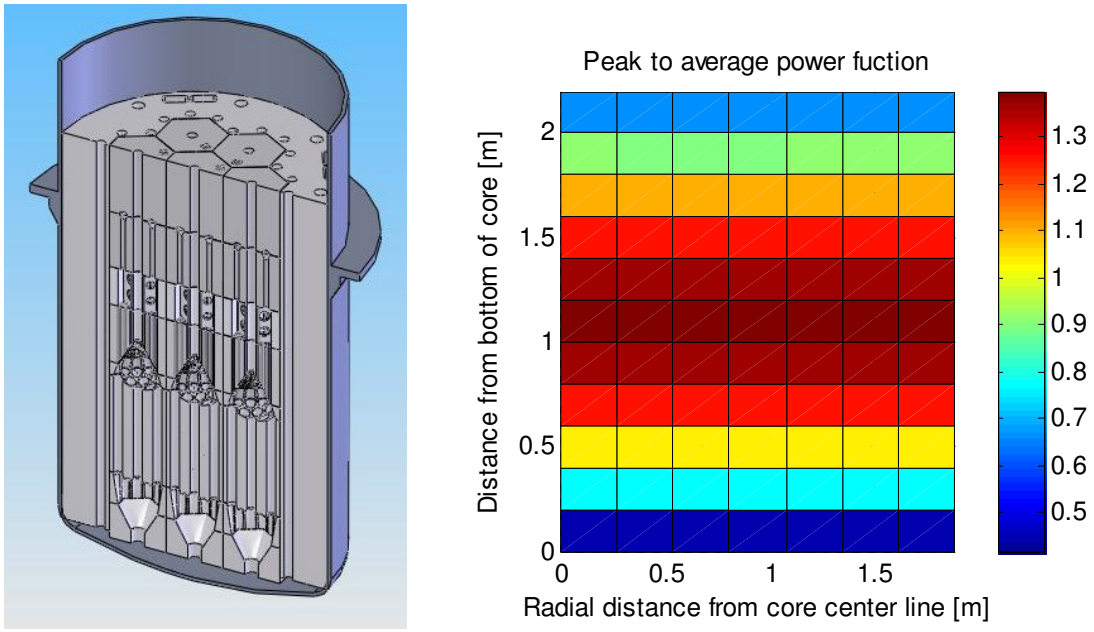

Fig. 3-6 Assembled core vertical cross section (left) and peak to average power shape function for active core region (right)

The figure above depicts the power shape function assumed for the thermal hydraulics analysis performed here. The meshing shown reflects the chosen level of discretization for numerical analysis of the reactor core. The details of the core discretization are discussed in the model construction section in chapter 5 along with the methodology.

3.2 MAIN HEAT EXCHANGER

The Intermediate Heat Exchanger (IHX) is the component which transports essentially all heat generated in the core to the intermediate cooling loop, which then transports the heat to the power conversion system, described in the next chapter. The current design of the IHX is derived from the heat exchanger design of the MSBR developed at ORNL in the 1970's. Both heat exchangers are single pass, shell and tube, counter-flow, disk and doughnut baffled, high power density designs. In both cases, the tubes have a knurled surface to enhance heat transfer on both the tube and the shell side of the heat exchanger. The differences however, are the specific geometric parameters of the heat exchangers, as well as a lower operating LMTD for the PB-AHTR.

3.2.1 IHX: Geometry, Material, Thermal-hydraulic performance

In the IHX, the bank of tubes is positioned vertically around an inner cylinder and position such that the spacing between tube centerlines is even both radially and circumferentially. The tubes are arranged neither in square or staggered configuration, but in a radial lattice, as shown in figure 3-7. The tubes are bent at the top end to accommodate thermal expansion during start up and thermal load variations.

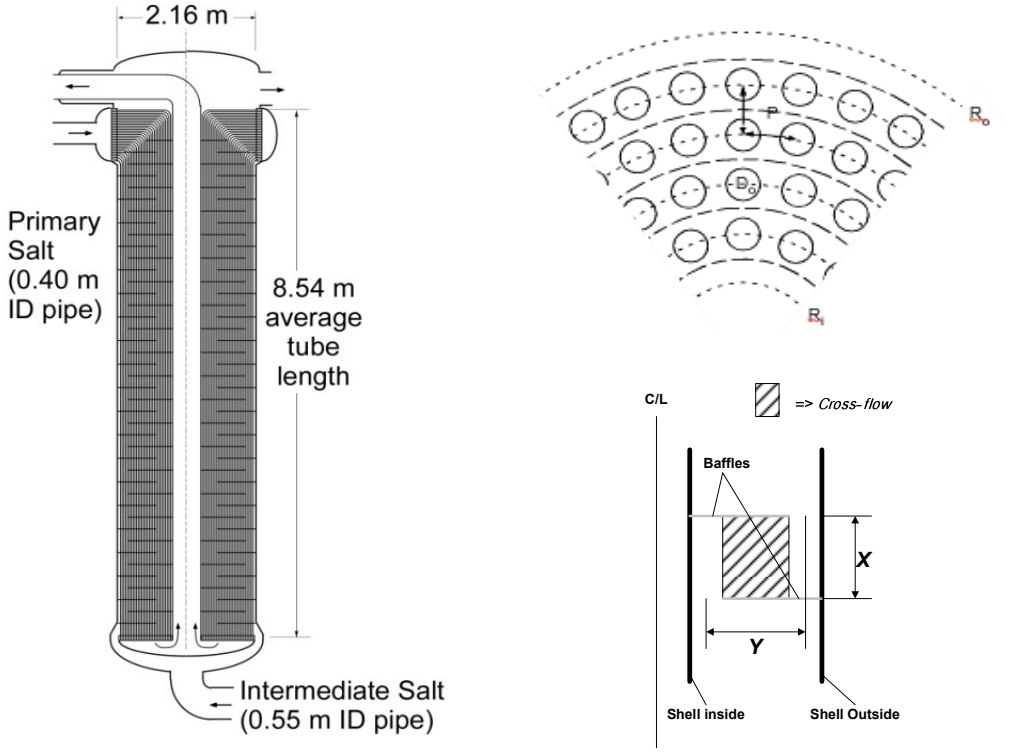

Fig. 3-7 IHX Geometric description

The primary, hot fluid enters the tube side of the heat exchanger at the top, then is collected at the bottom and carried to the top of the heat exchanger through the central tube, where coolant exits and returns to the reactor. The intermediate fluid enters the heat exchanger at the bottom, and then flows through a tortuous path perpendicular to the shell side of the tubes.

The baseline PB-AHTR design studied here employs Alloy 800H as the structural material for the vessel and components that are in contact with the salt coolant. Components such as coolant pumps, piping, heat exchanger pipes, shell, baffles, and tube sheet have a clad of Hastelloy N on the surfaces exposed to salt, for protection against corrosion. Alloy 800H is chosen for high temperature applications as the primary structural material given that its usage is code qualified up to 760 °C. The DOE VHTR program is also sponsoring a review of the Alloy 800H allowable stresses in the ASME Section III-NH code, also seeking to extend the code qualified operation to 900 °C. This effort will also include investigation of the alloy behavior under neutron radiation for high temperature applications.

3.3 PRIMARY PUMP

The primary pump of the PB-AHTR is a centrifugal pump with an overhung impeller and a special sealing mechanism to allow impeller operation with a dry main shaft. The pump design

basis considers the operation at high salt temperature and therefore special design requirements are taken into account.

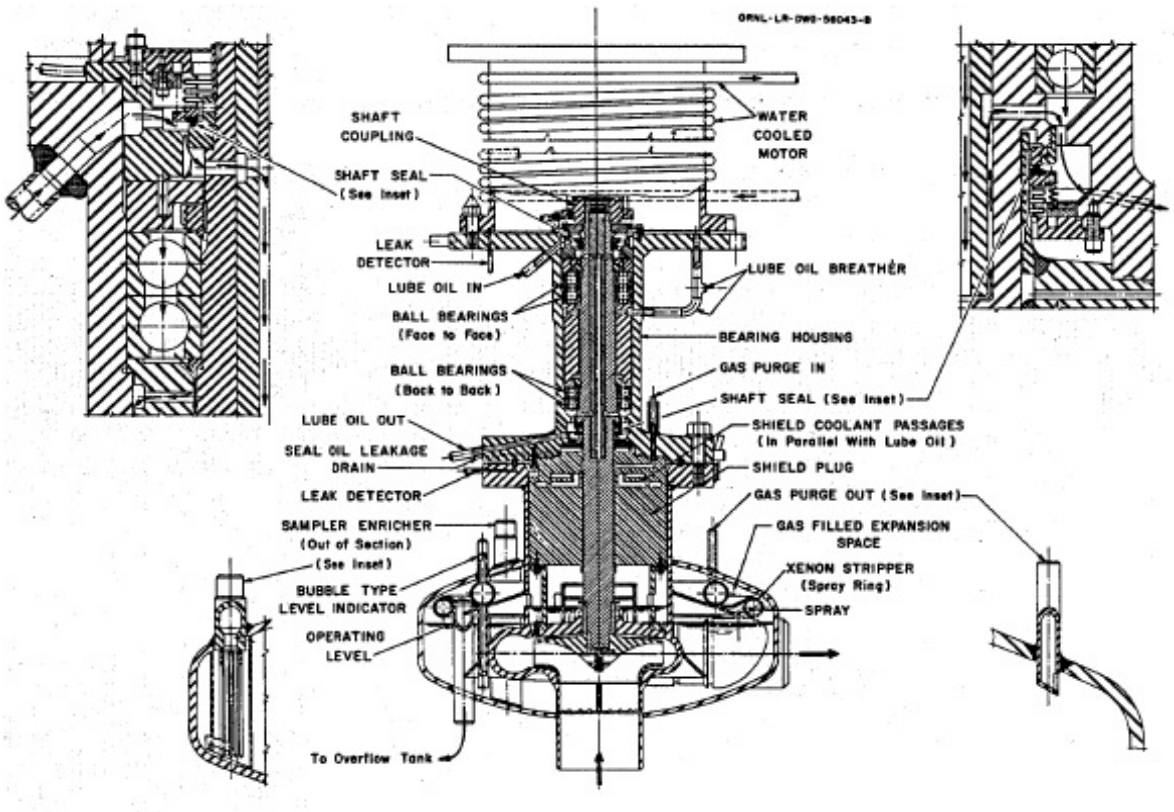

Fig. 3-8 MSBR primary pump vertical cross section view originating from ORNL report on MSRE system performance [11]

The figure above depicts the primary pump employed by MSBR. The pump design for the PB-AHTR is not expected to vary significantly from this pump design.

3.4 REACTOR CONTROL SYSTEMS

The PB-AHTR plant includes mechanisms designed to provide heat generation control. These mechanisms play a key role during reactor start-up, steady state full power output, load following, and reactor shutdown. The detail design of the reactor control mechanisms requires use of reactor physics tools, which were employed by Fratoni [5] in the analysis of inherent safety systems for the PB-AHTR. A general performance description of these control mechanisms is presented here.

There are three primary shutdown systems. 1) Active control system serves as the primary method for shutdown, and requires a signal for activation and interruption of energy input to shutdown-rod element latches 2) Passive control systems as the emergency control which do not require a signal or energy input and 3) Inherent control systems which do not require signal or

energy input, as the reserve control mechanism. The former two systems have been studied in detail and the reactivity effects resulting from the actuation of the mechanisms are presented in the section below.

In addition to shutdown elements, the reactor has control elements that are used to add and remove reactivity for the purpose of reactor control, including start-up, load-following and normal shutdown transients. The active control system requires the design of a system which employs energy input, in the form of electricity, magnetism or pneumatic to drive the insertion or removal of control elements from the core, and thus affecting the criticality. The system is designed to be operated from the control room and follow the reactor operators command according to the procedures. For the purposes of this study, it is assumed that the system can insert or remove variable amounts of reactivity taking various amounts of time for full insertion or removal as well as allowing a flexible delay time from signal to beginning of insertion.

3.4.1 Passive control: Reactivity worth, Insertion speed, Delay

The passive shutdown system is characterized by the activation without an external signal and also by acting without the input of energy, thus the designation as passive. This system consists of a neutrally buoyant shutdown rod which contains neutron absorbing material and is floating in a liquid salt channel that is located parallel to the pebble channel assemblies and extends from the bottom of the core all the way to the top of the upper plenum. In this configuration, the passive control rod sits above the core during full power operation and thus does not absorb neutrons significantly. During power excursions which cause the primary liquid salt core coolant to heat up, the density of the fluid becomes less than the density of the passive control rod, and causes the rod to sink inside the core, thus inserting a large amount of negative reactivity and shutting down the core. This mechanism is formally referred as the shutdown rods.

In order to study the performance of the shutdown rods, both, scaled experiments and simulations were set up by Blandford and Peterson [7] in order to measure the delay time which occurs from the onset of temperature rise until the shutdown rod begins to move, and also to estimate the amount of time the rod takes to insert inside the core. Fratoni [5] analyzed the shutdown rod reactivity worth using neutronics simulations. In both cases the information pertaining to this study is included in this section.

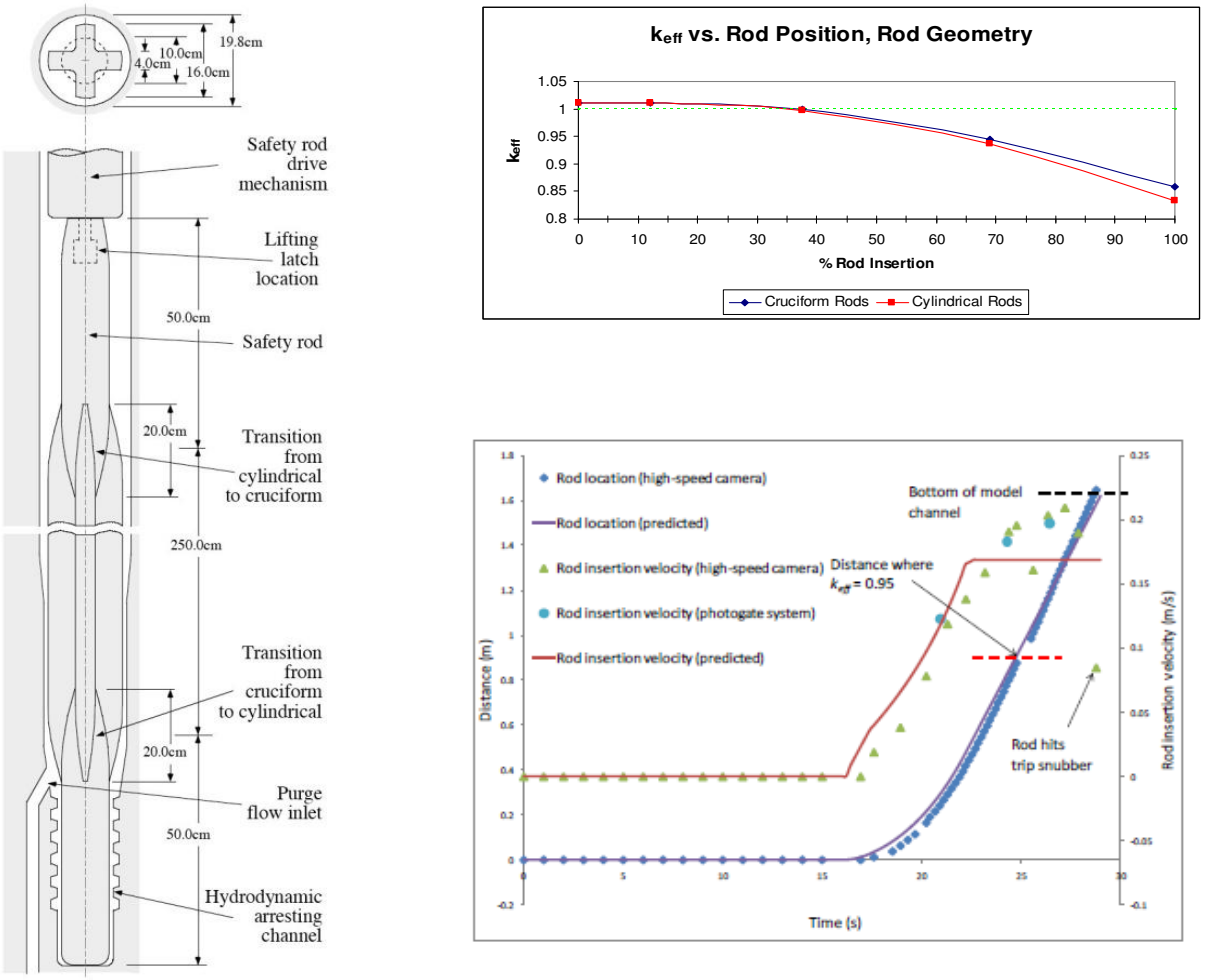

Fig. 3-9 Shutdown rod geometry in its inserted position inside the channel (left) core criticality predictions as a function of insertion depth (top) finally, insertion position and velocity following after onset of temperature increase resulting from studies by Blandford [7] and Fratoni [5].

The geometric design of the shutdown rod seeks to facilitate its insertion by minimizing the drag with the coolant in the channel as well as the contact between the rod and the channel walls. The design also considers potential stability issues for this floating body and finally, seeks to maximize the cross sectional area of the rod for neutron absorption. Based on these criteria, two designs are considered, using a cruciform-shaped rod and a cylinder-shaped rod.

The results of the analysis [5],[7] predict the total shutdown rod worth and the insertion delay and travel time of the inserting rod, for both designs, however experiments with the cruciform-shaped halted the analysis of this geometry early on. For this reason the data presented in the figures above refers to the cylindrical rod data only.

3.4.2 Inherent control: Feedback coefficients study.

The ultimate control mechanism is the inherent negative fuel and moderator temperature reactivity feedback. This engineered safety feature consists on designing the pebble fuel configuration to take advantage of the Doppler broadening effect on the epithermal absorption cross section of the fuel constituents, in special, of fertile fuel during temperature excursions. Similarly, the configuration of fuel and moderator material can be engineered such that effect of varying the overall moderator density due to thermal expansion results in the insertion of negative reactivity to the core. Fratoni [5] studied and quantified the reactivity insertion per unit of temperature variation of the fuel and moderator. While this study also discusses multiple fuel designs, the reactivity properties of the standard fuel pebble design and moderator at expected prototypical conditions are presented below.

Core average reactivity coefficients for 425-μm fuel kernel diameter and 12.5% TRISO packing factor

Feed-back mechanism	Value
Fuel temperature	-3.85 pcm/K
Coolant temperature[a]	-0.34 pcm/K
Moderator and fuel temperature[a]	-4.18 pcm/K
Moderator and coolant temperature[a]	-0.84 pcm/K

[a] Without leakage effect

Table 3-2 Temperature reactivity feedback coefficient for the fuel and moderator at average steady-state core burn-up levels [5]

Table 3-3 summarizes the values for the reactivity insertion that are assumed in this study for the different reactor control mechanisms.

Reactivity control parameters	**Active control mechanism**	**Passive shutdown rod mechanism**	**Inherent fuel reactivity control mechanism**	**Inherent moderator reactivity control mechanism**
Delay time from signal to initial response [s]	0	25	0	0
Travel time for full insertion [s]	1	37	0	0
Measure considered full insertion	Activation of insertion system	Complete sinking shutdown rod	Fuel temperature increase of 1500 °C	Moderator temperature increase of 500 °C
Total reactivity worth [$]	12.50	8.08	6.69	1.77

Table 3-3 Reactivity insertion parameters for reactor control systems

3.5 MODES OF OPERATION

3.5.1 Steady State

The PB-AHTR is designed for optimal operation under full power steady state conditions. In this mode, the passive safety cooling system removes a small amount of power and rejects heat to the outer surroundings. The power generation density is expected to vary within the reactor vessel spatially, and also throughout the fuel cycle. The temperatures exiting each core cooling channel are expected to vary as well, but effective mixing occurring at the upper plenum is expected to produce a homogeneous coolant temperature exiting the core into the heat exchanger.

3.5.2 Transient

Operation of the PB-AHTR during a transient is considered under a variety of situations which cause the transient to occur. For instance, changes in pump speed, changes in the secondary heat sink, and changes in the safety cooling systems are all events that will affect the rate of heat generation (reactivity changes) as well as the rate of heat removal (cooling capacity changes). The evaluation of transients is made for two distinct phases of the transients: short term fast variations and subsequent long term, slow variations.

During a transient, the fast variations cause the largest temperature and coolant flow rate changes in the core. These effects last in the order of minutes and involve forced flow conditions and high temperature difference heat transfer. For these reasons, the changes occur in the relative short time-scale. The secondary category of transient behavior belongs to short term, slow variations which are typically driven by buoyant flows and small temperature difference heat transfer. The threshold between short and long term events vary depending on each transient.

The evaluation of each transient requires the specification of precise bounding events which drive the changes of the plant operating conditions. The following section describes the applicable transients of interest for the PB-AHTR.

3.5.3 Initiating Events

SCRAM

The simplest transient to study is to shutdown the reactor by tripping the power conversion system and inserting the shutdown rods. At this point, the exact procedure to shut down the reactor has not been prepared, however, it is envisioned that the decay heat will be removed through the intermediate cooling system using a shutdown cooling system, with natural circulation of the primary and intermediate salts. Conceptually speaking, the procedure for shutting down the reactor must be designed to avoid overcooling of the primary salt, and therefore avoid causing coolant freezing which occurs at ~450 ^{o}C. The following are the three methods the reactor can be shut down, however, it is important to note that only the active and passive scram mechanisms will reduce the core power down to decay heat levels. The reactivity

due to feedback may not be sufficient to transition into decay heat mode, but certainly enough to lessen the heat generation rate significantly.

The reactor can be shut down employing a variety of mechanisms. The default mechanism consists of using the active control system, which inserts a large amount of negative reactivity by inserting neutron absorbing material into the core employing mechanical means. This method is the most effective and fastest to shut fission down, thus is typically used in nuclear reactors.

Another mechanism to shut down the reactor is by increasing the coolant temperature, either adjusting flow rates or primary heat sink and allow primary coolant temperatures to raise slightly and provoke the neutrally buoyant shutdown rod to insert into the core. This passive method is slow, however offers greatest reliability due to its passive nature.

Finally, the reactor core can also be shut down due to fuel and moderator negative reactivity thermal feedback effect, when the core increases its overall temperature sufficiently high. This passive method is the reactivity control mechanism that is considered after all other methods have been employed to shut the reactor down.

LOFC

The Loss of Forced Circulation (LOFC) transient refers to the inability to cool the reactor core through active, forced means. The most common scenario is to shut down both of the primary pumps.

Partial or total pump malfunction

The failure modes which produce this transient type may cause a partial or a total flow disruption. In the case of pump malfunction, a lessened net power supply to one or both of the primary pumps would produce smaller flow rates. Similarly, the introduction of excessive friction in the shaft bearings or the impeller points of contact, which would cause additional torque load to one of the pumps, thus reducing actual hydraulic power, that is, the cooling loop flow rate. A total failure of one of the pumps is perhaps the simplest scenario. Events such as the main shaft breakage or electric power supply interruption represent the total failure. Depending on the transient boundary conditions, the pump inertia may or may not be considered after a pump trip signal is in place.

Partial or total flow blockage

In the case of flow blockages, analogous to the pump failure case, malfunctions may alter the flow rates partially or completely. Given the tortuous path the primary coolant follows through the pebble bed and the small-diameter channels in the heat exchanger, these are the components most likely to show flow blockage disturbances. The case of complete flow blockage is less probable, but may occur if the temperature inside the loop drops sufficiently to freeze and plug across the entire flow area of the cooling loop.

Multi-component failure

The PB-AHTR employs two primary pumps which transport hot coolant through four heat exchangers. If only one of the pumps failed partially or completely, the flow in this loop would re-adjust based on the local flow conditions, affecting the flow distribution through the core and the heat exchangers. A flow blockage which occurs asymmetrically inside the core or heat exchanger would also have an impact locally, tending to allow uneven flows and rate of heat generation and removal.

LOHS

Loss of Heat Sink (LOHS) transients occur when the flow of salt through the intermediate system is altered or completely removed and thus disabling the cooling capacity of the intermediate heat exchangers. Other means of altering the heat sink is by considering degraded heat transfer rates due to fouling occurring at the liquid/metal interface.

Partial or total loss

LOHS transients may involve the complete loss of intermediate cooling, caused by an intermediate pump trip in all intermediate pumps. However this loss may be gradual as well, where only a fraction of the total mass flow rate on the intermediate cooling system is lost.

Multi-component loss

Finally, this transient can also involve cases where the loss does not occur to all components. For example, a pump trip for two/four intermediate pumps would reproduce a partial loss of heat sink, which would reflect in an asymmetric core cooling system, and thus causing core response to the perturbations that are difficult to predict.

LOCA

Loss of Coolant Accidents refers to the actual loss of liquid salt inventory. The pool design of the PB-AHTR includes the lining of buffer salt and a secondary retaining vessel guard which makes it essentially impossible for these transients to occur, since the buffer salt can ingress into the core due to gravity alone if the level of salt inventory decreases below the operation levels. A reserve tank of buffer salt is attached properly to provide ample supply if a loss would occur.

Small and Large break

Opposite to light water reactors, a loss of coolant accident is not sensitive to the size of the break, since the primary cooling system is not pressurized, resembling an open pool type reactor. In the current PB-AHTR design, the most likely LOCA event is a metallic structure failure outside the core causing coolant leakage or coolant mixing between the primary and intermediate salts inside the heat exchangers.

3.5.4 Safety limits

There are many safety considerations that limit the design of the PB-AHTR. These safety considerations results from the anticipation of several potential events that are likely to cause adverse effects to the integrity of the plant. These events are classified into the categories shown in Table 3-4 as presented by Peterson et al. [1] where each category contains a set of potential safety concerns from a licensing perspective.

Potential Safety Issues – Regulatory Design Criteria
Maintain control of radionuclides
Control heat generation (reactivity)
Control heat removal
Control coolant inventory
Maintain core and reactor vessel geometry
Maintain reactor building structural integrity

Table 3-4 Regulatory Design Criteria for safety

The DRACS system plays a key role by providing means of control of heat removal, although its design also affects essentially all other criterion in the table above. Given that the role of this mechanism is to remove decay heat, the design criteria follows the goal to achieve a system that can provide sufficient means to remove heat in case of failure of other primary means of heat removal, in this case, failure of the primary cooling system.

The safety concerns that arise due to a failed control of heat removal are many. The fuel and graphite core structures have very large margins to thermal damage, and thus cannot be easily damaged. Instead, overheating of the primary system would begin by causing accelerated thermal creep and mechanical failure of the metallic materials with the lowest thermal limits, in this case, structures such as pipes, pump components and the heat exchangers among others. Mechanical failure refers in this context to any consequence that compromises the components physical integrity. Thus, accelerated creep, fracture, deformation, rupture and melting are all mechanical failure modes among other modes. The failures described above are likely caused by reduced yield strength and accelerated creep deformation, but also by approaching melting temperature. The section below describes the limits chosen for safety.

Metallic thermal limits

Alloy 800H is ASME Code qualified for use up to 760 °C as reported by Peterson [1]. Alternatively, Alloy 316 stainless steel is code qualified for the use up to 800 °C. 316 SS offers a lower allowable stress loading compared to Alloy 800H. but has much better tolerance for neutron irradiation and has been shown to have low corrosion rates when used with clean flibe salt. Currently, an initiative exists by the U.S. DOE to evaluate and extend the operation limits for Alloy 800H up to 900 °C. Since the steady operation of the PB-AHTR employs salt exiting the core at ~704 °C, then a safety margin of 56 °C exists to remain within ASME Code limits

and accommodate coolant thermal variation during transients and accidents for Alloy 800H, and a somewhat larger margin for 316 SS.

Fuel thermal limits

Fuel failure begins to occur when pebble fuel reaches temperatures above 1600 °C as discussed by Peterson et al. [1]. The maximum temperatures envisioned in full power, steady operation occurs at the boundary between the graphite pebble core and the TRISO fuel layer and is calculated at 973 °C. This is the temperature of a fuel pebble located at the center of the core. The hottest pebble produces 3.77kW due to a peak to average axial peaking factor of 1.41. A different fuel design employing different sized TRISO particles or different packing fractions may change the effective thermal conductivity across the fuel layer to greater conductivity values of 15 W/m-K, thus reducing the maximum fuel temperature achieved in the fuel layer to 800-900 °C range. Likewise, the annular core design has lower pebble powers and temperatures. Minimizing the fuel temperature is highly desirable in order to reduce the peak coolant temperature during an Anticipated Transient Without Scram (ATWS) where the core is shut down due to negative reactivity feedback alone.

Assuming the fuel pebble design presented earlier in the chapter, there is a thermal margin of 630 °C until fuel could fail. At high temperature levels, pebble fuel fails due to many mechanisms that are discussed by Sterbentz [3] but failure primarily due to thermal stress which cause cracking of the sphere and leads to fission product release.

3.6 SUMMARY

The components of the core in addition to the primary system plant components are designs that are well defined in terms of its geometry and materials. The behavior of the nuclear core during transients requires the precise definition of the initiating events and boundary conditions to simulate secondary and sub-system plant components. The safety assessment of the core during transients is subject the margins of safety set by thermal and mechanical limits of the reactor constituents.

3.7 REFERENCES

[1] P. F. Peterson, et al., *Design, analysis and development of the modular PB-AHTR.* Proceedings of ICAPP ’08, Anaheim, CA, June (2008)

[2] H. J. Lim, P. F. Peterson *Conceptual design of the intermediate heat exchanger (IHX) for the PB-AHTR* UC Berkeley Report UCBTH-09-005, May 20 (2009)

[3] J. W. Sterbentz et. al., *Reactor physics parametric and depletion studies in support of TRISO particle fuel specification for the next generation nuclear plant.* Idaho National Engineering and Environmental Laboratory, September (2004)

[4] D. F. Williams, L. M. Toth, K. T. Clarno *Assesment of candidate molten salt coolants for the advanced high temperature reactor (AHTR)* Oak Ridge National Laboratory ORNL/TM-2006/12, March (2006)

[5] M. Fratoni *Development and applications of methodologies for the neutronic design of the pebble bed advanced high temperature reactor (PB-AHTR)* Ph.D. Dissertation, UC Berkeley (2008)

[6] A. Griveau *Modeling and Transient Analysis for the Pebble Bed Advanced High Temperature Reactor (PB-AHTR)* M.S. Project Report UCBTH-07-001 (2007)

[7] E. D. Blandford, P. F. Peterson *A novel buoyantly-driven shutdown rod design for passive reactivity control of the PB-AHTR.* 4th International Topical Meeting on High Temperature Reactor Technology (HTR-2008), Washington, DC (2008)

[8] D. Holcomb., *Personal communication* Oak Ridge National Laboratory, March (2011)

[9] N. Kohtz, H. Haque., *Meeting fuel temperature limits in an HTR-Module Reactor during depressurized core heat-up* Nuclear Engineering and Design 137 (1992) 115-124

[10] Idaho National Laboratory *NGNP High Temperature Materials White Paper* Next Generation Nuclear Plant Project INL/EXT-09-17187, June (2010)

[11] R. H. Guymon., *MSRE Systems and Components Performance.* Oak Ridge National Laboratory, ORNL-TM-3039 June (1973)

4. DESCRIPTION OF THE PB-AHTR PLANT SUB-SYSTEM DESIGNS

4.1 INTERMEDIATE SYSTEM

The reference PB-AHTR design uses a multiple reheat Brayton cycle for power conversion as heat transfers from the intermediate salt loop to the helium power conversion fluid. This system was chosen in order to achieve a high power conversion efficiency, as high as 46%. The information in this section is obtained from Caron et al. [1] and Peterson and Zhao [2] in addition to the input from Peterson [3] over the course of the research project. The picture below depicts the components of the power conversion system and the configuration with respect to the reactor core.

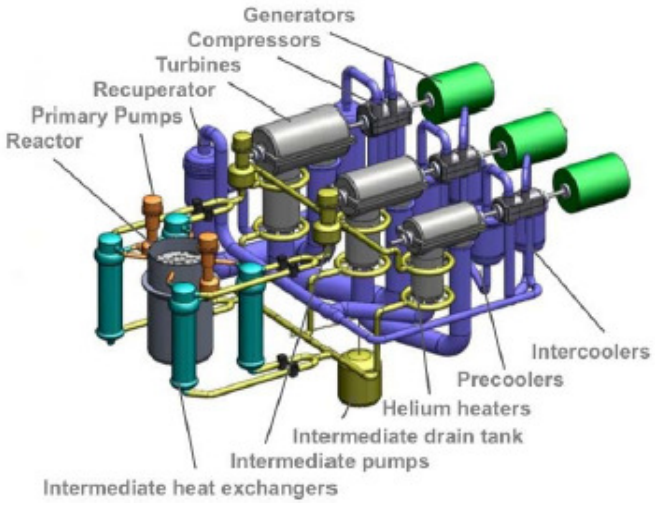

Fig. 4-1 Intermediate system and components

4.1.1 Salt to Helium heat exchanger

Design Challenges

The salt to helium heat exchanger design remains in schematic form. The design of this heat exchanger is challenging due to the 1) high pressure differential between the salt and helium loop and 2) high stress levels caused by large temperature drop on the heat exchanger. Figure 4-2 shows a schematic of the salt to helium heat exchanger and its configuration with respect to the power conversion system. The working salt in this heat exchanger is flinak (LiF-NaK-KF) and the power conversion system gas is helium.

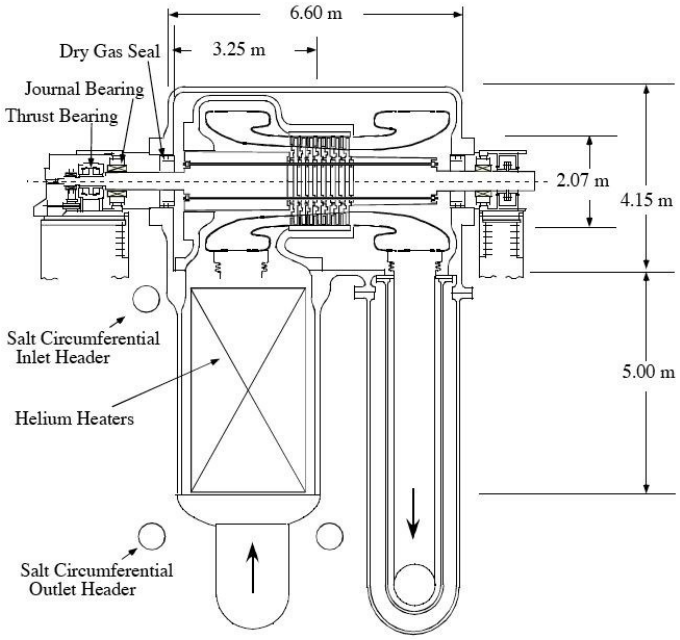

Fig. 4-2 Salt to helium heat exchanger and turbine location

4.1.2 Power conversion system

The overall concept is based on the Mitsubishi Heavy Industries power conversion system designed for the PBMR, which consists on conventional horizontal turbine and compressor, using dry gas seals and oil-lubricated bearings, shown in figure 4-3.

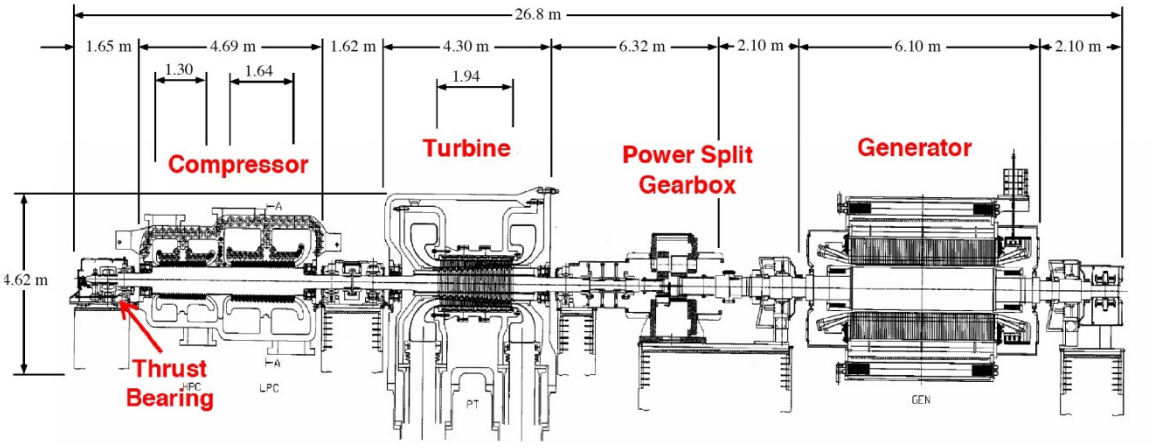

Fig. 4-3 Power conversion system schematic

4.1.3 Intermediate loop

The piping components which connect the power conversion system and the salt-to-helium heat exchanger components have not been designed. A detailed design is not very important for the purposes of the transient analysis, but the design of the overall system is important to understand the realistic transient analysis event breakdown, especially the loss of heat sink. Some assumptions can be made with regards to this transient, based on a parallel with light water reactor power conversion systems, however not with a strong basis. As it will be discussed in section 6.5.3, the approach assumed is the instantaneous total heat sink loss, as a conservative limit for how rapidly loss of heat sink occurs.

4.2 SAFETY SYSTEM DESIGN BASIS

The design basis for the safety system requires the implementation of the principle of passive safety. In order to fulfill this, the safety system employed by the PB-AHTR is passive and is designed to provide sufficient cooling capacity in addition to the primary heat removal system

DRACS Overview

The Direct Reactor Auxiliary Cooling System (DRACS) is a system consisting of various components designed to remove heat passively by means of natural circulation. The DRACS Heat Exchanger (DHX) is located above the core, where a bypass flow of the primary salt is diverted from the core inlet plenum is allowed to pass through the shell side of this heat exchanger. This heat exchanger is conceptualized as a single pass, disk and doughnut baffled, shell and tube type, similar in design to the IHX described in the section 3.2.1, but smaller in size and in the number of tubes. The flow diverted from the core inlet plenum is regulated by a component called a fluidic diode. The fluidic diode, analogous to an electric diode, is a device designed to impose a strong blockage for flows in the high resistance direction, while allowing almost free flow when flows occur in the opposite, low resistance direction. Heat absorbed by the DHX is rejected by the Natural Draft Heat Exchanger (NDHX) to the ambient by allowing air flow on the shell side at a rate controlled by intake dampers that are automated to open upon LOHS and loss of normal shutdown cooling, and can also be manually operated. These dampers are needed to control heat loss, since overcooling transients are also possible. Heat is convected by liquid salt in the DRACS loop which connects the outlet of the DHX to the inlet of the NDHX and vice versa, thus closing the passive loop which is entirely driven by buoyancy forces. Figure 4-4 depicts the DRACS system in relationship to the reactor core.

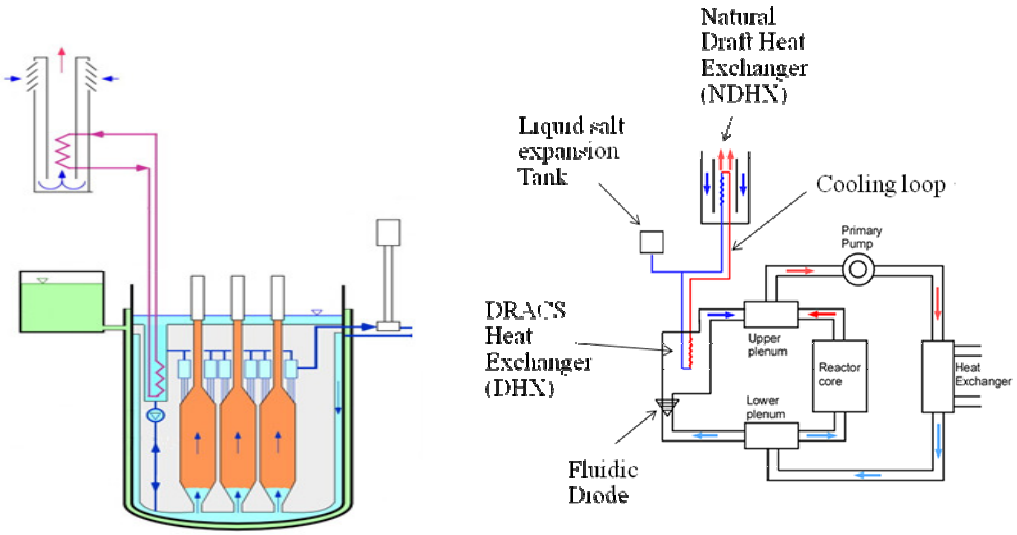

Fig. 4-4 PB-AHTR Passive safety system frontal diagram (left) and DRACS component scheme (right)

Fluids and Materials

For the reference design studied here, the working fluid for the DRACS system is LiF-NaF-KF salt, also referred as flinak. The overall heat transfer characteristics of this salt are very similar to flibe, the primary coolant, except that the cost of this salt is more accessible, thus preferred for heat transfer fluids where neutronic absorption is not of great concern. The melting temperature is very similar for both salts, therefore low temperatures margins to avoid freezing are essentially the same. Flinak and flibe do not show considerable corrosion rates, thus are not of concern in terms of potential chemical attack.

The wall materials for the DRACS heat exchangers and piping are envisioned as 316 stainless steel or Alloy 800H given that this material is code qualified for high temperature applications. However, the DRACS loop operates in lower temperatures than the core and may reach lower maximum temperatures during transient operation as well, thus potentially enabling the consideration of other metallic materials.

Finally, a factor of consideration in the material selection for the NDHX heat exchanger is the corrosion which may result from the interaction of the NDHX surface and water vapor among other air constituents at high temperatures. For these reason, the material evaluation is another aspect which needs to be considered in the detailed design of the DRACS system.

This section of the report offers a conceptual description of the design of the DRACS system, given that the actual design, optimization, verification and validation of the analysis, are subjects of this dissertation. The actual design process is detailed in section 5.3 DRACS Design, along with a description of the methodology.

4.2.1 DHX

The design basis for the DHX considers performance during the most challenging transient scenario. In this sense, most important transient is the Loss of Forced Circulation (LOFC) transient, where forced primary cooling stops, leaving natural circulation as the cooling mechanism. This section establishes the design basis for this component and considers the transient analysis for the purposes of setting the design basis. More detailed information on the transient analysis is presented in section 6.5.

DHX Heat Load Design Basis

The heat load capacity was selected to be 2% of the reactor power for various reasons. The logic established follows the principle that this set of heat exchangers are sought to be employed during severe LOFC transients only. The most severe LOFC transient assumes negligible heat loss due to natural circulation through the IHX. Irrespective of whether the reactor is scrammed or not, this transient will generate sufficient negative thermal reactivity feedback to effectively scram the reactor and switch the power mode to decay heat production. In this stage, the decay heat curve predicts a decaying heating curve to drop to about 2% of power at around 1000 sec (~15min) later and slowly dropping thereafter until it reaches 0.2% of power at around 1.5 weeks later. Following this logic, the heat generated during the first 1000 seconds will be in excess of heat removal capacity by the DHX. This excess will heat up the primary core cooling system components until the 2% power level is reached by the decay heat curve. The cooling system average temperatures will drop afterwards.

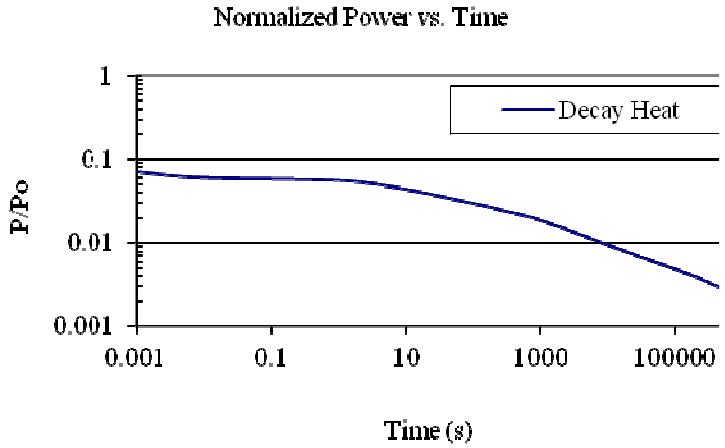

Fig. 4-5 Typical LWR core decay heat power history referenced form Schrock [9]

DHX Heat Load during Normal Reactor Operation

During full power steady state reactor operation, the DHX is passively removing heat; however, this amount of heat is controlled by two factors. First, the fluidic diode limits the amount of primary fluid passing through the shell side of the DHX, due to the high pressure drop across the

diode. Second, the amount of air flow rate allowed through the NDHX regulates heat release to the environment. Low air flow rates cause small coolant temperature change across the DHX Therefore, to reduce the rate of heat loss from the DRACS under normal power operation and under overcooling transients, the air flow rate at the NDHX chimney intake is controlled with inlet dampers to reduce the parasitic heat losses through the DRACS.

Geometric Design

The DHX is identical in design to the IHX, except they are smaller both in height and shell radius. This heat exchanger employs the same tube diameter as the IHX based on manufacturing and analysis considerations, and it is similarly held together by disk and doughnut baffles as shown in figure 4-6. The reader is referred to section 3.2.1for more details of the DHX geometry.

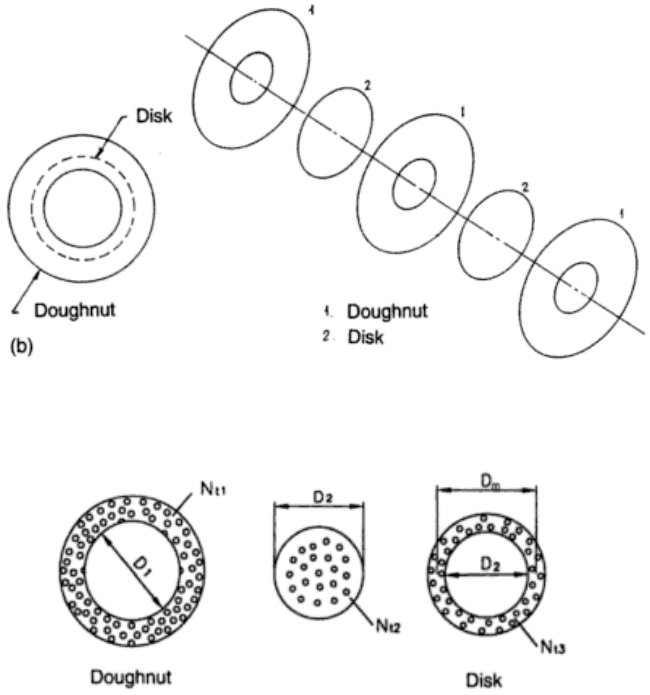

Fig. 4-6 Disk and doughnut heat exchanger internal component diagram illustrated by Kuppan [6]

Opposite to the IHX, the DHX carries primary, hot salt fluid through the shell side and the DRACS salt through the tube side of the heat exchanger. During steady-state full power, this heat exchanger transfers heat in parallel flow, but turns into a countercurrent heat exchanger during the LOFC transient, immediately after flow reversal is established through the DHX.

Both, the DHX and the IHX designs were developed employing the code PRIMEX in a study performed by Lim [10]. This code is relatively simple to use, since the input deck consists of nine input parameters, essentially, the inlet/outlet temperatures in addition to maximum outer radius and pressure losses. A parametric study was performed to obtain the smallest heat

exchanger design for the DHX under the expected operating conditions, since this heat exchanger is specially limited in space as it is located within the reactor vessel. The solution of the thermal-hydraulic problem was obtained after an algorithm was set up to run the executable multiple times and obtain a satisfactory design.

PRIMEX Overview

The design of the salt-to-salt heat exchangers, namely, the IHX and DHX requires the usage of a dedicated code which can predict specific geometric information for the construction and expected performance. The code PRIMEX was chosen for this application in the design of the PB-AHTR.

The Primary Heat Exchanger code PRIMEX was developed in an effort led by Bettis et. al. [11] at Oak Ridge National Laboratory in 1971 as part of the Molten Salt Breeder Reactor design effort, specifically, for the design of the primary heat exchanger for this reactor. The code then was reconstructed for PC usage in South Korea as part of the development for advanced molten salt reactor designs in their research institutions [10]. The primary benefit of the PRIMEX code is that the source code is available for manipulation.

The code PRIMEX was developed to analyze a tube and shell, counter flow single pass, disk and doughnut baffled heat exchanger embedded along the inner pipe at the center of the heat exchanger which carries the tube side fluid out of the heat exchanger with tubes arranged with identical circumferential and radial pitch and bent tubes in the upper part of the heat exchangers, identical in design to the IHX as presented in section 3.2.1. The code has a predetermined input file format which requires inlet and outlet temperatures for the two salts entering the heat exchanger. In addition, the code requires an upper bound on the allowed pressure drop for the tube and shell side, as well as the minimum required inner radius and the maximum allowed outer shell radius. The thermophysical properties of both fluids and the metallic structure of the exchanger are input into the source code as a function of temperature, therefore the flexibility to vary the constituents exists. Finally, there are a number of parameters that are fixed in the current version of the source code, but can be modified to evaluate other options. These parameters include the tube diameter and the tube pitch among others.

The code outputs detailed geometric information of the heat exchanger, the number of tubes and the total surface area for heat transfer. The code also outputs performance evaluation parameters, such as the overall heat load, the average heat transfer coefficients, average fluid velocities, average pressure drops, etc. Bettis et al. [11] list in detail the closure relations employed by the code for heat transfer and friction losses in addition to the basis for the geometric calculations.

4.2.2 Fluidic diode

The design of the fluidic diode is in current development at UC Berkeley in an effort led by Burnett *et al*. [5]. For this particular application, the fluidic diode design with the greatest

diodicity possible is desired. Diodicity is the ratio of form loss in the high resistance flow direction to the form loss in the low resistance direction. This requirement is chosen to minimize the bypass flow through the DHX during power operation, while minimizing flow resistance and the temperature drop during natural circulation removal of decay heat.

Geometry

This diode is the least developed element of the DRACS design and is therefore the most flexible component currently. There are several designs available but only two designs will be presented for conceptual purposes. First, the German fluidic diode design presented by Rothfuss [4], shown in Figure 4-7, consists of a mechanism that induces incoming flow in the high-resistance direction into a vortex and maintains the rotational flow as the vortex travels through the diode. To accomplish this, the diode employs guide blades as shown in the picture. In the low-resistance direction, flow travels linearly around the guide blades and exits the diode without having rotational flow induced. Similarly, the vortex diode design from NuVision Engineering [8] induces rotational flow as the fluid enters the reverse direction, but travels straight through in the forward direction.

In the case of the PB-AHTR other factors that must be considered in the design of the fluidic diode are the compatibility with high temperature fluids, the limited room available in the cavity located on the outer radius and the high diodicity required. The material chosen for the diode is likely to be similar to other components which come in contact with the primary coolant.

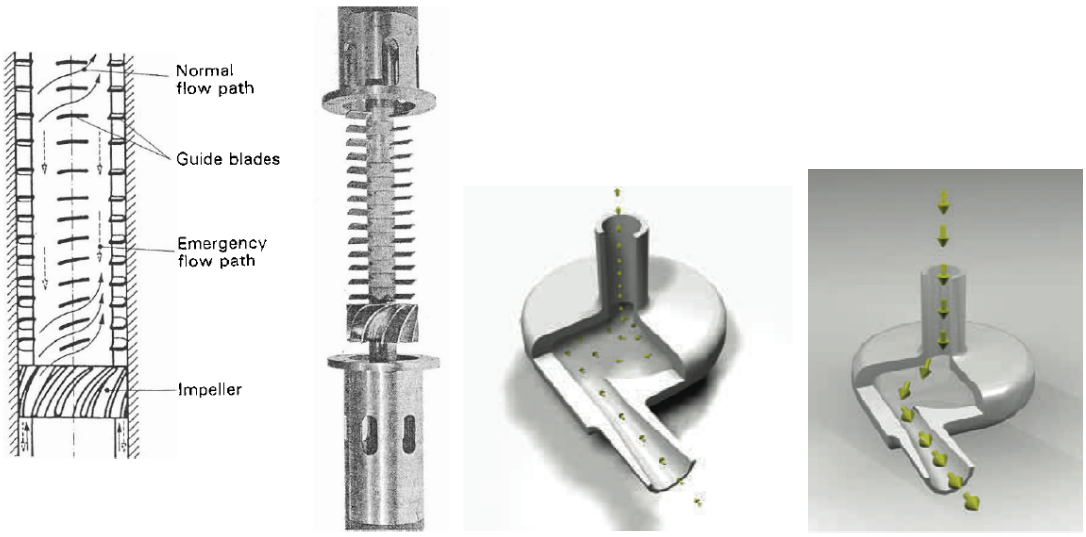

Fig. 4-7 Two types of fluidic diode available for investigation: Flow rectifier type (left) and vortex-diode type (right)

4.2.3 NDHX

Geometry

The Natural Draft Heat Exchanger (NDHX) consists of a bundle of helical tubes that transfers heat in a single pass, counter flow fluid configuration and is oriented vertically, located above the reactor core, as shown in figure 4-8. On the tube side, hot salt flows downward due to natural circulation inside the DRACS loop. On the shell side, air convection removes heat flowing upwards through the chimney, in cross flow through the helical tubes. At the base of the chimney, manual air intake dampers are controlled to reduce the amount of heat lost to the environment, thus improving the overall thermodynamic efficiency of the plant and providing control of the heat removal rate during overcooling transients. This damper, in case of transients where the safety removal heat system is needed, can be automatically or manually opened with small energy input, thus adhering to the principle of passive safety.

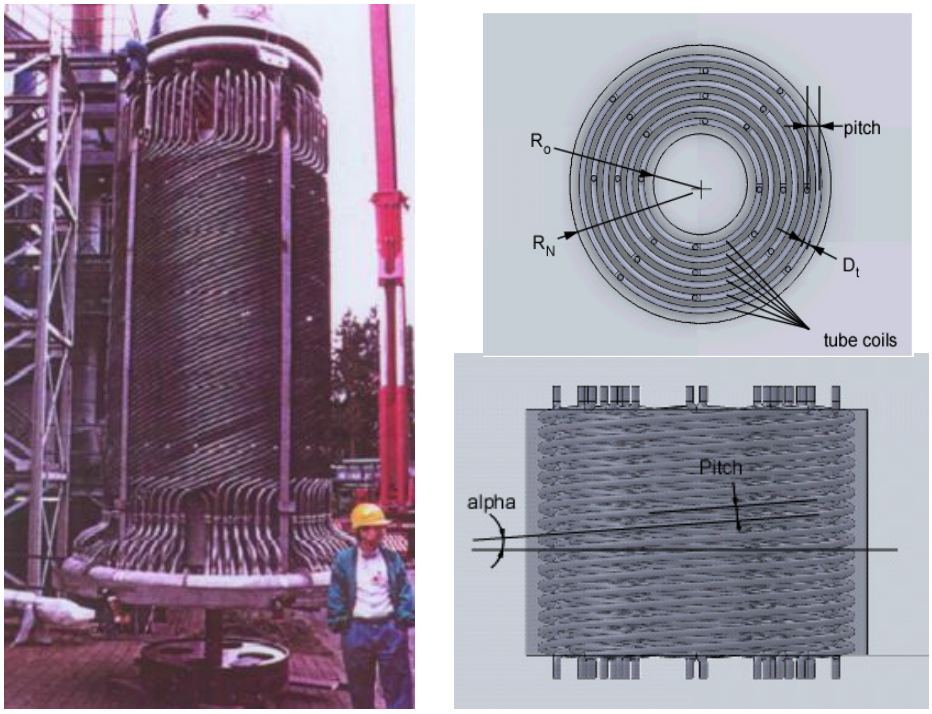

Fig. 4-8 Helical heat exchanger constructed for the European Breeder Reactor (left) served as the basis for the current PB-AHTR design. A diagram with key measurements for the PB-AHTR design (right)

A significant fraction of the heat being removed from the NDHX is transferred by thermal radiation between the hot tube surfaces and other surfaces. The amount of heat lost by this component through radiation can be significant, and is beneficial since it enhances overall heat transfer at high temperatures, and reduces heat transfer at lower temperatures, providing a stable heat transfer process.

Air flow through the NDHX is constrained in cylindrical structures composed of inner, middle and outer walls. Cold air coming in from the outside ambient flows downward between the outer and middle walls, then at the bottom flows towards the inner region, passing underneath the middle wall, and flows upwards in between the middle and inner wall, where air heats up as it removes heat from the surfaces of the helical tubes. Figure 4-4 shows a frontal cross section cut that displays the chimney geometry with respect to the helical tube bundle.

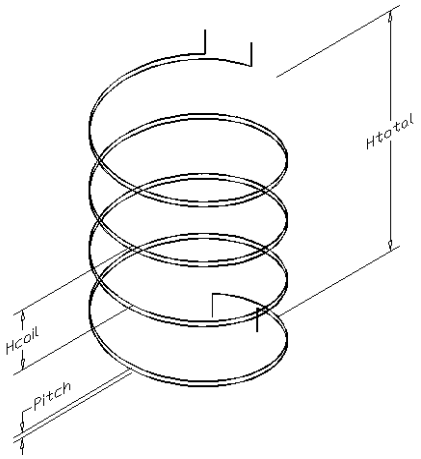

Fig. 4-9 Two helical tubes isolated in the heat exchanger structure and nomenclature employed in the geometric design

Each helical shaped tube forms a cylinder expanding along the main axis with an even tube separation pitch between each tube. Other helical shaped tubes form cylinders as well, however with different radiuses. The radius differences are approximately equal to the helical tube pitch such that a square tube lattice is formed; however, this is not quite the case, given that each layer of tube helixes are formed with inverted angles of attack in every other layer in order to eliminate the induction of rotational flow in air as it travels through the helical tubes. This geometry is illustrated in Figures 4-8 and 4-9.

Desired Performance

The NDHX is designed to reject heat to buoyant-driven air convection. The heat transfer coefficients on the air side are low, thus requiring large surface areas for effective cooling. The desired performance goal is to remove the required heat load employing the smallest structure possible. Also, it is desirable that the thermal inertia from the metallic structures can respond quickly and absorb excess heat effectively when the passive air convection is limited and is slow in inducing higher buoyant flow rate of the DRACS salt.

4.2.4 Salt loop

The numerous tube-side flows exiting the DHX all converge into an outlet plenum, then are collected and transported through a single pipe to the NDHX inlet plenum. The inlet plenum then

distributes the flow into each helical tube for heat rejection. Similarly, the flow exiting the NDHX is transported back to the DHX through a single pipe and connects to the DHX central tube.

Flow inside the DRACS coolant loop occurs purely due to natural circulation. Based on this consideration, it is important to minimize pressure drop due to friction in the loop, therefore reducing the length and maximizing the flow diameter. The diameter of the cooling loop is the parameter of interest.

4.2.5 Expansion tank

An expansion tank is connected to each DRACS cooling loop and it is designed to allow the thermal expansion or contraction of the fluid in the loop due to temperature changes without causing mechanical stress in the cooling loop. The expansion tank will be designed to have sufficient reserve coolant inventory to maintain the loop always filled with salt and sufficient room for expansion under the greatest envisioned temperature. The location of the tank with respect to the loop has not been defined yet, but likely to be located at the top of the loop and be designed to be heated by flow through the DRACS loop to prevent freezing.

4.2.6 Air flow chimney annulus

The chimney of the DRACS is designed to constrain and guide the fluid flow into the NDHX. It is desired to maintain the concrete external event structure of the chimney at low temperatures; therefore, ambient air that comes into the inlets at the top of the chimney flows down in an annulus, while the heated air flows up through an insulated duct in the center of the chimney. Since radiation heat transfer is important in this particular component, the heat shields must also consider this heat transfer mechanism. The chimney also requires that local air mixing between incoming cold air and exiting hot air does not occur. The detailed design needs to take these considerations into account.

4.3 OTHER CONCEPTUAL ASPECTS OF PLANT DESIGN

4.3.1 IHX piping

The specific size and layout of the piping system which connects the IHX to the reactor core inlet and outlet plenums are assumed to be simple pipes which maintain a constant flow area as they extend to connect the components and the primary pumps. The detailed configuration is needed in order to estimate the precise pressure drop due to form and friction as the fluid travels through the intermediate loop. The detailed design is of special importance for the transient analysis; in particular, for the events where the primary forced flow is lost and natural circulation flow is enabled. The time scale for the natural circulation onset is sensitive to the friction losses along the piping. For the purposes of this study, a constant flow area is assumed throughout the piping.

4.3.2 Active control drive system

While the passive buoyant control system of the reactor has been developed with fair detail, to the level of estimating the response delay and the insertion speed as discussed in section 3.4.1, the design for the active reactor control system has not been developed, however, it is expected to be capable of rapidly inserting shutdown elements. The reactivity control elements used for start up, load following, and normal shutdown are expected to have sufficiently slow response such that transients as LOFC will result in a reactor scram, and forced insertion of the shutdown elements. The reactivity worth of the shutdown elements are required to bring k_{eff} to below 0.95 and the corresponding reactivity worth was predicted by Fratoni [7]. In general, the insertion time is assumed to be 1 second, as this is standard for the electro-mechanical insertion of pressurized water reactor shutdown rods.

4.3.3 Plant component location and elevations: mechanical design constrains

Abbreb.	Length (m)
L_{AC}	2.2
L_{CHI}	20.0*
L_{CL}	5.5
L_{CLIL}	0.5
L_{D}	9.118
L_{DD}	2.912
L_{DHX}	2.6
L_{DIL}	0.5
L_{FDL}	5.05
L_{HLD}	0.5
L_{HLII}	1.0
L_{HLN}	1.0
L_{HLP}	4.5
L_{IHX}	7.33
L_{IL}	0.5
L_{ILD}	1.0
L_{ISD}	0.5
L_{LR}	1.85
L_{NDHX}	3.5*
L_{P}	1.0
L_{LP}	4.0
L_{LPH}	0.7
L_{R}	4.0
L_{RH}	1.5
L_{TPH}	0.7
L_{UP}	4.0
L_{UPH}	0.1
L_{UR}	1.068
L_{URH}	0.618
L_{VLL}	8.0*

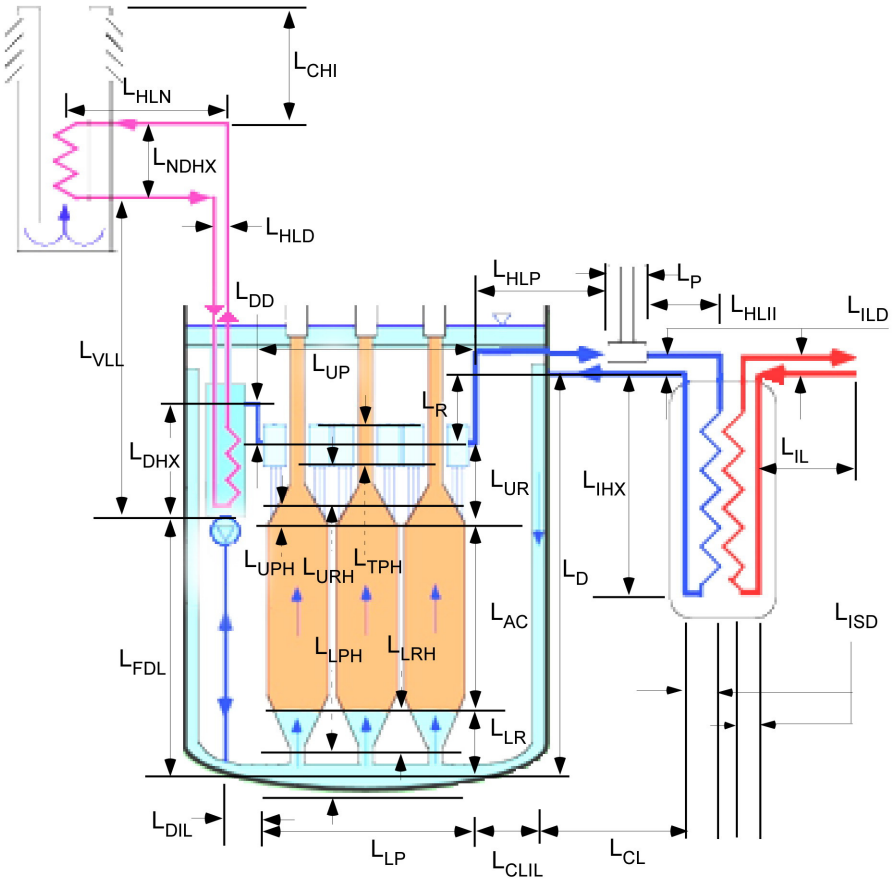

Fig. 4-10 Length diagram for plant component location and relative vertical height

Figure 4-10 shows the plant diagram and the relative heights. The quantities marked with a star are quantities which are subject of study in this investigation. The plant component placement relative to the reactor is based on building availability and existing plant component layout as discussed in [1]. The limiting parameters that are relevant for the NDHX design study are the available height difference between the NDHX and the DHX, as well as the available room to place the DHX inside the reactor cavity and the NDHX chimney, originating on the reactor building rooftop. Figure 4-11 shows the partial elevation view of the reactor building.

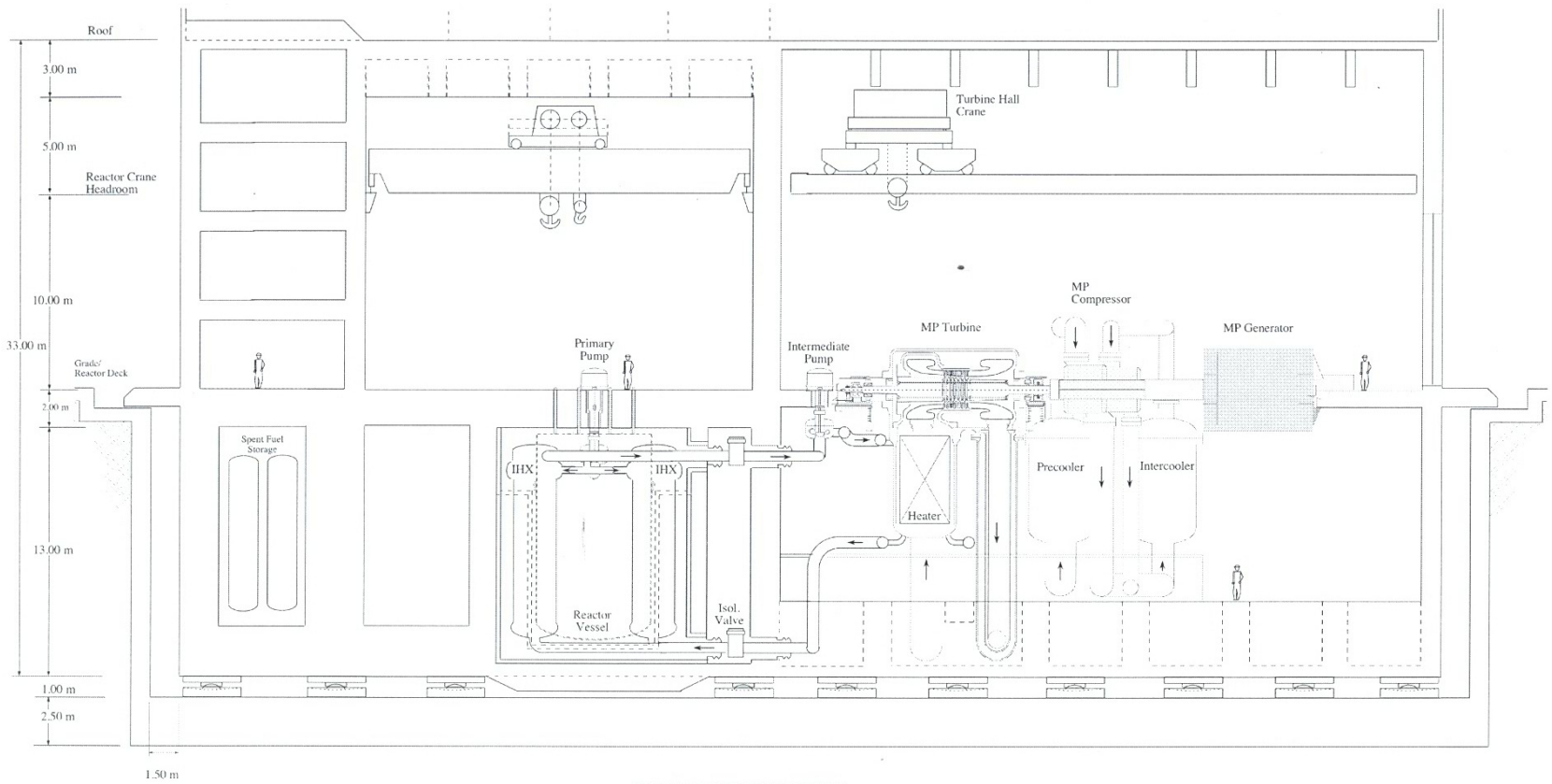

ELEVATION VIEW

Fig. 4-11 Reactor building elevation view

4.4 SUMMARY

The design of the secondary and sub-system components of the PB-AHTR are largely in a conceptual phase, while certain few components of the PB-AHTR have a well-established design basis, which allow its representation with fidelity and preciseness. Overall, sufficient information exists to effectively represent these components as a whole in the nuclear power plant model. In order to model parts and components not completely developed, simplifications and assumptions are required to model the reactor system and provide with boundary conditions for separate component analysis.

4.5 REFERENCES

[1] D. Caron, et. al., *A Modular Pebble-Bed Advanced High Temperature Reactor," NE-170 Senior Design Project, UC Berkeley Thermal Hydraulics Laboratory*. UCBTH-08-001, May (2008)

[2] P. F. Peterson, H. Zhao, *Passive decay heat removal for the advanced high temperature reactor.* UCBTH-03-005, February (2004)

[3] P. F. Peterson *Personal communication.* August 2010

[4] H. Rothfuss and F. Vogt, *Reactor Vessel Technology*. Nuclear Technology, 78 (1987) 245-246

[5] R. Burnett, D. Caso, J. Tang, P. F. Peterson *Fluidic diode development and optimization.* UCBTH-10-002, May (2010)

[6] T. Kuppan, *Heat Exchanger Handbook*. Eastern Hemisphere Distribution (2000)

[7] M. Fratoni *Development and applications of methodologies for the neutronic design of the pebble bed advanced high temperature reactor (PB-AHTR)* Ph.D. Dissertation, UC Berkeley (2008)

[8] NuVision Engineering *Vortex diode pumps: no moving part pumping systems.* Product profile information sheet, http://www.nuvisioneng.com/uploads/VortexDiodeProfile.pdf

[9] V. E. Schrock, *A Revised ANS Standard for decay heat from fission products.* Nucl. Technol. 46:323, (1979)

[10] H. J. Lim, P. F. Peterson *Conceptual design of the intermediate heat exchanger (IHX) for the PB-AHTR* UC Berkeley Report UCBTH-09-005, May 20 (2009)

[11] C. E. Bettis et. al., *Computer programs for MSBR heat exchangers.* Oak Ridge National Laboratory ORNL/TM-2815, June (1971)

5. DRACS DESIGN STUDY

This chapter explains the analysis rationale and methodology starting from the concept presented in the previous chapter and continues with the analysis procedure. The final section presents the point design obtained product of this analysis.

5.1 PROBLEM FORMULATION

The design of the DRACS system and its components is especially difficult since there aren't any readily available tools for the study of natural circulation driven air to natural circulation driven salt heat exchangers, let alone tools that have some degree of verification and validation for analysis reliability.

Based on the core and primary cooling system detailed design information, in addition to the concept presented in previous chapters, the task is to design a DRACS system which satisfies the goal to remove excess heat in case of transients, while satisfying size constraints and implementing general design guidelines learned from the design process of high temperature liquid salt systems.

The primary difficulty of this problem is to study all three natural circulation loops simultaneously. Figure 5-1 shows the air, salt cooling and core-DHX salt loops, when the reactor is operating under passive decay heat removal mode. Another difficulty is the lack of a reference design to start the study with. Finally, the study requires the implementation of accurate thermophysical properties for multiple fluids, as well as friction and heat transfer correlations for multiple geometries for multiple flow regimes.

5.2 PROBLEM GOVERNING EQUATIONS - SEPARATE PHENOMENA

Multidimensional Heat transfer in Heat Exchangers

The DRACS system is characterized for multidimensional heat transfer phenomena, occurring at the DHX and NDHX components, with greater extent on the shell side. In the case of the DHX, the disk-and-doughnut baffles constrain the flow of the shell side fluid to a combination of cross flow and parallel flow. The resulting convective heat transfer process is different in the two limiting cases (cross versus parallel flow) and is clearly dependent on the geometry. In the case of the NDHX, buoyant air flow perpendicular to the bank of tubes removes heat at different rates depending on the azimuthal location along the pipe circumference as discussed by Zukauskas [1]. Similarly, heat transfer rates are different for the rows of tubes downstream of the air flow compared to the first rows of tubes due to the temperature difference between these two fluids. This temperature difference is dependent on the axial location along the heat exchanger.

Multidimensional Fluid flow in Heat Exchangers

Similarly, the fluid flow is strongly dependent on the geometry of the heat exchangers, especially on the external flow. The fluid mechanics of molten salt are strongly affected by the temperature changes the fluid undergoes, since the viscosity of liquid salts changes by a factor of 5 over a change of 100 degrees Celsius as the fluid heats up or cools down. This may easily cause a change on the flow regime and thus strongly affect the pressure drop of the fluid flow through the components. Fluid flow is also difficult to predict on the inlet and outlet plenums as well as through the tube sheets of the heat exchangers.

The phenomena explained above are governed by the equations of conservation of mass, momentum and energy, which are presented below in their vector forms.

$$\frac{\partial(\rho)}{\partial t} = -\nabla(\rho\vec{v}) \tag{5.1}$$

$$\frac{\partial(\rho\vec{v})}{\partial t} = -\nabla p - [\nabla \cdot \rho\vec{v}\vec{v}] - [\nabla \cdot \underline{\underline{\tau}}] + \rho\vec{g} \tag{5.2}$$

$$\frac{\partial(\rho h)}{\partial t} + \rho(\vec{v} \cdot \nabla U) = k(\nabla^2 T) - (\vec{v} \cdot \nabla p) - (\underline{\underline{\tau}} \cdot \nabla\vec{v}) + q''' \tag{5.3}$$

The equations above need be solved simultaneously and in the appropriate coordinate system given the domain of the problem. In the case of the DRACS heat exchangers, the geometry is very complex where there is transport of momentum and energy occurring simultaneously.

5.3 SOLUTION TO GOVERNING EQUATIONS

The design of the DRACS systems requires the solution of Equations 5.1-5.3. The solution of these, non-linear, coupled equations can be achieved when certain simplifications and assumptions are made. The approach is to analyze the problem with a simple tool, which offers great flexibility for modification yet include acceptable precision in the analysis.

The following are the considerations made prior to the design, which allow the simplification of the problem:

- External cross flow in heat exchangers can be treated as 1-D flow, by employing heat transfer coefficients averaged over the tube circumference, thus independent of theta θ azimuthal pipe angle relative to the direction of flow.
- Pressure drop caused by baffles in heat exchangers can be represented by an effective pressure drop coefficient. This requires that the number of baffles is set and does not

change during a parametric study, as it is the case of the DHX heat exchanger. This allows the simplification of the problem into 1-D hydrodynamic problem.

- Large temperature between the bulk and the wall, especially in the case of internal flows can be taken into account by adjusting the heat transfer coefficients as recommended by Incropera [11].

- Connecting piping between heat exchangers are assumed to have uniform area of flow for each of the three natural circulation driven loops.

The considerations mentioned above, allow Equations 5.1-5.3 to be rewritten in 1-D along a reference loop, where the loop line coordinate is l and the 1-D simplified velocity vector field v is multiplied by the mean density ρ_m and expressed in terms of the mass flux G_m for all three equations.

$$\frac{\partial \rho_m}{\partial t} = -\frac{\partial G_m}{\partial l} \tag{5.4}$$

$$\frac{\partial G_m}{\partial t} + \frac{\partial}{\partial l}\left(\frac{G_m{}^2}{\rho_m}\right) = -\frac{\partial p}{\partial l} - f\,\frac{G_m{}^2}{2D_e\rho_m} - \rho_m g\cos\theta \tag{5.5}$$

$$\rho_m\frac{\partial h_m}{\partial t} + G_m\frac{\partial h_m}{\partial l} - \frac{\partial p}{\partial t} = \frac{q^{''}P_h}{A} + \frac{G_m}{\rho_m}\left(\frac{\partial p}{\partial l} + f\,\frac{G_m{}^2}{2D_e\rho_m}\right) \tag{5.6}$$

The equations shown above, are still non-linear, and require a simultaneous solution. Continuing with the analysis, further simplifications can be made, observing the following:

- All three natural circulation loops are designed assuming steady-state operation, therefore the time derivative *d/dt* terms can be neglected.

- Two of the natural circulation loops operate with liquid coolants, which can be treated as incompressible. In addition, the segments of the loop which represent the heat exchangers or the piping connecting heat exchangers are assumed to have constant area of flow. These two assumptions allow the $d(G_m^2/\rho_m)/dt$ term to be neglected.

- There is no source of external momentum addition to any of the loops, this is a natural circulation problem for all three loops, therefore *dp/dl* integrated over all three natural circulation loops can be neglected, including the air channel, where atmospheric pressure is the same for both inlet and outlet side of the loop.

- The pressure change energy storage, compared to the enthalpy change due to heating, is negligible, therefore it is neglected in the energy equation. Similarly, the friction energy dissipation is also neglected.

Neglecting the simplified conservation of mass, the arguments above reduce the governing equations to:

$$f \frac{G_m^{\ 2}}{2 D_e \rho_m} = \rho_m g \cos\theta \tag{5.7}$$

$$G_m \frac{\partial h_m}{\partial l} = \frac{q^{"} P_h}{A} \tag{5.8}$$

In the case of natural circulation where the working fluid is gaseous, the incompressible assumption is no longer valid, therefore the conservation of momentum equation becomes:

$$\frac{d}{dl}\left(\frac{G_m^{\ 2}}{\rho_m} \right) + f \frac{G_m^{\ 2}}{2 D_e \rho_m} = \rho_m g \cos\theta \tag{5.9}$$

Although the amount of energy dissipated in density changes along the loop for gases is greater than it is for liquid fluids, it is still much lesser than the overall enthalpy changes due to heating, and therefore the simplified conservation of energy equation remains the same as written in equation (5.8).

Equations (5.7) and (5.9) shown above are integrated over the corresponding flow loops. The primary simplification made is to reduce all eight DRACS loop into a single equivalent system, which behaves identically as all eight loops together. The following diagram represents the simplified loop schematic for the DRACS safety system presented in detail in figure 4.4 and discussed in section 4.2.

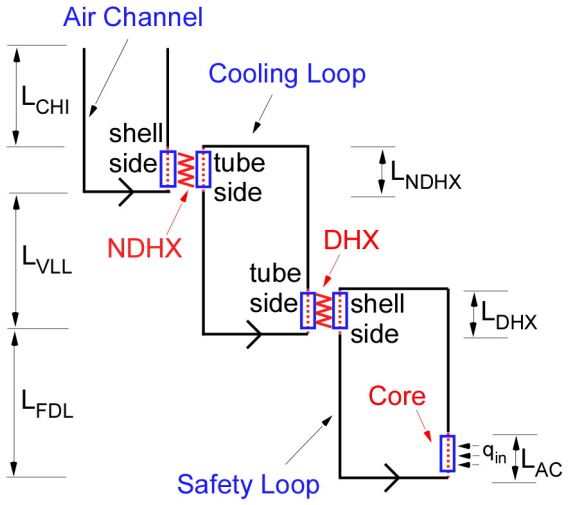

Fig. 5-1 Diagram and nomenclature for DRACS system cooling loops

It can be observed that both of the loops containing liquid fluid, namely, the safety loop and the cooling loop have similar geometry, therefore similar solution strategy can be applied when integrating over those loops. However, the air channel is composed of a heat source alone and requires different treatment. Integrating the friction term from equation (5.7) over the salt loops:

$$\oint_{safety-loop} f\frac{G_m^{\,2}}{2D_e\rho_m} = \int_{L_{AC}} f\frac{G_m^{\,2}}{2D_e\rho_m} + \int_{L_{DHX}} f\frac{G_m^{\,2}}{2D_e\rho_m} + \int_{Lpiping} f\frac{G_m^{\,2}}{2D_e\rho_m} \tag{5.10}$$

$$\oint_{cooling-loop} f\frac{G_m^{\,2}}{2D_e\rho_m} = \int_{L_{DHX}} f\frac{G_m^{\,2}}{2D_e\rho_m} + \int_{L_{NDHX}} f\frac{G_m^{\,2}}{2D_e\rho_m} + \int_{Lpiping} f\frac{G_m^{\,2}}{2D_e\rho_m} \tag{5.11}$$

The integrals above can be evaluated explicitly, implementing correlations to calculate the friction factor coefficient f according to the proper geometry, as explained in detail in section 2.8. Each of the integrals results in a pressure drop Δp due to friction.

Similarly, the gravity term from equation (5.7) is integrated. This term however, is equal to zero when the gravity vector field is perpendicular with the flow direction. When the flow is in the same direction as gravity, the integral is a net positive quantity, is negative in the opposite direction.

$$\oint_{safety-loop} \rho g\cos\theta dl = \int_{L_{FDL}} \rho_c g dl - \int_{L_{FDL}+L_{DHX}-L_{AC}} \rho_h g dl + \int_{L_{DHX}} \rho_{(l)} g dl - \int_{L_{AC}} \rho_{(l)} g dl \tag{5.12}$$

$$\oint_{cooling-loop} \rho g \cos\theta dl = \int_{L_{VLL}} \rho_c g dl - \int_{L_{VLL}+L_{NDHX}-L_{DHX}} \rho_h g dl + \int_{L_{NDHX}} \rho_{(l)} g dl - \int_{L_{DHX}} \rho_{(l)} g dl \tag{5.13}$$

The integrals over the non heating or cooling loop segments are straightforward. The density function $\rho_{(l)}$ can be assumed as a linear variation between the hot and cold densities. Todreas and Kazimi [8] analyzed the impact of assuming a linear variation, versus an exponential variation, which is most often the case for heat exchangers, but found little effect on the overall flow rate solution. Integrating over the heating or cooling elements:

$$\int_{L_{DHX}} \rho_{(l)} g dl - \int_{L_{AC}} \rho_{(l)} g dl = \frac{\rho_c + \rho_h}{2} g L_{DHX} - \frac{\rho_c + \rho_h}{2} g L_{AC} \tag{5.14}$$

$$\int_{L_{NDHX}} \rho_{(l)} g dl - \int_{L_{DHX}} \rho_{(l)} g dl = \frac{\rho_c + \rho_h}{2} g L_{NDHX} - \frac{\rho_c + \rho_h}{2} g L_{DHX} \tag{5.15}$$

Rearranging Equations (5.12) - (5.13) and implementing (5.14) and (5.15):

$$\oint_{safety-loop} \rho g \cos\theta dl = (\rho_c - \rho_h)\left(\frac{L_{DHX} + L_{AC}}{2} + L_{FDL} - L_{AC}\right) g \tag{5.16}$$

$$\oint_{cooling-loop} \text{`} \rho g \cos\theta dl = (\rho_c - \rho_h)\left(\frac{L_{NDHX} + L_{DHX}}{2} + L_{VLL} - L_{DHX}\right) g \tag{5.17}$$

In the case of salts, the density variation can be expressed solely as a function of a temperature change, since the coolant is considered incompressible. Employing the Bousinesq approximation:

$$\rho_{(T)} = \rho_{(T_o)}\left(1 - \beta(T - T_o)\right) \tag{5.18}$$

$$\rho_c - \rho_h = \beta \rho_c \Delta T \tag{5.19}$$

Integrating the left and right hand side of the energy equation (5.8) over the safety loop:

$$\oint_{safety-loop} G_m \frac{\partial h_m}{\partial l} \partial l = G_m \int_{L_{AC}} dh_m + G_m \int_{L_{DHX}} dh_m \tag{5.20}$$

$$\oint_{safety-loop} \frac{q^{"} P_h}{A} \partial l = \int_{L_{AC}} \frac{q^{"} P_h}{A} + \int_{L_{DHX}} \frac{q^{"} P_h}{A} \tag{5.21}$$

Applying the following principle and simplification:

$$\int dh_m = \int C_p dT = \overline{C_p}\Delta T \tag{5.22}$$

$$G_m A = \dot{m} \tag{5.23}$$

Equations (5.14)-(5.17) combined together over the appropriate integration range yield the following, in addition to the assumption of constant heat flux yield the following:

$$\dot{m}\overline{C_p}\Delta T = q'' A_{HT} = q \tag{5.24}$$

Rearranging

$$\Delta T = \frac{q}{\dot{m}\overline{C_p}} \tag{5.25}$$

Equation (5.19) combined with equation (5.25) is used to solve the set of governing equations (5.7) applied to both liquid salt loops as follows:

$$\int_{L_{AC}} f \frac{G_m^{\,2}}{2D_e\rho_m} + \int_{L_{DHX}} f \frac{G_m^{\,2}}{2D_e\rho_m} + \int_{Lpiping} f \frac{G_m^{\,2}}{2D_e\rho_m} = \beta\rho_c \frac{q}{\dot{m}\overline{C_p}}\left(\frac{L_{DHX}+L_{AC}}{2} + L_{FDL} - L_{AC}\right)g \tag{5.26}$$

$$\int_{L_{DHX}} f \frac{G_m^{\,2}}{2D_e\rho_m} + \int_{L_{NDHX}} f \frac{G_m^{\,2}}{2D_e\rho_m} + \int_{Lpiping} f \frac{G_m^{\,2}}{2D_e\rho_m} = \beta\rho_c \frac{q}{\dot{m}\overline{C_p}}\left(\frac{L_{NDHX}+L_{DHX}}{2} + L_{VLL} - L_{DHX}\right)g \tag{5.27}$$

The equations above can be solved to obtain the equilibrium flow rate which results from the buoyant force as the density changes when the loop coolant heats up and cools down. A similar process can be applied for the air channel, however, there are important differences which require special treatment, in this case, due to the compressibility of the fluid, and the large density variation of the fluid during heating.

Integrating equation (5.9) over all air channel segments:

$$\int_{air-channel} \frac{d}{dl}\left(\frac{G_m^{\,2}}{\rho_m}\right)dl + \int_{air-channel} f \frac{G_m^{\,2}}{2D_e\rho_m}dl = \int_{air-channel} \rho_m g\cos\theta dl \tag{5.28}$$

The first integral takes the acceleration of the thermal expansion into account. Given that this process only occurs in the section where heating occurs, the integral is performed over the heating section only. Introducing the Ideal Gas Law:

$$\rho(T) = \frac{P_o}{\overline{R}T} \tag{5.29}$$

The Ideal Gas Law is applicable to this study, since the working gas enters and exits at temperatures far away from its saturation temperature corresponding to the ambient pressure. At the inlet temperature and pressure, air is sufficiently superheated to justify the usage of the Ideal Gas Law. If the working fluid was steam, an evaluation of the applicability would be necessary prior to the implementation. Applying the ideal gas law, in addition to the linear density profile along the air heater:

$$\int_{air-channel} \frac{d}{dl}\left(\frac{G_m^{\,2}}{\rho_m}\right)dl = \frac{G_m^{\,2}}{2\rho_c g}\left(\frac{\rho_c}{\rho_h}-1\right) \tag{5.30}$$

$$\int_{air-channel} f\frac{G_m^{\,2}}{2D_e\rho_m}dl = \int_{L_{CHI-IN}} f\frac{G_m^{\,2}}{2D_e\rho_m} + \int_{L_{NDHX}} f\frac{G_m^{\,2}}{2D_e\rho_m} + \int_{L_{CHI-OUT}} f\frac{G_m^{\,2}}{2D_e\rho_m} \tag{5.31}$$

$$\int_{L_{NDHX}} f\frac{G_m^{\,2}}{2D_e\rho_m} = \frac{G_m^{\,2}}{2\rho_c g}\frac{\rho_c}{\overline{\rho}}\int_{L_{NDHX}} f\frac{A}{A_c D_e}dl \tag{5.32}$$

The integrals in equation (5.30) can be evaluated using the relations shown in section 2.9. The integration in equation (5.31) results from implementing the ideal gas law to express the density variation during heating. The ratio A/A_c is the ratio of friction area to flow area. Kays and London [3] discusses the proper calculation of this parameter.

The right hand side integral from equation (5.28) is evaluated applying the ideal gas law as well.

$$\int_{air-channel} \rho_m g\cos\theta dl = \int_{L_{CHI-IN}} \rho_c g dl - \int_{L_{NDHX}} \rho_{(l)} g dl - \int_{L_{CHI-OUT}} \rho_h g dl \tag{5.33}$$

In order to evaluate the integral over the heater section, it is necessary to assume a linear temperature distribution. The result of the integration is the following:

$$\int_{L_{NDHX}} \rho_{(l)} g dl = \frac{P_c}{\overline{R}\Delta T}\ln\left(\frac{T_c}{T_h}\right)\int_{L_{NDHX}} g dl \tag{5.34}$$

Employing equation (5.25), and replacing equation (5.30-5.33) into the governing relation (5.28), the following equation can be used to determine the equilibrium flow rate, which balances friction and gas expansion with buoyancy in the air channel.

$$\frac{G_m^{\,2}}{2\rho_c g}\left(\frac{\rho_c}{\rho_h}-1\right) + \int_{L_{NDHX-piping}} f\frac{G_m^{\,2}}{2D_e\rho_m}dl + \frac{G_m^{\,2}}{2\rho_c g}\frac{\rho_c}{\overline{\rho}}\int_{L_{NDHX}} f\frac{A}{A_c D_e}dl =$$

$$g\rho_c(L_{CHI}+L_{NDHX}) - g\frac{P_c}{\overline{R}\dfrac{q}{\dot{m}\overline{C}_p}}\ln\left(\frac{T_c}{T_h}\right)L_{NDHX} - g\rho_h L_{CHI} \tag{5.35}$$

Expressing the densities in terms of an inlet reference temperature and pressure, in addition to expressing the outlet temperature as a function of the inlet temperature as the following equation shows:

$$T_h = T_c + \frac{q}{\dot{m}\overline{\overline{C_p}}} \tag{5.36}$$

$$\rho_h = \rho(T_h) = \frac{P_o}{\overline{R}\left(T_c + \frac{q}{\dot{m}\overline{\overline{C_p}}}\right)} \tag{5.37}$$

Inserting equations (5.36) – (5.37) in (5.35)

$$\frac{G_m^{\,2}}{2\frac{P_o}{\overline{R}T_c}g}\left(\frac{T_c + \frac{q}{\dot{m}\overline{\overline{C_p}}}}{T_c} - 1\right) + \int_{L_{NDHX-piping}} f\frac{G_m^{\,2}}{2D_e\frac{P_o}{\overline{R}T_c}}dl + \frac{G_m^{\,2}}{2\frac{P_o}{\overline{R}T_c}g}\frac{T_c + \frac{q}{2\dot{m}\overline{\overline{C_p}}}}{T_c}\int_{L_{NDHX}} f\frac{A}{A_c D_e}dl =$$

$$g\frac{P_o}{\overline{R}T_c}(L_{CHI} + L_{NDHX}) - g\frac{P_c}{\overline{R}\frac{q}{\dot{m}\overline{\overline{C_p}}}}\ln\left(\frac{T_c}{T_c + \frac{q}{2\dot{m}\overline{\overline{C_p}}}}\right)L_{NDHX} - g\frac{P_o}{\overline{R}\left(T_c + \frac{q}{\dot{m}\overline{\overline{C_p}}}\right)}L_{CHI} \tag{5.38}$$

The equation above can be solved to determine an equilibrium mass flow rate ($\dot{m}$ or $G_m{\cdot}A_{flow}$) which balances the friction pressure drop (lhs) with the buoyancy lift due to the chimney effect (rhs). This solution requires the knowledge of an inlet temperature T_c, heat load q, a reference pressure P_o, in addition to the geometric characteristics of the problem.

All three natural circulation loops are tightly coupled in terms of the heat transfer phenomena. There are two heat exchangers which transfer heat generated by the core and is ultimately deposited in the air, as figure (5-1) shows. This coupling requires that the energy from one loop is transferred to the other adjacent loop, in addition, requires that the coolant temperatures are related for all loops. The equation below is the conservation of energy for heat exchangers.

$$q = UA\Delta T_{lm} \tag{5.39}$$

In the equation above, the logarithmic mean temperature difference ΔT_{lm} and the overall heat transfer coefficient U are dependent on the state of two adjacent cooling loops, which make up a heat exchanger. The equations below demonstrate this dependence:

$$\Delta T_{lm} = \frac{\left(T_{h,i} - T_{c,o}\right) - \left(T_{h,o} - T_{c,i}\right)}{\ln \dfrac{T_{h,i} - T_{c,o}}{T_{h,o} - T_{c,i}}} \tag{5.40}$$

$$\frac{1}{UA} = \frac{1}{h_i A_i} + \frac{\ln\left(\dfrac{D_i}{D_o}\right)}{2\pi k L} + \frac{1}{h_o A_o} \tag{5.41}$$

It can be inferred, that the heat transfer between loops strongly depends on the inlet and outlet temperatures of coolant within each loop, as well as the heat transfer rates as predicted by the local flow conditions.

The simultaneous solution of the problem governing equations (5.26) – (5.27) and (5.38) and the closure equation (5.39) requires the implementation of a numerical method, since these equations cannot be solved analytically as presented.

Equations (5.26) – (5.27) and (5.35) all have different *c* cold and *h* hot reference temperatures, in addition, the equations require the calculation of various geometric parameters, such as flow areas, surface areas, lengths and diameters. These equations also require the calculation of thermophysical and transport properties of the fluids and solid materials evaluated at various states. Finally, closure relations, i.e. friction and heat transfer coefficients are also needed, evaluated for multiple geometries at different flow conditions. The following section describes the numerical algorithm constructed to implement the solution of the governing equations for all natural circulation loops.

5.4 APPLICATION OF SIMPLIFIED GOVERNING EQUATIONS

A numerical code based on MATLAB was written to determine NDHX heat exchanger size which satisfies the design requirements.

Figure (5.3) is block diagram of the program developed, which implements and solves the governing equations of the problem, in addition to prepare auxiliary geometric calculations and thermophysical data for solution. The program source code is included in appendix B.

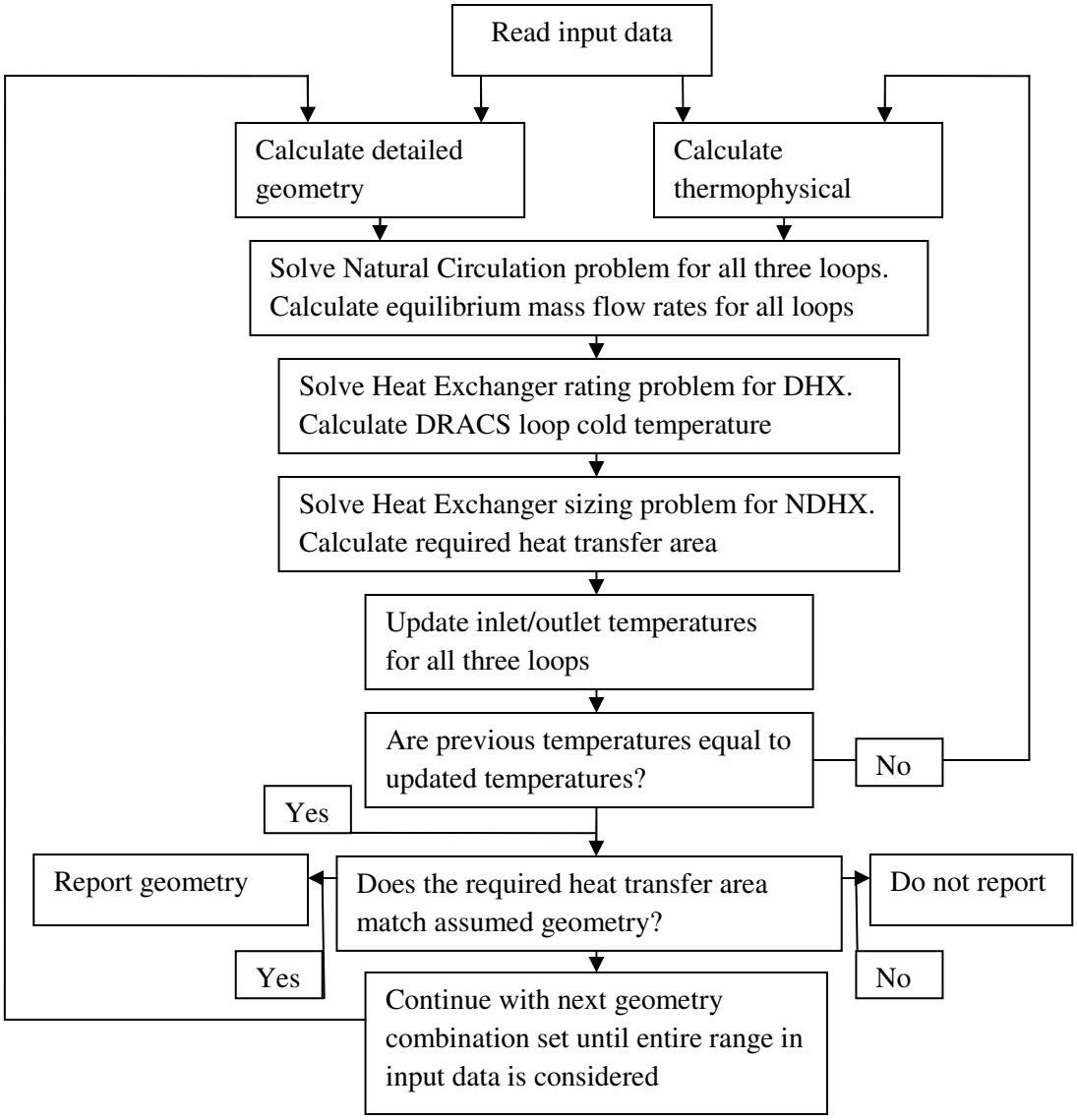

Fig. 5-2 Program block diagram

The program developed consists of five main sections: (1) input data, (2) pre-calculation, (3) problem solution, (4) solution convergence and (5) output data.

5.4.1 Reading Input Data

The input data required by the program is categorized in two groups: 1) data corresponding to the plant design, such as piping flow areas and vertical height positions, 2) specific geometry of the NDHX design, such as tube diameter, pitch, and the overall range of sizes considered for the heat exchanger design. The implementation of the data in the code is discussed in section 4.5.

The following table illustrates the data that is input into the code. Geometric variables correspond to figure 4-10 and figure 5-1.

Input data	
Plant parameters	Helical heat exchanger parameters

• Plant piping vertical height
  ○ L_{FDL}
  ○ L_{VLL}
  ○ L_{CHI}
• Plant piping flow area
  ○ A_{safety}
  ○ $A_{cooling}$
  ○ A_{chi}
• Plant component vertical height
  ○ L_{AC}
  ○ L_{DHX}
  ○ L_{NDHX}
	• Heat load
	• NDHX helical heat exchanger fixed parameters
	  ○ Ro
	  ○ Dto
	  ○ Dti
	  ○ P/D
	  ○ α
	• NDHX helical heat exchanger range parameters
	  ○ N_{lay}
	  ○ N_{win}
	• Initial guess for inlet and outlet temperature for three cooling loops
	• Coolant selection

Table 5-1 Input data variables for NDHX design algorithm

5.4.2 Performing pre-calculations

The module which performs the pre-calculation, prepares two sets of data that are necessary for the application of governing equations. The first set is the geometric properties and the second set are the thermophysical properties of the fluids.

Calculating Helical Heat Exchanger required geometric data

The geometry of the heat exchanger can be calculated based on geometric relations derived analytically for helical coil tubes. The following figures establish the parameters which describe the heat exchanger. Other values are calculated from these fundamental measurements. This section prepares the data required in order to solve the natural circulation and the heat exchanger problems.

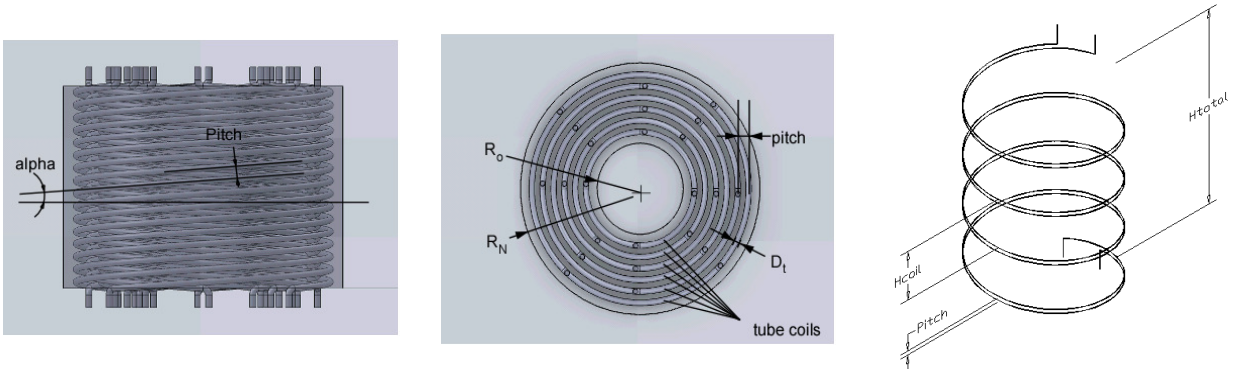

Fig. 5-3 NDHX geometric parameters for number of tubes and surface area calculation

Assuming a helical angle α corresponding to the coil which is located midway between the inner radius R_o and outer radius R_N, also, assuming a tube outer diameter D_{to}, tube inner diameter D_{ti}, tube pitch over diameter ratio P_oD, the total number of layers N_{lay} and the number of windings N_{win} one can determine the parameters listed below employing the following relations:

The number of tubes in a layer is calculated based on the tube at the center layer, with a radius of R_{cp}.

$$R_N = R_o + N_{lay} \cdot P_oD \cdot D_{to} \tag{5.42}$$

$$R_{cp} = \frac{R_o + R_N}{2} \tag{5.43}$$

A coil which spins a whole rotation at an angle α is has the following height:

$$H_{coil} = 4R_{cp} \tan(\alpha) \tag{5.44}$$

Tubes separated with a pitch to diameter ration of P_oD arranged as Figure 5.3 illustrates, in a single layer add up to the following number of tubes

$$N_{tubes-layer} = \frac{H_{coil}}{P_oD \cdot D_{to}} \frac{\sin(2\alpha)}{\sin(\alpha)} \tag{5.45}$$

The average arc length of a tube at the center layer is

$$AL_{ave} = N_{win} 2\pi \sqrt{R_{cp}^{\,2} + \frac{H_{coil}^{\,2}}{2\pi}} \tag{5.46}$$

It follows that length of the sum of all other tube layers is

$$AL_{total} = AL_{ave} \cdot N_{lay} \cdot N_{tubes-layer} \tag{5.47}$$

thus the number of tubes is

$$N_{tubes} = \frac{AL_{total}}{AL_{ave}} \tag{5.48}$$

Finally, the overall surface area is calculated from

$$HTA_o = \pi D_{to} \cdot AL_{total} \tag{5.49}$$

Calculating thermophysical properties

This module of the code calculates thermophysical properties of coolants evaluated at a proper reference temperature. For instance, certain heat transfer correlations require the evaluation of the viscosity at the tube surface and at the mean fluid temperature. This module also includes a proper method to average temperatures for its evaluation. In the case of gaseous coolant, a logarithmic averaging is performed as recommended by Kays and London [3].

The thermophysical and transport properties of the materials employed in the solution of the problem are as described in this section. The detailed expressions for the properties are included in the appendix A for fluids that are part of this study.

Air and Nitrogen

Air and nitrogen at the temperatures of operation of the NDHX behave as an ideal gas, since the saturation temperature of these gases at atmospheric pressure is much lower than the average gas temperature in the heat exchanger. The relations were obtained from Cengel and Boles [14] and White [12]. In addition, both of these fluids are also encoded in RELAP5-3D. The relations are compatible with the simpler analytical models based on observation during code runs.

Liquid Salts

The thermophysical properties of liquid salts are built in the code RELAP5-3D. These property files were added relatively recently and the source of the information is well documented by Davis [10] for all salts considered. The explicit relations employed by RELAP5-3D are also used analytically for hand calculations, since these relations were readily accessible.

Liquid Metals

In this study, other metals beyond the base liquid salt design were also considered. Thermo-physical properties of Sodium were obtained form Fink [7] in addition to those of Lead and Led-Bismuth from IAEA [6]. Additional supplementary data was obtained from Yang [4].

Solid structures

The properties pertaining to graphite H-451 and the effective TRISO fuel region were employed in the core model and the properties were obtained from Holcomb [2]. Similarly, Hastelloy N

was the metallic structure employed in the heat exchanger models and the properties of interest were obtained from Bettis et al. [13].

5.4.3 Solution

This part of the algorithm encompasses the largest part of the code. In this section, the solution of the equilibrium flow rate, expressed mathematically in equations (5.26), (5.27) and (5.38) is discussed. Additionally, the solution of the thermal coupling between the loops, show in equation (5.39) is discussed.

The first step in the algorithm is to solve for the equilibrium flow rate in all three loops. A mass flow rate is estimated assuming the largest temperature drop possible to initialize the calculation. The highest temperature assumed is the salt temperature limit of 760 ^{o}C and the minimum temperature is the salt freezing temperature of 450 ^{o}C, thus the minimum mass flow rates for both safety and cooling loops is:

$$\dot{m}_{\min} = \frac{q}{C_p \left(T_{high} - T_{low} \right)} \tag{5.50}$$

Then, starting from the minimum value from above, the mass flow rate is increased in each iteration *i* by an arbitrary addition factor.

$$\dot{m}_{i+1} = \dot{m}_i + \Delta\dot{m} \tag{5.51}$$

This iteration is continued until the corresponding governing equation (5.26-5.27, 5.38) is satisfied for each loop.

The second step in the algorithm is the solution of the inlet and outlet temperatures of the coolants of all three loops. There are two problems that are solved in this section, the *Heat Exchanger Rating* problem for the case of the DHX and the *Heat Exchanger Sizing* problem for the case of the NDHX. Both problems employ the same methodology, which is the Effectiveness-NTU Method as described by Incropera [11], however, the unknown variable is different for each problem.

Effectiveness-NTU Method

This solution methodology requires the calculation of various heat exchanger parameters in order to determine either a) required heat transfer area given expected performance b) expected performance given assumed heat transfer area. The overall strategy consists on calculating an overall heat transfer coefficient, the thermal capacities of the fluids, the effectiveness ratio and the number of thermal units (NTU). Once these values have been calculated for each heat exchanger, both sizing and rating type of problems can be solved.

Overall Heat Transfer Coefficient

In the analysis of heat exchangers, one key parameter is the overall heat transfer coefficient, which takes into account the heat transfer resistances from the both internal and external fluid flows and the conductive heat transfer resistance through the pipe wall. The effective heat transfer coefficient is calculated as reciprocal sum of the resistances mentioned. In this type of additions, the largest resistance usually dominates the overall effective resistance. The equation below shows how this calculation is performed based on the external, outer tube diameter.

$$U = \frac{1}{\left(\frac{1}{h_{out}} + \frac{1}{h_{cond}} + \frac{1}{h_{in}} \frac{D_{to}}{D_{ti}} \right)} \tag{5.52}$$

Where the resistance due to conduction across a pipe wall is:

$$\frac{1}{h_{cond}} = \frac{1}{\frac{k_{tube}}{D_{to} \cdot w_{thick}} \cdot \frac{2\, w_{thick}}{\ln\left(\frac{D_{to}}{D_{ti}} \right)}} \tag{5.53}$$

The internal and external heat transfer coefficients are calculated based on the geometry, the appropriate flow regime, the appropriate length scale and the appropriate reference temperature for thermophysical property evaluation. All correlations employed are described in section 2.3, 2.4 and 2.5. The research involving the correlation literature review demonstrated that multiple correlation authors often times employ different length scales as well as different reference temperature for thermophysical property evaluation, even when representing heat transfer in the same geometry and flow regime. For this reason, careful implementation of correlations is recommended.

Estimating outlet temperature: solving the rating problem

The solution of this type of problem is required for the DHX heat exchanger. In this configuration, the inlet temperature of the hot fluid is prescribed, and the outlet temperature of the hot fluid can be easily determined from the conservation of energy, applying the mass flow rate obtained from the solution of equation (5.26). On the cold side, the mass flow rate is determined by the solution of equation (5.27) and the temperature difference on this loop can be determined from the conservation of energy equation (5.25), however, the actual inlet or outlet temperature on the cold fluid is unknown. This section describes the solution for the inlet temperature of the cold fluid.

The rating problem requires fixed, well known heat exchanger geometry. In addition, the internal and external mass flow rates and the inlet temperature of the hot fluid is required. The overall heat transfer coefficient *U* can be calculated based on the mass flow rates and the geometry using

the appropriate heat transfer correlations using equation (5.52). First, the thermal capacities are calculated as follows:

$$C_H = \dot{m}_{hot}\, C_{p-hot} \tag{5.54}$$

$$C_C = \dot{m}_{cold}\, C_{p-cold} \tag{5.55}$$

The minimum of the above quantities is referred as $C_{\min}$ and the alternate $C_{\max}$. Employing equation (5.52) in addition to (5.54) – (5.55) the NTU factor can be calculated:

$$NTU = \frac{U \cdot A_{HT}}{C_{\min}} \tag{5.56}$$

The effectiveness of the heat exchanger in discussion can be calculated using equations (5.54) – (5.55) and the effectiveness relation for a cross flow single pass heat exchanger as follows:

$$\varepsilon = 1 - e^{-\frac{C_{\max}}{C_{\min}}\left(1 - e^{-\frac{C_{\min}}{C_{\max}} NTU}\right)} \tag{5.57}$$

In a rating type problem, the two inlet temperatures for the cold and hot fluid must be known as discussed by Mills [5]. Alternatively, if the heat load is known, one of the inlet temperatures can be estimated based on the other. Using equation (5.57) and the knowledge of the net heat load and the inlet temperature of the hot fluid, the maximum heat load and the inlet temperature of the cold fluid can be estimated as follows:

$$\dot{q}_{\max} = \frac{\dot{q}_{net}}{\varepsilon} \tag{5.58}$$

$$T_{cold,in} = T_{hot,in} - \frac{\dot{q}_{\max}}{C_{\min}} \tag{5.59}$$

Thus, the outlet temperature of the cold fluid is calculated as follows:

$$T_{cold,out} = T_{cold,in} + \frac{\dot{q}_{net}}{\dot{m}_{cold}\, C_{p-cold}} \tag{5.60}$$

The solution above requires the knowledge of mass flow rate through the natural circulation loops. These flow rates come from the solution obtained from equation (5.26) in the case of the safety loop and equation (5.27) for the cooling loop. The net heat is a prescribed parameter that remains constant through the natural circulation and heat exchanger problem solution.

Estimating required heat transfer area: sizing problem solution

The solution of this type of problem is required in order to characterize the NDHX. The inlet and outlet temperatures of the hot fluid in this heat exchanger take the value of equations (5.59) and (5.60). The mass flow rate in this loop is also known as a result from equation (5.27). In the cold side, air enters the heat exchanger at a known inlet temperature and a known mass flow rate, which comes from the solution of the natural circulation equilibrium equation (5.38). The air outlet temperature can be determined from the energy conservation equation (5.36) however, what is not determined is the heat exchanger size in order to satisfy the performance requirements, as constrained by the pressure drop and temperature drops on both the hot and the cold side. The Effectiveness-NTU method is employed in order to calculate this.

The first step is to assume the NDHX geometry. The overall heat transfer coefficient U can be calculated from the known mass flow rates and equation (5.40) and the appropriate heat transfer correlations. The flow thermal capacities are also established based on the known salt inlet and outlet temperatures from equations (5.54) and (5.55). After assigning $C_{\min}$ to the smallest capacity of the two, the max heat removal rate can be obtained as follows:

$$\dot{q}_{\max} = C_{\min}\left(T_{hot,in} - T_{cold,in}\right) \tag{5.61}$$

Then the effectiveness factor and the capacity ratio can be calculated:

$$\varepsilon = \frac{\dot{q}_{net}}{\dot{q}_{\max}} \tag{5.62}$$

The Number of Transfer Units can be calculated directly from the effectiveness-NTU relations, in this case, the relation for a cross-flow single pass heat exchanger is chosen.

$$NTU = -\frac{C_{\max}}{C_{\min}}\ln\left(\frac{C_{\min}}{C_{\max}}\ln\left(1-\varepsilon\right)+1\right) \tag{5.63}$$

The knowledge of the NTU, in addition to the overall heat transfer coefficient leads to the prediction of the required surface area for heat transfer.

$$A_{HT} = NTU\,\frac{C_C}{U} \tag{5.64}$$

The approach taken in order to solve this problem, is to assume a heat exchanger geometry, then solve the natural circulation problem for both the hot and cold sides to obtain the inlet and outlet temperatures and mass flow rates. Then apply the Effectiveness-NTU method to determine the required heat transfer area, if the heat transfer area output matches the surface area of the assumed geometry, then the solution was obtained. If not, the assumed geometry is varied until the assumed surface area matches the required surface area for performance.

5.4.4 Convergence

The criterion for convergence is based on two parameters. First, the problem is iterated under the same geometric parameters allowing all temperatures reach a steady condition, thus thermophysical properties change no longer. It was chosen to stop iteration after the temperatures are within a 0.5 ^{o}C of difference between the previous and current iteration.

The second criterion for convergence consists on matching the required overall heat transfer area to the assumed heat transfer area by 5% margin. This provided sufficient flexibility to allow the code reach convergence quickly, without having the code solve the problem over small sizing intervals which would slow down the convergence. Both of these cut-off convergence parameters were chosen arbitrarily, procuring solution speed entirely.

5.5 ANALYSIS PROCEDURE AND EVALUATION

The input arguments of the program built, shown in Table (5-1) can be categorized in two sections: a) invariable parameters and b) variable parameters. The invariable parameters arise from the design requirements explained in section 4.2 for the NDHX. The variable parameters are set in order to observe the effect of each in the overall design. The program built was run under several combinations of variable input parameters to determine a suitable design which satisfies both types of constrains simultaneously. Following is a discussion of the invariable parameters, and the values selected for the analysis.

5.5.1 Invariable parameters

Heat Load

The NDHX is designed to remove 2% of the total reactor thermal power divided over all eight heat exchangers. This corresponds to 18MW total or 2.25 MW per loop. As was discussed in section 4.2, the rationale behind choosing this heat capacity is to allow the fluid and thermal absorbing graphite reflectors to heat up to a limit point assuming no cooling capacity while the natural circulation flow is established. It results that the decay heat power history exponentially decays from the initial 7% core power from the moment the core is shut down to a 2% core power level in ~15 minutes. The amount of energy released in this interval is allowed to elevate the temperature of the reactor core internal, as well as the reactor vessel fluid to a limit of 760 °C.

This calculation is conservative, as it assumes no heat is removed by fluid and pump impeller inertia or buoyancy driven natural circulation through the IHX. This calculation also assumes that heat is evenly distributed through all core components, but in fact, some components will heat up to greater levels compared to others. Finally, this calculation assumes the ideal decay heat history curve; however the precise amount of heat released by the core once on decay heat

mode will depend on the fission product constituents and concentration resulting from fuel burnup levels.

Another factor supporting the decision to construct a passive heat exchanger to remove 2% of the power instead of 7% of the power is based on economic reasons. Minimizing the size of the emergency decay heat sink grants low construction cost, in addition to reducing the salt inventory as much as possible. Certainly, a detailed economic study is necessary to evaluate the impact of the NDHX size on the overall plant construction cost.

Inlet and Limit temperatures for cooling loops

The salt temperatures of the cooling loop and the safety loop as indicated in Figure (5-1) are expected to be above the salt freezing point of 450 °C as indicated by Williams [9] and remain below the maximum permissible temperature set for safety limits of 760 °C. Therefore, the analysis is performed constraining fluid temperatures between those margins for both loops. The inlet temperature of the hot fluid of the DHX heat exchanger is set to the maximum of 760 °C. In the case of the air loop, the temperatures are constrained using the same upper limit, however the lower limit is imposed to 20 °C, given that this is the assumed inlet temperature for the NDHX air side refrigerant.

Core and DHX Geometry

The geometric parameters which correspond to the core and the DHX are considered invariant, since their design is fixed. Further information on these components is offered in section 3.1 and section 4.2.1 for the core and DHX respectively. The safety system design and analysis assumes the following as fixed parameters, and they refer to parameters illustrated in Figure (4-10) and table (5-1).

- Pebble bed effective area of flow $A_{AC} = 1.74\ m^2$
- Pebble bed length $L_{AC} = 2.2$ m
- DHX effective area of flow $A_{DHX} = 0.164\ m^2$
- Vertical distance between core and DHX $L_{FDL} = 2.2$ m
- DHX effective length $L_{DHX} = 2.2$ m

5.5.2 Variable parameters

The parameters listed below are not constrained. In order to obtain a point design, the following parameters must take a value. The values shown below come from the estimate of available space for the heat exchanger allocation, in addition to the application of engineering judgment as well as some trial and error with the code constructed. Figure 4-10 illustrates the plant design cross section, which serves as a reference for vertical height availability within the building. Section 8.4 evaluates the impact of the variation of these parameters in the overall design for optimization. The following variables are illustrated in Figure (4-10) and Table (5-1).

Plant Parameters

The distance between the bottom of the NDHX and the bottom of the DHX and the chimney length above the NDHX respectively:

- L_{VLL} = 8.0 m
- L_{CHI} = 20.0 m

Flow areas for component connecting pipes between core and DHX, between DHX and NDHX and chimney respectively:

- A_{safety} = 0.06 m^2
- $A_{cooling}$ = 0.07 m^2
- A_{chi} = 5.0 m^2

Helical Heat Exchanger Parameters

The parameters below describe the geometric configuration of the NDHX. Figures (xx-xy) illustrate these parameters.

NDHX helical heat exchanger fixed parameters

- Ro = 0.1 m
- Dto = 0.056 cm
- Dti = 0.050 cm
- P/D = 1.85
- A = 15^o

NDHX helical heat exchanger range parameters

Valid designs for the NDHX are explored in the following range of values, for the number of radial tube layers, and the number of whole loop rotations or windings respectively.

- N_{lay} = 40 - 60
- N_{win} = 0.2 - 1.3

The following parameters are calculated by the program as a function of any given geometric configuration:

- Air side flow area
- Air side tube bank length
- Salt side flow area

- Salt side tube arc length

The final parameter which is also varied as part of this study, is the working coolant selected for the cooling loop and the air loop. The following are the coolants considered

- Flibe
- Flinak
- Flinabe
- Lead
- Lead-Bismuth Eutectic
- Sodium

The air loop can assume air, or pure nitrogen as the working gas. Nitrogen was added in order to match the available working fluid used in RELAP5-3D to benchmark transient analysis.

The point design reported in the next section assumes flibe, flinak and nitrogen as the working fluids for the safety, cooling and air loops respectively. Following the primary simplification discussed at beginning of this chapter, the following section presents results for the single equivalent conceptual loop represented in figure (5-1).

5.6 RESULTS

The results output by the program constructed are described in this section. The data presented appears in a scattered fashion due to the set constrains for convergence. The code uses an iterative technique to obtain heat exchanger designs which satisfactory pass the two convergence test. The designs are searched covering the combination of possible heights and outer radiuses for a range of values, and with a number of intervals in each range. The code reports values which satisfy the equations with the convergence criteria selected. Under certain geometry arrangements, the code may not find a suitable combination when it is expected. These are shown as empty data points in the plots. Larger intervals and smaller convergence constrain are expected to represent data with greater consistency, however at a cost of unreasonable computation time.

5.6.1 Multiple NDHX configurations

The following figure shows the number of tube layers the helical heat exchanger needs as a function of helical heat exchanger height.

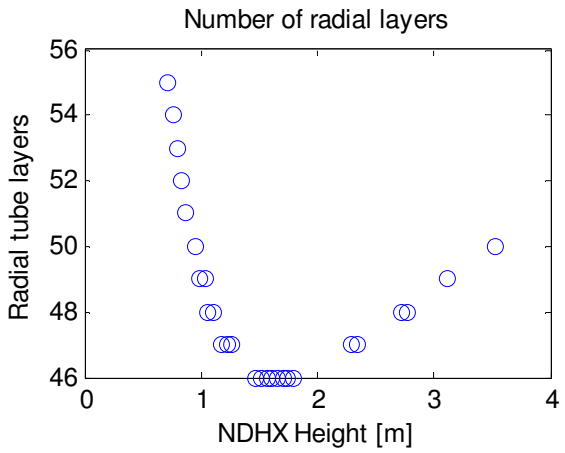

Fig. 5-4 Number of radial layers of tubes as function of heat exchanger height

It can be observed from the figure above, that short heat exchangers require numerous radial layer of tubes, as the heat exchanger shortens, the number of layer reaches a minimum and starts increasing after a minimum is reached. The figure below indicates the amount of surface area based on tube outer diameter as a function of heat exchanger height.

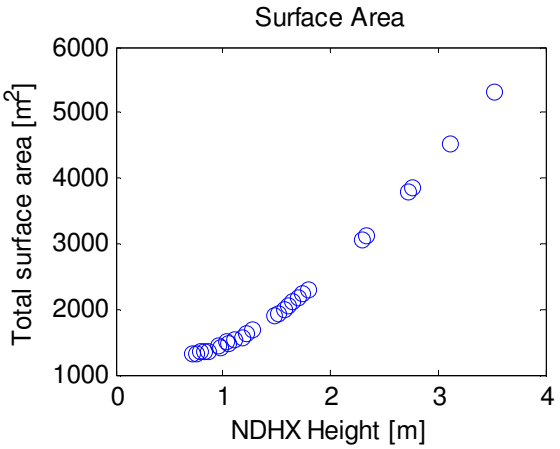

Fig. 5-5 Total tube surface area based on outer diameter for corresponding heat exchanger configuration from previous figure

Figures 5-4 and 5-5 indicate the multiple configurations of the NDHX which can be employed to remove excess decay heat from the reactor. While these multiple configurations satisfy the design requirements, the performance is different for all of them. It is expected that those configurations short with height will be characterized by low residence time of air, thus the outlet temperature of air is expected to be low. Analogously, a tall heat exchanger is expected to heat air to high temperatures, near those of liquid salt in the DRACS loop (right). The figures illustrate the performance of the NDHX from above as a function of height.

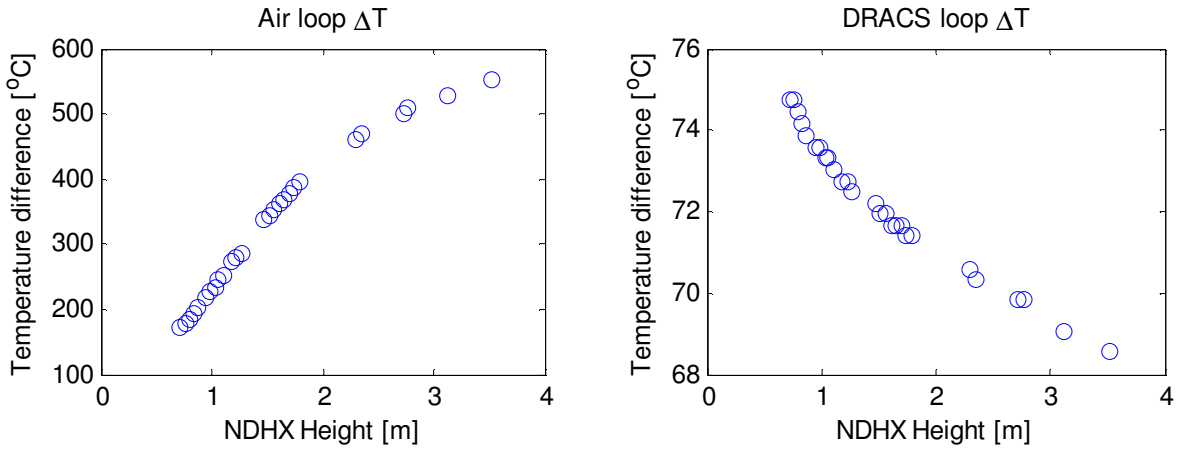

Fig. 5-6 Temperature difference for multiple heat exchanger configurations

The figures above show the temperature difference necessary to drive the flow due to the chimney effect on the air side (left) and to the natural circulation on the DRACS loop. The temperature difference on the air side of the NDHX greatly increases as the heat exchanger length increases, whereas the temperature variation is small for the tube side, liquid salt coolant temperature difference.

The mass flow rates which balance the friction head loss and the buoyancy head in these loops are shown in the following figure.

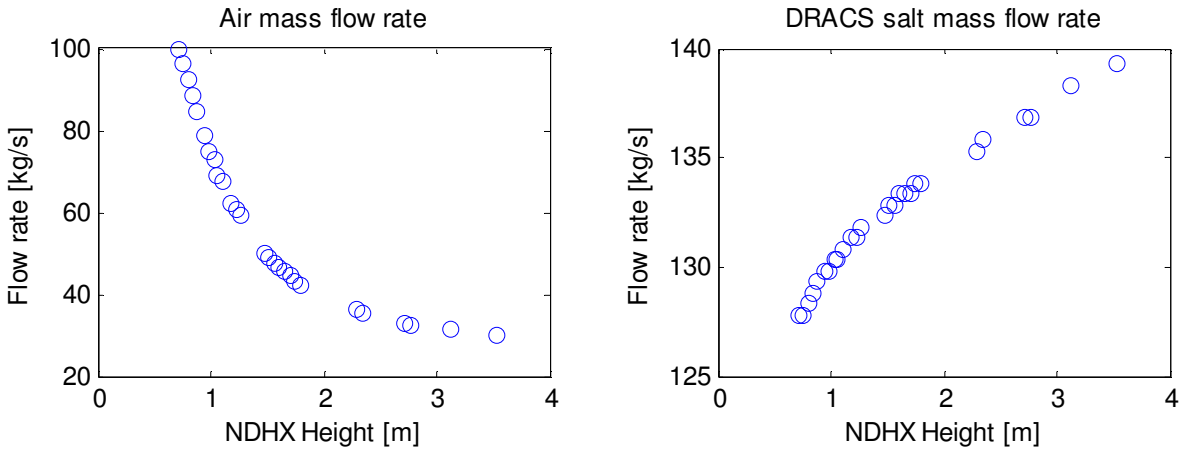

Fig. 5-7 Equilibrium flow rate for the air and cooling loops for various NDHX configurations

It can be observed that the equilibrium mass flow rate of air is highly dependent on the geometric configuration of the NDHX, whereas the liquid salt coolant is not very sensitive. The axial air flow rate is a strong function of the heat exchanger height since the air pressure drop increases as the heat exchanger lengthens. This requires greater air temperature difference across the air loop to increase the buoyancy and balance friction. Although the liquid salt tube side pipe length also increases as the heat exchanger lengthens, the increased pressure drop is overshadowed by the

pressure drop in other parts of the DRACS loop. For this reason, neither salt temperature difference nor salt flow rate is significantly increased. The figures below display the pressure drop and buoyancy head for the air and salt cooling channels.

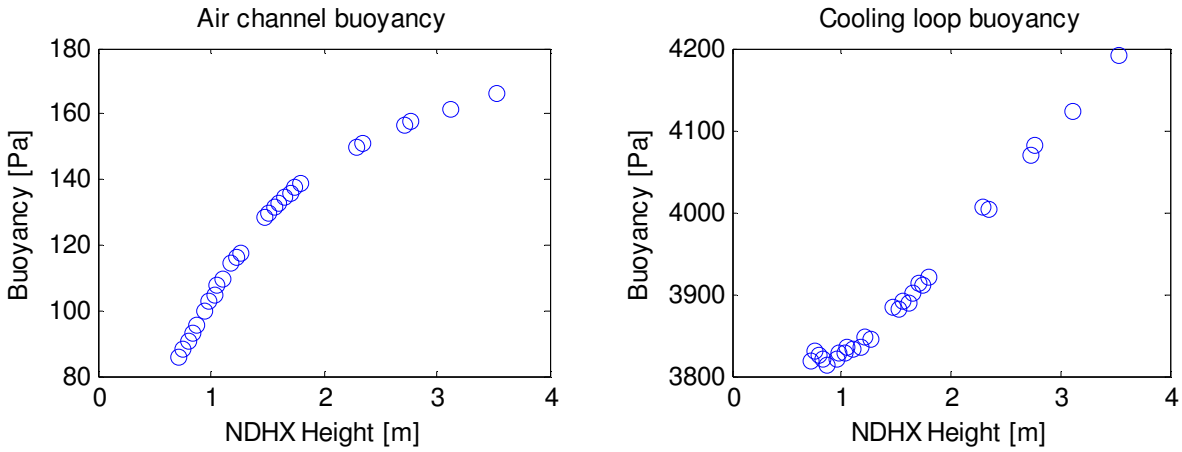

Fig. 5-8 Buoyancy pressure for air and liquid salt loops available to drive natural circulation flow

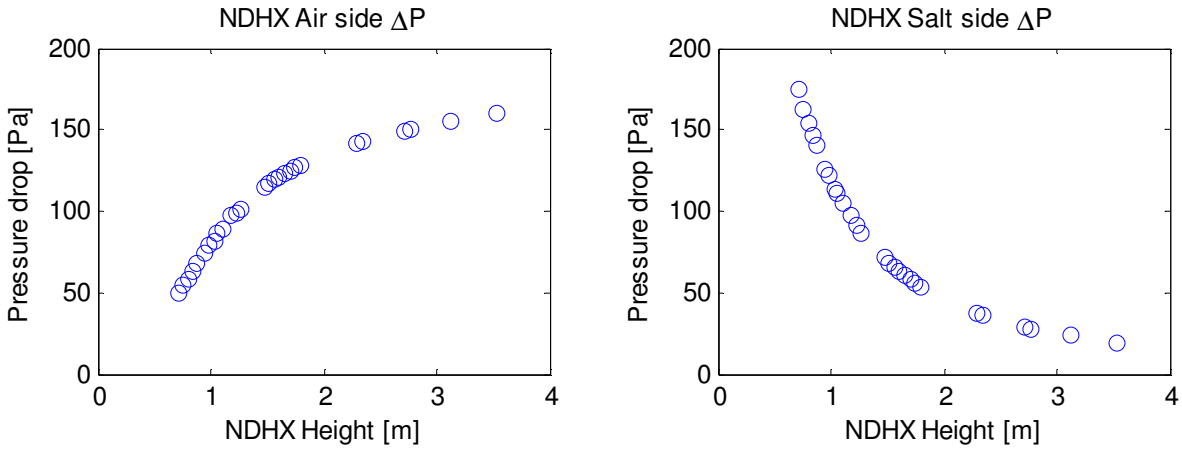

Fig. 5-9 Friction pressure for air and liquid salt loops through the heat exchanger.

Figure 5-6 and 5-7 shows buoyancy and friction pressure relationships. In the air side of the NDHX, it can be observed that the chimney buoyancy head is slightly above the friction losses through the heat exchanger. This implies that friction losses on the air loop external to the NDHX are small. In the other hand, friction losses are very small compared to the loop buoyancy head in the salt side, thus indicating that other parts of the loop cause greater friction loses.

The friction pressure drop on the salt side of the NDHX is small mainly due to a large pipe diameter, which is taken as 5cm. In general, friction pressure drop increase as mass flow rate increases, however, figure 5-7 and Fig 5-9 indicate the opposite relation for liquid salt flow. This occurs because the mass flow rate increases at a much slower rate as the total tube side flow area since the NDHX requires more radial tube layers as the NDHX height increases, therefore the

liquid salt flows at a lower mean velocity through the NDHX as the heat exchanger lengthens, thus causing less pressure drop as compared to shorter heat exchanger configurations.

Finally, the different flow rates through the heat exchanger are expected to show varying average heat transfer coefficients. The figure below indicates this relationship.

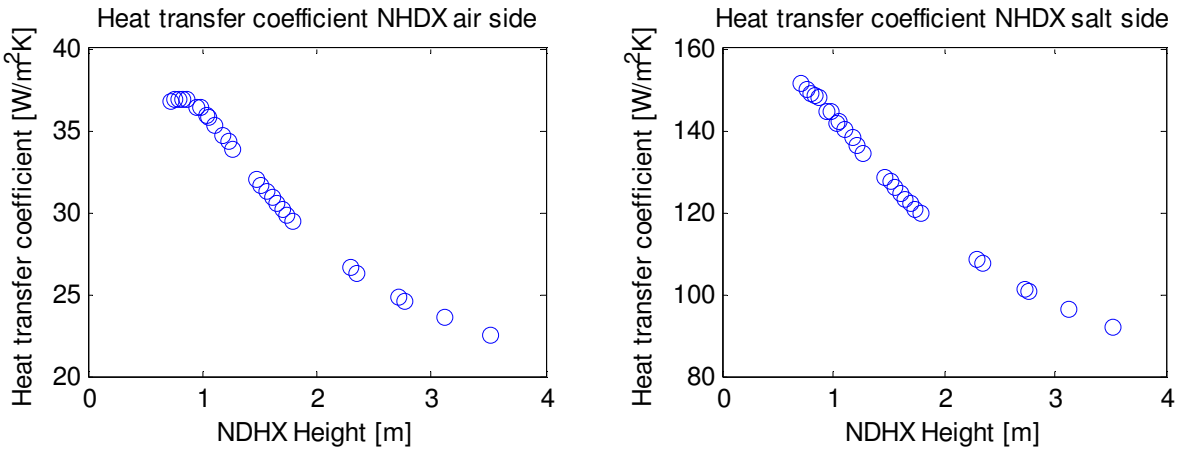

Fig. 5-10 Average heat transfer coefficients for air and liquid salt side through the heat exchanger.

As expected, the heat transfer coefficient on the air side of the heat exchanger decreases as the mass flow rate decreases. In the case of the salt side, the heat transfer coefficient decreases while the mass flow rate increases for the same reason as the pressure drop decreases, the liquid salt velocity decreases since the flow area increases as the heat exchanger configuration is varied. The following figure demonstrates this relationship by plotting the Reynolds number of the air and liquid salt through the heat exchanger.

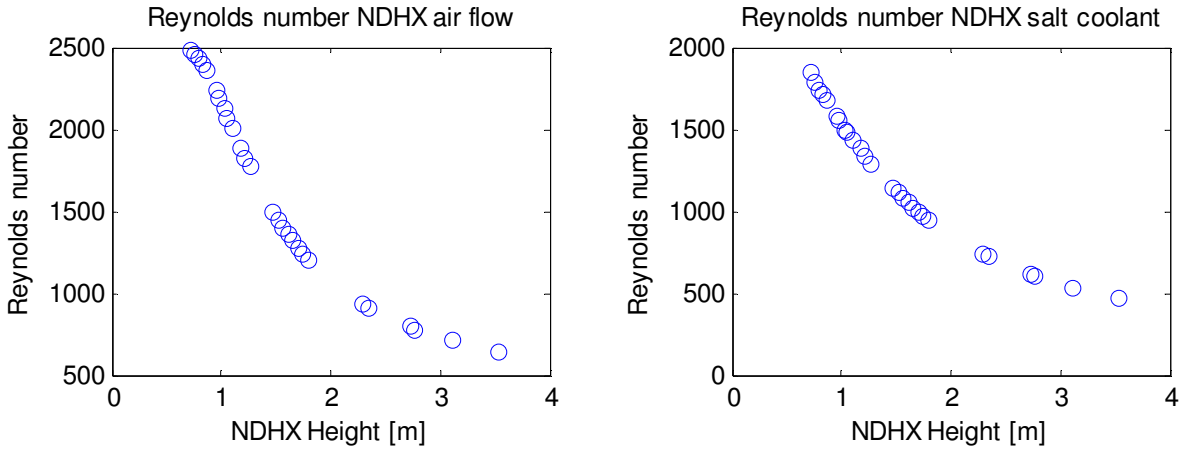

Fig. 5-11 Reynolds number for air and liquid salt side through the heat exchanger.

5.6.2 DRACS Point design

Evaluating the results presented above, a single configuration is chosen to employ as the DRACS point design.

The point design was chosen is a preliminary chosen for convenience of analysis. It was observed that a preliminary analysis of the NDHX design using RELAP5-3D behaves in a more stable manner when the pressure drop of the air side is large, than when it is small. This occurrence is explained in detail in section 6.5. In order to assure stability, a tall design was chosen for the NDHX point design; however the optimization of this point design is evaluated in section 8.4. The following table provides the data which characterizes the DRACS system reference point design.

NDHX Natural Draft Heat Exchanger - Geometric data			
Tube outer diameter	5.60 cm	Radial rows of tubes	56
Tube wall thickness	0.3 cm	Pipe horizontal inclination angle	15^{o}
Average tube length	18.3 m	Coil height	2.82 m
Nominal length	3.50 m	Aflow internal	3.32 m^2
Total number of tubes	1690	Tube pitch to diameter ratio	1.85
OD Heat transfer area	5510 m^2	Area flow external	40.8 m^2
Central coil radius	2.2 m		

Table 5-2 Geometric description of single equivalent NDHX heat exchanger

NDHX Natural Draft Heat Exchanger – Rated performance data			
Heat transfer rate per unit	18.0 MW_{th}	Number of units required	1
Natural Draft coolant	Nitrogen	DRACS salt	LiF-NaF-KF
Mass flow rate of primary shellside air	32.3 kg/s	Mass flow rate of DRACS tubeside salt	139.5 kg/s
Pressure drop in shellside	159 Pa	Pressure drop in tubeside	20 Pa
Average heat transfer coefficient shell side	22.5 (W/ m^2 °C)	Average heat transfer coefficient tube side	90.6 (W/ m^2 °C)
Inlet temperature of primary shell side air	20 °C	Inlet temperature of DRACS tube side salt	556 °C
Outlet temperature of primary shell side air	570 °C	Outlet temperature of DRACS tube side salt	624 °C
LMTD	210 °C	Average Reynolds tubeside	633.5
		Average Reynolds shellside	451.0

Table 5-3 Performance characteristics of single equivalent NDHX heat exchanger

The results presented above refer to the single equivalent NDHX. In order to scale down to the prototype design, where the heat load is transported through eight salt-to-air heat exchangers a

methodology of scaling is applied. This methodology is presented in the next chapter, where a transient analysis of the nuclear reactor plant is performed. In order to accomplish this, other plant components also require adequate scaling to represent in a single element the behavior of multiple elements. Clearly, only the geometric parameters are scaled, since it is necessary to preserve the performance similarity between scaled model and prototype

5.7 SUMMARY

In this chapter, a methodology of solution of the governing equations and the numerical implementation of this solution is presented. As a result, a computer program was built to determine suitable heat exchanger designs which satisfy the design requirements and constrains appropriate for the operation of the passive safety system. Estimates from the plant component allocation design in addition to numerical stability of solution allow the selection of a heat exchanger point design, which serves as a reference for sensitivity analysis, where the impact of the variation of plant parameters is analyzed. This point design also serves as a reference for transient analysis of the plant.

5.8 REFERENCES

[1] A. Zukauskas, *Heat transfer from tubes in crossflow.* Advances in Heat Transfer 18 (1987) 87-134

[2] D. Holcomb., *Personal communication* Oak Ridge National Laboratory, March (2011)

[3] W. M. Kays, A. L. London, *Compact Heat Exchangers 3rd Edition* McGraw-Hill Book Company (1984)

[4] Y. S. Yang, *Thermal analysis of Liquid Metal Fast Breeder Reactors,* American Nuclear Society, La Grange Park, IL (1978)

[5] A. F. Mills *Basic Heat & Mass Transfer 2nd edition*. Prentice-Hall, Upper Saddle River, New Jersey (1999)

[6] *Thermophysical properties of Materials for Nuclear Engineering: A Tutorial and Collection of Data*, IAEA, Vienna (2008)

[7] Fink, J. K. *Thermodynamic and Transport Properties of Sodium Liquid and Vapor,* Argonne National Laboratoy – Reactor Engineering Division. ANL/RE-95/2, January (1995)

[8] N. E. Todreas, M. S. Kazimi *Nuclear Systems I Thermal Hydraulic Fundamentals.* Taylor & Francis (1993)

[9] D. F. Williams, L. M. Toth, K. T. Clarno *Assessment of candidate molten salt coolants for the advanced high temperature reactor (AHTR)* Oak Ridge National Laboratory ORNL/TM-2006/12, March (2006)

[10] C. Davis *Implementation of molten salt properties into RELAP5-3D/Athena* Idaho National Engineering and Environmental Laboratory INEEL/NXT-05-02658 January (2005)

[11] F. P. Incropera, D. P. Dewitt *Fundamentals of Heat and Mass Transfer 5th edition.* John Wiley and Sons, New York (2001)

[12] F. M. White *Fluid Mechanics 5th edition.* McGraw-Hill, New York (2003)

[13] C. E. Bettis et. al., *Computer programs for MSBR heat exchangers.* Oak Ridge National Laboratory ORNL/TM-2815, June (1971)

[14] Y. A. Cengel, M. A. Boles *Thermodynamics An Engineering Approach 4th edition.* McGraw-Hill, New York (2002)

6. SAFETY SYSTEM TRANSIENT ANALYSIS

6.1 PROBLEM FORMULATION

The approach to developing the initial design for the DRACS safety system for the PB-AHTR assumes quasi-steady-state operation of the DRACS, in isolation from other plant components and without consideration of the initial transient processes involved as the DRACS system starts up. Part of the subsequent design process is the transient analysis of the design when coupled to the complete nuclear plant design, and evaluating its performance under design basis events such as Loss of Forced Circulation (LOFC).

6.2 PROBLEM GOVERNING EQUATIONS – INTEGRAL PHENOMENA

The design approach for the DRACS system assumes steady state heat removal, where there is no net energy storage and heat is removed at a certain rate based upon a percentage of the reactor full thermal power. Under this assumption, each component of the DRACS system can be studied separately using analytical models. But because the actual system operates under transient conditions where decay heat drops with time and thermal inertia plays a large role, the transient response of the system must also be evaluated to verify that it has sufficient heat transport capacity to keep reactor structures and fuel inside their thermal limits. During a transient, the boundary conditions that are applied to each component vary and affect the performance of the heat exchanger. This variation affects all the components of the system, although in different degrees. For instance, a heat source temperature increase would cause an increase of the natural circulation within the DRACS, also causing increased pressure drops within the heat exchangers, but the pressure drop is not necessarily the same in each component, since the fluid regime may differ for each component. Thus in the case of transients, the study of the DRACS system must be performed integrally.

It is important to note that during transients, the performance of the heat exchanger never reaches steady conditions. As it was mentioned, the DRACS system is expected to passively cool down the core, but the heat generation rate of the core is also dependent on the temperature of the inlet core coolant, which is a function of the amount of heat transported by the DRACS. If the reactor has not been scramed (anticipated transient without scram, or ATWS), the coolant temperature affects the core primarily due to the temperature and density feedback mechanisms that are detailed by Ott [3] by affecting the rate of nuclear reactions occurring within the core. For this reason, the study of the performance of the DRACS system must be done integrally along the core and any other cooling components active during the transients, which may affect the coolant temperature and thus the heat generation rate.

The equation below is the equation of neutron transport, which includes time dependent terms and space dependent terms, in addition to external source terms. One factor affecting the transport of neutrons is the cross section functions symbolized by sigma Σ, with the subscripts s for neutron scattering and t for total rate of reaction. These factors depend strongly on the

material temperature reactions occur. For this reason, it desirable to solve the transport of mass, momentum and energy equations (5.1-5.3) coupled with the neutron transport equations simultaneously.

$$\frac{1}{v}\frac{\partial \psi(\vec{r},E,\vec{\Omega},t)}{\partial t}+\vec{\Omega}\cdot\nabla\psi(\vec{r},E,\vec{\Omega},t)+\psi(\vec{r},E,\vec{\Omega},t)\Sigma_{to}(\vec{r},E) \tag{6.1}$$

$$=s(\vec{r},E,\vec{\Omega},t)+\int_{\Omega'\to 4\pi}\int_{E'=0}^{\infty}\psi(\vec{r},E,\vec{\Omega},t)\Sigma_{sc}(\vec{r},E'\to E,\vec{\Omega}'\to\vec{\Omega})dE'd\vec{\Omega}'$$

6.3 SOLUTIONS TO GOVERNING EQUATIONS

As it can be noted from the governing equations discussed above, the exact solution of these equations is near to impossible due to the non-linear, multi-dimensional, unsteady and multi-variable nature of the problem, in addition to the implicit aspect of the variables common to all governing equations. The common approach in the study of nuclear reactor systems is the application of numerical solutions to the coupled equations of transport in a simplified version. In order to accomplish this task, a commercial nuclear analysis package was adopted.

6.3.1 RELAP5-3D Overview

The code RELAP5-3D (Reactor Excursion and Leakage Analysis Program) has been used in the past to analyze transients in earlier versions of the PB-AHTR as documented by Niquille [9] and Griveau [10]. Results obtained from these previous work contributed to the overall point design of the core as detailed in section 3.1 presented earlier in this report. RELAP5-3D is a well-known, highly flexible reactor transient response code that was originally developed to assess the safety and reliability of Light Water Reactor (LWR) designs under various transients [8]. The development of RELAP5-3D is an ongoing effort at Idaho National Laboratory (INL) since its initial version, and is constantly growing in terms of the availability of special models, fluid libraries, and graphic user interface options to simplify the usage of this complex code. In 2005, INL added molten salt properties for 4 different salts to the built-in fluid library in this computer program. This enabled the usage of this software for the analysis of the PB-AHTR.

The code includes many generic component models from which thermal-hydraulic systems can be simulated. The component models include pumps, valves, pipes, heat releasing or absorbing structures, reactor kinetics, electric heaters, jet pumps, turbines, separators, annuli, pressurizers, accumulators, and power control system components. In addition, special process models are included for effects such as form loss, flow at an abrupt area change, branching, choked flow, and non-condensable gas transport.

The multi-dimensional component in RELAP5-3D was developed to model the multi-dimensional flow behavior in many LWR components. Typically this will be the lower plenum,

core, upper plenum and down comer. However, the model is general, and is not restricted to use in the core vessel.

6.3.2 Numerical Solution scheme

RELAP5-3D utilizes a semi-implicit numerical scheme to solve integral equations for the conservation of mass, momentum and energy across the boundaries of the discretized solution domain. The equations of transport can be simplified given certain conditions, which are reasonable assumptions in the representation of certain nuclear reactors.

Governing Equations

The equations solved by RELAP5-3D are presented in Eq. 5.1-5.3 after certain simplifications are applied. The first simplification comes when 3-D thermal-hydraulic phenomena is simplified to 1-D such as fluid flow in uniform area channels or heat conduction when the temperature gradient is much greater in one direction (radially) compared to other directions (axially) in case of tubes where heating or cooling occurs. This simplification allows the usage of mean values for velocity and internal energy of fluid.

The second simplification consists on the application of the point reactor kinetics model discussed in Duderstadt [13] to describe the transient fission power within the reactor core. This model is used whenever the neutron flux can be expressed as the product of a time-independent space-dependent shape factor, and a time-dependent space-independent amplitude factor. This assumption is invalid in certain cases, for example, the ejection of a control rod with high reactivity worth. This event causes a strong deviation from the assumed shape factor, invalidating the point reactor kinetics model.

The transport equations to be solved are partial differential equations. In general, these equations can be solved analytically for all variables in few circumstances when the boundary conditions along with some simplifications allow for a direct analytical solution, as an example the solution to the heat equation applied to the semi infinite one-dimensional solid with a step change in temperature at the surface is demonstrated in Incropera [11]. The following is the governing equation and the necessary transformation to obtain the analytical solution in for both variables.

$$\frac{\partial^2 T}{\partial x^2} = \frac{1}{\kappa}\frac{\partial T}{\partial t} \qquad \text{(1-D heat equation)} \tag{6.2}$$

$$\eta = \frac{x}{\sqrt{4\kappa t}} \qquad \text{(transformation)} \tag{6.3}$$

$$\frac{T(x,t) = T_s}{T_i - T_s} = erf\left(\frac{x}{2\sqrt{\kappa t}}\right) \qquad \text{(solution)} \tag{6.4}$$

Unfortunately, the governing equations of the thermal – hydraulic phenomena within the reactor core, heat exchanger and other components are multi-variable, non-linear and time dependent. For this reason a numerical scheme is applied to solve for the simplified transport equations of mass momentum and energy in the system and across components as a function of time. The following are the simplified equations as reported by the RELAP5-3D Code Development Group [8]

Conservation of Mass

$$\frac{\partial \rho}{\partial t} + \nabla \cdot \left(\rho \bar{v} \right) = 0 \tag{6.5}$$

Conservation of Momentum

$$\rho \left(\frac{\partial \bar{v}}{\partial t} + \bar{v} \cdot \nabla \bar{v} \right) = -\nabla P + \bar{\sigma} + \rho \bar{f} \tag{6.6}$$

Conservation of Energy

$$\rho \left(\frac{\partial U}{\partial t} + \bar{v} \cdot \nabla U \right) = -\nabla \cdot \bar{q} - P \nabla \cdot \bar{v} + tr(\bar{S} \cdot \nabla \bar{v}) + \rho Q \tag{6.7}$$

Neutron point reactor kinetics

$$\phi(t) = \phi_o \left[\frac{\beta_T}{\beta_T - \rho_R} e^{\frac{(\gamma \cdot \rho_R)}{\beta_T - \rho_R} t} - \frac{\rho_R}{\beta_T - \rho_R} e^{-\frac{(\beta_T - \rho_R)}{l} t} \right] \tag{6.8}$$

The conservation equations of mass, momentum and energy are solved over all cell volumes and time intervals that added together define the problem in time and in space. The point reactor kinetics equation is applied to every cell volume that constitutes a heat generation component subject to power fluctuations due to reactivity variations. Every heated mesh element is affected in the same manner, however reactivity feedback coefficients can have weighting multipliers to account for core power density space-dependence. The discretization of the components depends on the numerical scheme employed in order to solve these equations. RELAP5-3D does not discretize in space the same way when solving for vector quantities as opposed to scalar quantities, thus solution schemes for temperature and velocity use different spatial discretization. Figure 6-1, obtained from Ref. [8], shows the solution scheme over a sample mesh cell.

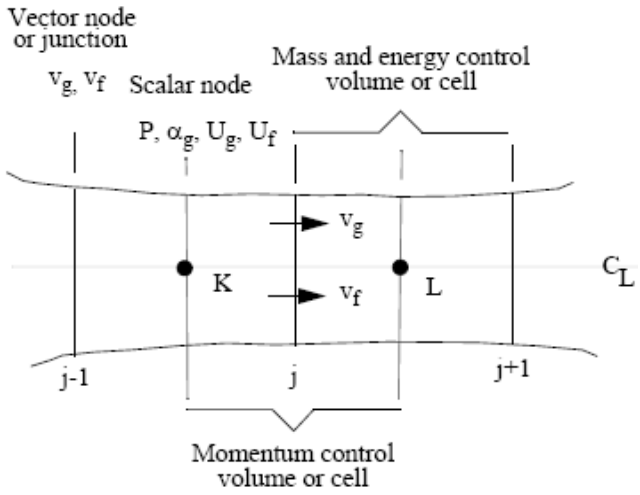

Fig. 6-1 Scalar and vector property spatial solution scheme in RELAP5-3D [8]

Numerics

In order to solve equations (6.5) – (6.7), these partial differential equations are replaced by difference equations. These difference equations result from integrating the differential equations over a control volume (or mesh cell) in which mass and energy are conserved by equating the accumulation to the rate of mass and energy in through the cell boundaries minus the rate of mass and energy out through the cell boundaries plus the source terms. This model averages properties for all mesh cells and requires the knowledge of velocities at the volume boundaries. The velocities at boundaries are most conveniently defined through use of momentum control volumes (cells) centered on the mass and energy cell boundaries. This approach results in a numerical scheme having a shifted spatial mesh. The scalar properties (pressure, specific internal energies, and void fraction) of the flow are defined at cell centers, and vector quantities (velocities) are defined on the cell boundaries. Equations (6.9), (6.10) and (6.11) depict the difference equations for the 2-phase mixture balance of mass, energy and momentum.

$$\left(\alpha_g\rho_g+\alpha_f\rho_f\right)_j^{n+1}-\left(\alpha_g\rho_g+\alpha_f\rho_f\right)_j^{n}+\left\{\left(\left(\alpha_g^n\rho_g^n v_g\right)_{j+1/2}^{n+1}+\left(\alpha_f^n\rho_f^n v_f\right)_{j+1/2}^{n+1}\right)A_{j+1/2}\right.$$
$$\left.-\left(\left(\alpha_g^n\rho_g^n v_g\right)_{j-1/2}^{n+1}+\left(\alpha_f^n\rho_f^n v_f\right)_{j-1/2}^{n+1}\right)A_{j-1/2}\right\}\left(\Delta t/V_j\right)=0 \qquad (6.9)$$

$$
\begin{aligned}
&\left(\alpha_f \rho_f u_f\right)_j^{n+1} - \left(\alpha_f \rho_f u_f\right)_j^{n} + P_j^n \left(\alpha_f^{n+1} - \alpha_f^n\right)_j \\
&+\left(\left(\alpha_f \rho_f u_f\right)_{j+1/2}^{n} + \left(\alpha_f^n\right)_{j+1/2} P_j^n\right)\left(v_f\right)_{j+1/2}^{n+1} A_{j+1/2}\left(\Delta t / V_j\right) \\
&-\left(\left(\alpha_f \rho_f u_f\right)_{j-1/2}^{n} + \left(\alpha_f^n\right)_{j-1/2} P_j^n\right)\left(v_f\right)_{j-1/2}^{n+1} A_{j-1/2}\left(\Delta t / V_j\right) \\
&=\left\{\left(h_f / (h_g - h_f)\right)^n q_{wf}^{n+1} + \left(h_g / (h_g - h_f)\right)^n q_{wg}^{n+1}\right. \\
&\left.+q_{wf}^n + DISS_f^n\right\}_j \Delta t
\end{aligned}
\tag{6.10}
$$

$$
\begin{aligned}
&\left(\left(\alpha_g \rho_g\right)_{j+1/2}^{n}\left(v_g^{n+1} - v_g^n\right)_{j+1/2} + \left(\alpha_f \rho_f\right)_{j+1/2}^{n}\left(v_f^{n+1} - v_f^n\right)_{j+1/2}\right)\Delta x_{j+1/2} \\
&+\frac{1}{2}\left(\alpha_g \rho_g\right)_{j+1/2}^{n}\left(\left(v_g^2\right)_{j+1}^{n} - \left(v_g^2\right)_j^n\right)\Delta t \\
&+\frac{1}{2}\left(\alpha_f \rho_f\right)_{j+1/2}^{n}\left(\left(v_f^2\right)_{j+1}^{n} - \left(v_f^2\right)_j^n\right)\Delta t - \frac{1}{2}\left(\left(\alpha_g \rho_g\right)_{j+1/2}^{n} VISG_{j+1/2}^n\right. \\
&\left.+\left(\alpha_f \rho_f\right)_{j+1/2}^{n} VISF_{j+1/2}^n\right)\Delta t = -\left(P_{j+1} - P_j\right)^{n+1}\Delta t + \left[\rho_{j+1/2}^n B_x\right. \\
&-\left(\alpha_g \rho_g\right)_{j+1/2}^{n}\left(v_g\right)_{j+1/2}^{n+1} FWG_{j+1/2}^n - \left(\alpha_f \rho_f\right)_{j+1/2}^{n}\left(v_f\right)_{j+1/2}^{n+1} FWF_{j+1/2}^n \\
&\left.-\left(\Gamma_g\right)_{j+1/2}^{n}\left(v_g - v_f\right)_{j+1/2}^{n}\right]\Delta x_{j+1/2}\Delta t
\end{aligned}
\tag{6.11}
$$

The difference equations shown above result from the application of the governing equations over the sample mesh element shown in figure (6-1) as reported by Ambrossini [2]. The terms evaluated at the new time step are superscripted with n+1 notation, and the terms donored are subscripted with j+1/2. These donored terms take values advected from neighbor cells based on the selected spatial marching scheme.

In the process of replacing the partial differential equations for difference equations, it is necessary to expand the time derivatives. In order to do so, there are two potential approaches, an explicit scheme, where the time derivative uses previous time step information and the implicit scheme, where the time derivative is evaluated at the new time step.

The semi-implicit numerical solution scheme is based on evaluating carefully selected time derivatives at the new time step information. The terms evaluated implicitly are identified as the scheme is developed. The implicit terms are formulated to be linear in the dependent variables at new time. This results in a linear time-advancement matrix that is solved by direct inversion using the default border-profile LU solver. Thus, an N x N system of equations must be solved simultaneously at each time step. N is the total number of control volumes used to simulate the fluid system.

Closure Relations

The coupling of the hydrodynamic and heat transfer at each mesh element is performed explicitly. However, an option exists to implicitly couple the time advancement of the hydrodynamic and heat structure models. 1-D and some cases 2-D heat conduction is used to compute temperature distributions within heat structures. Hydrodynamic and heat structure conditions are coupled through heat structure boundary conditions.

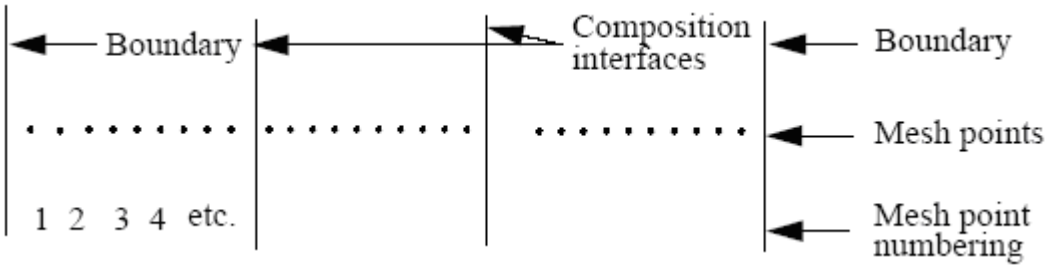

Fig. 6-2 Heat transport interface and structure nomenclature in RELAP5-3D

$$q'' = h_g \left(T_w - T_{REFg}\right) + h_f \left(T_w - T_{REFf}\right) \quad (6\text{-}12)$$

The heat conduction equations have additional terms related to fluid temperatures introduced by the boundary conditions. This larger set of simultaneous equations, however, is solved with only a modest increase in computations compared to the explicit coupling. Implicit coupling can be used with either the semi-implicit or nearly-implicit advancement. The purpose of the implicit coupling of hydrodynamic and heat structure time advancement is to more accurately model the exchange of energy between the structures and fluid in the volumes, to avoid numerical instabilities due to explicit coupling, and to achieve reduction of computing time through larger time steps.

Finally, in order to complete the thermal-hydraulic computations, the code requires the use of closure relations to properly couple the different phenomena occurring at the interface between constituents in the problem domain. Namely, the wall friction and the wall heat transfer correlations which can be manually modified as needed. Ref [8] provides more detailed information on the numerical part and the theoretical basis for the closure relations employed.

6.3.3 RELAP5-3D Code Limitations

For the purposes of this study, the primary limitation of the code is the use difficulty and steep learning curve. This code is very powerful primarily because of the rich variety of special process models that are appropriate for the study of LWR including two-phase flow phenomena, stratification and fluid-vapor separation among others. The problem occurs when a simple system such as the PB-AHTR is represented; there are a number of parameters which must take a

value and are non-intuitive for any user not dealing with two-phase flow problems. Based on input documented by ref. [5] RELAP5-3D is a code for advanced users, and does not possess any level of automation which users modeling simple systems can take advantage of. However, the developing team from INL has noted this observation from other users and has started working on a more advanced version which allows the user to select the level of fidelity a model needs to represent.

Other important limitation of the code is the absence of the exact wall friction loss and wall heat transfer correlations for the multiple geometries employed in this study. The existing correlations are appropriate for LWR components and require their manipulation to reproduce the expected coefficients for wall friction and heat transfer in pebble beds. This limitation can easily be modified at the source code level by the staff at INL, however this requires a contract which may be sought in the future.

6.4 MODEL CONSTRUCTION

6.4.1 Plant Components

The plant components corresponding to the primary system are modeled based on the information from sections 3.1 – 3.4 and 4.2 – 4.3. This information, in addition to the recently obtained reference design parameters for the safety cooling DRACS listed in section 5.6, can be used to construct a computational model that serves to study the performance of the overall plant in steady state full power, and in response to transient events of interest. A complete plant model is necessary to perform the integral evaluation of the plant systems; especially during transients given that the boundary conditions which drive the transport of heat and momentum through the multiple components of the plant are constantly changing and are dependent of one another. The following sections explain how the computational model is built based on the collected plant design data.

6.4.2 Plant Model Scaling

In order to study and evaluate the DRACS system point design listed in section 5.6.2 it is necessary to couple this model to the existing model of the PB-AHTR which has been previously developed and documented by [7]. However, the existing RELAP5-3D model is an inconvenient model to study the DRACS system for the following reasons:

- The existing PB-AHTR model is too detailed, making it difficult to add new components to the model while not conflicting with existing component ID numbers and satisfy maximum number of components allowed by the code.
- The existing model is complete and represents the current point design of the reactor, including all components accurately represented. In order to add the DRACS system, all 8 DRACS loops would be required to be input. Since it is expected to vary the parameters of the DRACS during the study, the modification of all DRACS components for all DRACS loops becomes cumbersome and unnecessary.

- The addition of 8 DRACS loops significantly slows computation time even further, especially during transients.
- Data analysis becomes significantly more complex since results of simulations need to be read for every DRACS loop, and since the transients studied affects all loops equally and simultaneously, then there is no real need to simulate all systems but simulate one effective equivalent system.
- Analytical benchmarking is very difficult if all DRACS loops are represented, but it is simpler if one equivalent loop is employed.

For the reasons shown above, it was decided to represent the multiple components and loops in the PB-AHTR model into equivalent lumped components and loops which behave identically and respond identically in case of transients. Below is the general criterion for the scaling of multiple components and loops into a single component and loop:

- Scaled components must employ tubes of the same length and diameter as the prototype (NDHX, IHX, and DHX).
- Scaled components must use the same coolants at the same pressures and temperatures.
- Scaled components must preserve geometric similarity.
- Scaled components must be placed in the same vertical height location relative to the core.

The scaling of the DHX heat exchangers is specially challenging, primarily due to the complex geometry arising from the usage of baffles on the primary-coolant shell side. In disk-and-doughnut baffled heat exchangers, there are three distinct characteristic flow areas, the inner and outer window flow areas, where fluid travels partially in parallel flow with the heat exchanger tubes, and partially in cross flow. The third region is the center cross flow region. These different areas are not proportional to the outer radius or the number of tubes employed, but rather, proportional to the multiplication of the outer radius and the uniform baffle space distance. In order to represent scaled heat exchangers properly, the following criteria is established.

Scaling Strategy

The strategy employed in the problem of combining of multiple components into a single component is to preserve the key phenomena that are important for the adequate representation of the component as part of the system.

The problem of scaling was analyzed from an external and internal point of view. From the external point of view, all scaled components are assumed equal to the prototypical components in terms of the functions they perform and under the conditions the components perform. This implies that a single equivalent primary pump drives the overall mass flow rate through the core and the primary loop under the same overall head as the 2 prototypical pumps that are in part of the plant design with the same fluid at the same temperatures. Similarly, a single equivalent IHX

removes the heat of 4 prototypical IHX under the combined mass flow rate of all components with the same fluids at the same temperature difference and efficiency. Finally, a single equivalent DRACS system removes the same amount of heat as 8 prototypical DRACS systems under the combined mass flow rate of all components with the same fluids at the same temperature difference and efficiency.

An important note is that under natural circulation, the flow driving mechanism is entirely different compared to forced flow. In the case of natural circulation, the driving force is proportional to the vertical height which separates the heat source from the heat sink. An additional external point of view to the problem then is the requirement that the equivalent model must preserve the plant geometry to ensure equivalent behavior when forced flow conditions are no longer present.

From the internal point of view, the parameters that are considered important are the rates of transport of momentum and energy, namely the friction loss and heat transfer, both as a function of flow conditions and spatial dependence.

Starting from the assumptions provided by the external point of view and the requirements arising from the internal point of view the scaling laws for equivalency are developed.

The following are the relations for friction losses in our study:

Internal flow friction factor

$$\Delta P = f \frac{L}{D_h} \rho \frac{V^2}{2} \tag{6.13}$$

where the friction factor f is a function of Re number as discussed in section 2.8. This relation is applicable for straight tubes as it is the case of the salt-salt heat exchangers. For the salt-air heat exchanger, the laminar flow friction drop inside the curved pipe is slightly higher than in straight pipes reported by Mori [4] and the modified equation is

$$\frac{f_{curved}}{f_{straight}} = 0.108 \,\mathrm{Re} \sqrt{\frac{a}{Rc}} \tag{6.14}$$

where a is the radius of the curved tube and Rc is the radius of the coil.

External form loss factor

$$\Delta P = K \rho \frac{V^2}{2} \tag{6.15}$$

In the equation above, K is the form loss factor. In the case of external cross flow through a bank of tubes, the factor K is the following as indicated in [6].

$$K = N\chi \tag{6.16}$$

N is the number of restrictions in the direction of the flow. For the IHX and DHX case, where the tubes are arranged neither aligned nor staggered, but are rather radially expanding lattice, Bergelin et al. [6] suggest that the N is the sum of restrictions in the cross-flow region plus only half of those located in the inner window region and half of those located in the outer region. The report also suggests letting X take the value of 0.6 for this radial lattice system. Only in the case of the IHX and DHX, the overall pressure drop is the sum of the pressure drop calculated within each baffle over all baffle spaces along the heat exchangers. In other words:

$$\Delta P_{total} = \frac{N_{baffles}}{2} \Delta P_{baffle-space} \tag{6.17}$$

$$\Delta P_{baffle-space} = \left(\frac{N_{out-window}}{2} + N_{cross-flow} + \frac{N_{out-window}}{2} \right) \chi \cdot \rho \frac{V^2}{2} \tag{6.18}$$

Based on the relations discussed above, the scaling laws dictate that the following parameters need to be maintained for similarity between model and prototype representations.

Fluid velocity

The preservation of fluid velocity allows similar friction factors on the flow, thus preserving the friction loss rates. In order to maintain fluid velocity, the area of flow must be proportional to the ratio of mass flow rates between model and prototype heat exchangers and piping interconnecting components. This is a requirement both for internal and external flows.

Fluid residence time

This requires that the fluid travel time is the same both in the scaled and prototype models. Given that geometrically, the components preserve the vertical height due to the natural circulation requirement, then by maintaining identical tube length on the heat exchangers in addition to proportional total flow area to mass flow rate, the residence time of the fluids are preserved also. In the shell side, the effective residence time is the ratio of the shell side volume to the average flow area. This imposes the requirement that the ratio of volume to area for the prototype is identical to the model.

Number of restrictions

In the case of the NDHX, this requirement is automatically met by maintaining the tube diameter, the tube pitch and the overall height of the helical heat exchanger. In the case of the IHX and DHX, the number of restriction is met by selecting the appropriate inner and outer radius for the heat exchanger such that the number of restrictions is the same between scaled and prototype models.

Heat transfer rate

The heat transfer rate predicts the gain or loss of heat as a result of convection. The important factors for heat transfer process are the total heat transfer surface area, heat transfer coefficient and the temperature difference between the hot and cold fluid. Newton's cooling law states this as follows:

$$\dot{q} = hA\left(T_{surface} - T_{fluid}\right) \tag{6.19}$$

The objective is that the scaled model removes the equivalent amount of heat as all other heat exchangers under similar flow conditions and identical temperatures, then the following results in the case of the IHX:

$$\dot{q}_{scale} = 4 \cdot \dot{q}_{prototype} \tag{6.20}$$

$$A_{scale} = 4 \cdot A_{prototype} \tag{6.21}$$

This allows the design of the scaled parameters such that the heat transfer coefficient is identical, since the temperature difference is taken as identical based on the general requirement for component scaling outlined earlier.

Heat transfer coefficient

The relations for heat transfer coefficient for internal flows are functions of Re and Pr numbers. Since the fluid temperatures are preserved, as well as the mean fluid velocity, then the heat transfer coefficient is preserved. Similarly for the case of external flows, the preservation of Re and Pr can is achieved by maintaining an adequate external flow area such that the external fluid flow velocity is identical for the scale and prototype models.

Heat transfer surface area

The requirement is to preserve the ratio of heat transfer area with the ratio of heat load. This is accomplished easily by also imposing the ratio of total number of tubes to be proportional in the same manner as well between scaled and prototype models, under the assumption of equal tube lengths. This last assumption is one of the general requirements explained earlier in this section in order to preserve overall component height and fluid residence time.

The requirements imposed above do not conflict one another. For this reason the scaling process of the components with an advanced design was performed without any problems, this is the case of the DHX, IHX and primary pumps. In the case of the NDHX, the process outlined above is used to downscale from a single equivalent heat exchanger into eight prototypical heat exchangers. Next section includes detailed design data for scaled and prototypical heat exchanger as a result of this study.

6.4.3 Model to prototype tables

The following tables display the geometric parameters employed in the construction of the reactor model. In addition reference performance parameters are also shown to illustrate the expected deviations from employing scaled versus prototypical component representations. The data for the IHX and DHX in tables 6-1 and 6-2 was obtained using the PRIMEX code. Data for the NDHX was obtained using the code described in section 5.5.

	Prototype IHX	**Up-scaled IHX**	**Ratio Scale/Prototype**
Radial rows of tubes	43	37	1.16
Total number of tubes	9728	38450	3.95
Heat load	225 MW_{th}	900MW_{th}	4.00
Nominal length	8.33m	8.28m	0.99
External Aflow	0.566m^2	2.19m^2	3.87
Internal Aflow	0.359m^2	1.419m^2	3.95
O.D. Heat Transfer area	2.59x10^4 m^2	1.03x10^4 m^2	3.97
ΔPtube	1.27x10^5 Pa	1.31x10^5 Pa	1.03
ΔPshell	1.43x10^5 Pa	1.43x10^5 Pa	1.00
LMTD	30.3 K	30.3 K	1.00

Table 6-1 Scaling parameters ratio for the IHX

	Prototype DHX	**Up-scaled DHX**	**Ratio Scale/Prototype**
Radial rows of tubes	4	4	1.0
Total number of tubes	504	3841	7.62
Heat load	2.25 MW_{th}	18MW_{th}	8.00
Nominal length	2.65m	2.58 m	0.97
External Aflow	0.082m^2	0.641m^2	7.81
Internal Aflow	0.019m^2	0.142m^2	7.88
O.D. Heat Transfer area	45.8 m^2	349.4 m^2	7.63
ΔPtube	2.82x102 Pa	2.69x102 Pa	0.95
ΔPshell	1.38x102 Pa	1.38x102 Pa	1.00
LMTD	91.8 K	91.8 K	1.00

Table 6-2 Scaling parameters ratio for the DHX

	Prototype NDHX	**Up-scaled NDHX**	**Ratio Scale/Prototype**
Radial rows of tubes	7	56	8
Total number of tubes	211	1690	8.01
Heat load	2.25 MW_{th}	18MW_{th}	8.0
Nominal length	3.50 m	3.50 m	1.0
External Aflow	5.1 m^2	40.8 m^2	8.0
Internal Aflow	0.41 m^2	3.32 m^2	8.1
O.D. Heat Transfer area	680 m^2	5510 m^2	8.1
Horizontal tube angle	15.0^o	15^o	1.0
LMTD	210 K	210 K	1.00

Table 6-3 Scaling parameters ratio for the NDHX

6.4.4 Plant Nodalization

A nodalization diagram was built to demonstrate the plant model constructed in RELAP5-3D. This diagram includes all the plant components, such as the core (1-8), the IHX (43), intermediate loop (52), the DHX (25), the NDHX (62). The model is explained in further detail in appendix C where all geometric properties are listed, along with the input file itself. The nodalized diagram is illustrated in figure (6-3).

6.4.5 Thermal-Hydraulic Initial and Boundary Conditions, Closure Relations and Decay Heat

Initial conditions are important in order to allow the computational tool to reach convergence to a solution at every time step. There are two types of problems that can be solved using RELAP5-3D and the model built: steady state problems and transient problems. Steady state problems are run until the code reaches steady conditions in temperature and fluid velocity over all mesh volumes and cell junctions. Once this condition is satisfied, the user can employ an option within the code to rewrite the problem input file updating the initial conditions, such that an updated problem may be started from steady state conditions.

Transient problems require that the problem is initiated from steady-state conditions. A proper transient problem may be initiated from at the start of the transient being studied, or some time into the transient, to allow the user observe the steady nature of the problem prior to the transient event.

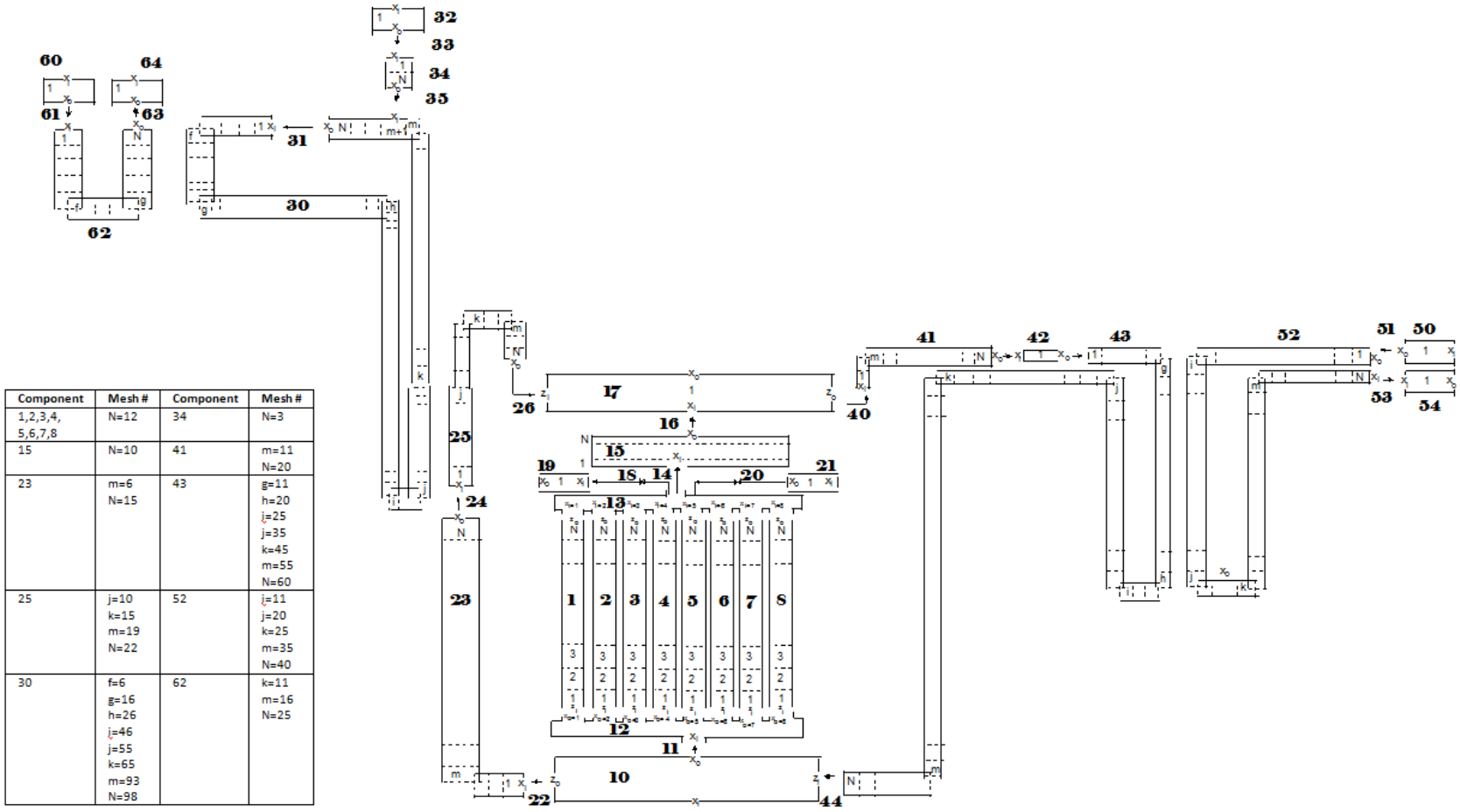

Component	Mesh #	Component	Mesh #
1,2,3,4, 5,6,7,8	N=12	34	N=3
15	N=10	41	m=11 N=20
23	m=6 N=15	43	g=11 h=20 i=25 j=35 k=45 m=55 N=60
25	j=10 k=15 m=19 N=22	52	i=11 j=20 k=25 m=35 N=40
30	f=6 g=16 h=26 i=46 j=55 k=65 m=93 N=98	62	k=11 m=16 N=25

Fig. 6-3 Plant Nodalization diagram

The closure relations for friction and form losses, as well as wall heat transfer for the multiple geometries in the problem are input manually, except for the simple pipe geometries, where the code can automatically predict the friction and heat coefficients. For the case of pebbles, curved pipe, cross-flow on a bank of tubes and other geometries, the correlations presented in section 2.3 - 2.5 and 2.7 – 2.9 are specified in the RELAP5-3D model.

Finally, the study also requires the input of the decay heat time history for the core immediately after a reactor shutdown. RELAP5-3D includes the ANS-79 decay heat curve which is discussed by Todreas and Kazimi [1] as a function of time after reactor scram. This curve was employed in previous analysis and has been adopted for the study of transients, although future use of an alternate curve of the expected decay heat curve for the pebble bed, TRISO fueled core is recommended.

6.5 ANALYSIS PROCEDURE AND DATA EVALUATION

6.5.1 Steady state convergence

Once the model is assembled, the geometric parameters properly input, the boundary conditions set appropriately, and reasonable initial conditions are inserted, the code is run and the results are evaluated. The first run always starts in transient mode. The reason is that the initial conditions for fluid velocity and temperatures cannot be the true values at steady state, since these values vary for every mesh cell in a component, and the initial conditions are known roughly and single values can be estimated for the whole component, not for every mesh cell.

The solution algorithms will update the scalar and vector parameters of the problem as the code marches in time, until the problem time limit is reached. Since the temperatures change during the convergence, these changes lead to artificial reactivity insertion, which causes energy generations variation in the reactor core. To avoid this, it is important to input appropriate initial conditions for the problem.

RELAP5-3D contains a sub-routine called PYGMALION, which can be run to re-write an input file by replacing all the initial condition cards with the information provided by a problem already run. The idea is that after the code is run, steady state conditions can be reached, and the information can be used as the input for another input file, where the only difference between the previous and current input files are the initial conditions. This process can be repeated manually several times until the initial conditions are sufficiently good to allow the code to run without making significant changes in the problem sub domain properties, therefore reaching a true steady state condition. This process is also recommended to achieve faster run times once true steady state problems are run.

6.5.2 Performing transient analysis

Once the true steady state RELAP5-3D model was built based on the analytical relations output by the NDHX calculation sheets, in addition to the geometric data for the DHX output by the PRIMEX code appropriately converted to SI units, the analysis consisted of investigating the parameters which affected the system cooling ability during the worst transient conceptually envisioned as outlined in section 3.5.2. A change in the parameters affecting the any the DRACS heat removal mechanism requires of application of the steady state convergence process anew to determine the effect of the variation prior to a transient study.

6.5.3 Transient description

The plausible transient events subject to analysis are described in section 3.5.3, where LOFC, LOHS and LOCA transients are described, including their respective variations due to the magnitude of the assumed failure, such as break size, asymmetric and partial heat removal capacity loss. The transients analyzed in this section are particularly interesting in analyzing the performance of the DRACS design presented in the previous chapter during the transient. Previous work by Galvez et. al. [7] has analyzed the performance other safety systems, such as the active scram, the passive core shutdown and the negative reactivity feedback control system. Instead, this report focuses on the performance of the DRACS system as a passive heat removal system.

To best illustrate the behavior of the DRACS, the transient selected assumes a complete loss of primary heat sink simultaneous with the primary pump trip and the reactor scram. This is accomplished by switching to decay heat mode, tripping the primary and secondary pumps and also blocking the primary coolant flow path to the IHX, to eliminate natural circulation cooling through the core-IHX loop. Previous analyses have demonstrated that in a LOFC transient, the IHX provides significant early cooling to the shutdown core due to the thermal inertia of the metallic structure of the heat exchanger.

The pump trip is very short, forcing the pump to stop completely in 0.1 seconds. This allows the fluid motion to continue due to inertia alone. The heat sink is removed in 0.2 seconds. This is the smallest value which can be used to stop the secondary side flow and block the IHX flow path without causing numerical instabilities and other undesired phenomena. Finally, the decay heat mode is turned by imposing the power history curve shown in figure 4-5 as the net power output by the core. This switch occurs instantaneously at the time of the transient.

The transient occurs at 100 seconds, given that the problem is started from the steady state full power initial conditions. This allows a transient to be started from the beginning if necessary, but 100 seconds is chosen for illustration purposes.

6.5.4 Criteria for acceptability

The acceptability criteria for the point design of the DRACS system is most importantly based on the requirement to preserve the peak core outlet temperature under 760 °C at any time during the selected transient. Another criteria for acceptability is that the DRACS system's overall size meets the constrains imposed by the reactor building design, included available vertical height from core to the helical heat exchangers and the available space for the NDHX chimney. Finally the requirement to maintain the DRACS salt coolant temperature above freezing point and preserve a reasonable margin for freezing is also important.

6.6 RESULTS

The insertion of the shutdown control elements into the core is expected to bring the reactor power down very quickly. As a consequence, the average fuel temperatures come down rapidly as the power per pebble is reduced greatly from the full-power value; however, pebble fuel layer temperatures are always higher than coolant surface temperatures, as the reactor is still producing a decay heat. The following curve is the primary safety indicator of the transient study. This figure seeks to demonstrate, that the reactor core does not exceed thermal safety limits for fuel and metallic structures in contact with core outlet coolant.

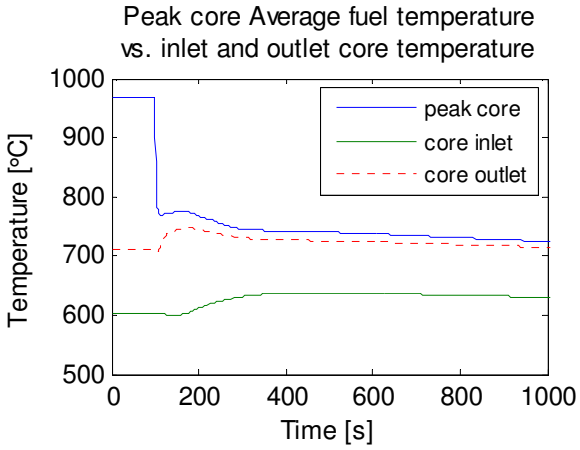

Fig. 6-4 Comparison of peak core average fuel temperature to inlet and outlet core coolant temperatures

Natural circulation loops performance

The following figures are detailed representations of what happens within safety, cooling and air passive natural-circulation driven coolant loops in the mentioned order. In each loop, the inlet and outlet temperatures, along the flow rate history, the corresponding pressure drop of each loop component and the temperature difference driving the flow are shown. Figure (5-1) illustrates the corresponding loop and the nomenclature employed.

Safety loop

The DHX inlet temperature is below the outlet temperature prior to the transient due to the restricted flow in parallel with the core. Once the transient is initiated, a flow reversal is ensued short after, and this can be observed with the temperature history shown in the figure below.

The DHX inlet temperature reaches a maximum of ~750 ^{o}C at around two minutes into the transient. This is also the core peak outlet temperature during the transient.

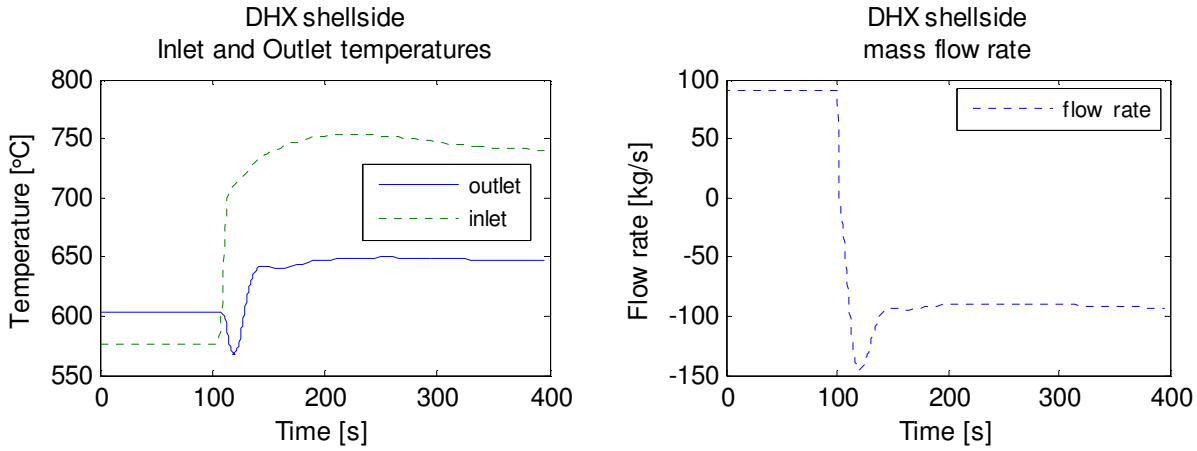

Fig. 6-5 Safety loop hot and cold fluid temperatures during transient (left), mass flow rate through the safety loop (right)

The mass flow rate profile of the safety loop indicates a smooth flow reversal in the DHX from steady full power, where a bypass flow exists through the fluidic diode, to decay heat removal mode through the DHX where hot salt enters the top of the DHX and is cooled, flowing downward back to the core bottom inlet plenum. The flow rate history reaches a maximum spike, then reaches an equilibrium flow rate, quickly dampening reduced oscillatory behavior shown quickly after reaching the maximum reversed flow rate value.

The temperature difference across the safety loop quickly reaches steady value of ~100 kg/s, which then slowly decreases. The initial temperature spike observed is due to the short, temporary trough in the DHX outlet during flow reversal.

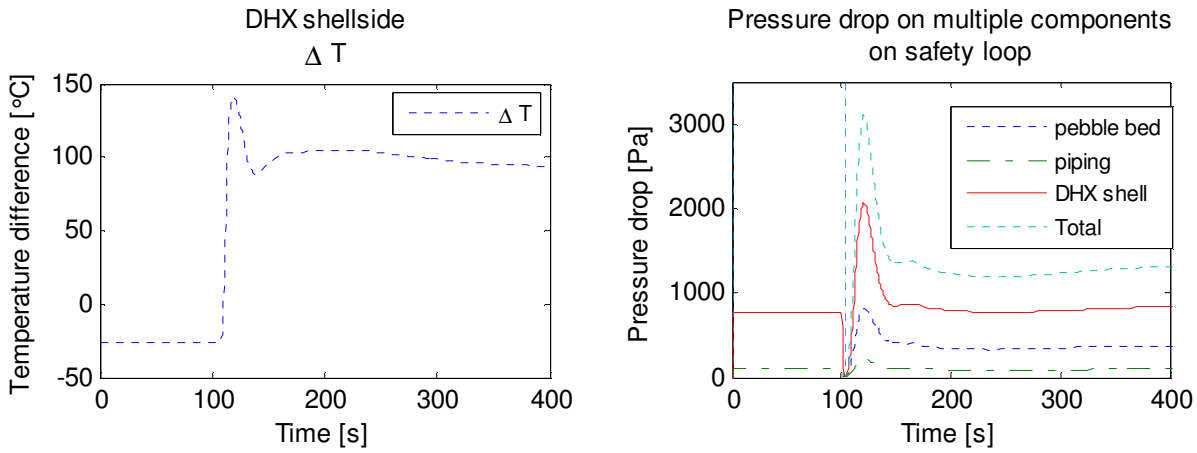

Fig. 6-6 Safety loop temperature difference (left), pressure drop of components in the safety loop during transient (right)

The pressure drop of each component in the safety loop is in constant prior to the transient. The pressure drop across the pebble bed is very large, and is not included in the scale of the plot. The pressure spike shown by all components is due to the spike in the mass flow rate, early in the transient. Shortly after, steady values are reached.

The pressure drop across the DHX shell is larger than the pressure drop at the core, due to the much smaller flow area and high resistance of baffle restricted cross flow. Pressure drop through all components are, however in comparable order of magnitude. The total pressure drop is the amount of buoyancy head that is required to establish natural circulation flow.

Cooling loop

The cooling loop steady inlet and outlet temperatures are plotted. During the transient, the DHX heat exchanger switches from a parallel-flow to a counter flow heat exchanger. In addition, the hot shell side temperatures are much higher than during steady state full power. For this reason, the hot temperature of the cooling loop quickly rises and reaches a steady level, when natural circulation becomes established.

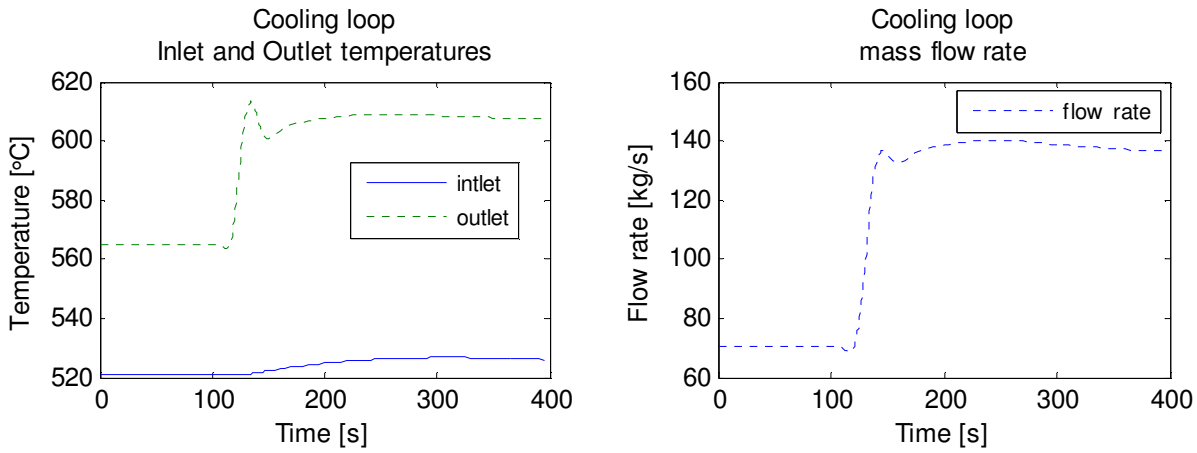

Fig. 6-7 Cooling loop hot and cold fluid temperatures during transient (left), mass flow rate through the cooling loop (right)

The mass flow rate history during the transient, similarly quickly establishes to the steady cooling mode at higher flow rates. The peak value is reached at ~2 minutes into the transient and drops slowly thereafter.

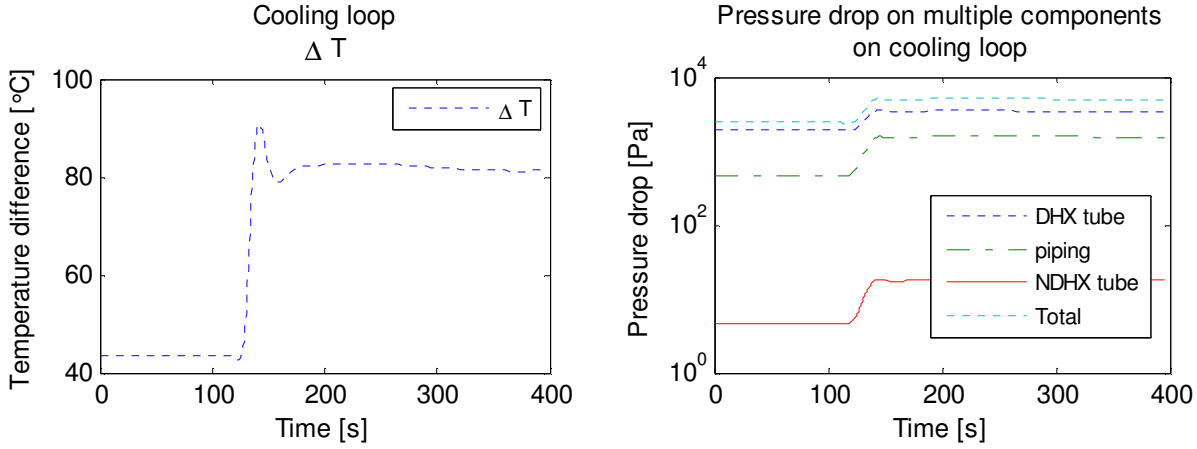

Fig. 6-8 Cooling loop temperature difference (left), pressure drop of components in the cooling loop during transient (right)

The pressure drop distribution shows that the pressure drop of the coolant through the DHX tube side and the connecting pipe are two orders of magnitude higher than the pressure drop through the NDHX tube side coil. This is because the flow area combined of all NDHX tubes is much greater than the DHX, in addition to a much larger pipe inner diameter. The total friction pressure drop amounts to ~ 4300 Pa, which is the buoyancy head at this temperature difference across the DRACS loop.

Air channel

Prior to the transient, air flow is restricted through the air inflow dampers. This reduces the air flow rate and increases the residence time of air as it travels through the chimney. Once the transient begins, the dampers are opened fully, and mass flow rate of air is incremented. At higher flow rates, air exits the chimney at lower temperatures. The temperature difference across the chimney rapidly changes after the transient.

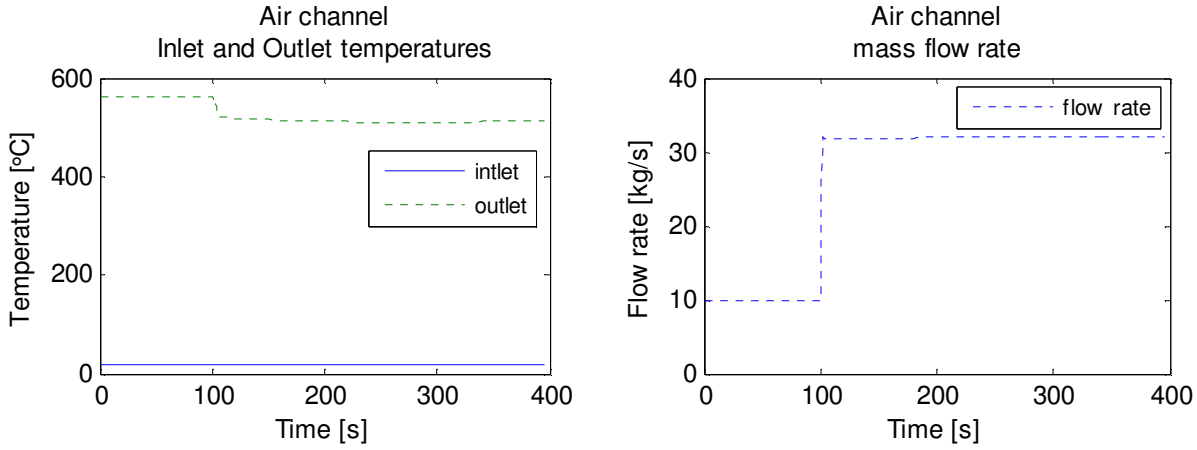

Fig. 6-9 Air channel hot and cold gas temperatures during transient (left), mass flow rate through the air channel (right)

The pressure drop prior to the transient is very high, primarily due to the near-closed air dampers. Upon the scram signal, the dampers are opened near immediately and high air flow is quickly established. For a brief period of time, air flows at higher rates under the same surface temperature in the NDHX. When the surface temperature distribution is altered, the thermophysical properties of air are altered, and a higher flow resistance is reached.

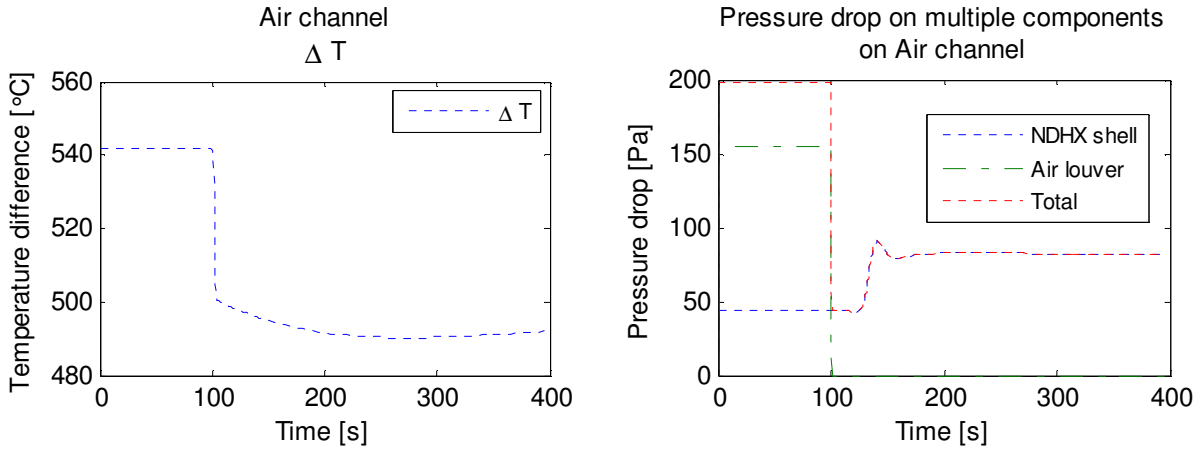

Fig. 6-10 Air channel temperature difference (left), pressure drop of components in the air channel during transient (right)

Energy transfer

In order to understand the transient, it is important to understand the heat flow process in this multi-component system. The energy generated after shutdown by decay heat is expected to be released to the environment as heated air through the NDHX, however, during the transient, the amount of decay heat varies, and early on exceeds the heat exchanger capacity. In this period, excess heat is absorbed by the solid constituents of the system, and by the loop fluids. The first set of curves represents the heat flow between heat sources and sinks connected by their corresponding loop. The second set of loops represents the transient heat absorbed by the metallic heat exchanger structures, in this case, the tubes as the volume of the outer casing and internals are not taken into consideration. The last set of curves represents the heat absorbed by the fluid volumes within each natural circulation loop.

Figure 6-11 shows the heat flow distribution and the heat produced by the core. Early in the transient, ~ 45 MW of heating power is released by the core, but only ~ 22 MW is removed by the safety loop. Similarly, ~20 MW is removed by the cooling loop, and only ~ 18 MW is removed by the secondary air flow in the NDHX. This trend continues until ~700 seconds, when the reactor decay heat curve drops below the heat removal rate of the safety loop. The graph on the right shows that after ~ 1000 seconds, the amount of heat removed by both, the safety and cooling loops slightly exceeds the decay heat curve, and closely follows this in a decaying trend.

The air loop continues to remove ~18 MW, closely matching the design basis heat load power and does come down along with the decay heat curve. The fact that the air loop removes a nearly constant heat load is reasonable, because the NDHX is designed to have the largest LMTD and thermal resistance of any component in the DRACS system, to minimize the potential for freezing of the salt. Thus the heat transferred to the air is quite insensitive to the temperature of the salt. Furthermore, this shows that the air dampers can be used to effectively control the heat removal rate by the DRACS, since the heat removal rate is closely linked to the air flow rate. This is a positive feature, because this means that the DRACS system can be closely controlled to prevent overcooling from occurring.

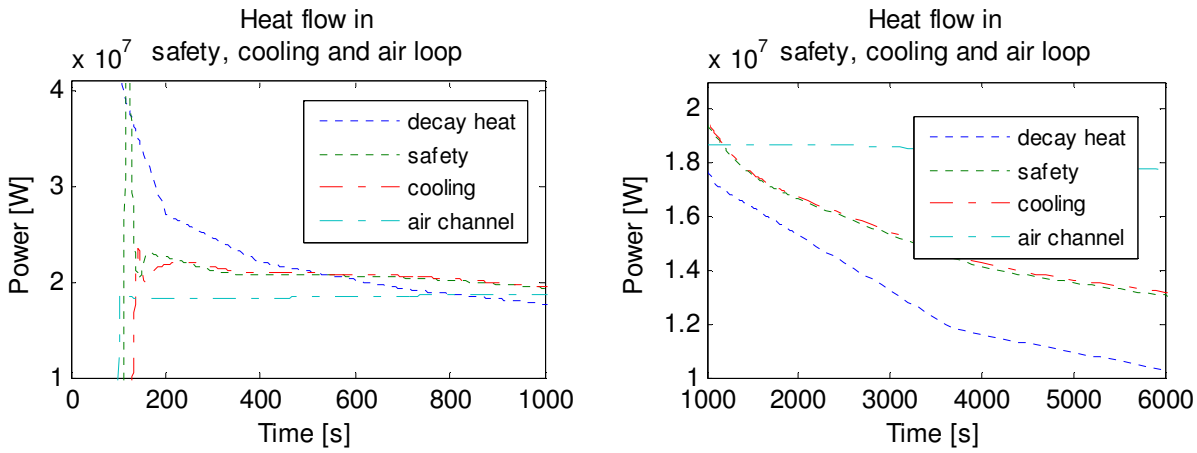

Fig. 6-11 Heat flow in natural circulation loops during first 1000 seconds (left), during the next 5000 seconds into the transient (right)

The response of the NDHX air side shows that the air dampers will need to be restricted to reduce heat removal at a time ~1200 seconds (20 minutes) into the transient. The amount of air restriction to maintain temperatures and its time variation was not investigated here.

Energy storage

The following figures illustrate the amount of heat absorbed by the solid materials that have sufficient thermal capacity to absorb or release a significant amount of heat during the transient.

Safety loop components

In the safety loop, the pebble bed, its corresponding graphite moderators and the upper reflector are large voluminous graphite structures that are expected to absorb and release heat. Immediately after the transient, the thermal inertia of the core moderators absorbs the excess heat, while the upper reflectors and the pebble bed thermal inertia release heat to the surrounding fluid. At around 600 seconds into the transient, the DRACS heat removal capability exceeds decay heat generation and all core structures are effectively releasing heat at ~ 500 kW as shown in Figure 6-11.

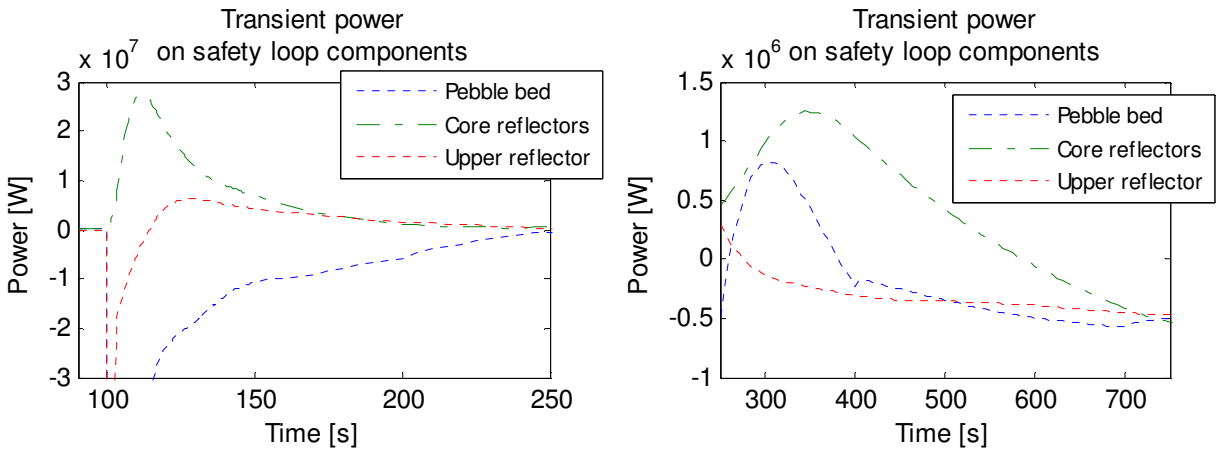

Fig. 6-12 Transient heat flow in heat releasing or absorbing structures in the core during the first 250 seconds (left), during the next 750 seconds into the transient (right)

Cooling loop

The metallic structure of the DHX also absorbs energy during the transient temporarily. The Figure 6-13 indicates that immediately after the transient, the DHX gives off a small amount of heat, due to the cold fluid reversal, then a peak occurs and reaches ~13 MW of power, which is absorbed by the DHX and quickly drops to a low positive value which implies heating of the structure until ~ 200 seconds, when the structure starts to cool down at a low cooling rate.

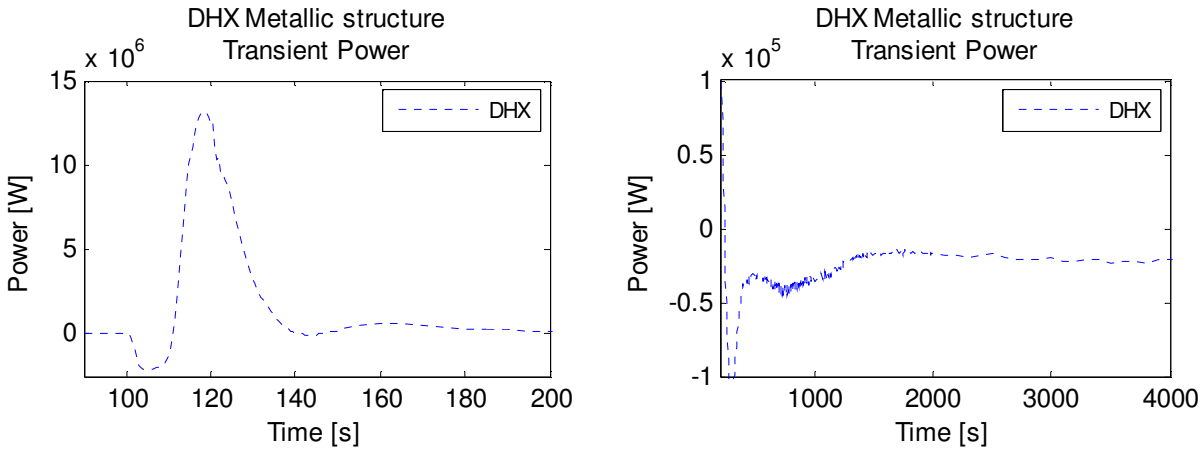

Fig. 6-13 Transient heat flow in the DHX metallic structure during the first 200 seconds (left), during the next 3800 seconds into the transient (right)

Air loop

The NDHX releases heat immediately after the transient due to the sudden step variation of the air flow rate on the external side. ~ 400 seconds after the transient is initiated, steady average metallic structures are reached and the metallic structure beings to heat up for another ~ 1400, when the metallic structures start to cool off, releasing heat until the dampers are re-adjusted. In

this simulation, the dampers are not closed to preserve temperatures in the NDHX and prevent overcooling.

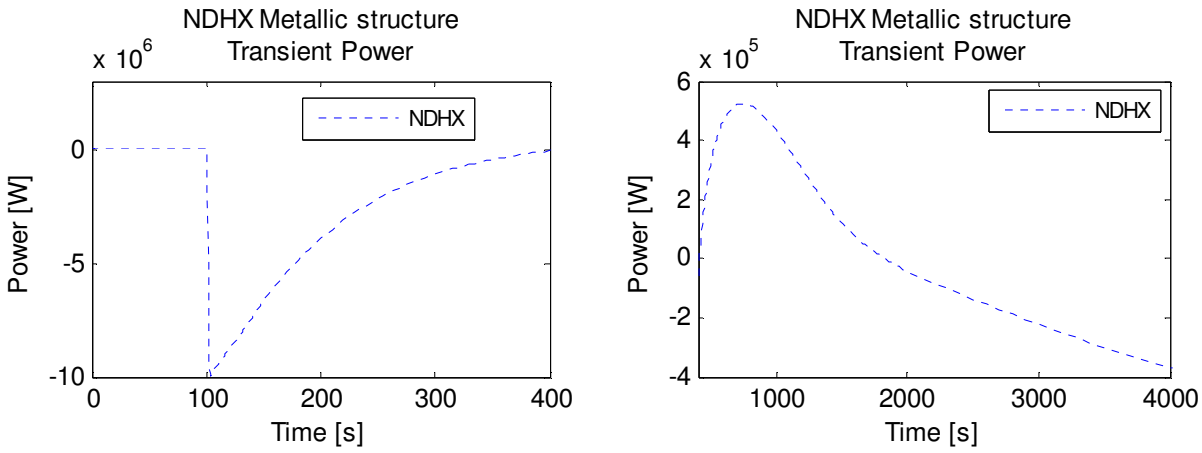

Fig. 6-14 Transient heat flow in the NDHX metallic structure during the first 400 seconds (left), during the next 3600 seconds into the transient (right)

Fluid Thermal storage

In addition to the solid structures, the average temperatures of the safety and cooling bulk fluids increase early in the transient, as these fluids absorb excess energy which the heat exchangers cannot remove for brief periods of time, as steady hydrodynamic conditions are reached. The figure below shows the thermal storage of energy of the fluids during the transient and is calculated as follows:

$$\dot{q} = \rho V C_p \frac{d\bar{T}}{dt} \qquad (6\text{-}22)$$

where the fluid volume is predicted from geometric calculations, density and heat capacity are approximated as constants and evaluated at their average values. The bulk temperature for time derivative evaluation is calculated based upon the volume average for all of the salt volume as follows:

$$\bar{T} = \frac{1}{V}\oint T dV \qquad (6\text{-}23)$$

The calculated transient thermal storage heating rates are shown for the safety and cooling loops, in two different scales. The left plot of Figure 6-15 shows the first 400 seconds into the transient, and the plot in the right shows the reminder 5600 seconds, where much lesser storage heating magnitudes are observed. The numerical instability observed is likely caused by the calculation of the temperature time derivative. In this stage of the transient, the code automatically varies the time step of the solution constantly thus causing this variation.

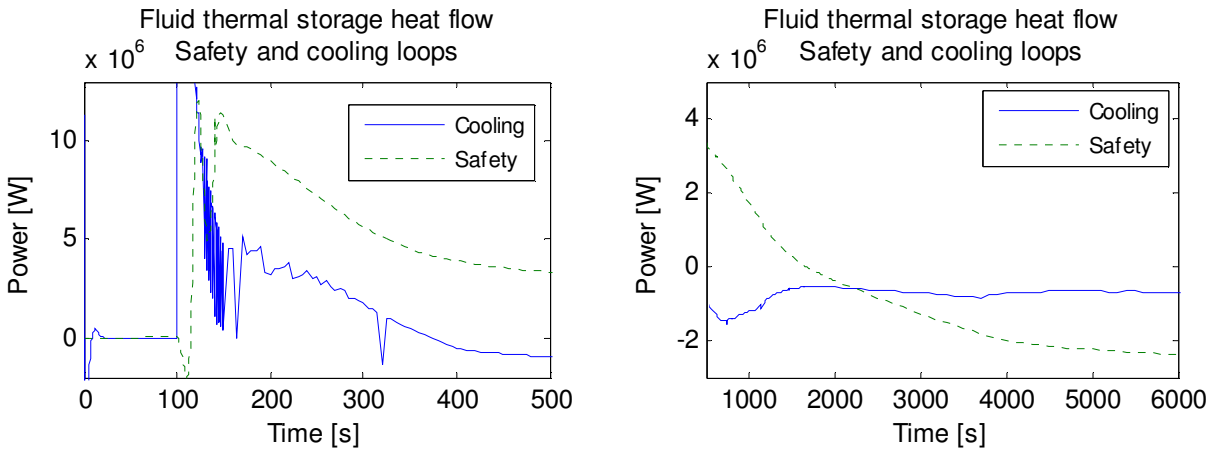

Fig. 6-15 Fluid transient thermal energy storage in the safety and cooling loops during the first 500 seconds (left), during the next 5500 seconds into the transient (right)

It can be observed that a significant amount of heat is absorbed early in the transient by the fluid alone. This is the amount of energy released during decay heat removal and not transferred and dumped as waste heat. At the peak, 15 MW of energy is absorbed by the primary coolant. The cooling loop fluid shows numeric instability in the calculation, however, similar quantity is observed. The spike observed, but not shown reaches very large power levels and this is caused by the large temperature time derivative and does not represent necessarily accurate power levels. After 1000 seconds, the power levels have dropped to below 3 MW, and decreases below zero indicating overall temperature decrease in the safety loop. This switch occurs ~500 seconds earlier in the case of the DRACS loop.

Solid structure temperature distribution

Figure 6-16 represents the average temperature of the heat transfer solid constituents. The temperature distribution along the core shows the temperature averaged over the pebble over core axial region. A short period of time after the transient starts the temperature profile drops to the steady value 650 ^{o}C and 750 ^{o}C at the inlet and outlet core regions respectively. These values compare well with the corresponding inlet and outlet primary coolant temperatures of 645 ^{o}C and 740 ^{o}C.

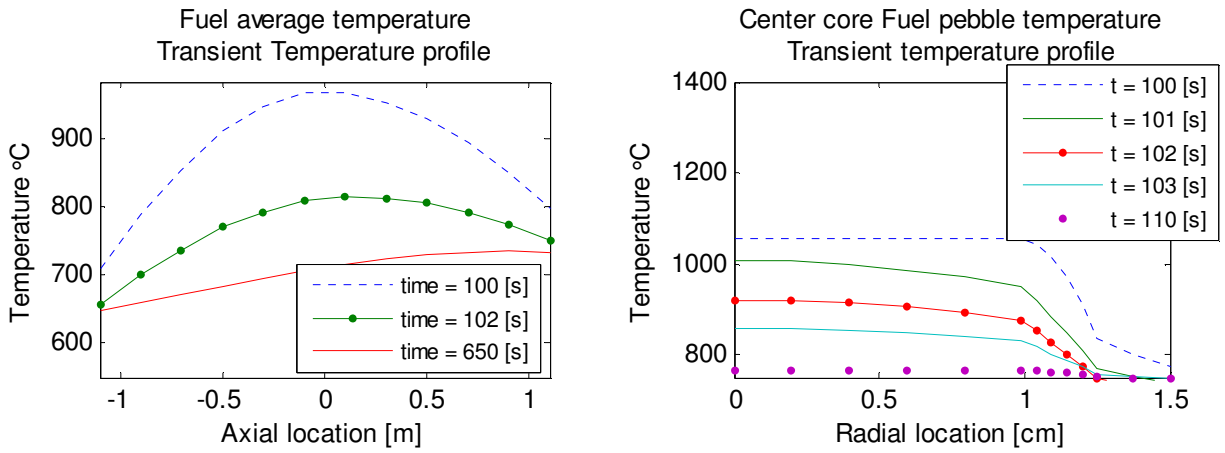

Fig. 6-16 Transient average fuel temperature profile along the core (left) and DHX transient average metallic structure temperature (right) for before and after the transient

The temperature profile of each pebble is shown in the left plot of Figure 6-16 for various times during the transient. The temperature sharply decreases within a few seconds into the transient, reaching a near flat temperature across the pebble during steady decay heat mode.

The profile of the average metallic structure temperature of the DHX is also plotted. During the transient, it can be observed that for a brief period, the temperature in the lower side is higher than the upper side of the heat exchanger and this is caused by flow reversal. The axial temperature distribution rises to a near linear temperature distribution from 625 ^{o}C to 700 ^{o}C. This distribution remains essentially constant during the rest of the transient.

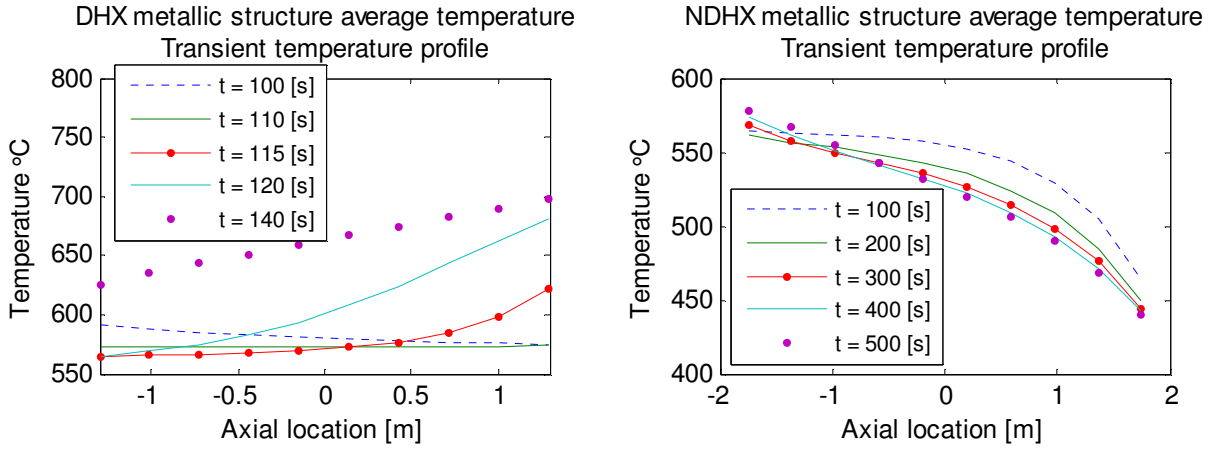

Fig. 6-17 NDHX transient average metallic structure temperature (left) and radial profile transient temperature distribution of a pebble located in the central region of the core (right)

Similarly, the temperature profile of the NDHX metallic structure is plotted in Figure 6-17. The changes observed during the transient are smaller in magnitude compared to those observed in

the DHX. In this case, the bottom of the NDHX corresponds to the rightmost positive axial location.

6.7 SUMMARY

The transient analysis performed in this chapter demonstrate the transient transfer of heat is a complex process, where fluids and solid structures interact temporarily storing energy as the fluid flow rates fluctuates during hydrodynamic transition. The analysis tool employed in this study demonstrates the capacity to provide an insight into the physical process occurring during a transient. The analysis shows that the DRACS passive heat removal system accomplishes the goal of maintaining the peak coolant temperature below the safety limit operating in natural circulation. The study also determined that air flow rates must be throttled beginning about 20 minutes after the transient to control overcooling of the reactor.

6.8 REFERENCES

[1] N. E. Todreas, M. S. Kazimi *Nuclear Systems I Thermal Hydraulic Fundamentals.* Taylor & Francis (1993)

[2] W. Ambrosini, *Basic concepts on numerical methods and Relap5equations*. RELAP5-3D Course, San Pierdo a Grado, Pisa, Italy. April (2008)

[3] K. O. Ott, R. J. Neuhold, *Introductury Nuclear Reactor Dynamics.* ANS Publications, La Grange Park, Illinois (1985)

[4] Y. Mori, W. Nakayama *Study on forced convective heat transfer in curved pipes (1st report laminar region).* Int. J. Heat Mass Transfer. 8 (1965) 67-82

[5] Users problem report session. *International Relap5 Users Group* C*onference proceedings '10*. Idaho National Laboratory West Yellowstone, MT (2010)

[6] 0. P. Bergelin, G. A. Brown, and A. P. Colburn, *Heat Transfer and Fluid Friction During Flow Across Bank of Tubes -V: A Study of a Cylindrical Baffled Exchanger Without Internal Leakage.* Trans. ASME, 76 (1954) 841-850.

[7] C. Galvez, et. al., *Modeling and Transient Simulation of the PB-AHTR using RELAP5-3D.* Proceedings of ICAPP '10, San Diego, CA, June (2010)

[8]. RELAP5-3D CODE DEVELOPMENT TEAM, RELAP5-3D Code Manual Volume I: Code Structure, Systems Models and Solution Methods rev. 2.3, 1-1, Idaho National Laboratory, Idaho Falls, (2005)

[9] A. Niquille *Modeling and Transient Analysis for the Modular Pebble Bed Advanced High Temperature Reactor (PB-AHTR)* M.S. Project Report UCBTH-07-002 (2007)

[10] A. Griveau et al., *Transient thermal response of the PB-AHTR to Loss of Forced Cooling.* Global 2007, Boise, Idaho, September 9-13, 2007.

[11] F. P. Incropera, D. P. Dewitt *Fundamentals of Heat and Mass Transfer 5th edition.* John Wiley and Sons, New York (2001)

[13] J. J. Duderstadt, L. J. Hamilton *Nuclear Reactor Analysis* John Wiley and Sons, New York (1976)

7. VERIFICATION STUDIES

7.1 ARGUMENT FOR VERIFICATION

In this dissertation, two different studies were performed thus far 1) The design of a passive heat exchanger given a heat load and the heat sink and heat source temperatures; and 2) the transient analysis of this design employing a nuclear reactor design. The results were presented in the appropriate sections of the document including a discussion of the significance of the results.

The overall objective of this study is to demonstrate that the resulting design can satisfy the safety criteria in this reactor. However, the results documented in section 5.6 and section 6.6 of this dissertation are not sufficient to demonstrate the efficacy of the safety system, since the analysis performed cannot be benchmarked against existing data deriving from the operation of passive safety systems and transient operation of pebble-bed, salt cooled nuclear reactors, simply due to the inexistence of this information. Similarly, there is an absence of readily available simulation tools to perform this present study using other computational tools. The comparison with data from alternate studies or operational data would provide an estimate on the accuracy and preciseness of the models developed in this study. Cacuci [5] illustrates the relation between model verification and model qualification through the following diagram.

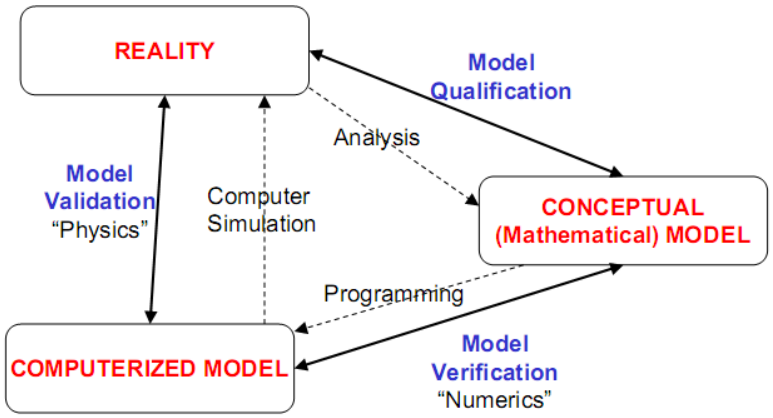

Fig. 7-1 Model verification relationship

In light of this, it is necessary to obtain other sources of reference data to compare the present findings against, thus establishing a benchmark for the results and a verification of the methodology. The following sections establish a comparison between the present safety system design versus comparable safety system designs for comparable nuclear reactor systems and an alternative approaches to perform transient analysis of the nuclear reactor system subject to this study.

7.2 SAFETY SYSTEM DESIGN COMPARISON

A literature review within the Journal of Nuclear Design and Engineering provided information of the technical design of the passive safety system employed in the European Fast Reactor (EFR) and the Demonstration Fast Breeder Reactor (DFBR), a Japanese design. Both are heavily documented by Farrar [1]

	Parameter	**unit**	**Description**				
DRACS description	Reactor design		PB-AHTR		DFBR	EFR	
	Total reactor thermal power	MW	900	900	1600	3600	3600
	Coolant type and flow mechanism		Flinak Nat. C.	Sodium Nat. C.	Sodium Forced	Sodium Nat. C.	Sodium Forced
	Number of lops		8	8	4	6	6
	Power per loop	MW	2.25	2.25	11	15	15
	Total power (% of full power)	MW	18 (2%)	18 (2%)	44(2.75%)	90 (2.5%)	90 (2.5%)
Primary side	DHX type		Straight	Straight	Straight	U tube	Straight
	Heat transfer area per loop	m^2	55.27	55.27	41	96	68.8
	Height	m	2.6	2.6	6.1	5.08	5.08
	Primary flowrate per loop	kg/s	8.62	8.62	39.7	161	178.4
	Primary side ΔP	Pa	465	465	785	611	757
	Inlet/outlet temperature	^oC	760/656	760/656	550/333	530/456	530/464
Loop side	HX Height difference	m	8.0	8.0	21.2	34.1	34.1
	Loop flow rate per loop	kg/s	17.37	12.44	46.1	68	71.7
	Loop ΔP	Pa	4211	2855	23540	13770	18000
	Cold/hot leg temperature	^oC	556/626	568/712	285/472	333/505	329/494
Air side	NDHX type		Helical	Helical	Serpentine	Helical	Serpentine
	Heat transfer area per loop	m^2	688.8	503.7	1500	2980	1282
	Stack height	m	20.0	20.0	34	37.4	37.4
	Air flow rate	kg/s	4.04	3.31	59.7	69.9	105.7
	Air side ΔP	Pa	159	161	2200	170	500
	Inlet/outlet temperature	^oC	20/570	20/645	50/231	35/245	35/174

Table 7-1 Comparison with other DRACS design

The table above refers to values from the DRACS point design reported in section 5.6. The alternate sodium cooled DRACS design, is a point design taken from the analysis performed in section 8.5.2 with a comparable height as the reference salt cooled DRACS point design.

The designs obtained for the salt and sodium version of the DRACS are comparable to the natural circulation sodium design for the EFR, however, the hot temperatures for the air, loop and primary side largely distinguish the PB-AHTR with the other two reference designs. This is due to the requirement to preserve primary and safety loop salts well above the freezing point, which is around 450 ^oC.

Both PB-AHTR safety DRACS designs presented here are not optimized designs, rather reference point designs. The criteria and methodology for optimization is discussed in the next chapter.

7.3 SOURCES OF DISTORTION

The primary source of potential error identified in the analysis performed, is the calculation of the equilibrium flow rate established by the balance between buoyancy and friction in the air channel. The derivation of the air density distribution along the heat exchanger assumes a linear temperature change, from cold to hot conditions.

$$T_{(x)} = \frac{T_h - T_c}{L} x + T_c \tag{7-1}$$

Applying the ideal gas law:

$$\rho_{(x)} = \frac{P_c}{\overline{R} T_{(x)}} \tag{7-2}$$

This density function is then integrated along the air heater channel to yield the following

$$\int_{L_{NDHX}} \rho_{(l)} g dl = \frac{P_c}{\overline{R} \Delta T} \ln\left(\frac{T_c}{T_h}\right) \int_{L_{NDHX}} g dl \tag{7-3}$$

This is the term which contributes to the overall buoyancy of the air chimney. The contribution is small however, in the case of tall hot air stacks, as it is the case of this study; the hot air stack is much larger in length compared to the heat exchanger tube bank length.

The linear assumption is questionable. The following figures are air temperature profile of the NDHX along the tube bank and the corresponding gas density profile, both obtained from steady decay heat removal mode RELAP5-3D calculations.

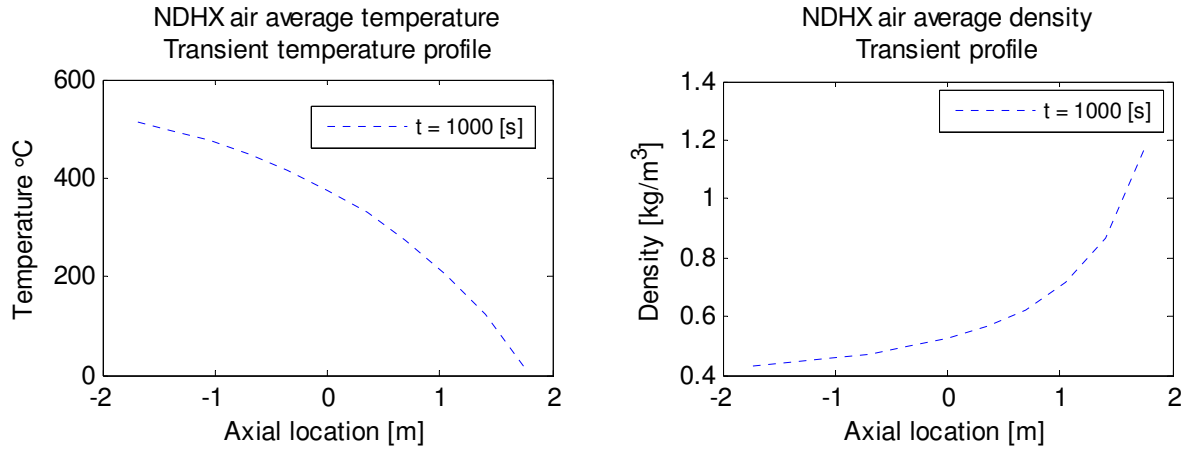

Fig. 7-2 Temperature profile of NDHX tube bank

As it can be observed, the temperature relation is not linear, but it is not far from linearity either. The density profile resulting from a linear temperature distribution follows in similar form as the figure from the right, due to negative exponential of temperature from equation (7-2). This may be due to the low temperature change liquid salts experience travelling on the tube side, relative to the large change of air in the shell side.

Another error contributing factor is the calculation of air pressure drop in the tube bank. Kays and London [6] report that pressure drop calculations in tube banks follow the following form:

$$\frac{\Delta P}{P_1} = \frac{G^2}{2g_c}\frac{v_1}{P_1}\left((1-\sigma^2)\left(\frac{v_2}{v_1}-1\right)+f\frac{A}{A_c}\frac{v_m}{v_1}\right) \tag{7-4}$$

Neglecting the area change due to free to frontal area ratio σ, expressing the specific volumes υ_1, υ_2 and υ_m as densities of incoming cold, hot and average density fluids respectively, and replacing the friction area to flow area ratio to the traditional length to hydraulic diameter ratio, the equations above takes the following familiar form:

$$\Delta P = \frac{G^2}{2\rho_c}\left(\left(\frac{\rho_c}{\rho_h}-1\right)+f\frac{L}{D_h}\frac{\rho_c}{\rho_m}\right) \tag{7-5}$$

The equation above involves two dynamic pressure multipliers. The first term is the acceleration component, which takes into account the expansion gases experience as heat is added, this expansion represents a force against the direction of flow, thus expressed as a pressure drop. The second term is the friction factor for tube banks in cross flow; however, this factor is multiplied by the ratio of the cold density and average fluid density. This once again, relies on the initial assumption of the linear temperature profile and the effect on the estimate average density. The proper manner to calculate this mean density is as follows:

$$\rho_m = \frac{1}{A}\int_{L_{NDHX}} \rho dA \tag{7-6}$$

From figure 7-1, one can observe that the average air density is far from the mean average of hot and cold densities, in fact, the average density is much closer to the hot density than it is to the cold density.

The integral shown in equation (7-6) is impossible to perform without knowing *a-priori* the temperature distribution. The present study assumed an exponentially decaying density distribution and obtained the mean density based on the endpoint densities.

The biggest discrepancy occurred when NDHX performance estimates were compared against steady state RELAP5-3D calculations, and moderate disparities were found particularly corresponding to pressure drop calculations.

The proper friction factors were input into the code input file. The spatial advancement scheme for the conservation of momentum in RELAP5-3D takes into account the volume expansion as air travels through the heat exchanger. The initial assumption was that friction factors at every mesh element would be automatically adjusted by the cold-to-average density ratio multiplier in each mesh element. However, C. Davis [7] indicated that RELAP5-3D calculates the pressure drop based on the density of the upstream volume. Thus, it does not include the cold-to-average density ratio factor and will underestimate the form loss when there is a large density change between two mesh elements. After this information was obtained, this multiplier was manually added to the input file, and results with greater agreement with the reference design were obtained.

7.4 TRANSIENT ANALYSIS VERIFICATION

Todreas [2] and Wylie [3] offer a methodology to perform analytical hydraulic transient analysis in loops, however their approach is limited to systems where a) transitions from laminar to turbulence flow regimes do not occur from component to component connected in a loop and b) friction factors can be expressed as a function of Reynolds number elevated to the same power everywhere in the loop. While this approach is useful to establish first order estimates, the existence of multiple components where the friction factors are functions part independent and part dependent of Reynolds numbers render this approach nearly to impossible to apply.

A suitable solution for the non linear differential equation arising from the application of the conservation of momentum equation along the loop requires complex numerical techniques. In addition, the problem of natural circulation of salts and gases, where both of the fluids undergo large temperature and density changes make it difficult to estimate average thermophysical properties, which are intended to represent the effective property of fluids for segments of the loop. Constructing a code which solves these equations maintaining the time dependence is a large effort, which results equivalent to constructing a smaller version of the RELAP5-3D code. Instead, the approach for verification of the transient analysis presented in section 6.6 is to employ other codes, which are commercially available and have been used for similar applications.

Other codes available for thermal hydraulic analysis of nuclear systems indicated by Ransom [4] are TRACE, CATHARE and RETRAN. These codes are used by the industry and the international community to study transients in nuclear power plants. The current limitation is the availability of thermophysical property libraries that encompass the fluids considered in this study. Another significant limitation expected in the usage of any other code is the availability of non-typical friction loss and heat transfer correlations. In this context, non-typical geometries refer to pebble beds, curved pipes, and cross flow configurations.

A complementary process to the verification of the transient analysis, is the validation of the transient models through experimentation and data analysis. Cacuci [5] describes the process of validation as a comparison of computational solution with the correct answer provided by

experimental data from benchmark cases or validation experiments. The experiments require careful design in order to replicate the key phenomena, as specified through a Phenomena Identification and Ranking Table (PIRT). The experiments require sufficient detailed data collection to allow conclusive comparisons of computations with experimental data to quantify model fidelity and model credibility.

7.5 SUMMARY

Verification of results for both the DRACS safety system design and the PB-AHTR transient analysis requires the implementation of a similar study employing different tools to obtain alternate data and use this as a basis for comparison. Design parameters for DRACS safety system of similar reactor designs were presented and compared against the reference design obtained in this study. Overall similarity was observed, and significant variations in the comparison were explained. Alternate tools to perform transient analysis exist, however are not readily available and may be subject to applicability limitations when studying liquid-salt cooled, pebble bed reactors.

7.6 REFERENCES

[1] B. Farrar et. al., *Fast reactor decay heat removal: Approach to the safety system design in Japan and Europe.* Nuclear Engineering and Design 193 (1999) 45-55

[2] N. E. Todreas, M. S. Kazimi *Nuclear Systems II Elements of Thermal Hydraulic Design.* Hemisphere Publishing Corporation (1990)

[3] B. Wylie, L. Streeter *Fluid transient in Systems*. Prentice Hall (1993)

[4] V. Ransom *Nuclear Reactor Systems: Thermal Hydraulic Modeling* Modeling, Experimentation and Validation Summer School, Idaho National Laboratory, June (2010)

[5] D. Cacuci, *Data Assimilation for Model Validation and Calibration* First International Verification and Validation for Nuclear Systems Analysis Workshop, Idaho Falls (2008)

[6] W. M. Kays, A. L. London, *Compact Heat Exchangers 3rd Edition* McGraw-Hill Book Company (1984)

[7] C. Davis, *Personal communication* Idaho National Laboratory, February (2011)

8. OPTIMIZATION APPROACH

8.1 OVERVIEW

In this chapter, multiple criteria for optimal design of the DRACS passive safety system are presented. First, the general considerations for the overall design of the nuclear plant are reviewed based on the reactor operation mode. In addition, more specific criteria corresponding to the design of the safety system is presented, including economic aspects, performance considerations and safety requirements. Finally, a study is performed evaluating the sensitivity of plant parameters, NDHX geometric parameters and coolant selection on the performance of the system.

8.2 OPTIMIZATION CRITERIA – HEAT GENERATION MODE

During steady state operation of the PB-AHTR power plant, it is desirable to operate using air dampers to control the cool air inlet flow rate through the NDHX, The use of the dampers helps maximize thermodynamic efficiency of plant by reducing heat losses to the environment, and is also necessary to control heat removal to prevent overcooling of the reactor. The current point design assumes air dampers valves which are at 85 % area of flow closed and in this position, 5.6 MW of heating power are removed through the air chimney.

After the transient is initiated, the air dampers are fully opened rapidly, and remain opened to remove the design heat removal requirement of 18 MW. This amount of heat is removed as long as the liquid salt temperature is higher than air temperatures, and this condition remains even after the core produces less than 18 MW of decay heat. For this reason, it is necessary to design an electro-mechanical air damper, which closes up gradually after DRACS salt temperatures decrease on average, which occurs after approx. 20 minutes. In order to prevent liquid salt from freezing, electrical heaters must be employed once decay heat power levels are lower than heat losses to the environment, as when long term core shutdown is envisioned.

During the early part into the transient, the temperatures of metallic materials change rapidly in the structural material. The design of both the DHX and NDHX heat exchanger must allow the expansion and contraction in metallic tubes. This is accomplished by employing bends and curves on pipes prior to junction with the inlet and outlet manifold.

8.3 OPTIMIZATION CRITERIA – OPERATION AND SAFETY

8.3.1 Normal Start-up and Shutdown

The usage of electric heaters around the DRACS cooling loop can maintain salt coolant in liquid phase during start-up. Similarly, usage of electric heaters can maintain a minimum coolant temperature and allow the DRACS loop to remain in liquid phase during core outage. In case of heat exchanger maintenance, liquid salt may be drained to a tempered storage tank to preserve salt in liquid phase.

8.3.2 Under cooling and overcooling

These undesired conditions occur when air louver is not set to accommodate air flow heat removal rate at identical nuclear heat generation rate.

To prevent under cooling, the passive safety system must be designed with a conservative margin of safety, which allows the sudden increase in cooling ability in case of insufficient cooling capacity. This can be accomplished by designing the air conveyance system of the DRACS assuming a reduced maximum aperture of the air damper. For instance, the design of the air conveyance system can assume a 75% flow area opening for the design basis of the system. In the event of under cooling, this louver gate can be fully opened, instantly providing additional cooling ability previously unavailable.

To prevent overcooling, the DRACS system must be able to adjust the amount of cooling, and this is accomplished by reducing the air flow through the chimney by throttling the air louver, located at the air inlet side. Another mechanism to control overcooling of the reactor core, is to add heat to the cooling loop by employing electric heaters, which can be the same heaters used during reactor start-up operations. Adding heat to the loop can compensate for heat removed to the environment and thus prevent overcooling events.

8.3.3 Diversity and Redundancy

The design of the DRACS safety system for the PB-AHTR assumes fully passive, natural circulation heat removal for all eight loops. In this design, the criteria for redundancy is clearly satisfied, since there are multiple loops available to perform a single task. However, all cooling loops and heat exchangers are identical and this configuration does not follow the criteria for diversity.

The adopted approach in the design of safety systems for the Gas Cooled Fast Reactor (GCFR) includes the development of diverse systems as discussed by Medwid [1], where a core auxiliary cooling system is designed independent of the shutdown cooling system, which incorporates natural circulation capabilities on the helium, water, and air sides as a backup to normal forced circulation capabilities. Additionally, Farrar [2] discusses a different approach taken by the European Fast Reactor (EFR) safety system design. In this reactor design, the direct reactor cooling consist of two diverse systems, one comprising of three loops operating in natural convection and the other three loops operating in forced convection, designed to remove the same amount of heat per loop, however the forced convection loop can also operate under natural circulation removing ~2/3 of the rated forced flow power per loop.

Based on the cited examples, the criteria for redundancy and diversity of the safety systems currently employed by the PB-AHTR can be optimized by implementing a similar approach as the GCFR and EFR designs employing different heat transport process on similar systems which accomplish identical goals of removing heat from the reactor through diverse and redundant

systems. Therefore the PB-AHTR also has a normal shutdown cooling system that can remove heat by natural circulation through the intermediate heat exchangers under shutdown conditions.

8.4 OPTIMIZATION CRITERIA – SIZING AND PERFORMANCE

The overall objective of this criterion is to reduce the amount of metallic material employed constructing the passive safety system. In this section, a detailed evaluation of the impact of varying the a) plant geometric parameters and b) helical heat exchanger geometric parameters previously assumed as invariable in section 5.5 and during the transient evaluation of the system.

8.4.1 Effect of Plant parameters variation

NDHX thermal elevation sensitivity

The reference design assumes a distance of 8 m between the bottom of the NDHX and the bottom of the DHX. An increased height is expected to cause an increase in the buoyancy of the salt loop. Greater buoyancies produce greater flow rates, which in turn, reduce the temperature difference across the loop and increase the effectiveness of the DHX heat exchanger, bringing the cold fluid outlet temperature closer to the hot fluid inlet temperature. These effects are observed in Figures 8-1 to 8-3.

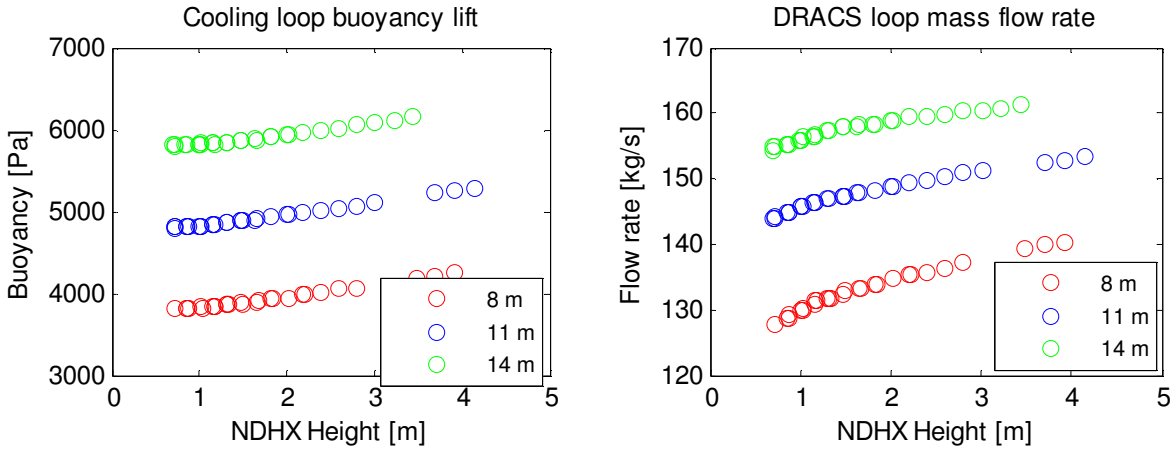

Fig. 8-1 Cooling loop buoyancy lift (left) and flow rate (right) assuming three elevation differences as a function of various NHDX designs.

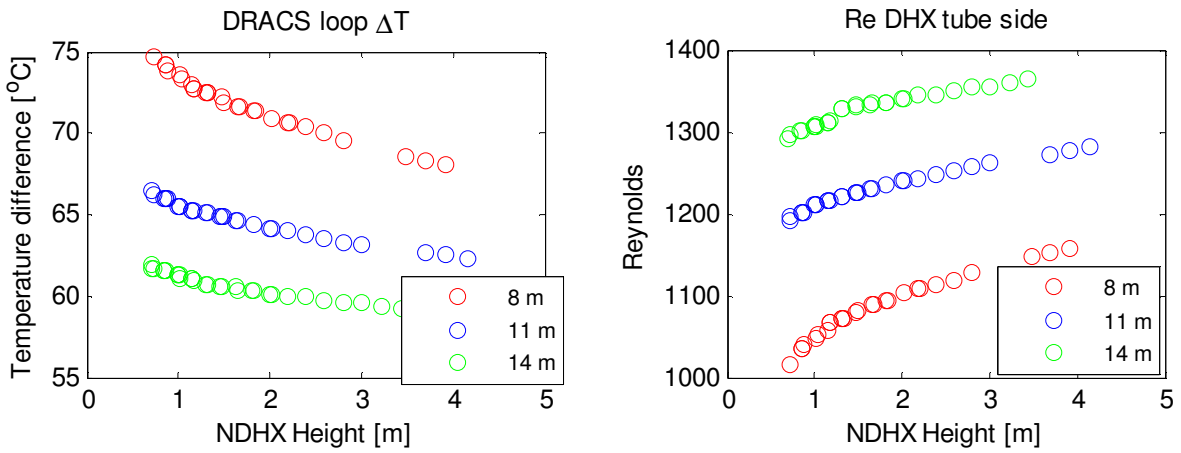

Fig. 8-2 Temperature difference across the DRACS loop (left) and Reynolds number in the DHX tube side of the loop (right) assuming three elevation differences for various NDHX designs.

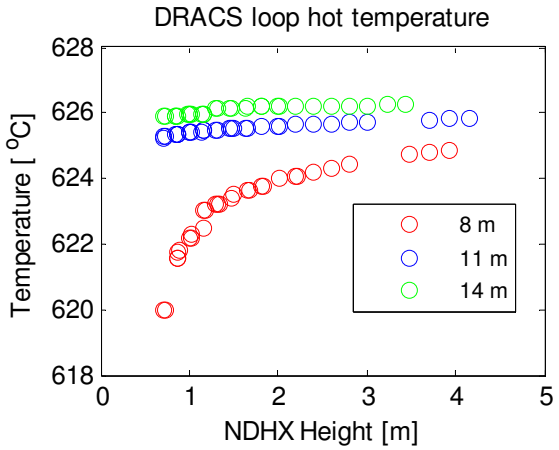

Fig. 8-3 DRACS loop hot temperature assuming three elevation differences for various NDHX designs.

The effect of greater elevation difference between the DHX and NDHX is a) increases flow rates, enhancing heat transfer and driving higher average liquid salt temperatures b) decreases sensitivity of the NDHX performance to the height of the NDHX itself. Based on freezing margin considerations, larger distance is desirable, however at the expense of economic considerations due to the added salt inventory.

NDHX Chimney stack height sensitivity

Air heat removal is driven by the buoyancy forces. The stack height is an important component of the buoyancy, due to the storage of hot, low density gas, which creates pressure difference sufficient to move air across the NDHX tubes. A higher stack represents higher buoyancy, which then requires greater flow rates to balance with friction.

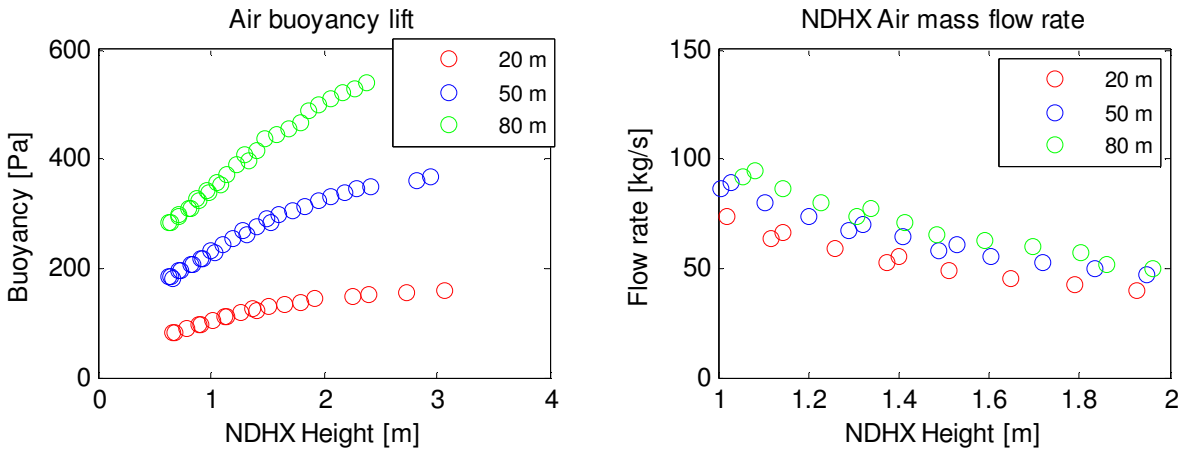

Fig. 8-4 Air buoyancy and air flow rates through NDHX

The effect of greater mass flow rates of air through the heat exchanger is expected to reduce the temperature gain. This is also due to the reduced residence time air spends as it travels through the heat exchanger at higher speeds. Proportionally to the velocity, the Reynolds number reflects this increase. The following figures display this.

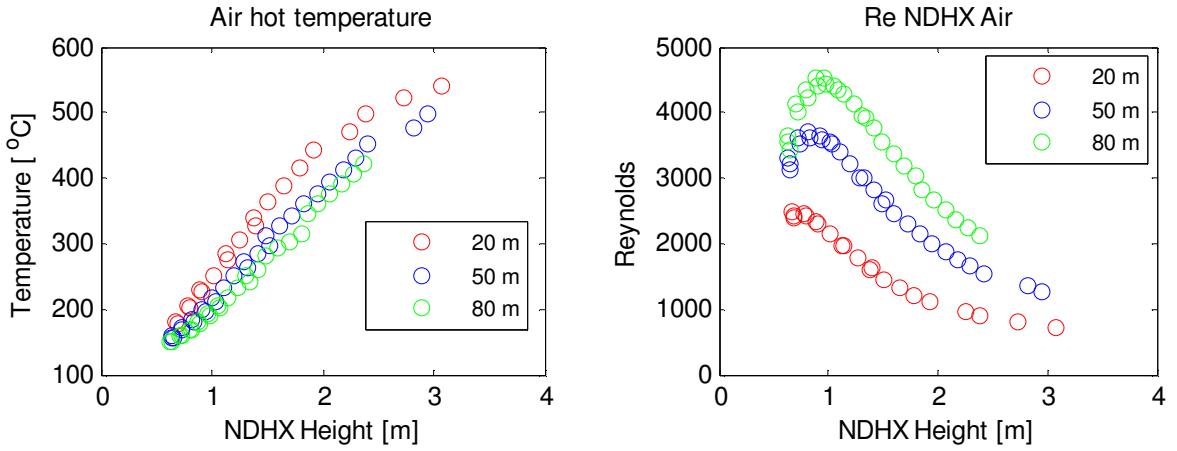

Fig. 8-5 Air hot temperatures and air Reynolds

In the case of air flow, the heat transfer coefficient in cross flow is very sensitive to the flow rate. The overall heat transfer coefficient for the NDHX is severely limited by the air side coefficient, as the salt side is an order of magnitude greater under a range of conditions. Thus, greater air heat transfer coefficient changes the overall heat transfer coefficient of the NDHX. The following figures demonstrate these relationships

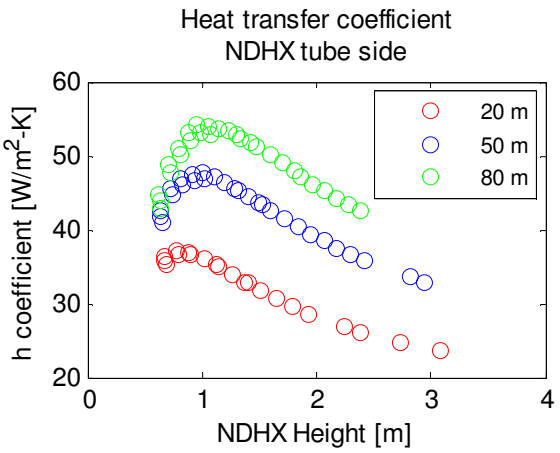

Fig. 8-6 Air Heat transfer coefficients

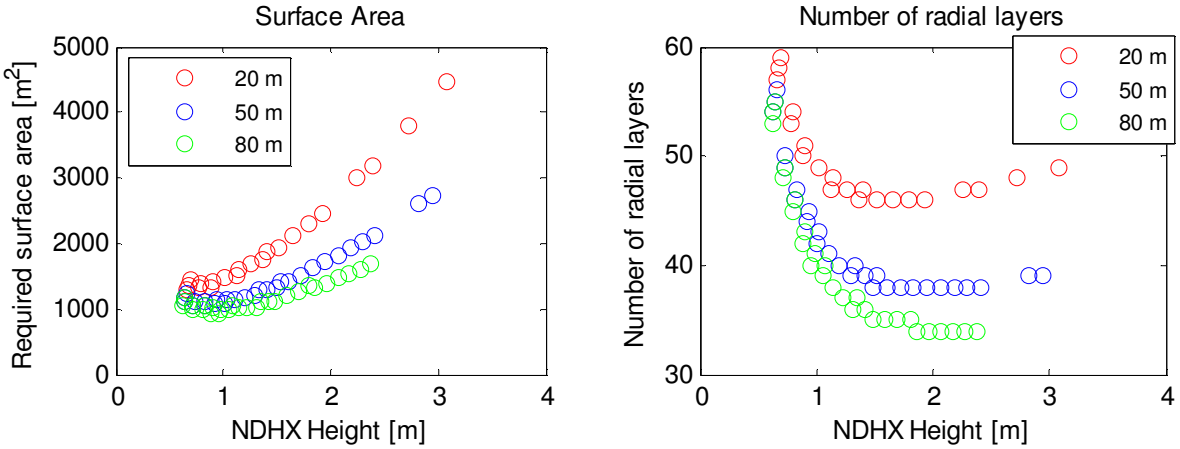

Fig. 8-7 Surface area and outer radius

The variation of the flow areas of the connecting pipe between the NDHX and the DHX salt fluid, and the chimney pipe diameter are not evaluated since the system response is easily predictable. As the flow areas assumed are reduced the salt inventory is also reduced, however a resulting higher friction pressure drop requires a smaller flow rate. This in turn, causes an increased temperature difference across the safety loop. The magnitude of the increased pressure is proportional to the flow area shrinkage. A similar phenomenon occurs for the air chimney, since the pressure drop through in cross flow through the NDHX tubes is much greater than the chimney friction drop.

8.4.2 Effect of Helical Heat Exchanger Parameter Variation

Pipe Diameter

Changing the helical coil pipe diameter affects hydraulic and heat transfer processes in both, internal and external sides of the NDHX heat exchanger. As a consequence, the overall

performance of the system is also altered. This study assumes internal pipe diameters of 4.0cm, 5.0cm and 6.0cm and analyzes the effects in each side of the heat exchanger separately.

Air side

Smaller pipe diameters in a bank of tubes with identical pitch to diameter ratios lead to higher air friction coefficients. These higher friction coefficients lead to higher pressure drop traveling through the same overall tube bank length. The following figure shows this relationship.

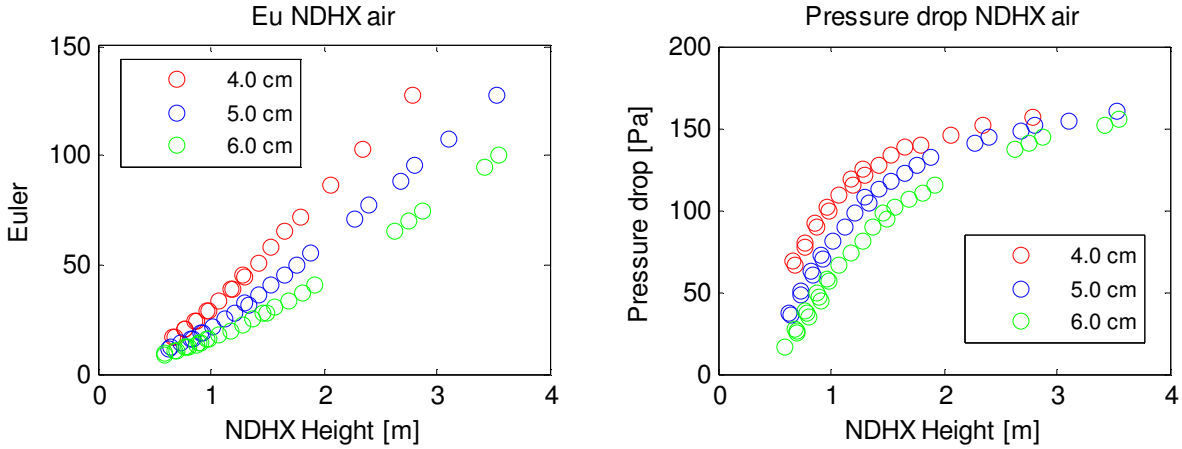

Fig. 8-8 Air flow Euler number and pressure drop through the NDHX for various pipe diameters

The non-dimensional Euler number is chosen to illustrate how the pressure drop increases for smaller pipe diameters. Pressure drop in gases, is also a function of the acceleration as gas expands due to heat addition. From Figure 8-8 it can be observed that the relationship between Euler number and the pressure drop is proportional, but not linear in nature.

Higher pressure drop in tube banks with smaller pipe diameter cause mass flow rates to be reduced. Smaller flow-rates are compensated with higher air temperature rise to balance the net power output.

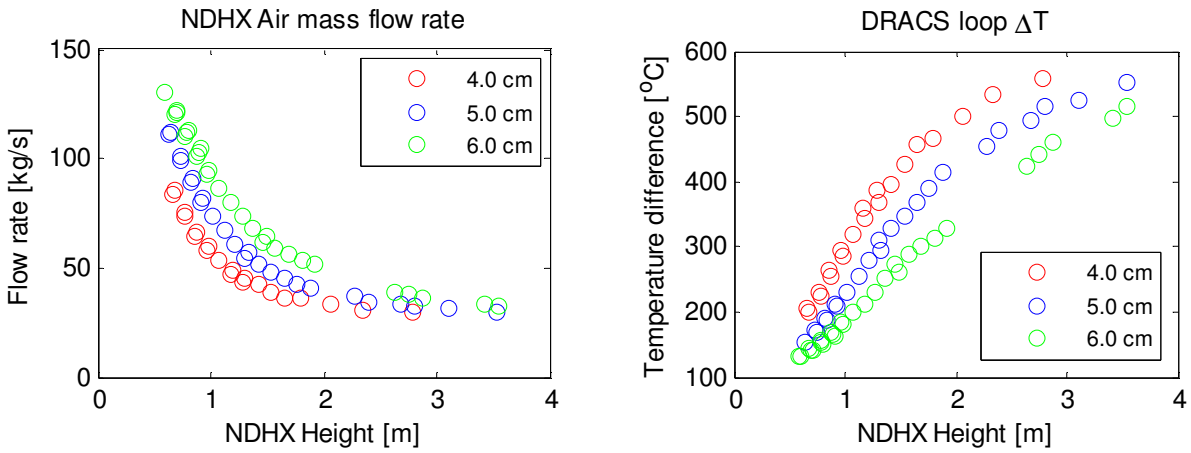

Fig. 8-9 Flow rate and temperature increase

Air flowing at higher mass flow rates will in consequence have greater heat transfer coefficients, consequence of higher Reynolds numbers, also due in part to larger hydraulic diameter for larger pipe diameters.

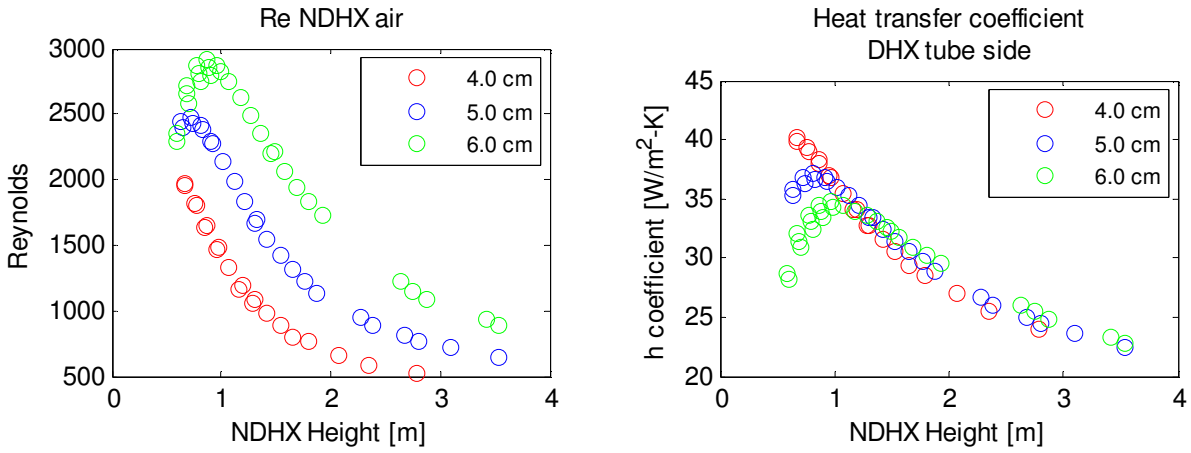

Fig. 8-10 Reynolds number and heat transfer coefficient

The figure above show higher heat transfer coefficient for larger tube diameter for the taller NDHX configurations, and a sharp decrease for shorter configurations. This is because the Reynolds number sharply decreases for NDHX heights below the smallest surface area resulting from the optimal combination of radial layers and number of helical tube rotations. The pictures below show this point, at least for the 6 cm pipe.

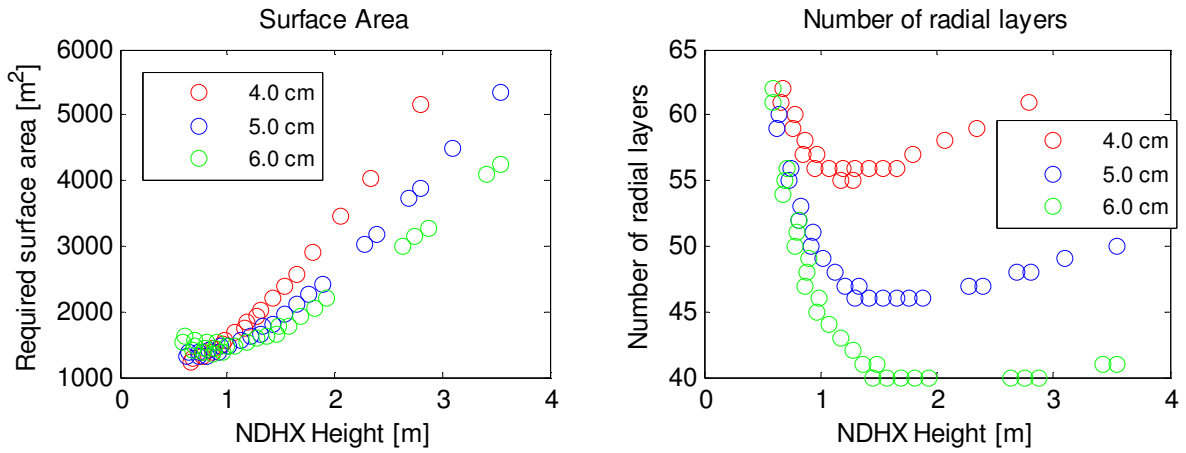

Fig. 8-11 Surface area and number of radial layers

It can be observed that the NDHX design requires less number of radial tube layers as the pipe diameter increases. Similarly, heat exchangers with larger pipes, require less overall heat transfer areas, primarily due to the enhanced air heat transfer coefficient caused by higher flow rates.

On the tube side

Obtaining satisfactory NDHX designs employing smaller tube diameter forces the code to employ larger total number of tubes. The net effect is a greater overall area of flow when more numerous, smaller tubes are used. Given that the total mass flow rate of the DRACS cooling loop remains unaffected, smaller pipe diameters represent smaller flow velocity and thus smaller Reynolds numbers.

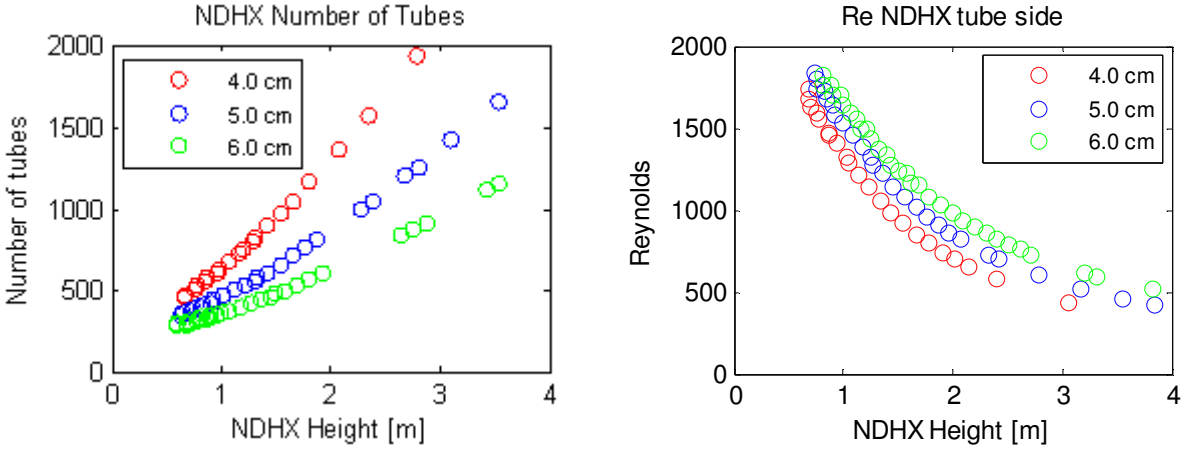

Fig. 8-12 Number of tubes in the NDHX (left) and Reynolds number of liquid salt flow through the coils for multiple inner tube diameters.

Adjusting the coil pipe inner diameter is expected to affect the pressure drop and heat transfer numbers beyond the influence of Reynolds number. The friction factor and heat transfer coefficient in curved pipes are functions of the ratio of pipe diameter to coil diameter. When

different diameters are employed, the average coil radius varies, the ratio of tube diameter to coil diameter becomes unpredictable. Moreover, the correlation for friction factors employed in this study is a complex logarithmic function of this ratio. The overall results of the code for the heat transfer coefficient, Euler number and salt pressure drop are presented in the Figures 8-13 and 8-14 respectively.

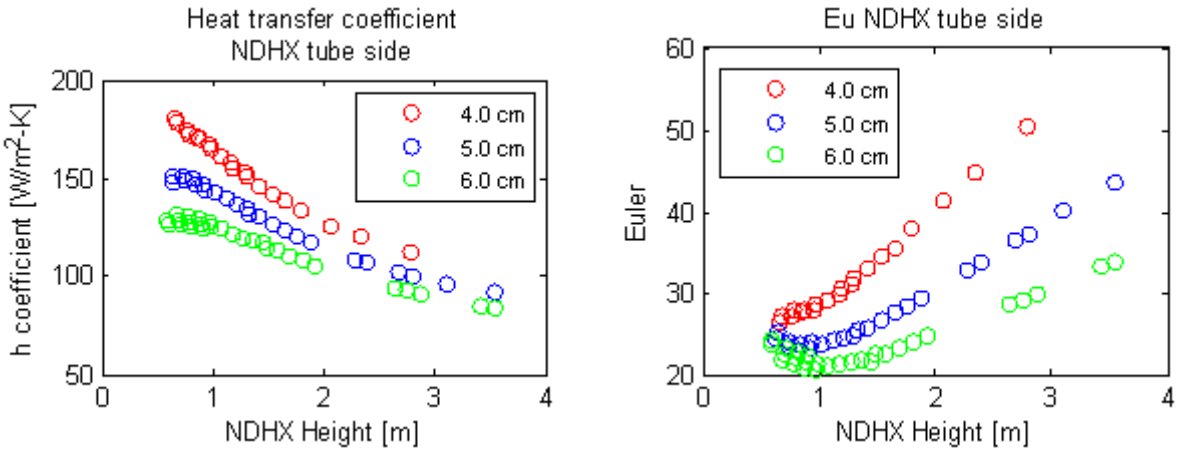

Fig. 8-13 NDHX liquid salt heat transfer coefficient (left) and characteristic Euler number of internal flow through the coils for multiple inner tube diameters.

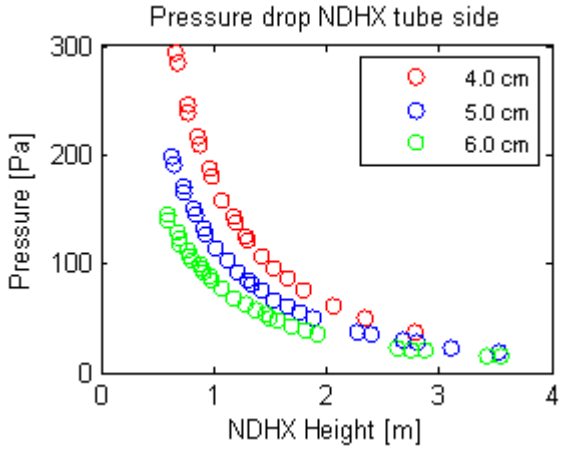

Fig. 8-14 Pressure drop of liquid salt through the coils for multiple inner tube diameters.

Taking into consideration the overall effect of the air and tube sides, smaller pipe diameters lead to more voluminous heat exchangers with high surface areas for heat transfer. Large diameter heat exchangers require similar liquid salt volumes with the added benefit of smaller surface area and smaller outer radius. For these reasons, large pipe diameters are preferable.

Pitch to Diameter ratio

Similarly to the analysis of tube diameter variation, the effects are studied separately for the air and salt sides. Three pitch to diameter ratios are studied, 1.7, 1.85 and 2.0.

Air side

Tighter tube lattices are characterized for higher friction factors. This implies lower air flow rates, higher pressure drops, lower heat transfer coefficients, and therefore higher required heat transfer areas. Lower flow rates also require higher temperature difference across the loop to deliver the required heat load. Figures 8-15 to 8-17 illustrate these relationships.

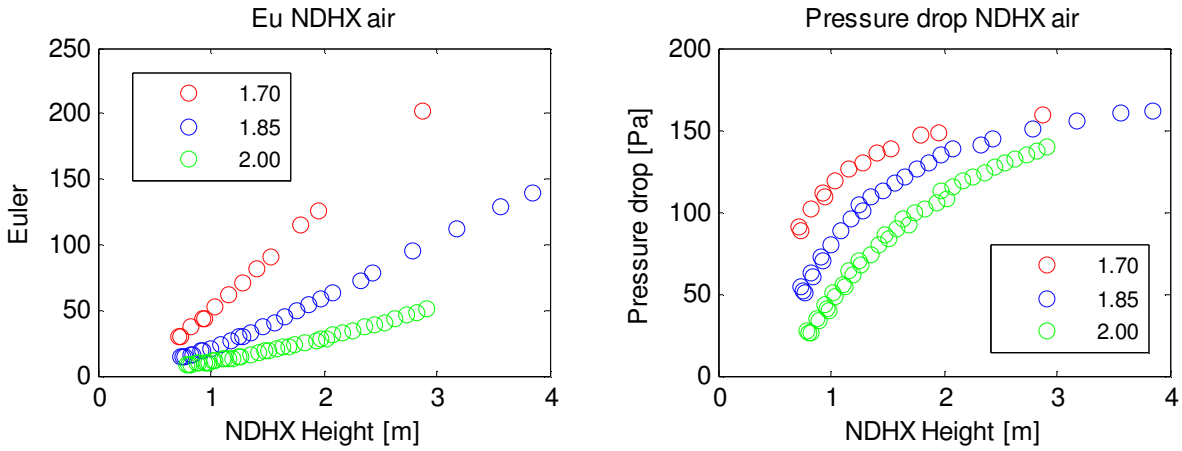

Fig. 8-15 Characteristic air Euler number (left) and corresponding pressure drop (right) across the NDHX coils for varying pitch to diameter tube lattice arrangements.

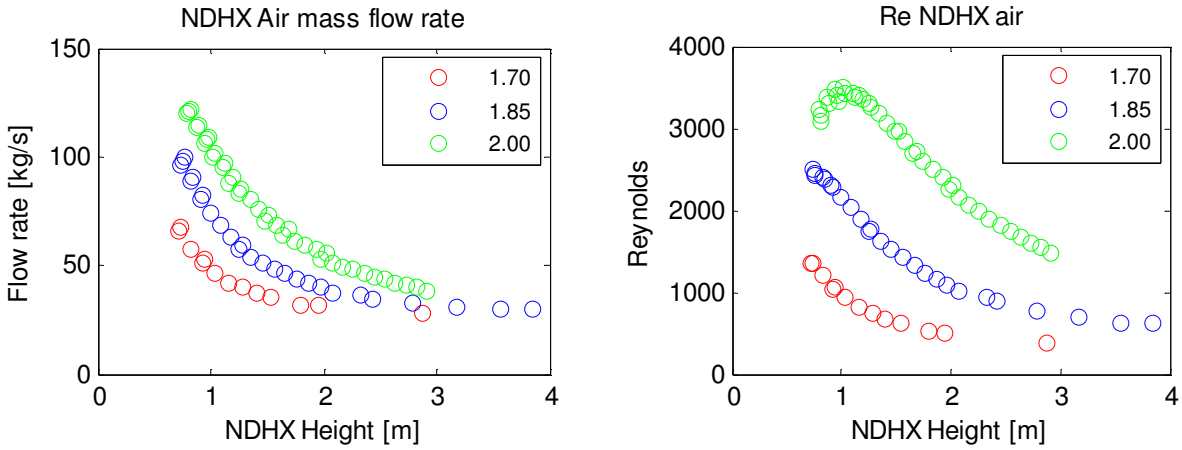

Fig. 8-16 NDHX air flow rate (left) and corresponding Reynolds number (right) across the NDHX coils for various pitch to diameter ratio tube lattice.

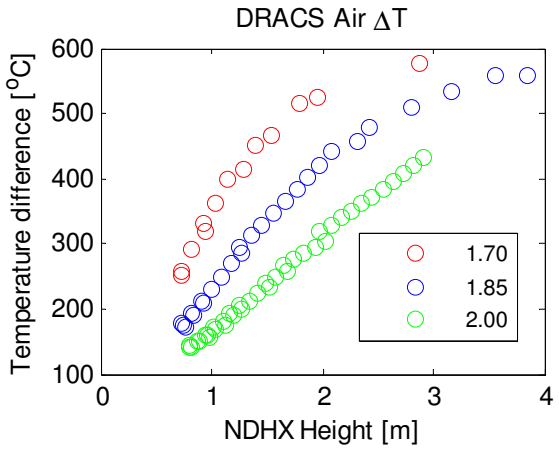

Fig. 8-17 Air outlet to inlet temperature difference across the NDHX shell side, for various pitch to diameter ratio tube lattice.

Tube side

Similarly to the case of smaller pipe diameter, tighter lattice configurations require greater number of tubes and in turn, greater area of flow for salt is available. At essentially identical salt flow rates, Reynolds numbers are lower for low pitch to diameter ratios.

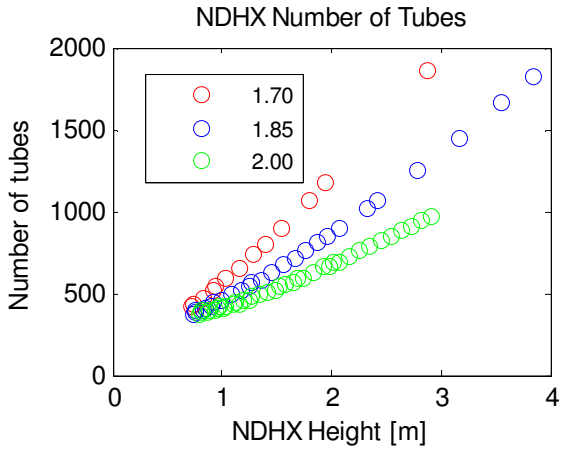

Fig. 8-18 Number of tubes required in NDHX design for different pitch to diameter ratios for various heat exchanger heights

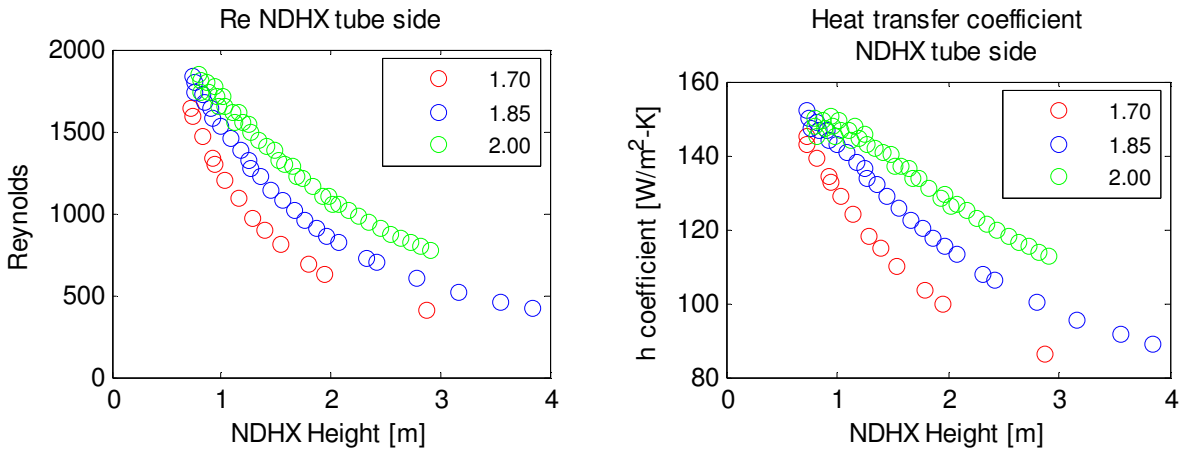

Fig. 8-19 Characteristic Reynolds number (left) and heat transfer coefficient (right) assuming different pitch to diameter ratios for various NDHX designs

Lower Reynolds numbers generate lower heat transfer rates in the salt side as well an increased friction factor, since friction factors in curved pipes are proportional to Re to the –0.5 power. This is observed in a higher Euler numbers characteristic of the flow. The overall pressure drop however, is greater for higher pitch to diameter tube arrangements, which have higher Reynolds numbers.

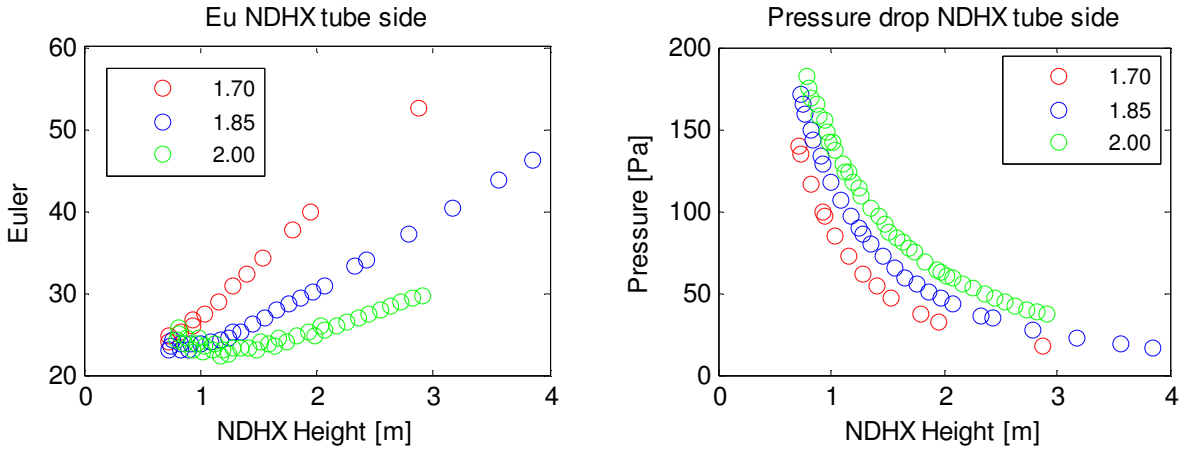

Fig. 8-20 Characteristic air Euler number (left) and corresponding liquid salt pressure drop (right) within the NDHX coils for varying pitch to diameter tube lattice arrangements.

Overall, the NDHX requires greater heat transfer surface area as well as greater number of radial layers of tubes when small pitch to diameter ratios is employed.

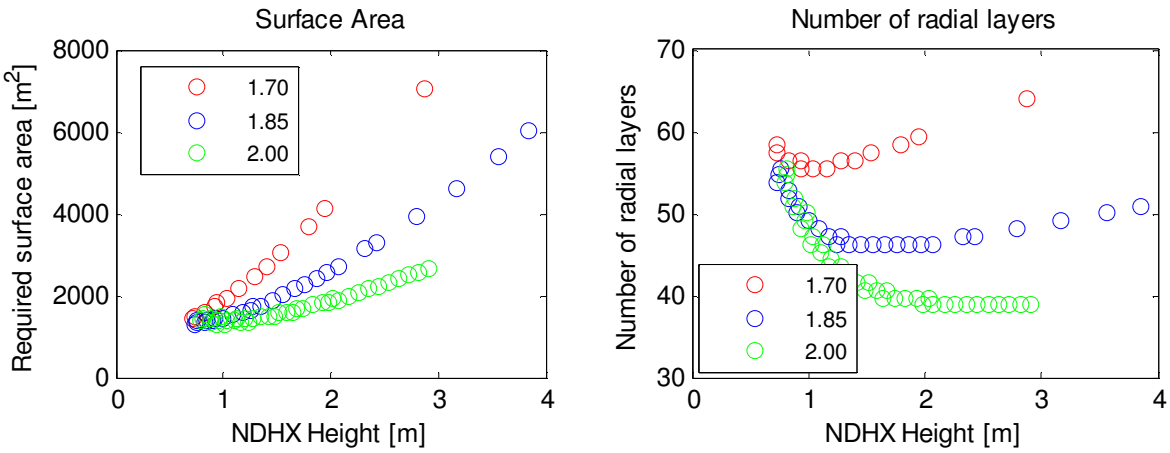

Fig. 8-21 Surface area (left) and number of radial layers (right) for various pitch to diameter ratios in the NDHX design

Based on the considerations discussed above, the NDHX design can be optimized increasing the tube diameter increasing the pitch to diameter ratio to reduce surface area and coil outer diameter. On the other hand, tighter tube lattice and smaller tube diameters output hotter air at shorter NDHX lengths. In order to best select the proper NDHX size, the metrics of performance must be established and prioritized.

8.5 OPTIMIZATION CRITERIA – COOLANT TYPE SELECTION

There are multiple coolant candidates that can be employed as the working fluid for the DRACS natural circulation loop, also referred as the cooling loop chapter 5, which discusses the design of the system. Given the high temperature environment, and the requirement to operate in liquid phase, the two candidate coolant types for the DRACS are liquid salts and liquid metals. The table below evaluates the thermophysical properties at the average temperature of 665 ^{o}C for various liquid salts and liquid metals.

Thermo-physical property comparison for liquid salts and liquid metals evaluated at 665 ^{o}C (938 K)						
	Flibe	Flinak	Flinabe	Lead	Lead-Bismuth	Sodium
P [kg/m^3]	1995.0	2044.7	1779.4	10204.0	9822.3	797.46
-dρ/dT [kg/m^{3}K]	0.488	0.73	0.711	1.35	1.38	0.242
β [K^{-1}]	2.446E-4	3.571E-4	3.996E-4	1.323E-4	1.405E-4	3.036E-4
C_p [J/kgK]	2386	1884	1507	142.57	146.51	1251.4
μ [Pa·s]	0.006354	0.00341	0.000955	0.00142	0.00110	0.000200
k [W/mK]	1.1	0.8	0.5	15.648	16.471	60.32
Pr	13.78	8.03	2.87	0.0129	0.0098	0.0042
Melt. pt. [^{o}C]	458	454	385	327	123.5	97.7

Table 8.1 Thermo physical property comparison of salts and metals

In order to evaluate the performance of the six coolants under consideration, all geometric properties presented in chapter 5 as the reference design for the passive safety system design are employed. The only variant is the coolant selection for the DRACS cooling loop. The analysis in the section below evaluates the coolant candidates in the following category a) liquid salts, b) liquid metals and c) single liquid salt vs. single liquid metal.

8.5.1 Comparison of Liquid salts

The primary differences observed for the three candidate salts can be inferred from the table above. Flibe has smaller volumetric expansion coefficient, compared to the other salts. From this observation, it is expected that the buoyancy head in the DRACS loop is smallest for the flibe case. Also, due to the low buoyancy head in the flibe loop, the mass flow rate required to create identical friction head must also be smaller, to the case for other salts. The figure below shows these relationships.

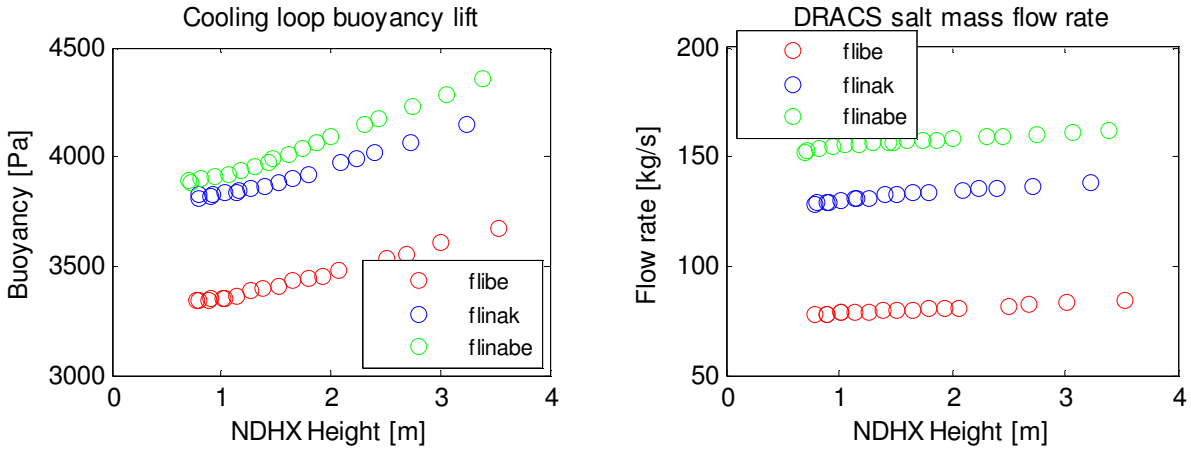

Fig. 8-22 Buoyancy head and mass flow rate for multiple NDHX design configurations for the three candidate salts.

The high buoyancy shown by flinak and flinabe suggest that, similar performance as flibe can be achieved under smaller thermal center vertical height difference.

Given that the mass flow rate is the lowest for the flibe case and considering that the heat capacity for all three salts are similar, the temperature difference across the loop is roughly inversely proportional to the mass flow rate, and for flibe is expected to be high in order to maintain the heat load requirement.

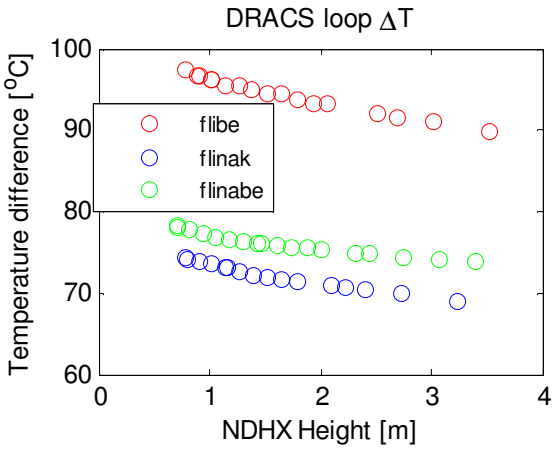

Fig. 8-23 Temperature differences across the DRACS loop for multiple NDHX design configurations.

Another observation from the table of thermophysical properties is that flinabe has much lower viscosity than other salts. This is expected to amplify the Reynolds number significantly, even when coolant travels at comparable flow rates. The figure below demonstrates this effect.

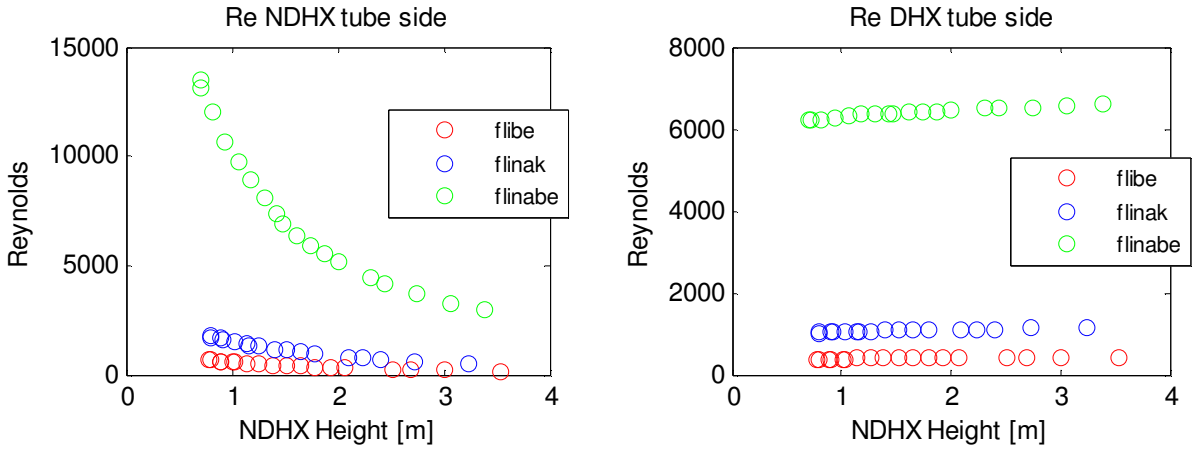

Fig. 8-24 Non-dimensional Reynolds number on the tube side of the NDHX and DHX for multiple NDHX designs, employing the three candidate salts.

The increased Reynolds number for the salt loop using flinabe causes an increased heat transfer rate on the same side in each corresponding heat exchanger.

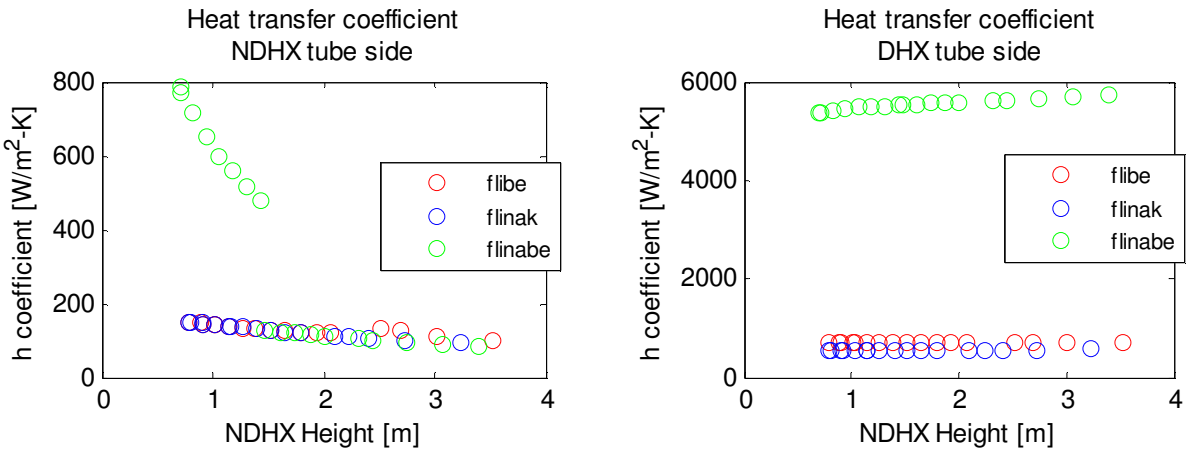

Fig. 8-25 Heat transfer coefficient on the tube side of the NDHX and DHX for multiple NDHX designs, employing the three candidate salts.

For the short NDHX configuration (height<1.5m) with flinabe, the salt Reynolds number is high enough such that flow is turbulent, and therefore, causes elevated heat transfer coefficients. From figure 8-4, this transition is observed to occur at Reynolds number of ~6000. As it was discussed in chapter 2, the transition from laminar to turbulent regimes is shifted from the transition in straight pipes due to the curvature of the pipe. Similarly, in the DHX, higher heat transfer coefficients are observed and no transition occurs, since the flow is always in the turbulent regime.

Higher tube side heat transfer coefficients can have a large effect on the overall effectiveness of each heat exchanger as long as the shell side heat transfer coefficient is larger. This is the case of the DHX, where cross flow heat transfer coefficients are very large. Combined, a higher overall heat transfer coefficient results, which increases the DHX effectiveness and thus, bringing closer the outlet temperature of the cold fluid to the inlet temperature of the hot fluid, which is set to 760 ^{o}C. This increase is also reflected in the cold temperature of the cold fluid. Figure 8-26 demonstrates this relationship.

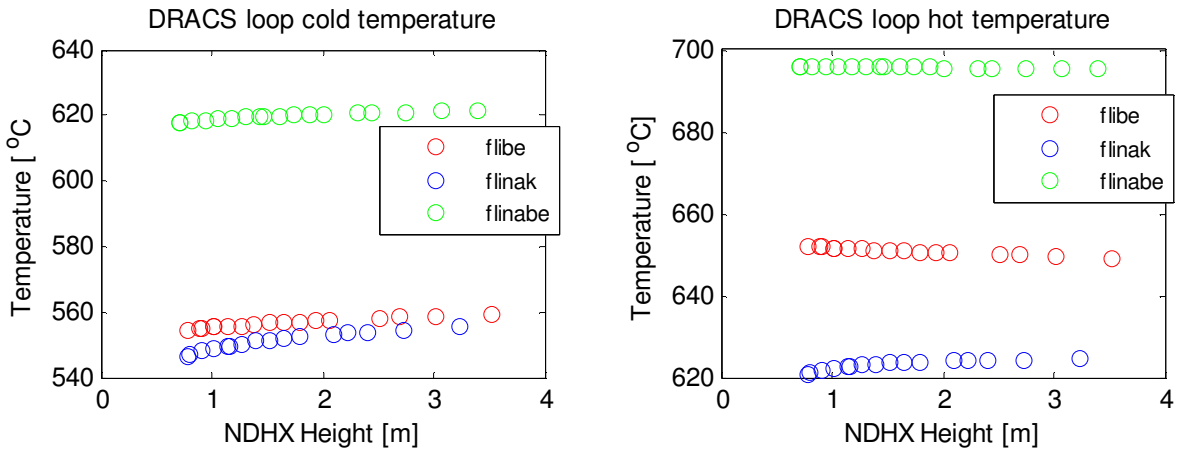

Fig. 8-26 Hot and cold coolant temperatures for various NDHX designs employing the three candidate salts

An increased heat transfer coefficient on the tube side of the NDHX does not change the heat exchanger effectiveness, since the shell side heat transfer coefficient, driven by air, is very low.

Based on the observations from the cases above, the conclusions are the following 1) flibe loops require higher vertical thermal height difference to perform similarly other two salts, 2) in this configuration, flibe loops require higher temperature difference across the loop to deliver the same amount of power and 3) the low viscosity of flinabe makes the fluid reach turbulent conditions without reaching high flow rates, and this helps enhance the effectiveness of the DHX, elevating the DRACS salt temperatures. This is important, since higher DRACS loop temperature provides greater margin of safety against salt freezing in the DRACS.

8.5.2 Comparison of Liquid metals

The thermophysical properties of the liquid metals considered are shown in Table 8-1. It is noted that both lead and lead-bismuth eutectics are very similar, except the former has a lower melting temperature, which is a desired characteristic for greater margin of safety in case of freezing.

When establishing a figure of merit for the buoyancy head of natural circulation loops, the volumetric expansion coefficient is important, but not as much as the derivative of density with respect to temperature. The following equations illustrate this:

$$\Delta P_B = \beta \rho_o \Delta T g \Delta L \qquad (8\text{-}1)$$

But, for non-compressible fluids, the volumetric expansion coefficient is as follows:

$$\beta = -\frac{1}{\rho}\frac{d\rho}{dT} \qquad (8\text{-}2)$$

Inserting equation (8-2) into (8-2) and assuming that $\rho_o/\rho = 1$, it follows

$$\Delta P_B = -\frac{d\rho}{dT}\Delta T g \Delta L \qquad (8\text{-}3)$$

While the thermal expansion coefficient of lead and sodium are similar, the derivative of density with respect to temperature for sodium is smaller by a factor of five than lead. This means that the expected buoyancy will be significantly smaller compared to lead, assuming similar temperature difference. The following picture demonstrates this relationship

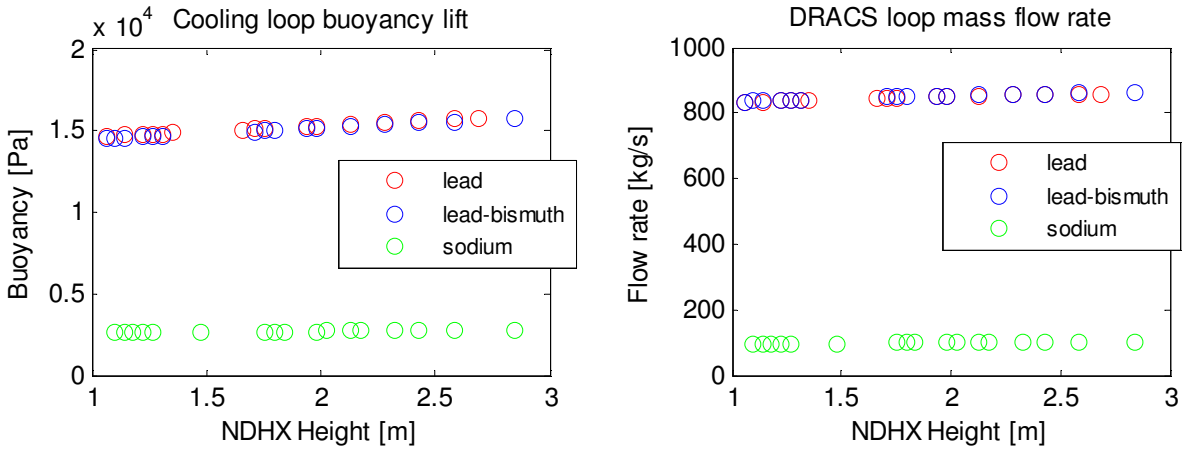

Fig. 8-27 Buoyancy head and mass flow rate for multiple NDHX design configurations for the three candidate liquid metals

This behavior suggests that a lead or lead-bismuth cooling loop generates similar buoyancy forces as a sodium loop at significantly lower vertical thermal height difference.

Under this configuration, in order to compensate for larger buoyancy, lead and lead-bismuth loops require higher mass flow rates for greater friction head. Figure 8-27 shows this relationship.

In order to compensate a reduced mass flow rate, sodium loops are expected to have a much higher temperature difference across the loop compared to lead or lead-bismuth loops. However, this is not the case, since, oddly enough, the heat capacity of sodium is much higher than that of lead and lead-bismuth. Interestingly, in this particular configuration, the ratio of heat capacities is inversely proportional to the ratio of flow rates, cancelling the effect on overall heat load capacity, thus allowing similar temperature drop across the loop. Figure 8-28 depicts this relationship.

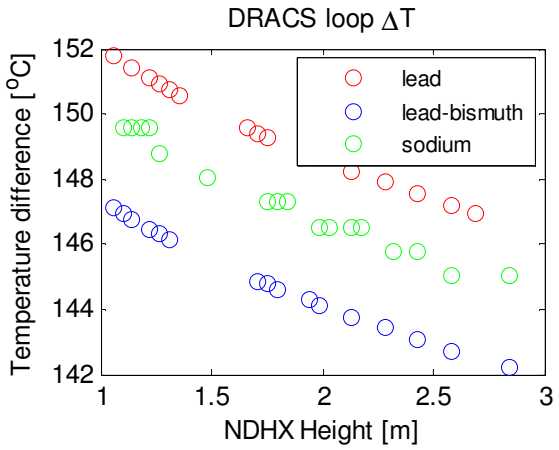

Fig. 8-28 Temperature difference across the DRACS loop for multiple NDHX design configurations.

Greater mass flow rates are expected to drive, in this case, lead and lead bismuth loops to high Reynolds numbers in the tube sides of both DHX and NDHX heat exchangers. In addition, the unusually low values of viscosity characteristic of liquid metals further drive a higher Reynolds number in the loop.

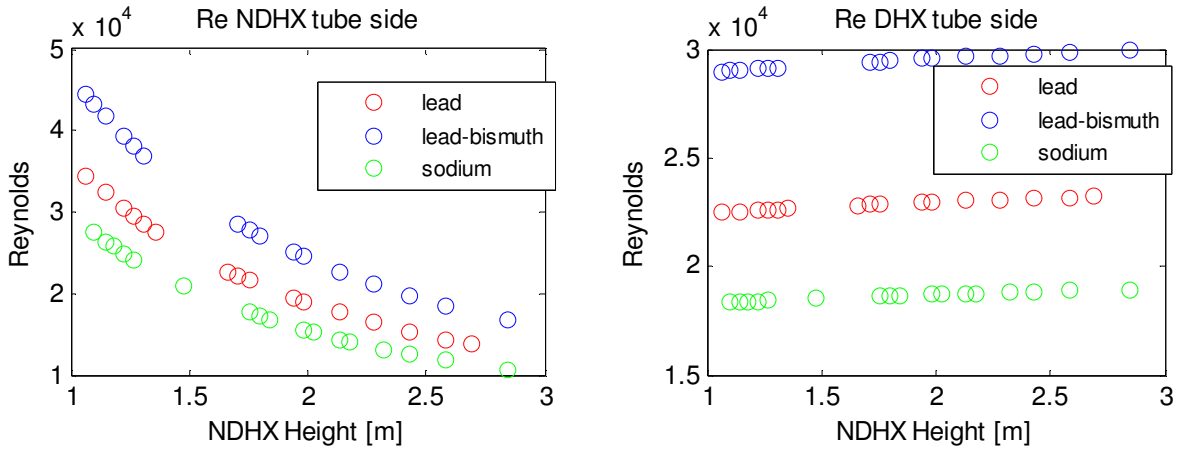

Fig. 8-29 Non-dimensional Reynolds number on the tube side of the NDHX and DHX for multiple NDHX designs, employing the three candidate metals.

The turbulent flow regimes present under all NDHX configurations are expected to produce high heat transfer coefficients. As this was demonstrated in the analysis of the salt candidates, higher heat transfer coefficient only enhances the effectiveness of the DHX. Thus, the outlet temperature of the cold side of the DHX is expected to near the inlet hot temperature of the shell side, independent of the NDHX design. The following demonstrates this.

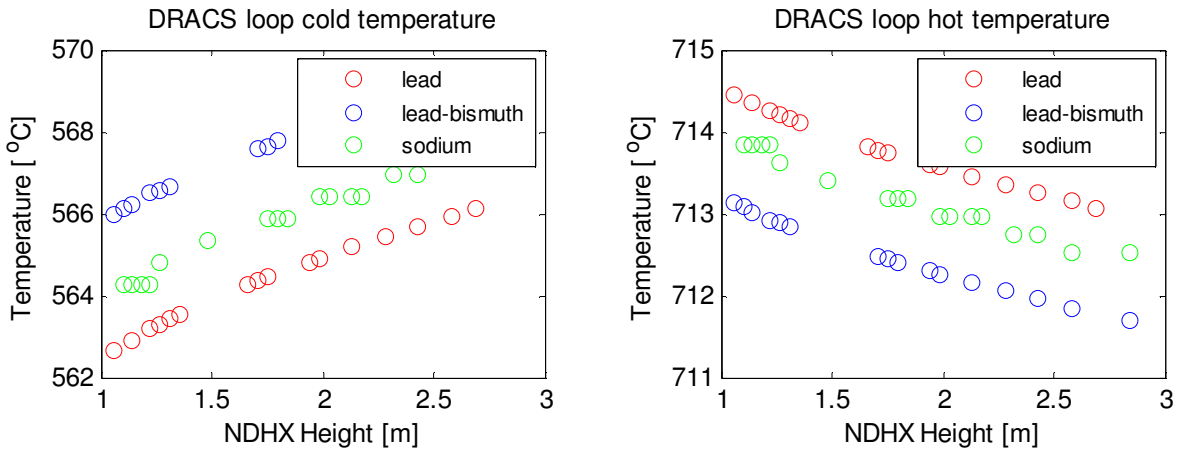

Fig. 8-30 Hot and cold coolant temperatures for various NDHX designs employing the three candidate metals

The observations from above show that a) high density derivative with respect to temperature creates large buoyancy and large mass flow rates in lead and lead bismuth loops, b) low viscosity and high conductivity of all three liquid metals result in high heat transfer coefficients, which enhances the effectiveness of the DHX heat exchanger to the limit imposed by the shell side heat transfer and c) due to the inversely proportional relationship of heat capacity and the derivative of density with respect to temperature between lead or lead-bismuth and sodium, a loop of the same height performs very similarly in both cases under very different coolant flow rates.

8.5.3 Comparison of salts vs. metals

In order to perform this evaluation, the selected salt is flinabe, since this salt demonstrated tendency to display turbulent flow conditions due to the low viscosity at relatively low flow rates in the assumed geometry. Similarly, sodium is the selected liquid metal for evaluation.

Under identical geometric conditions, the higher time derivative of density of flinabe is expected to generate higher buoyancy head when compared to sodium loops. As a consequence, higher flow rates are also expected in the salt loop. This relationship is shown in the following figure.

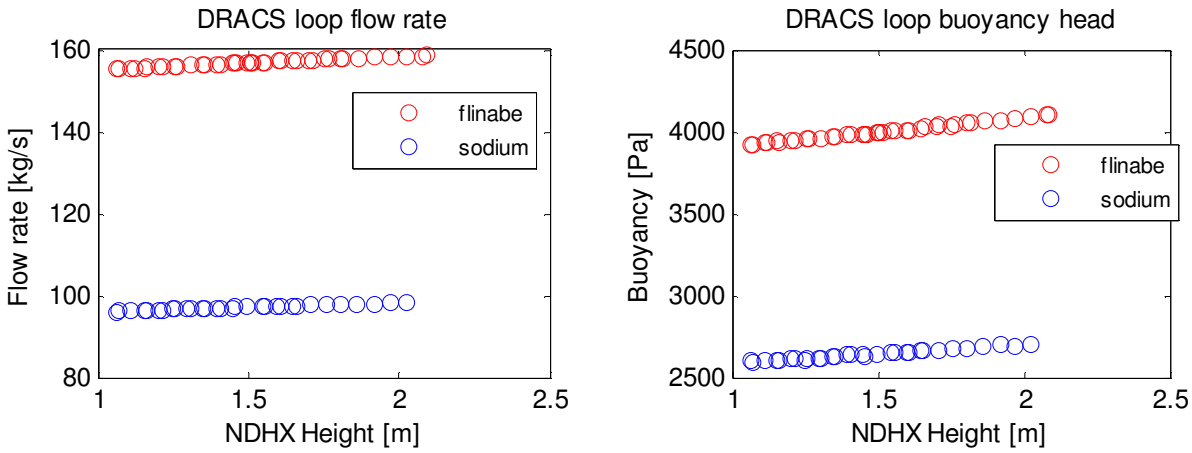

Fig. 8-31 Buoyancy and flow rates comparison for sodium and flinabe

Flinabe and sodium posses similar values of heat capacity, for this reason the temperature difference across the DRACS loop is expected to be roughly proportional to the flow rate ratios, in order to deliver equal amounts of heat.

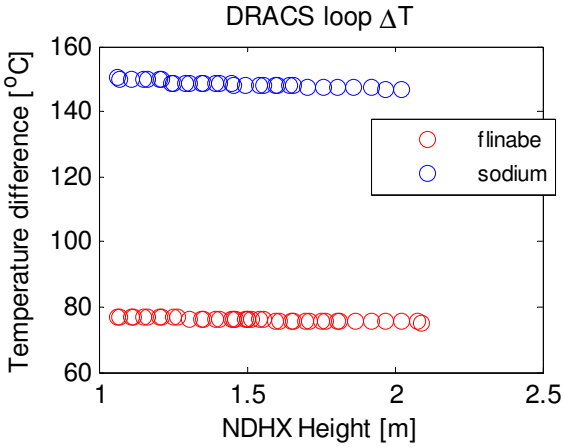

Fig. 8-32 Temperature difference across loop comparison for sodium and flinabe

Despite a lower sodium flow rate through the loop as shown in Figure 8-31, a higher heat transfer coefficient for both heat exchangers is observed, principally due to the higher heat conduction coefficient, which is 120 times greater than salt. This enhances the effectiveness of the DHX, which drives the DRACS loop hot temperatures closer to the safety loop hot temperature. The cold temperature, however, is below the cold temperature for the flinabe loop, due to the greater temperature difference across the loop necessary for sodium. Figure 8-33 demonstrate this relationship.

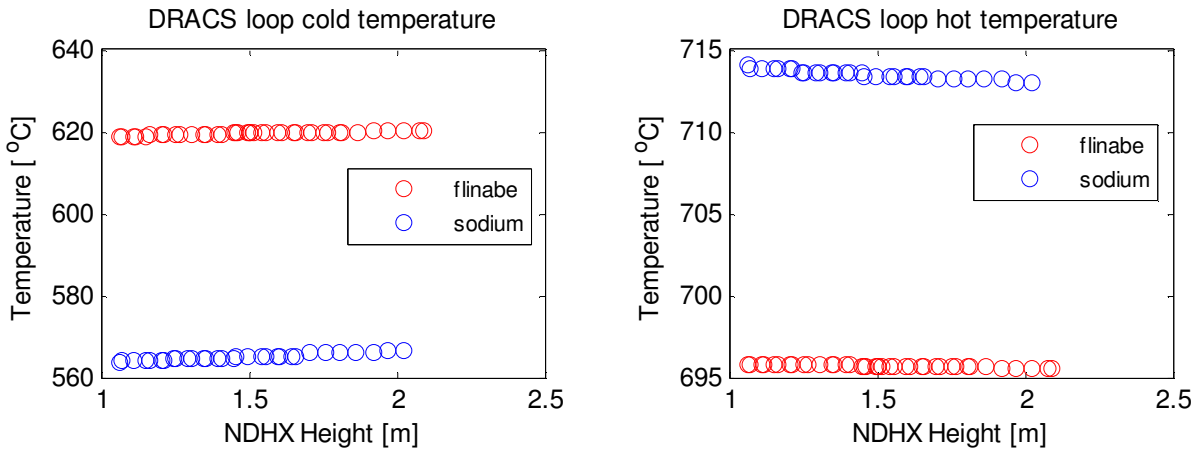

Fig. 8-33 Hot and cold temperatures for loop comparison for sodium and flinabe

Liquid salts are characterized to have much higher Prandtl numbers than liquid metals. This indicates that the thermal diffusivity is much greater than the momentum diffusivity for liquid metals and as a consequence, the thermal sublayer is much greater than the momentum sublayer as indicated by Kays and Crawford [3], causing the heat transport to be a weaker function of the local hydrodynamic conditions, as opposed to liquid salts. This implies that a natural circulation cooling loop employing liquid metals can be expected to show high heat transfer coefficients at low flow rates, thus requiring little flow rate which translates into smaller friction pressure drop, and thus requiring a smaller buoyancy head to drive the flow. This is investigated by evaluating the sodium loop, however under a reduced vertical height of 2 m, instead of the reference 8 m. For comparison, the liquid salt loop case assumes the reference height.

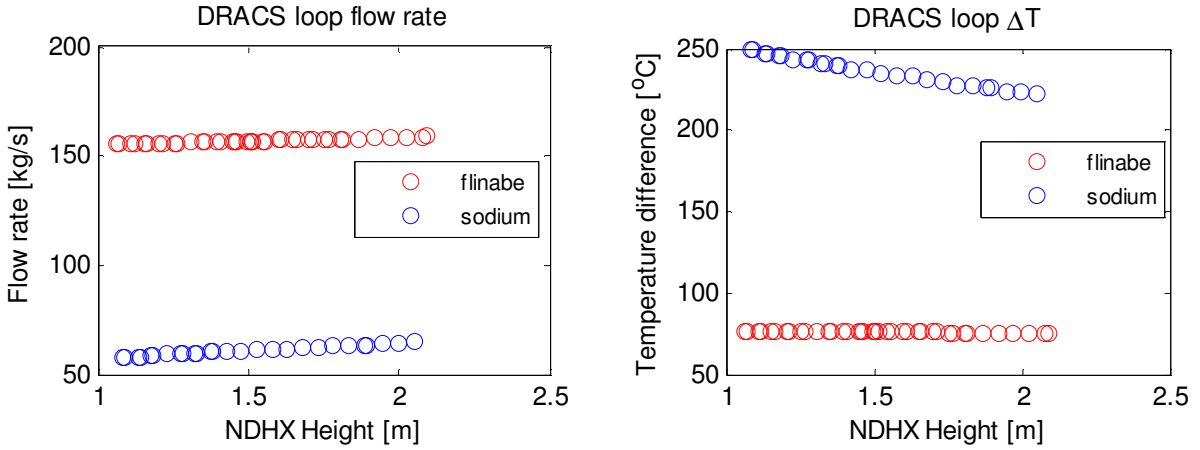

Fig. 8-34 Sodium loop at reduced thermal elevation versus reference salt design temperature difference across loop

Figure 8-34 shows that, although similar heat transfer rates are achieved at lower flow rates for the sodium loop, the small flow rates in addition to the small heat capacity of sodium force the

loop to experience a larger temperature change. This raises the concern of thermal stresses in the metallic structures and reduces the margin for freezing of the sodium loop.

The final insight when comparing the effect of coolant choice in the heat exchanger is to compare the relative sizes required for the heat exchanger. This information can be obtained from evaluating the total outer surface area and the number of radial layers for the NDHX. This assumes the reference geometry for both loops.

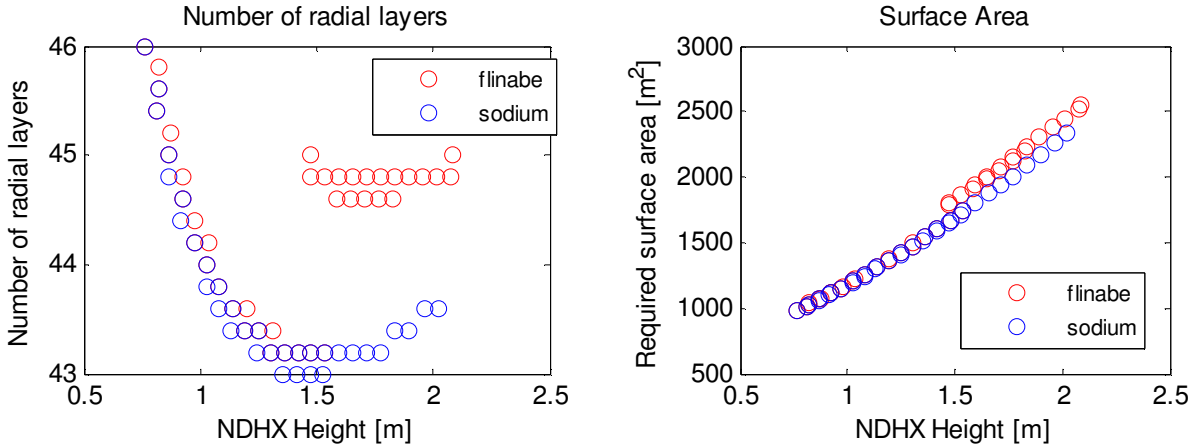

Fig. 8-35 Number of radial layers required and total surface area for NDHX design for flinabe and sodium working fluids.

Based on the Figure 8-35, a sodium-cooled design for the NDHX requires slightly lesser radial layers, however, for short-height NDHX designs, the salt flow in the tube side become turbulent, as it can be observed from Fig 8-35 and this causes the overall design to require lesser radial layer and lesser overall surface area, effectively behaving as a sodium loop.

Overall, the comparison between flinabe and sodium has shown the following: a) liquid metals require greater temperature differential to deliver same amount of heat load for the same loop height, b) liquid metals can have high heat transfer rates at very low mass flow rates, requiring small thermal height between sink and source, however at the expense of greater temperature difference and c) liquid metals require slightly less surface area as compared to salt loops.

8.6 SUMMARY

The program constructed allows the flexibility to obtain heat exchanger designs assuming up to three distinct parameters, thus providing with an estimate on the impact of each variation on the overall DRACS design. The parameters varied in this study are: 1) plant parameters such as area of flow and vertical relative elevation 2) salt-to-air heat exchanger parameters, such as tube diameter and pitch to diameter ratio and 3) coolant type selection, including liquid salts and liquid metals. The impact of each variation was discussed and it was observed that heat exchanger size largely depend and desired air outlet temperature. Smaller heat exchangers output

low air temperatures, transferring heat to high air flow rates. In the range of possible DRACS salt temperatures, these small heat exchangers operate in the lower end, reducing the margin for freezing. In the evaluation of liquid metals as cooling candidates, the low heat capacity typical of these fluids causes the natural circulation loop to operate with a large temperature difference, which is undesirable for material thermal loading concerns, however liquid metals offer greater margin for freezing than salts. The proper balance requires correct prioritization between margin for freezing, desired air outlet temperature taking into consideration economic factors.

8.7 REFERENCES

[1] Medwid, W. A. *Design, Analysis and Verification of Natural Circulation in the GCFR* General Atomic Company, San Diego, CA

[2] B. Farrar et. al., *Fast reactor decay heat removal: Approach to the safety system design in Japan and Europe.* Nuclear Engineering and Design 193 (1999) 45-55

[3] W.M. Kays, M.E. Crawford, Convective Heat and Mass Transfer, 2nd edition., McGraw-Hill, New York, (1987)

9. CONCLUSIONS

An investigation leading to the design and performance analysis during transients of the passive safety system employed by the PB-AHTR was conducted. The guiding principle in this study adhered to the overall nuclear reactor system design process, employing liquid salt, high temperature technology. Work performed by previous researchers internal and external to UC Berkeley served as a strong basis, proving key information on the overall reactor design and the analysis methodology. As a result, a methodology to perform comprehensive safety studies at the plant level and with greater plant detail than previously accomplished was implemented. The importance of this study lies on the feedback provided to plant designers to improve the overall design towards greater safety, improved economy and design robustness.

The objectives set prior to the investigation were accomplished. A methodology for the design of passive safety systems was developed. In addition, a methodology for the transient analysis of the plant was also developed. As a result, a detailed design of the safety system was originated, and the response of the plant during a specific transient was analyzed. Finally, an approach to verify the results obtained and to optimize the passive safety system design was discussed and demonstrated.

In this study, wealth of mathematical expressions for physical phenomena was employed. The applicability of the models was discussed extensively and applied correspondingly. Due to the complex and diverse geometry in the heating and cooling channels in this plant design, the primary remaining challenge is to demonstrate the validity of the heat transfer correlations for high Prandtl fluids, such as liquid salts near the laminar – turbulence transitioning flow region, for the geometries considered.

Sufficient and accurate descriptive information exists to construct a model of the core and primary systems. Also, moderately detailed designs of the primary and safety heat exchangers are available. Secondary and auxiliary cooling systems remain in conceptual design phase, but sound assumptions can be made to represent these components in the overall plant model.

A computer program was constructed, based on the models developed to represent the coupled heat transfer in natural circulation loops subject to temperature constrains problem. The methodology employed provided information on the momentum and energy distribution in the natural circulation loops enabling reactor designers quantify overall effectiveness of the system preventing core overheat when no other heat removal mechanisms are present. The program also provided with a reference point design of the DRACS safety system. It was determined that the reference point design is voluminous and requires moderately elevated temperature difference to operate. The primary source of wall friction is within the tubes of the DHX. Given that these component are located within the reactor pressure vessel, they are subject to size constrains and therefore, a re-evaluation of the selected heat exchanger design must be made. Also, it was found that short and compact NDHX heat exchanger designs can be employed, at the expense of high

air flow rates and low air outlet temperatures, predecessor conditions for rapid overcooling. Finally, it was found the solution algorithm employed simplifies the heat transfer process to a space-independent problem. In this approach, it is imperative that the average a value representing the spatial distribution is carefully made, especially in the case of compressible fluid flow with heat addition and friction losses. This observation occurred when results of the computer program output were compared with results from the analysis with RELAP5-3D, which is a space dependent code.

The transient analysis of the loss of forced cooling event shows slow transition from forced to natural circulation cooling in the core and the DHX. As a result, the peak coolant temperature does not rise above the safety limit imposed at 760 ^{o}C and the peak fuel temperature remains far below the limit of 1600 ^{o}C. The passive cooling system shows a smooth and rapid transition from air louver-suppressed waste heat release to full capacity decay heat removal mode. It was found that the 2% of the full power heat load design basis mark is proper, since the system demonstrated the ability to absorb excess heat in the fluid and metallic structures, internal and external to the core in the early phase of the transient, when greater amounts of heat are generated. These effects are observed within the first 5 minutes of the transient. After 15 minutes heat output is matched with removal capacity and stable heat transfer is sustained. At this point, the air louvers need to be gradually throttled to reduce passive cooling capacity to match heat output. If air louvers are not throttled, DRACS salt reaches the freezing point in approximately 3 hours. While this study assumed an immediate scram response to the LOFC event, it would be interesting to perform this study assuming a failure to immediately scram and allow the passive shutdown rods to scram the reactor after the insertion and travel delay.

Transient analysis with RELAP5-3D re-affirms the need to have the precise correlations employed implemented into the code. Additionally, RELAP5-3D requires careful air flow friction factor weighting due to the numerical scheme employed in the solution architecture.

A simple verification process was discussed that provided initial confidence that the DRACS design matches comparable designs for other similar reactor concepts. Similar DRACS designs employed 2.5-2.75% range as the full power fraction for design basis heat load further adding confidence in the selected fundamental constrains in this study. In addition, the effect of multiple variations to the reference passive safety design were analyzed and the findings provided guidance towards the proper selection of component location, air heat exchanger tube configuration and geometry, and ideal coolant type. The selection of these parameters requires a set criterion which properly balances safety, economy and robustness in the optimization process.

The study presented is the first analyzing passive safety system design and performance for the PB-AHTR. Multiple other studies are required to validate the results obtained. As a suggestion for future analysis complementary to this study, is the quantification of uncertainties, the verification through alternate transient analysis tools, experimental investigation of liquid salt

heat transfer process in laminar-turbulent transition regimes, studies of various options for heat transfer enhancement, and the comparison of transients with Integral Effects Test (IET) experiments to validate the methods and models presented here.

10. APPENDIX

Appendix A: Thermophysical property expressions for various coolants

Appendix B: Program source code listing

Appendix C: RELAP5-3D input file and detailed geometric description

Appendix A

Thermophysical property expressions for various coolants

I. $^{7}Li_2BeF_4$ (Flibe)

$$C_p(K) = 2386\left[\frac{J}{kg \cdot K}\right]$$

$$\rho(K) = -0.4884(T - 273.15) + 2279.7\left[\frac{kg}{m^3}\right]$$

$$\mu(K) = 1.16x10^{-4} e^{\frac{3755}{T}}\left[\frac{kg}{m \cdot s}\right]$$

$$k(K) = 1.1\left[\frac{W}{m \cdot K}\right]$$

II. LiF-NaK-KF (Flinak)

$$C_p(K) = 2386\left[\frac{J}{kg \cdot K}\right]$$

$$\rho(K) = -0.4884(T - 273.15) + 2279.7\left[\frac{kg}{m^3}\right]$$

$$\mu(K) = 1.16x10^{-4} e^{\frac{3755}{T}}\left[\frac{kg}{m \cdot s}\right]$$

$$k(K) = 1.1\left[\frac{W}{m \cdot K}\right]$$

III. LiF-BeF_2-NaF (Flinabe)

$$C_p(K) = 2386\left[\frac{J}{kg \cdot K}\right]$$

$$\rho(K) = -0.4884(T - 273.15) + 2279.7\left[\frac{kg}{m^3}\right]$$

$$\mu(K) = 1.16x10^{-4} e^{\frac{3755}{T}}\left[\frac{kg}{m \cdot s}\right]$$

$$k(K) = 1.1\left[\frac{W}{m \cdot K}\right]$$

IV. NaK

$$C_p(K) = 2386\left[\frac{J}{kg \cdot K}\right]$$

$$\rho(K) = -0.4884(T - 273.15) + 2279.7\left[\frac{kg}{m^3}\right]$$

$$\mu(K) = 1.16x10^{-4} e^{\frac{3755}{T}}\left[\frac{kg}{m \cdot s}\right]$$

$$k(K) = 1.1\left[\frac{W}{m \cdot K}\right]$$

V. Pbbi

$$C_p(K) = 2386\left[\frac{J}{kg \cdot K}\right]$$

$$\rho(K) = -0.4884(T - 273.15) + 2279.7\left[\frac{kg}{m^3}\right]$$

$$\mu(K) = 1.16x10^{-4} e^{\frac{3755}{T}}\left[\frac{kg}{m \cdot s}\right]$$

$$k(K) = 1.1\left[\frac{W}{m \cdot K}\right]$$

VI. Na

$$C_p(K) = 1658.2 - 8.479x10^{-1}T + 4.454x10^{-4}T^2 - 2.992x10^{6}T^{-2}\left[\frac{J}{kg \cdot K}\right]$$

$$\rho(K) = 5.638x10^{-9}T^3 - 1.956x10^{-5}T^2 - 0.2197T + 1016.1\left[\frac{kg}{m^3}\right]$$

$$\mu(K) = e^{-6.4406 - 0.3958\ln(T) + \frac{556.835}{T}}\left[\frac{kg}{m \cdot s}\right]$$

$$k(K) = 124.67 - 0.1138T + 5.5226x10^{-5}T^2 - 1.1842x10^{-8}T^3\left[\frac{W}{m \cdot K}\right]$$

VII. Air

$$C_p(K) = \frac{1}{28.97x10^{-3}}\left(28.11 + 0.1967x10^{-2}T + 0.4802x10^{-5}T^2 - 1.996x10^{-9}T^3\right)\left[\frac{J}{kg \cdot K}\right]$$

$$\rho(K) = \frac{101215}{287T}\left[\frac{kg}{m^3}\right]$$

$$\mu(K) = 1.71x10^{-5}\left(\frac{T}{273}\right)^{\frac{2}{3}}\left(\frac{273+110.4}{T+110.4}\right)\left[\frac{kg}{m \cdot s}\right]$$

$$k(K) = \mu(T)\left(C_p(T) + \frac{5}{4}\frac{\overline{R}}{28.02x10^{-3}}\right)\left[\frac{W}{m \cdot K}\right]$$

VIII. Nitrogen

$$C_p(K) = \frac{1}{28.02x10^{-3}}\left(28.90 + 0.1571x10^{-2}T + 0.8081x10^{-5}T^2 - 2.873x10^{-9}T^3\right)\left[\frac{J}{kg \cdot K}\right]$$

$$\rho(K) = \frac{101215}{297T}\left[\frac{kg}{m^3}\right]$$

$$\mu(K) = 1.76x10^{-5}\left(\frac{T}{293}\right)^{\frac{2}{3}}\left[\frac{kg}{m \cdot s}\right]$$

$$k(K) = \mu(T)\left(C_p(T) + \frac{5}{4}\frac{\overline{R}}{28.97x10^{-3}}\right)\left[\frac{W}{m \cdot K}\right]$$

Appendix B

Computer source code listing

The following diagram establishes the name of the functions listed in the following sections. The module labeled Master is the primary algorithm which calls all other supplementary functions in the solution. The diagram below is identical to Fig. 5-2 and the solution methodology is described in section 5.2 in detail.

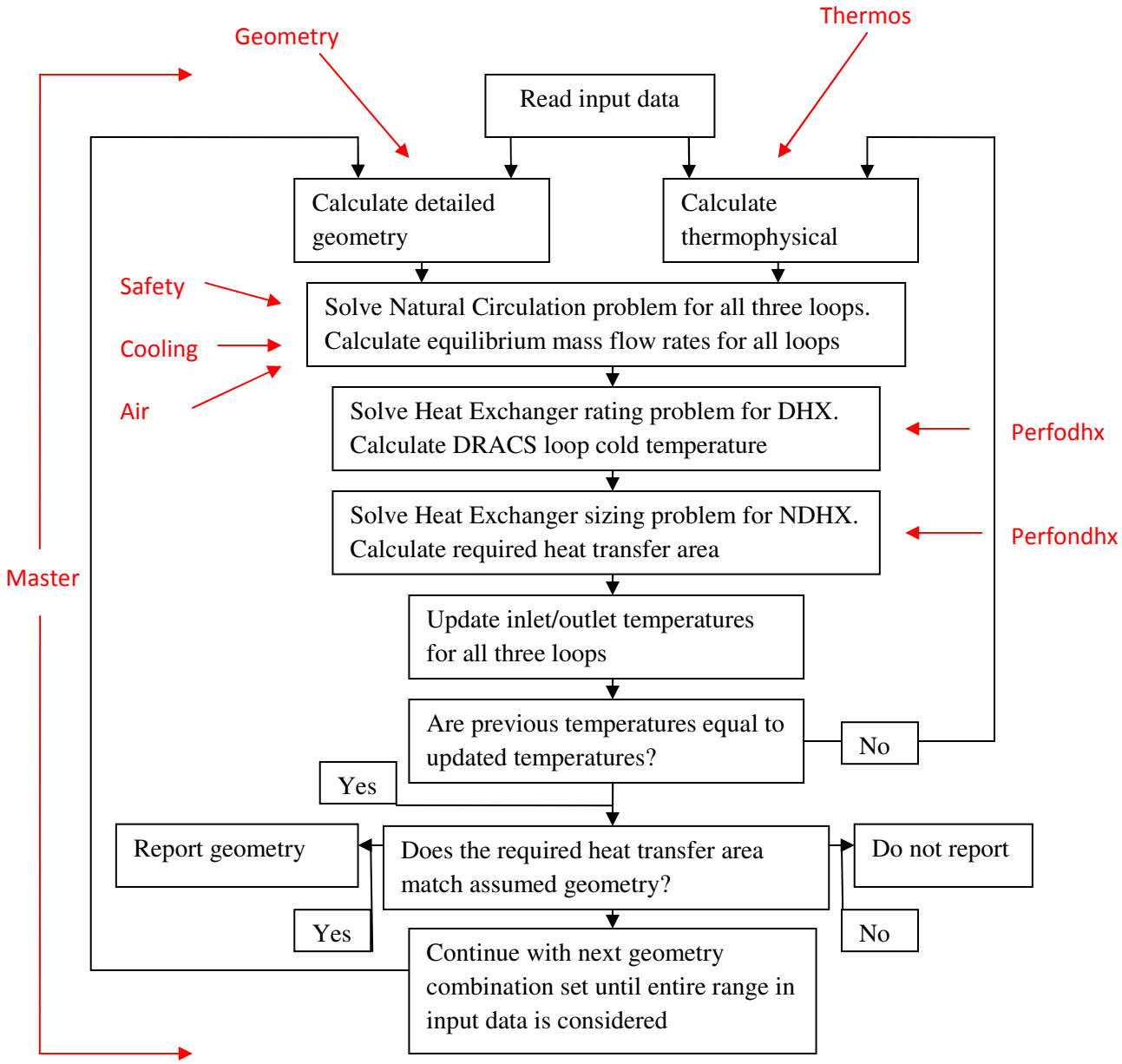

I. Master

```
clear all, close all;

heat=18e6;
%lower nwin range
lnwr=0.2;%0.0;%0.5;
%upper nwin range
unwr=1.35;%1.625;%2.0;
%lower nlay range
lnlr=36;%0;%10;
%upper nlay range
unlr=64;%24;%30;
%NUMBER of nwin intervals
nwit=30;%1;%20;%%%%%%%%%%%%%%%%%%%%%%%%%%%%%%%%%%%%
%NUMBER of i nlay intervals
nlit=30;%1;%20;%%%%%%%%%%%%%%%%%%%%%%%%%%%%%%%%%%%%
%calc i (nlay) multiplier
imul=(unlr-lnlr)/nlit;
%calc j (nwin) multiplier
jmul=(unwr-lnwr)/nwit;

for aa=1:3
    k=0;

    for i=1:nlit;
        for j=1:nwit;
            diagnostic=[aa i j]
            %COIL HEAT EXCHANGER SIZE
            nlay=lnlr+i*imul;
            nwin=lnwr+j*jmul;
            %nwin=0.9+j/100;
            %DISK-DOUGHNUT PARAMETER
            htdha=442.218;
            dtouh=0.0095;
            dtinh=0.0069;
            afdho=0.2383;
            afdhi=0.1798;
            ldhx=2.6;
            across=21.34;
            %COIL HEAT EXCHANGER PARAMETERS
            rinn=0.1;
            dtin=0.04+(aa-1)*0.01;
            dtou=dtin+0.006;
            podr=1.85;%1.70+(aa-1)*0.15;
            alce=15;
            %PLANT PARAMETERS
            afpis=0.07;
            aori=0.035;
            afpi=0.06;
            afpia=5.0;
            lfdl=5.0;
            lvll=8.0;
            lchi=20.0;
            %FLUID SELECTION
            ssaf=1;
            scoo=2;
            sair=2;
            %TEMPERATURES
            tins=765+273;
            thos=tins;
            tina=20+273;
            tcoa=tina;
            %Assume initial temps;
            tcoc=700+273;
            thoc=750+273;
            tcos=730+273;
            thoa=500+273;
            err1=3;
            err2=1;
            while err2>=1%err1>=3&err2>=1
                %THERMO PROPERTY CALLING
                [cpsa,cpco,cpai,...
                    c2sa,c2co,...
                    rhsa,rhco,rhav,rhah,rhac,...
                    musa,muco,muai,...
                    musash,mucosc,mucosh,muaic,muaih...
                    kcsa,kcco,kcai,...
                    prsa,prco,prai]=...
                    thermos(ssaf,scoo,sair,...
                    tcos,thos,...
                    tcoc,thoc,...
                    tcoa,thoa);

                %FUNCTION CALLING

[g1,g2,g3,g4,g5,g6,g7,g8,g9,g10,g11,g12,g13]=...

geometry(rinn,nlay,nwin,dtou,dtin,podr,alce);
                [s1,s2,s3,s4,s5,s6,s7,s8,s9]=...
```

```
                    safety(heat,afpis,lfdl,...
                    afdho,dtouh,ldhx,across,aori,...
                    cpsa,c2sa,rhsa,musa);

[c1,c2,c3,c4,c5,c6,c7,c8,c9,c10,c11,c12]=...

cooling(heat,g1,g2,g4,g3,g8,afpi,lvll,afdhi,...
                    cpco,c2co,rhco,muco);
                [a1,a2,a3,a4,a5,a6,a7,a8,a9,a10,a11]=...

air(heat,g5,g7,g3,afpia,lchi,podr,...

cpai,rhav,rhah,rhac,muai,muaic,muaih,tcoa);
                [pd1,pd2,pd3,pd4,pd5]=...

perfodhx(heat,dtouh,dtinh,htdha,tins,scoo...
                    ,s1,c1,s2,c2,...

kcsa,prsa,cpsa,kcco,prco,cpco,muco,mucosh);
                [pn1,pn2,pn3]=...
                    perfondhx(heat,g2,g7,g8,g9,...
                    podr,thoc,scoo,tina,...
                    c4,a1,c2,a2,...

kcai,cpai,kcco,prco,cpco,muco,mucosc);
                [sca1,sca2,sca3,sca4]=...
                    scaled(rinn,g10,g13);
                [done]=riter(afpis,afpi,afpia,aori,...
                    dtin,dtou,dtinh,dtouh,g7,...
                    g6,htdha,...
                    afdho,g5,g1,afdhi,...
                    a10,a11,0.15,c11,c12,0.5,across,...
                    lfdl,ldhx,g4,g3,lvll,lchi);
                %computing outlet temps;
                tcoc_old=tcoc;
                thoc_old=thoc;
                thoa_old=thoa;
                tcoc=pd1;
                thoc=pd1+c3;
                tcos=thos-s3;
                thoa=tcoa+a3;
                err1=abs(thoa_old-thoa);
                err2=abs(thoc_old-thoc);
            end
```

```
                dummy=pn1/g6;

                if
(isreal(pn1)>0&a8>1)&(dummy<1.05&dummy>0.95)

                    k=k+1;
                    if aa==1;
                        ge(k,1)=g3;
                        ge(k,2)=g8;

ge(k,3)=(g6/(pi*dtou))*pi*(dtin/2)^2;
                        ge(k,4)=g1/(pi*(dtin/2)^2);
                        ge(k,5)=g4;
                        ge(k,6)=nlay;
                        ge(k,7)=g10;
                        ge(k,8)=nwin;
                        ge(k,9)=g11;
                        ge(k,10)=g12;

                        mf(k,1)=a2;%mflow
                        mf(k,2)=c2;
                        mf(k,3)=s2;
                        dpb(k,1)=a4;
                        dpb(k,2)=c5;
                        dpb(k,3)=s4;

                        t(k,1)=tcoa;
                        t(k,2)=thoa;
                        t(k,3)=tcoc;
                        t(k,4)=thoc;
                        t(k,5)=tcos;
                        t(k,6)=thos;
                        dt(k,1)=a3;
                        dt(k,2)=c3;
                        dt(k,3)=s3;

                        re(k,1)=a1;
                        re(k,2)=c4;
                        re(k,3)=c1;
                        re(k,4)=s1;
                        eu(k,1)=a9;
                        eu(k,2)=c10;
                        eu(k,3)=c9;
                        eu(k,4)=s8;%eu ext dhx
                        ht(k,1)=pn2;%ndhx air
```

```
                    ht(k,2)=pn3;%ndhx tube
                    ht(k,3)=pd3;%dhx tube
                    ht(k,4)=pd2;%dhx shell

                    dpf(k,1)=100*(a6+a7)/a4;
                    dpf(k,2)=100*c8/c5;
                    dpf(k,3)=100*s7/s4;
                    dpf(k,4)=dummy;
                    dpf(k,5)=pn1;

                    lmtd(k,1)=((thos-thoc)-(tcos-
tcoc))/...
                        log((thos-thoc)/(tcos-tcoc));
                    lmtd(k,2)=((thoc-thoa)-(tcoc-
tcoa))/...
                        log((thoc-thoa)/(tcoc-tcoa));

                    dp(k,1)=a6;%cold pipe
                    dp(k,2)=a5;%heater
                    dp(k,3)=a7;%hot pipe
                    dp(k,4)=c6;%heater
                    dp(k,5)=c8;%piping
                    dp(k,6)=c7;%cooler
                    dp(k,7)=s5;%heater
                    dp(k,8)=s7;%piping
                    dp(k,9)=s6;%cooler

                    sc(k,1)=sca1;
                    sc(k,2)=sca2;
                    sc(k,3)=sca3;
                    sc(k,4)=sca4;

                    per(k,1)=pd4;
                    per(k,2)=pd5;

                    ppp=ge(:,1);
                elseif aa==2
                    ge2(k,1)=g3;
                    ge2(k,2)=g8;

ge2(k,3)=(g6/(pi*dtou))*pi*(dtin/2)^2;
                    ge2(k,4)=g1/(pi*(dtin/2)^2);
                    ge2(k,5)=g4;
                    ge2(k,6)=nlay;
                    ge2(k,7)=g10;
                    ge2(k,8)=nwin;
                    ge2(k,9)=g11;
                    ge2(k,10)=g12;


                    mf2(k,1)=a2;%mflow
                    mf2(k,2)=c2;
                    mf2(k,3)=s2;
                    dpb2(k,1)=a4;
                    dpb2(k,2)=c5;
                    dpb2(k,3)=s4;

                    t2(k,1)=tcoa;
                    t2(k,2)=thoa;
                    t2(k,3)=tcoc;
                    t2(k,4)=thoc;
                    t2(k,5)=tcos;
                    t2(k,6)=thos;
                    dt2(k,1)=a3;
                    dt2(k,2)=c3;
                    dt2(k,3)=s3;

                    re2(k,1)=a1;
                    re2(k,2)=c4;
                    re2(k,3)=c1;
                    re2(k,4)=s1;
                    eu2(k,1)=a9;
                    eu2(k,2)=c10;
                    eu2(k,3)=c9;
                    eu2(k,4)=s8;%eu ext dhx
                    ht2(k,1)=pn2;%ndhx air
                    ht2(k,2)=pn3;%ndhx tube
                    ht2(k,3)=pd3;%dhx tube
                    ht2(k,4)=pd2;%dhx shell

                    dpf2(k,1)=100*(a6+a7)/a4;
                    dpf2(k,2)=100*c8/c5;
                    dpf2(k,3)=100*s7/s4;
                    dpf2(k,4)=dummy;
                    dpf2(k,5)=pn1;

                    lmtd2(k,1)=((thos-thoc)-(tcos-
tcoc))/...
                        log((thos-thoc)/(tcos-tcoc));
```

```
                    lmtd2(k,2)=((thoc-thoa)-(tcoc-
tcoa))/...
                        log((thoc-thoa)/(tcoc-tcoa));

                    dp2(k,1)=a6;%cold pipe
                    dp2(k,2)=a5;%heater
                    dp2(k,3)=a7;%hot pipe
                    dp2(k,4)=c6;%heater
                    dp2(k,5)=c8;%piping
                    dp2(k,6)=c7;%cooler
                    dp2(k,7)=s5;%heater
                    dp2(k,8)=s7;%piping
                    dp2(k,9)=s6;%cooler

                    sc2(k,1)=sca1;
                    sc2(k,2)=sca2;
                    sc2(k,3)=sca3;
                    sc2(k,4)=sca4;

                    ppp2=ge2(:,1);
                else
                    ge3(k,1)=g3;
                    ge3(k,2)=g8;

ge3(k,3)=(g6/(pi*dtou))*pi*(dtin/2)^2;
                    ge3(k,4)=g1/(pi*(dtin/2)^2);
                    ge3(k,5)=g4;
                    ge3(k,6)=nlay;
                    ge3(k,7)=g10;
                    ge3(k,8)=nwin;
                    ge3(k,9)=g11;
                    ge3(k,10)=g12;

                    mf3(k,1)=a2;%mflow
                    mf3(k,2)=c2;
                    mf3(k,3)=s2;
                    dpb3(k,1)=a4;
                    dpb3(k,2)=c5;
                    dpb3(k,3)=s4;

                    t3(k,1)=tcoa;
                    t3(k,2)=thoa;
                    t3(k,3)=tcoc;
                    t3(k,4)=thoc;
                    t3(k,5)=tcos;
                    t3(k,6)=thos;
                    dt3(k,1)=a3;
                    dt3(k,2)=c3;
                    dt3(k,3)=s3;

                    re3(k,1)=a1;
                    re3(k,2)=c4;
                    re3(k,3)=c1;
                    re3(k,4)=s1;
                    eu3(k,1)=a9;
                    eu3(k,2)=c10;
                    eu3(k,3)=c9;
                    eu3(k,4)=s8;%eu ext dhx
                    ht3(k,1)=pn2;%ndhx air
                    ht3(k,2)=pn3;%ndhx tube
                    ht3(k,3)=pd3;%dhx tube
                    ht3(k,4)=pd2;%dhx shell

                    dpf3(k,1)=100*(a6+a7)/a4;
                    dpf3(k,2)=100*c8/c5;
                    dpf3(k,3)=100*s7/s4;
                    dpf3(k,4)=dummy;
                    dpf3(k,5)=pn1;

                    lmtd3(k,1)=((thos-thoc)-(tcos-
tcoc))/...
                        log((thos-thoc)/(tcos-tcoc));
                    lmtd3(k,2)=((thoc-thoa)-(tcoc-
tcoa))/...
                        log((thoc-thoa)/(tcoc-tcoa));

                    dp3(k,1)=a6;%cold pipe
                    dp3(k,2)=a5;%heater
                    dp3(k,3)=a7;%hot pipe
                    dp3(k,4)=c6;%heater
                    dp3(k,5)=c8;%piping
                    dp3(k,6)=c7;%cooler
                    dp3(k,7)=s5;%heater
                    dp3(k,8)=s7;%piping
                    dp3(k,9)=s6;%cooler

                    sc3(k,1)=sca1;
                    sc3(k,2)=sca2;
                    sc3(k,3)=sca3;
                    sc3(k,4)=sca4;
```

```
                    ppp3=ge3(:,1);
                end
            else
            end

        end

    end

end



%plots
if aa==1

    subplot(3,3,1);plot(ppp,ge(:,2),'o');title('Surface
Area')
    subplot(3,3,2);plot(ppp,ge(:,3),'o');title('Fluid
Volume')
    subplot(3,3,3);plot(ppp,ge(:,4),'o');title('Number
of Tubes')
    subplot(3,3,4);plot(ppp,ge(:,5),'o');title('Ave tube
length')
    subplot(3,3,5);plot(ppp,ge(:,6),'o');title('Number
of radial layers')
    subplot(3,3,6);plot(ppp,ge(:,7),'o');title('Outer
Radius')
    subplot(3,3,7);plot(ppp,ge(:,8),'o');title('Number
of windings')
    subplot(3,3,8);plot(ppp,ge(:,9),'o');title('alpha
in')
    subplot(3,3,9);plot(ppp,ge(:,10),'o');title('alpha
out')
    figure

    subplot(3,8,1);plot(ppp,mf(:,1),'o');title('Air cold
mflow')
    subplot(3,8,9);plot(ppp,mf(:,2),'o');title('cooling
mflow')
    subplot(3,8,17);plot(ppp,mf(:,3),'o');title('safety
mflow')
    subplot(3,8,2);plot(ppp,dpb(:,1),'o');title('Air
buoyancy lift')

subplot(3,8,10);plot(ppp,dpb(:,2),'o');title('Cooling
loop buoyancy lift')
    subplot(3,8,18);plot(ppp,dpb(:,3),'o');title('Safety
buoyancy lift')
    subplot(3,8,6);plot(ppp,t(:,1),'o');title('Air cold
Temp')
    subplot(3,8,7);plot(ppp,t(:,2),'o');title('Air hot
temp')
    subplot(3,8,14);plot(ppp,t(:,3),'o');title('Cooling
loop cold temp')
    subplot(3,8,15);plot(ppp,t(:,4),'o');title('Cooling
loop hot temp')
    subplot(3,8,22);plot(ppp,t(:,5),'o');title('Safety
loop cold temp')
    subplot(3,8,23);plot(ppp,t(:,6),'o');title('Safety
loop hot temp')
    subplot(3,8,8);plot(ppp,dt(:,1),'o');title('Air DT')
    subplot(3,8,16);plot(ppp,dt(:,2),'o');title('Cooling
DT')
    subplot(3,8,24);plot(ppp,dt(:,3),'o');title('Safety
DT')
    subplot(3,8,3);plot(ppp,dp(:,1),'o');title('dPf in-
chi air')
    subplot(3,8,4);plot(ppp,dp(:,2),'o');title('dP-f
heater air')
    subplot(3,8,5);plot(ppp,dp(:,3),'o');title('dP-f
out-chi air')
    subplot(3,8,11);plot(ppp,dp(:,4),'o');title('dP-f
heater cooling')
    subplot(3,8,12);plot(ppp,dp(:,5),'o');title('dP-f
piping cooling')
    subplot(3,8,13);plot(ppp,dp(:,6),'o');title('dP-f
cooler cooling')
    subplot(3,8,19);plot(ppp,dp(:,7),'o');title('dP-f
heater safety')
    subplot(3,8,20);plot(ppp,dp(:,8),'o');title('dP-f
piping safety')
    subplot(3,8,21);plot(ppp,dp(:,9),'o');title('dP-f
cooler safety')
```

```
    figure
    subplot(3,4,1);plot(ppp,re(:,1),'o');title('Re air
heater')
    subplot(3,4,2);plot(ppp,re(:,2),'o');title('Re ndhx
coolant')
    subplot(3,4,3);plot(ppp,re(:,3),'o');title('Re dhx
coolant')
    subplot(3,4,4);plot(ppp,re(:,4),'o');title('Re dhx
flibe')
    subplot(3,4,5);plot(ppp,eu(:,1),'o');title('Eu air
heater')
    subplot(3,4,6);plot(ppp,eu(:,2),'o');title('Eu ndhx
coolant')
    subplot(3,4,7);plot(ppp,eu(:,3),'o');title('Eu dhx
coolant')
    subplot(3,4,8);plot(ppp,eu(:,4),'o');title('Eu dhx
flibe')
    subplot(3,4,9);plot(ppp,ht(:,1),'o');title('h ndhx
air')
    subplot(3,4,10);plot(ppp,ht(:,2),'o');title('h ndhx
coolant')
    subplot(3,4,11);plot(ppp,ht(:,3),'o');title('h dhx
coolant')
    subplot(3,4,12);plot(ppp,ht(:,4),'o');title('h dhx
flibe')


    figure

subplot(2,2,1);plot(ppp,sc(:,1),'o');title('prototype
inner radius')

subplot(2,2,2);plot(ppp,sc(:,2),'o');title('prototype
outer radius')

subplot(2,2,3);plot(ppp,sc(:,3),'o');title('prototype
inner alpha')

subplot(2,2,4);plot(ppp,sc(:,4),'o');title('prototype
outer alpha')
    figure
    subplot(2,2,1);plot(ppp,per(:,1),'o');title('U')
    subplot(2,2,2);plot(ppp,per(:,2),'o');title('NTU')

elseif aa==2
```

```
subplot(3,3,1);plot(ppp,ge(:,2),'or',ppp2,ge2(:,2),'ob')
;title('Surface Area')

subplot(3,3,2);plot(ppp,ge(:,3),'or',ppp2,ge2(:,3),'o');
title('Fluid Volume')

subplot(3,3,3);plot(ppp,ge(:,4),'or',ppp2,ge2(:,4),'o');
title('Number of Tubes')

subplot(3,3,4);plot(ppp,ge(:,5),'or',ppp2,ge2(:,5),'o');
title('Ave tube length')

subplot(3,3,5);plot(ppp,ge(:,6),'or',ppp2,ge2(:,6),'o');
title('Number of radial layers')

subplot(3,3,6);plot(ppp,ge(:,7),'or',ppp2,ge2(:,7),'o');
title('Outer Radius')

subplot(3,3,7);plot(ppp,ge(:,8),'or',ppp2,ge2(:,8),'o');
title('Number of windings')

subplot(3,3,8);plot(ppp,ge(:,9),'or',ppp2,ge2(:,9),'o');
title('alpha in')

subplot(3,3,9);plot(ppp,ge(:,10),'or',ppp2,ge2(:,10),'o'
);title('alpha out')
    figure


subplot(3,8,1);plot(ppp,mf(:,1),'or',ppp2,mf2(:,1),'o');
title('Air cold mflow')

subplot(3,8,9);plot(ppp,mf(:,2),'or',ppp2,mf2(:,2),'o');
title('cooling mflow')

subplot(3,8,17);plot(ppp,mf(:,3),'or',ppp2,mf2(:,3),'o')
;title('safety mflow')

subplot(3,8,2);plot(ppp,dpb(:,1),'or',ppp2,dpb2(:,1),'o'
);title('Air buoyancy lift')
```

```
subplot(3,8,10);plot(ppp,dpb(:,2),'or',ppp2,dpb2(:,2),'o
');title('Cooling loop buoyancy lift')

subplot(3,8,18);plot(ppp,dpb(:,3),'or',ppp2,dpb2(:,3),'o
');title('Safety buoyancy lift')

subplot(3,8,6);plot(ppp,t(:,1),'or',ppp2,t2(:,1),'o');ti
tle('Air cold Temp')

subplot(3,8,7);plot(ppp,t(:,2),'or',ppp2,t2(:,2),'o');ti
tle('Air hot temp')

subplot(3,8,14);plot(ppp,t(:,3),'or',ppp2,t2(:,3),'o');t
itle('Cooling loop cold temp')

subplot(3,8,15);plot(ppp,t(:,4),'or',ppp2,t2(:,4),'o');t
itle('Cooling loop hot temp')

subplot(3,8,22);plot(ppp,t(:,5),'or',ppp2,t2(:,5),'o');t
itle('Safety loop cold temp')

subplot(3,8,23);plot(ppp,t(:,6),'or',ppp2,t2(:,6),'o');t
itle('Safety loop hot temp')

subplot(3,8,8);plot(ppp,dt(:,1),'or',ppp2,dt2(:,1),'o');
title('Air DT')

subplot(3,8,16);plot(ppp,dt(:,2),'or',ppp2,dt2(:,2),'o')
;title('Cooling DT')

subplot(3,8,24);plot(ppp,dt(:,3),'or',ppp2,dt2(:,3),'o')
;title('Safety DT')

subplot(3,8,3);plot(ppp,dp(:,1),'or',ppp2,dp2(:,1),'o');
title('dPf in-chi air')

subplot(3,8,4);plot(ppp,dp(:,2),'or',ppp2,dp2(:,2),'o');
title('dP-f heater air')

subplot(3,8,5);plot(ppp,dp(:,3),'or',ppp2,dp2(:,3),'o');
title('dP-f out-chi air')

subplot(3,8,11);plot(ppp,dp(:,4),'or',ppp2,dp2(:,4),'o')
;title('dP-f heater cooling')

subplot(3,8,12);plot(ppp,dp(:,5),'or',ppp2,dp2(:,5),'o')
;title('dP-f piping cooling')

subplot(3,8,13);plot(ppp,dp(:,6),'or',ppp2,dp2(:,6),'o')
;title('dP-f cooler cooling')

subplot(3,8,19);plot(ppp,dp(:,7),'or',ppp2,dp2(:,7),'o')
;title('dP-f heater safety')

subplot(3,8,20);plot(ppp,dp(:,8),'or',ppp2,dp2(:,8),'o')
;title('dP-f piping safety')

subplot(3,8,21);plot(ppp,dp(:,9),'or',ppp2,dp2(:,9),'o')
;title('dP-f cooler safety')

    figure

subplot(3,4,1);plot(ppp,re(:,1),'or',ppp2,re2(:,1),'o');
title('Re air heater')

subplot(3,4,2);plot(ppp,re(:,2),'or',ppp2,re2(:,2),'o');
title('Re ndhx coolant')

subplot(3,4,3);plot(ppp,re(:,3),'or',ppp2,re2(:,3),'o');
title('Re dhx coolant')

subplot(3,4,4);plot(ppp,re(:,4),'or',ppp2,re2(:,4),'o');
title('Re dhx flibe')

subplot(3,4,5);plot(ppp,eu(:,1),'or',ppp2,eu2(:,1),'o');
title('Eu air heater')

subplot(3,4,6);plot(ppp,eu(:,2),'or',ppp2,eu2(:,2),'o');
title('Eu ndhx coolant')

subplot(3,4,7);plot(ppp,eu(:,3),'or',ppp2,eu2(:,3),'o');
title('Eu dhx coolant')

subplot(3,4,8);plot(ppp,eu(:,4),'or',ppp2,eu2(:,4),'o');
title('Eu dhx flibe')

subplot(3,4,9);plot(ppp,ht(:,1),'or',ppp2,ht2(:,1),'o');
title('h ndhx air')
```

```
subplot(3,4,10);plot(ppp,ht(:,2),'or',ppp2,ht2(:,2),'o')
;title('h ndhx coolant')

subplot(3,4,11);plot(ppp,ht(:,3),'or',ppp2,ht2(:,3),'o')
;title('h dhx coolant')

subplot(3,4,12);plot(ppp,ht(:,4),'or',ppp2,ht2(:,4),'o')
;title('h dhx flibe')
    figure

subplot(2,2,1);plot(ppp,sc(:,1),'or',ppp2,sc2(:,1),'o');
title('prototype inner radius')

subplot(2,2,2);plot(ppp,sc(:,2),'or',ppp2,sc2(:,2),'o');
title('prototype outer radius')

subplot(2,2,3);plot(ppp,sc(:,3),'or',ppp2,sc2(:,3),'o');
title('prototype inner alpha')

subplot(2,2,4);plot(ppp,sc(:,4),'or',ppp2,sc2(:,4),'o');
title('prototype outer alpha')
else


subplot(3,3,1);plot(ppp,ge(:,2),'or',ppp2,ge2(:,2),'ob',
ge3(:,1),ge3(:,2),'og');title('Surface
Area');legend('1','2','3')

subplot(3,3,2);plot(ppp,ge(:,3),'or',ppp2,ge2(:,3),'ob',
ppp3,ge3(:,3),'og');title('Fluid
Volume');legend('1','2','3')

subplot(3,3,3);plot(ppp,ge(:,4),'or',ppp2,ge2(:,4),'ob',
ppp3,ge3(:,4),'og');title('Number of
Tubes');legend('1','2','3')

subplot(3,3,4);plot(ppp,ge(:,5),'or',ppp2,ge2(:,5),'ob',
ppp3,ge3(:,5),'og');title('Ave tube
length');legend('1','2','3')

subplot(3,3,5);plot(ppp,ge(:,6),'or',ppp2,ge2(:,6),'ob',
ppp3,ge3(:,6),'og');title('Number of radial
layers');legend('1','2','3')

subplot(3,3,6);plot(ppp,ge(:,7),'or',ppp2,ge2(:,7),'ob',
ppp3,ge3(:,7),'og');title('Outer
radius');legend('1','2','3')

subplot(3,3,7);plot(ppp,ge(:,8),'or',ppp2,ge2(:,8),'ob',
ppp3,ge3(:,8),'og');title('Nwinn');legend('1','2','3')

subplot(3,3,8);plot(ppp,ge(:,9),'or',ppp2,ge2(:,9),'ob',
ppp3,ge3(:,9),'og');title('alpha
in');legend('1','2','3')

subplot(3,3,9);plot(ppp,ge(:,10),'or',ppp2,ge2(:,10),'ob
',ppp3,ge3(:,10),'og');title('alpha
out');legend('1','2','3')
    figure


subplot(3,8,1);plot(ppp,mf(:,1),'or',ppp2,mf2(:,1),'ob',
ppp3,mf3(:,1),'og');title('Air cold mflow')

subplot(3,8,9);plot(ppp,mf(:,2),'or',ppp2,mf2(:,2),'ob',
ppp3,mf3(:,2),'og');title('cooling mflow')

subplot(3,8,17);plot(ppp,mf(:,3),'or',ppp2,mf2(:,3),'ob'
,ppp3,mf3(:,3),'og');title('safety mflow')

subplot(3,8,2);plot(ppp,dpb(:,1),'or',ppp2,dpb2(:,1),'ob
',ppp3,dpb3(:,1),'og');title('Air buoyancy lift')

subplot(3,8,10);plot(ppp,dpb(:,2),'or',ppp2,dpb2(:,2),'o
b',ppp3,dpb3(:,2),'og');title('Cooling loop buoyancy
lift')

subplot(3,8,18);plot(ppp,dpb(:,3),'or',ppp2,dpb2(:,3),'o
b',ppp3,dpb3(:,3),'og');title('Safety buoyancy lift')

subplot(3,8,6);plot(ppp,t(:,1),'or',ppp2,t2(:,1),'ob',pp
p3,t3(:,1),'og');title('Air cold Temp')

subplot(3,8,7);plot(ppp,t(:,2),'or',ppp2,t2(:,2),'ob',pp
p3,t3(:,2),'og');title('Air hot temp')

subplot(3,8,14);plot(ppp,t(:,3),'or',ppp2,t2(:,3),'ob',p
pp3,t3(:,3),'og');title('Cooling loop cold temp')
```

```
subplot(3,8,15);plot(ppp,t(:,4),'or',ppp2,t2(:,4),'ob',p
pp3,t3(:,4),'og');title('Cooling loop hot temp')

subplot(3,8,22);plot(ppp,t(:,5),'or',ppp2,t2(:,5),'ob',p
pp3,t3(:,5),'og');title('Safety loop cold temp')

subplot(3,8,23);plot(ppp,t(:,6),'or',ppp2,t2(:,6),'ob',p
pp3,t3(:,6),'og');title('Safety loop hot temp')

subplot(3,8,8);plot(ppp,dt(:,1),'or',ppp2,dt2(:,1),'ob',
ppp3,dt3(:,1),'og');title('Air DT')

subplot(3,8,16);plot(ppp,dt(:,2),'or',ppp2,dt2(:,2),'ob'
,ppp3,dt3(:,2),'og');title('Cooling DT')

subplot(3,8,24);plot(ppp,dt(:,3),'or',ppp2,dt2(:,3),'ob'
,ppp3,dt3(:,3),'og');title('Safety DT')

subplot(3,8,3);plot(ppp,dp(:,1),'or',ppp2,dp2(:,1),'ob',
ppp3,dp3(:,1),'og');title('dPf in-chi air')

subplot(3,8,4);plot(ppp,dp(:,2),'or',ppp2,dp2(:,2),'ob',
ppp3,dp3(:,2),'og');title('dP-f heater air')

subplot(3,8,5);plot(ppp,dp(:,3),'or',ppp2,dp2(:,3),'ob',
ppp3,dp3(:,3),'og');title('dP-f out-chi air')

subplot(3,8,11);plot(ppp,dp(:,4),'or',ppp2,dp2(:,4),'ob'
,ppp3,dp3(:,4),'og');title('dP-f heater cooling')

subplot(3,8,12);plot(ppp,dp(:,5),'or',ppp2,dp2(:,5),'ob'
,ppp3,dp3(:,5),'og');title('dP-f piping cooling')

subplot(3,8,13);plot(ppp,dp(:,6),'or',ppp2,dp2(:,6),'ob'
,ppp3,dp3(:,6),'og');title('dP-f cooler cooling')

subplot(3,8,19);plot(ppp,dp(:,7),'or',ppp2,dp2(:,7),'ob'
,ppp3,dp3(:,7),'og');title('dP-f heater safety')

subplot(3,8,20);plot(ppp,dp(:,8),'or',ppp2,dp2(:,8),'ob'
,ppp3,dp3(:,8),'og');title('dP-f piping safety')

subplot(3,8,21);plot(ppp,dp(:,9),'or',ppp2,dp2(:,9),'ob'
,ppp3,dp3(:,9),'og');title('dP-f cooler safety')
```



```
    figure

subplot(3,4,1);plot(ppp,re(:,1),'or',ppp2,re2(:,1),'ob',
ppp3,re3(:,1),'og');title('Re air heater')

subplot(3,4,2);plot(ppp,re(:,2),'or',ppp2,re2(:,2),'ob',
ppp3,re3(:,2),'og');title('Re ndhx coolant')

subplot(3,4,3);plot(ppp,re(:,3),'or',ppp2,re2(:,3),'ob',
ppp3,re3(:,3),'og');title('Re dhx coolant')

subplot(3,4,4);plot(ppp,re(:,4),'or',ppp2,re2(:,4),'ob',
ppp3,re3(:,4),'og');title('Re dhx flibe')

subplot(3,4,5);plot(ppp,eu(:,1),'or',ppp2,eu2(:,1),'ob',
ppp3,eu3(:,1),'og');title('Eu air heater')

subplot(3,4,6);plot(ppp,eu(:,2),'or',ppp2,eu2(:,2),'ob',
ppp3,eu3(:,2),'og');title('Eu ndhx coolant')

subplot(3,4,7);plot(ppp,eu(:,3),'or',ppp2,eu2(:,3),'ob',
ppp3,eu3(:,3),'og');title('Eu dhx coolant')

subplot(3,4,8);plot(ppp,eu(:,4),'or',ppp2,eu2(:,4),'ob',
ppp3,eu3(:,4),'og');title('Eu dhx flibe')

subplot(3,4,9);plot(ppp,ht(:,1),'or',ppp2,ht2(:,1),'ob',
ppp3,ht3(:,1),'og');title('h ndhx air')

subplot(3,4,10);plot(ppp,ht(:,2),'or',ppp2,ht2(:,2),'ob'
,ppp3,ht3(:,2),'og');title('h ndhx coolant')

subplot(3,4,11);plot(ppp,ht(:,3),'or',ppp2,ht2(:,3),'ob'
,ppp3,ht3(:,3),'og');title('h dhx coolant')

subplot(3,4,12);plot(ppp,ht(:,4),'or',ppp2,ht2(:,4),'ob'
,ppp3,ht3(:,4),'og');title('h dhx flibe')

    figure

subplot(2,2,1);plot(ppp,sc(:,1),'or',ppp2,sc2(:,1),'ob',
ppp3,sc3(:,1),'og');title('prototype inner
radius');legend('1','2','3')
```

```
subplot(2,2,2);plot(ppp,sc(:,2),'or',ppp2,sc2(:,2),'ob',
ppp3,sc3(:,2),'og');title('prototype outer
radius');legend('1','2','3')

subplot(2,2,3);plot(ppp,sc(:,3),'or',ppp2,sc2(:,3),'ob',
ppp3,sc3(:,3),'og');title('prototype inner
alpha');legend('1','2','3')

subplot(2,2,4);plot(ppp,sc(:,4),'or',ppp2,sc2(:,4),'ob',
ppp3,sc3(:,4),'og');title('prototype outer
alpha');legend('1','2','3')
end

set(gcf, 'PaperOrientation', 'landscape');
set(gcf, 'PaperPositionMode', 'manual');
set(gcf, 'PaperUnits', 'inches');
set(gcf, 'PaperPosition', [-0.5 -0.5 12 9]);
```

II. Thermos

```
function [cpsa,cpco,cpai,...
    c2sa,c2co,...
    rhsa,rhco,rhav,rhah,rhac...
    musa,muco,muai,...
    musash,mucosc,mucosh,muaic,muaih...
    kcsa,kcco,kcai,...
    prsa,prco,prai]=...
    thermos(ssaf,scoo,sair,...
    tcos,thos,...
    tcoc,thoc,...
    tcoa,thoa)
% ssaf=1;
% scoo=1;
% sair=1;
% tcos=938;
% thos=938;
% tcoc=938;
% thoc=938;
% tcoa=400;
% thoa=410;
if ssaf==1
    %flibe
    t=(0.7*thos+0.3*tcos);
    tsh=(thos+thoc)/2;
    cpsa=2386;
    c2sa=0.488;
    rhsa=-0.4884*(t-273.15)+2279.7;
    musa=1.16e-4*exp(3755/t);
    musash=1.16e-4*exp(3755/tsh);
    kcsa=1.1;
    prsa=cpsa*musa/kcsa;

elseif ssaf==2
    %flinak
    t=(0.7*thos+0.3*tcos);
    tsh=(thos+thoc)/2;
    cpsa=1884;
    c2sa=0.73;
    rhsa=-0.73*(t-273.15)+2530.0;
    musa=4.0e-5*exp(4170/t);
    musash=4.0e-5*exp(4170/tsh);
    kcsa=0.8;
    prsa=cpsa*musa/kcsa;
end

if scoo==1
    %flibe
    t=(0.7*thoc+0.3*tcoc);
    tsh=(thoc+thos)/2;
    tsc=(tcoc+thoa)/2;
    cpco=2386;
    c2co=0.488;
    rhco=-0.4884*(t-273.15)+2279.7;
    muco=1.16e-4*exp(3755/t);
    mucosc=1.16e-4*exp(3755/tsc);
    mucosh=1.16e-4*exp(3755/tsh);
    kcco=1.1;
    prco=cpco*muco/kcco;

elseif scoo==2
    %flinak
    t=(0.7*thoc+0.3*tcoc);
    tsh=(thoc+thos)/2;
    tsc=(tcoc+thoa)/2;
    cpco=1884;
    c2co=0.73;
    rhco=-0.73*(t-273.15)+2530.0;
    muco=4.0e-5*exp(4170/t);
    mucosc=4.0e-5*exp(4170/tsc);
    mucosh=4.0e-5*exp(4170/tsh);
    kcco=0.8;
    prco=cpco*muco/kcco;

elseif scoo==3
    %flinabe
    t=(0.7*thoc+0.3*tcoc);
    tsh=(thoc+thos)/2;
    tsc=(tcoc+thoa)/2;
    cpco=1507;
    c2co=0.711;
    rhco=-0.711*(t-273.15)+2252.1;
    muco=8.77e-5*exp(2240/t);
    mucosc=8.77e-5*exp(2240/tsc);
    mucosh=8.77e-5*exp(2240/tsh);
    kcco=0.5;
    prco=cpco*muco/kcco;
elseif scoo==4
    %pb
```

```
    t=(0.7*thoc+0.3*tcoc);
    tsh=(thoc+thos)/2;
    tsc=(tcoc+thoa)/2;
    cpco=175.1-4.961e-2*t-1.52e6*t^(-2)+1.985e-5*t^2-
2.099e-9*t^3;
    c2co=1.35;
    rhco=10660-1.35*(t-600);
    muco=6.57e-3-1.68e-5*(t-273)+1.81e-8*(t-273)^2-
6.75e-12*(t-273)^3;
    mucosc=6.57e-3-1.68e-5*(tsc-273)+1.81e-8*(tsc-
273)^2-6.75e-12*(tsc-273)^3;
    mucosh=6.57e-3-1.68e-5*(tsh-273)+1.81e-8*(tsh-
273)^2-6.75e-12*(tsh-273)^3;
    kcco=31.58-4.69e-2*t+4.54e-5*t^2-1.44e-8*t^3;
    prco=cpco*muco/kcco;

elseif scoo==5
    %pbbi
    t=(0.7*thoc+0.3*tcoc);
    tsh=(thoc+thos)/2;
    tsc=(tcoc+thoa)/2;
    cpco=146.51;
    c2co=1.38;
    rhco=11116.74-1.38*t;
    muco=4.9e-4*exp(760.1/t);
    mucosc=4.9e-4*exp(760.1/tsc);
    mucosh=4.9e-4*exp(760.1/tsh);
    kcco=12.41-3.37e-2*t+7.75e-5*t^2-3.94e-8*t^3;
    prco=cpco*muco/kcco;
elseif scoo==6
    %na
    t=(0.7*thoc+0.3*tcoc);
    tsh=(thoc+thos)/2;
    tsc=(tcoc+thoa)/2;
    cpco=1658.2-8.479e-1*t+4.454e-4*t^2-2.992e6*t^(-2);
    c2co=0.00003912*t-1.6914e-8*t^2+0.2197;
    rhco=5.638*10^-9*t^3-0.00001956*t^2-0.2197*t+1016.1;
    muco=exp(-6.44-0.39*log(t)+556.83/t);
    mucosc=exp(-6.44-0.39*log(tsc)+556.83/tsc);
    mucosh=exp(-6.44-0.39*log(tsh)+556.83/tsh);
    kcco=124.67-0.11*t+5.52e-5*t^2-1.18e-8*t^3;
    prco=cpco*muco/kcco;

end
```

```
if sair==1
    %air
    tc=tcoa;
    th=thoa;
    t=(0.7*thoa+0.3*tcoa);
    tsc=tcoa;
    tsh=thoa;
    cpai=1/28.97e-3*(28.11+0.1967e-2*t+...
        0.4802e-5*t^2-1.966e-9*t^3);
    rhac=101215/(287*tc);
    rhah=101215/(287*th);
    rhav=101215/(287*t);
    muai=1.71e-5*(t/273)^(2/3)*(273+110.4)/(t+110.4);
    muaic=1.71e-
5*(tsc/273)^(2/3)*(273+110.4)/(tsc+110.4);
    muaih=1.71e-
5*(tsh/273)^(2/3)*(273+110.4)/(tsh+110.4);
    kcai=muai*(cpai+5/4*8.314/28.02e-3);
    prai=cpai*muai/kcai;
elseif sair==2
    %nitrogen
    tc=tcoa;
    th=thoa;
    t=(0.7*thoa+0.3*tcoa);
    tsc=tcoa;
    tsh=thoa;
    cpai=1/28.02e-3*(28.90-0.1571e-2*t+...
        0.8081e-5*t^2-2.873e-9*t^3);
    rhac=101215/(297*tc);
    rhah=101215/(297*th);
    rhav=101215/(297*t);
    muai=1.76e-5*(t/293)^0.67;
    muaic=1.76e-5*(tsc/293)^0.67;
    muaih=1.76e-5*(tsh/293)^0.67;
    kcai=muai*(cpai+5/4*8.314/28.97e-3);
    prai=cpai*muai/kcai;
end
```

III. Geometry

```
function
[afndc,dhndi,lndhx,lntube,afnda,htsurfo,dhndo,ator,dodi,
rnnn,alpi,alpo,hcoi] =...
    geometry(rinn,nlay,nwin,dtou,dtin,podr,alce)
%INPUT PARAMETERS
    %sent from function master
%OUTPUT PARAMETERS
rnnn=rinn+(nlay)*podr*dtou;
rave=(rinn+rnnn)/2;
hcoi=2*(rnnn+rinn)*tan(alce*pi/180);
alpi=(180/pi)*atan(hcoi/(4*rinn));
alpo=(180/pi)*atan(hcoi/(4*rnnn));
htot=hcoi*nwin;
arclave=2*pi*(((rinn+rnnn)/2)^2+(hcoi^2)/(2*pi))^0.5;
arclall=arclave*nlay*(hcoi/(2*podr*dtou)*...
    ((sin(alce*2*pi/180))/(sin(alce*pi/180))))*nwin;
ntubes=arclall/arclave;
htsurfo=pi*dtou*arclall;
aflowi=ntubes*pi*(dtin/2)^2;
aflowe=pi*(rnnn^2-rinn^2)*(1-1/podr);
dhndo=aflowe*htot/(arclall*pi*dtou);
ator=dtin/rave;
dodi=dtou/dtin;
%PASSED VARIABLES
%cooling
afndc=aflowi;
dhndi=dtin;
lndhx=htot;
lntube=arclave;
%air
afnda=aflowe;
dhnd=dtou;
arcl=arclall;
```

IV. Safety

```
%         pdh  pdh  inf inf, inf,inf,inf
function [redh,mflow,dt,dpbs,dph,dpc,dpp,eu,dpd]=...
    safety(heat,afpis,lfdl,...
    afdh,dhdh,ldhx,across,aori,...
    cpfb,c2fb,rhfb,mufb)
%             m     m
    %AREAS
    afac=1.74;
    %HYDRO DIAMS
    dhac=0.0242;
    dhpi=2*((afpis/3.1416)^0.5);
    %FRICTION LENGTHS
    lac=2.2;
    ldd=2.9;
    llpi=lfdl+ldd;
    %HEIGHT DIFFERENCES
    llr=1.85;
    lthe=lfdl+0.5*ldhx-(llr+0.5*lac);
    %upper ul and lower ll temperature limits
    ulfb=765+273;
    llfb=450+273;
    mfmi=heat/(cpfb*(ulfb-llfb));
    mflow=0;
    orie=1;
    flag=1;
    i=0;
%ALGORITHM-----------------------------------------------
------------------
while orie==1&flag==1
    mflow=mfmi+i/2;
    %buoyancy
    dpbs=9.81*lthe*(heat/(mflow*cpfb))*(c2fb/rhfb)*rhfb;
    %friction
    veac=mflow/(rhfb*afac);
    reac=rhfb*dhac*veac/mufb;
    %ffac=3.5+300/reac;


    vepi=mflow/(rhfb*afpis);
    repi=rhfb*dhpi*vepi/mufb;
    if  repi>0&repi<2200
        ffpi=64/repi;
    elseif repi>=2200&repi<=3000
        ffpi=(3.75-
8250/repi)*(1/(1.8*log10(6.9/3000))^2-64/2200)+64/2200;
    else
        ffpi=1/(1.8*log10(6.9/repi))^2;
    end

    %diode pressure loss
    et=aori/afpis;
    ec=0.62+0.38*(et^3);
    kori=(1-1/(ec*et))^2;
    dpd=kori*(rhfb*(vepi^2)/2);




    vedh=mflow/(rhfb*afdh);
    redh=rhfb*vedh*dhdh/mufb;


    dph=150*(lac/dhac^2)*mufb*(veac)+...
         1.75*(lac/dhac)*rhfb*(veac^2);
    dpp=ffpi*(llpi/dhpi)*rhfb*(vepi^2)/2;
    dpc=(mflow^2/(rhfb*afdh^2))*(1/2)*across;
    %dpc=rhfb*vedh^2/2*51;
    eu=dpc/(rhfb*(vedh^2)/2);
    dpfs=dph+dpc+dpp+dpd;

    delt=dpbs-dpfs;
    orie=sign(delt);
    if abs(delt)<1
        flag=-1;
        %fprintf('sucess')
    else
    end
    i=i+1;
end
%END OF ALGORITHM-----------------------------------------
------------------
dt=heat/(mflow*cpfb);
vedhd=vedh;
kori;
rhfb*(vepi^2)/2;
reac;
dph/(rhfb*(veac^2)/2);
```

V. Cooling

```
%         pdh  pndh pdh pndh, inf,inf,inf,inf,inf,inf
function
[redh,mflow,dt,rend,dpbs,dph,dpc,dpp,euh,euc,coefa,coefb
]=...

cooling(heat,afndc,dhndi,lntube,lndhx,ator,afpi,lvll,afd
h,...
    cpfk,c2fk,rhfk,mufk)
%             gf    gf     gf    gp   m     m
    dhdh=0.006855;
    dhpi=2*((afpi/pi)^0.5);
    %FRICTION LENGTHS
    ldhx=2.45;
    llpi=lvll+lvll+lndhx-ldhx;
    %HEIGHT DIFFERENCES
    lthe=lvll+0.5*lndhx-0.5*ldhx;
    %initial temp vars
    ulfk=765+273;
    llfk=450+273;
    %min mflow
    mfmi=heat/(cpfk*(ulfk-llfk));
    mflow=0;
    orie=1;
    flag=1;
    i=0;
%ALGORITHM-----------------------------------------
------------------
while orie==1&flag==1
    mflow=mfmi+i/2;
    %buoyancy
    dpbs=9.81*lthe*(heat/(mflow*cpfk))*(c2fk/rhfk)*rhfk;
    %friction
    vedh=mflow/(rhfk*afdh);
    redh=rhfk*dhdh*vedh/mufk;
    if  redh>0&redh<2200
        ffdh=64/redh;
    elseif redh>=2200&redh<=3000
        ffdh=(3.75-
8250/redh)*(1/(1.8*log10(6.9/3000))^2-64/2200)+64/2200;
    else
        ffdh=1/(1.8*log10(6.9/redh))^2;
    end

    vepi=mflow/(rhfk*afpi);
    repi=rhfk*dhpi*vepi/mufk;
    if  repi>0&repi<2200
        ffpi=64/repi;
    elseif repi>=2200&repi<=3000
        ffpi=(3.75-
8250/repi)*(1/(1.8*log10(6.9/3000))^2-64/2200)+64/2200
    else
        ffpi=1/(1.8*log10(6.9/repi))^2;
    end

    vend=mflow/(rhfk*afndc);
    rend=rhfk*dhndi*vend/mufk;
    if  rend>0&rend<10000
        %k=rend*ator^0.5;
        %ffnd=(64/rend)*(21.5*k/(1.56+log10(k))^5.73);
        %coef=64*0.108*ator^0.25;
        %ffnd=64*0.108*ator^0.25*rend^-0.5;
        ffnd=64*0.108*ator^0.25*rend^(-0.5);
    %elseif rend>=2200&rend<=3000
%         k=rend*ator^0.5;
%         ffnd=((3.75-
8250/rend)*(1/(1.8*log10(6.9/3000))^2-
64/2200)+64/2200)*...
%             (21.5*k/(1.56+log10(k))^5.73);
    else
        ffnd=(0.029+0.304*(rend*ator^2)^-0.25)*ator^0.5;
    end

    coefa=ffnd*(lntube/dhndi);
    %coefb=64*0.108*ator^0.25*(lntube/dhndi);
    coefb=0;
    dph=ffdh*(ldhx/dhdh)*rhfk*(vedh^2)/2;
    euh=dph/(rhfk*(vedh^2)/2);

    dpp=ffpi*(llpi/dhpi)*rhfk*(vepi^2)/2;

    dpc=ffnd*(lntube/dhndi)*rhfk*(vend^2)/2;
    euc=dpc/(rhfk*(vend^2)/2);

    dpfs=dph+dpc+dpp;

    delt=dpbs-dpfs;
```

```
    orie=sign(delt);
    if abs(delt)<1
        flag=-1;
        %fprintf('sucess');
    else
    end
    i=i+1;
end

%END OF ALGORITHM-------------------------------------
------------------
dt=heat/(mflow*cpfk);
vedh;
vendd=vend;
```

VI. Air

```
%to       pnd pnd   inf inf,infinfinfinf,
function
[rend,mflow,dt,dpbs,dph,dppc,dpph,i,eu,coefa,coefb]=...
    air(heat,afnda,dhndo,lndhx,afpia,lchi,podr,...
    cpai,rhav,rhah,rhac,muai,muaic,muaih,tini)
%         gf   gf     gf     m    m  m
pres=1.013e5;
unic=0.2968e3;
%GEOMETRY-----------------------------------------------
------------------
dhpi=2*((afpia/3.1416)^0.5);
llpi=lndhx+lchi;
%initial temperature
%     tini=293;
%     tave=450;
%     tout=600;
%upper ul and lower ll temperature limits
ulai=765+273;
llai=120+273;
mfmi=heat/(cpai*(ulai-llai));
mflow=0;
orie=1;
flag=1;
i=0;
%test=1;
%ALGORITHM----------------------------------------------
------------------
while orie==1&flag==1
    mflow=mfmi+i/30;
    %test=isreal(mflow);
    %buoyancy
    dpbs=9.81*lndhx*rhac+...

9.81*lndhx*pres/(unic*(heat/(cpai*mflow)))*log(tini/(tin
i+(heat/(cpai*mflow))))+...
        9.81*lchi*(rhac-rhah);
    %friction

    vepic=mflow/(rhac*afpia);
    repic=rhac*dhpi*vepic/muaic;
    if  repic>0&repic<2200
        ffpic=64/repi;
    elseif repic>=2200&repic<=3000
        ffpic=(3.75-
8250/repic)*(1/(1.8*log10(6.9/3000))^2-64/2200)+64/2200;
    else
        ffpic=1/(1.8*log10(6.9/repic))^2;
    end

    vepih=mflow/(rhah*afpia);
    repih=rhah*dhpi*vepih/muaih;
    if  repih>0&repih<2200
        ffpih=64/repih;
    elseif repih>=2200&repih<=3000
        ffpih=(3.75-
8250/repih)*(1/(1.8*log10(6.9/3000))^2-64/2200)+64/2200;
    else
        ffpih=1/(1.8*log10(6.9/repih))^2;
    end

    vend=mflow/(rhav*afnda);
    rend=rhav*dhndo*vend/muai;
    %ffnd=4*0.070;%from kays london
    ffnd=4*(0.044+0.08*(podr)*(podr-1)^(-0.43-
1.13*podr))*rend^(-0.15);
    dppc=ffpic*(llpi/dhpi)*rhac*(vepic^2)/2;
    dpph=ffpih*(lchi/dhpi)*rhah*(vepih^2)/2;
    dph=(ffnd*(lndhx/dhndo)*(rhac/rhav)+2*(rhac/rhah-
1))...
        *rhac*(vend^2)/2;
    eu=dph/(rhac*(vend^2)/2);

    %coefa=2*(rhac/rhah-1);
    %coefa=0.0;
    coefa=ffnd*(lndhx/dhndo)*(rhac/rhav);
    %coefb=f(L/d)*(rhac/rhav)
    %coefb=4*(0.044+0.08*(podr)*(podr-1)^(-0.43-
1.13*podr))*...
    %    (lndhx/dhndo)*(rhac/rhav);

    %coefb=4*(0.044+0.08*(podr)*(podr-1)^(-0.43-
1.13*podr))*(lndhx/dhndo)*(rhac/rhav);
    coefb=0.0;

    dpfs=dph+dppc+dpph;

    delt=dpbs-dpfs;
    orie=sign(delt);
```

```
    if abs(delt)<0.3
        flag=-1;
        %fprintf('sucess')
    else
    end
    i=i+1;
end

%END OF ALGORITHM-------------------------------------
------------------

dt=heat/(mflow*cpai);
vend;
```

VII. Perfodhx

```
%   to     pnd  inf  inf
function [tinc,hout,hinn,uuuu,ntu]=...

perfodhx(heat,dhdho,dhdhi,htda,tins,scoo,redhs,redht,mfl
ows,mflowc,...

ksaave,prsaave,cpsaave,kcoave,prcoave,cpcoave,muco,mucos
h)
%              gf   gf    m    m    m    saf   cool  saf
cool

kwal=30.0;
%OUTPUT

if (scoo==5||scoo==6)||scoo==4
    nuin=7+0.025*(redht*prcoave)^0.8;
else
    if redht<2300
        %nuin=4.36;
        %nuin=4.36+(0.023*redht*prcoave*dhdhi/.1)/...
        %    (1+0.0012*redht*prcoave*dhdhi/.1)

%nuin=0.027*redht^0.8*prcoave^0.333*(muco/mucosh)^0.14;
        nuin=4.36;
    %elseif redht>=2300&redht<=10000
        %nuin=0.012*(redht^0.87-
280)*prcoave^0.4*(muco/mucosh)^0.11;
    else

nuin=0.027*redht^0.8*prcoave^0.333*(muco/mucosh)^0.14;
    end

end

if redht<1000
    efi=1;
elseif redht>=1000&redht<=10000
    efi=1+((redht-1000)/9000)^0.5;
else
    efi=2.0;
end

hinn=kcoave*nuin*efi/dhdhi;

nuou=0.346*redhs^0.618*prsaave^.333;

if redhs<1000
    efo=1;
elseif redhs>=1000&redhs<=10000
    efo=1+0.3*((redhs-1000)/9000)^0.5;
else
    efo=1.3;
end

hout=ksaave*nuou*efo/dhdho;



uuuu=1/(...
    dhdho/(dhdhi*hinn)+...
    1/hout+...
    dhdho*log(dhdho/dhdhi)/(2*kwal)...
    );

ch=mflows*cpsaave;
cc=mflowc*cpcoave;
if cc<ch
    cmin=cc;
    crat=cc/ch;
else
    cmin=ch;
    crat=ch/cc;
end

ntu=uuuu*htda/cmin;
%effe=(1/crat)*(1-exp(-crat*(1-exp(-ntu))));
effe=1-exp(-crat^(-1)*(1-exp(-crat*ntu)));
qmax=heat/effe;
tinc=tins-qmax/cmin;
```

VIII. Perfondhx

```
%     to   m    inf  inf
function [htar,hout,hinn]=...

perfondhx(heat,dhndi,dhndo,ator,dodi,podr,tinc,scoo,tina
,rendt,rends,mflowc,mflowa,...
    kaiave,cpaiave,kcoave,prcoave,cpcoave,muco,mucosc)
%              gf     gf   gp   pdh, m      m   m
coo   air   coo   air
kwal=30.0;
%OUTPUT
if (scoo==5||scoo==6)||scoo==4
    nuin=7+0.025*(rendt*prcoave)^0.8;
else
    if rendt*ator^0.5>40&rendt*ator^0.5<1e3
        si=2/11*(1+(1+77/4*1/(prcoave^2))^0.5);

nuin=0.1979*(rendt*ator^0.5)^0.5/si*1/(1+37.05/si*(1/40-
17/120*si+...

(1/(10*si)+13/30)*1/(10*prcoave))*(rendt*ator^0.5)^-
0.5);
    else

nuin=1/41*rendt^(5/6)*ator^(1/12)*(1+0.061/(rendt*ator^2
.5)^(1/6))...
            *prcoave^0.4;
    end

end
hinn=kcoave*nuin/dhndi;

if podr>=1.5&podr<=4.0
    c=0.1306*podr^2-0.5806*podr+0.8542;
    m=-0.0458*podr^2+0.2015*podr+0.4149;
    nuou=c*rends^m;
else
    nuou=6.66e-3*rends+10.06;
end
hout=kaiave*nuou/dhndo;
uuuu=1/(...
    dodi/hinn+...
    1/hout+...
    dodi*dhndi*log(dodi)/(2*kwal)...
    );

ch=mflowc*cpcoave;
cc=mflowa*cpaiave;
if cc<ch
    cmin=cc;
    crat=cc/ch;
else
    cmin=ch;
    crat=ch/cc;
end
qmax=cmin*(tinc-tina);
effe=heat/qmax;
%ntu=-log(1+1/crat*log(1-effe*crat));
ntu=-(1/crat)*log(crat*(log(1-effe))+1);

htar=ntu*cmin/uuuu;

crat;
%VARIABLES PASSED
```

Appendix C
Transient input file

```
=Full input file for simplified model
*******************************************************
*Problem options
*******************************************************
100  newath transnt
102  si si
120  30010000 26.050  ms3
121  10010000 0.0000  ms1
122  52010000 11.118  ms3
123  62250000 26.050  n2
201  150.000   1.0-6 0.5 15011   1 1000 1000
202  2000.00   1.0-6 1.0 15011   5 1000 1000
203  10000.0   1.0-6 10.0 15011 10 1000 1000

*************************
* Primary system
*************************
*-------pipe 1
*card name component
10000 core_1 pipe
*card #-of-elements
10001 12
*card angle-type option#
10002 sph 3
*card flow-A-vols which-vols
10101 0.0137672,12
*card flow-A-int-juncs which-int-juncs
10201 0.0137672,11
*card length which-vols
10301 0.18333,12
*card azimuth-angle which-vols
10501 0.0,12
*card vertica-angle which-vols
10601 90.0,12
*card wall-rough,hydroD,which-vols (local x coords)
10801 0.0,0.0242495,12
*card fwd loss rev loss which-juncs
10901 28.866518 28.866518 11
*card volume-control-flags tlpvbfe,which-vols
11001 0000010,12
*card junction-control-flags efcahs,which-juncs
11101 0,11
*card vols-init-conds-option P, T,
unused,unused,unused,which-vols
11201 0   5213236. 354593.  354593.  0. 0. 1
11202 0   5179302. 371138.  371138.  0. 0. 2
11203 0   5145335. 393186.6 393186.6 0. 0. 3
11204 0   5111326. 419833.  419833.  0. 0. 4
11205 0   5077262. 448778.  448778.  0. 0. 5
11206 0   5043139. 478630.  478630.  0. 0. 6
11207 0   5008952. 507575. 507575. 0. 0. 7
11208 0   4974700. 534222. 534222. 0. 0. 8
11209 0   4940388. 557663. 557663. 0. 0. 9
11210 0   4906022. 576959. 576959. 0. 0. 10
11211 0   4871610. 591205. 591205. 0. 0. 11
11212 0   4837164. 599947. 599947. 0. 0. 12
*card initial-cond-mass-flow
11300 0
*card juncs-init-conds-cntrl liquid-vel gas-vel which-
juncs
11301 1.017472 1.017472 0. 1 * 27.78993
11302 1.019213 1.019213 0. 2 * 27.78993
11303 1.021541 1.021541 0. 3 * 27.78993
11304 1.024369 1.024369 0. 4 * 27.78993
11305 1.027458 1.027458 0. 5 * 27.78993
11306 1.030664 1.030664 0. 6 * 27.78993
11307 1.03379  1.03379  0. 7 * 27.78993
11308 1.036684 1.036684 0. 8 * 27.78993
11309 1.039245 1.039245 0. 9 * 27.78993
11310 1.041364 1.041364 0. 10 * 27.78993
11311 1.042931 1.042931 0. 11 * 27.78993
*card juncs-hyd-diam flood vapor slope which-juncs
11401 0.0242495,0.0,1.0,1.0,11
*card  Bf       Cf  Br       Cr  junc num
13001  2474.278,1.0,2474.278,1.0,11
*-------pipe 2
*card name component
20000 core_2 pipe
*card #-of-elements
20001 12
*card angle-type option#
20002 sph 3
*card flow-A-vols which-vols20101 0.0825808,12
*card flow-A-int-juncs which-int-juncs
20201 0.0825808,11
*card length which-vols
```

```
20301 0.18333,12
*card azimuth-angle which-vols
20501 0.0,12
*card vertica-angle which-vols
20601 90.0,12
*card wall-rough,hydroD,which-vols (local x coords)
20801 0.0,0.0242495,12
*card fwd loss rev loss which-juncs
20901 28.866518 28.866518 11
*card volume-control-flags tlpvbfe,which-vols
21001 0000010,12
*card junction-control-flags efcahs,which-juncs
21101 0,11
*card vols-init-conds-option P, T,
unused,unused,unused,which-vols
21201 0   5213236. 354596.  354596.  0. 0. 1
21202 0   5179301. 371134.  371134.  0. 0. 2
21203 0   5145335. 393189.  393189.  0. 0. 3
21204 0   5111326. 419837.  419837.  0. 0. 4
21205 0   5077262. 448785.  448785.  0. 0. 5
21206 0   5043139. 478650.  478650.  0. 0. 6
21207 0   5008952. 507598. 507598. 0. 0. 7
21208 0   4974700. 534246. 534246. 0. 0. 8
21209 0   4940388. 557677. 557677. 0. 0. 9
21210 0   4906022. 576974. 576974. 0. 0. 10
21211 0   4871610. 591218. 591218. 0. 0. 11
21212 0   4837164. 599946. 599946. 0. 0. 12
*card initial-cond-mass-flow
21300 0
*card juncs-init-conds-cntrl liquid-vel gas-vel which-
juncs
21301 1.01747  1.01747  0. 1 * 166.6942
21302 1.019212 1.019212 0. 2 * 166.6942
21303 1.02154  1.02154  0. 3 * 166.6942
21304 1.024368 1.024368 0. 4 * 166.6942
21305 1.027458 1.027458 0. 5 * 166.6942
21306 1.030665 1.030665 0. 6 * 166.6942
21307 1.033792 1.033792 0. 7 * 166.6942
21308 1.036685 1.036685 0. 8 * 166.6942
21309 1.039246 1.039246 0. 9 * 166.6942
21310 1.041365 1.041365 0. 10 * 166.6942
21311 1.042932 1.042932 0. 11 * 166.6942
*card juncs-hyd-diam flood vapor slope which-juncs
21401 0.0242495,0.0,1.0,1.0,11
*card  Bf       Cf  Br       Cr  junc num
23001  2474.278,1.0,2474.278,1.0,11
*-------pipe 3
*card name component
30000 core_3 pipe
*card #-of-elements
30001 12
*card angle-type option#
30002 sph 3
*card flow-A-vols which-vols
30101 0.1651616,12
*card flow-A-int-juncs which-int-juncs
30201 0.1651616,11
*card length which-vols
30301 0.18333,12
*card azimuth-angle which-vols
30501 0.0,12
*card vertica-angle which-vols
30601 90.0,12
*card wall-rough,hydroD,which-vols (local x coords)
30801 0.0,0.0242495,12
*card fwd loss rev loss which-juncs
30901 28.866518 28.866518 11
*card volume-control-flags tlpvbfe,which-vols
31001 0000010,12
*card junction-control-flags efcahs,which-juncs
31101 0,11
*card vols-init-conds-option P, T,
unused,unused,unused,which-vols
31201 0   5213236. 354593.  354593.  0. 0. 1
31202 0   5179301. 371134.  371134.  0. 0. 2
31203 0   5145334. 393189.  393189.  0. 0. 3
31204 0   5111325. 419837.  419837.  0. 0. 4
31205 0   5077262. 448785.  448785.  0. 0. 5
31206 0   5043139. 478650. 478650. 0. 0. 6
31207 0   5008952. 507598. 507598. 0. 0. 7
31208 0   4974700. 534246. 534246. 0. 0. 8
31209 0   4940388. 557680. 557680. 0. 0. 9
31210 0   4906022. 576977. 576977. 0. 0. 10
31211 0   4871610. 591221. 591221. 0. 0. 11
31212 0   4837164. 599952. 599952. 0. 0. 12
*card initial-cond-mass-flow
31300 0
*card juncs-init-conds-cntrl liquid-vel gas-vel which-
juncs
31301 1.01747  1.01747  0. 1 * 333.388
```

```
31302 1.01921  1.01921  0. 2 * 333.388
31303 1.02154  1.02154  0. 3 * 333.388
31304 1.024368 1.024368 0. 4 * 333.388
31305 1.027457 1.027457 0. 5 * 333.388
31306 1.030664 1.030664 0. 6 * 333.388
31307 1.033792 1.033792 0. 7 * 333.388
31308 1.036685 1.036685 0. 8 * 333.388
31309 1.039245 1.039245 0. 9 * 333.388
31310 1.041365 1.041365 0. 10 * 333.388
31311 1.042932 1.042932 0. 11 * 333.388
*card juncs-hyd-diam flood vapor slope which-juncs
31401 0.0242495,0.0,1.0,1.0,11
*card  Bf       Cf  Br       Cr  junc num
33001  2474.278,1.0,2474.278,1.0,11
*-------pipe 4
*card name component
40000 core_4 pipe
*card #-of-elements
40001 12
*card angle-type option#
40002 sph 3
*card flow-A-vols which-vols
40101 0.1651616,12
*card flow-A-int-juncs which-int-juncs
40201 0.1651616,11
*card length which-vols
40301 0.18333,12
*card azimuth-angle which-vols
40501 0.0,12
*card vertica-angle which-vols
40601 90.0,12
*card wall-rough,hydroD,which-vols (local x coords)
40801 0.0,0.0242495,12
*card fwd loss rev loss which-juncs
40901 28.866518 28.866518 11
*card volume-control-flags tlpvbfe,which-vols
41001 00000010,12
*card junction-control-flags efcahs,which-juncs
41101 0,11
*card vols-init-conds-option P, T,
unused,unused,unused,which-vols
41201 0   5213236. 354593.  354593.  0. 0. 1
41202 0   5179301. 371134.  371134.  0. 0. 2
41203 0   5145334. 393189.  393189.  0. 0. 3
41204 0   5111325. 419837.  419837.  0. 0. 4
41205 0   5077262. 448785.  448785.  0. 0. 5
41206 0   5043139. 478650. 478650. 0. 0. 6
41207 0   5008952. 507598. 507598. 0. 0. 7
41208 0   4974700. 534246. 534246. 0. 0. 8
41209 0   4940388. 557680. 557680. 0. 0. 9
41210 0   4906022. 576977. 576977. 0. 0. 10
41211 0   4871610. 591221. 591221. 0. 0. 11
41212 0   4837164. 599952. 599952. 0. 0. 12
*card initial-cond-mass-flow
41300 0
*card juncs-init-conds-cntrl liquid-vel gas-vel which-
juncs
41301 1.01747  1.01747  0. 1 * 333.388
41302 1.01921  1.01921  0. 2 * 333.388
41303 1.02154  1.02154  0. 3 * 333.388
41304 1.024368 1.024368 0. 4 * 333.388
41305 1.027457 1.027457 0. 5 * 333.388
41306 1.030664 1.030664 0. 6 * 333.388
41307 1.033792 1.033792 0. 7 * 333.388
41308 1.036685 1.036685 0. 8 * 333.388
41309 1.039245 1.039245 0. 9 * 333.388
41310 1.041365 1.041365 0. 10 * 333.388
41311 1.042932 1.042932 0. 11 * 333.388
*card juncs-hyd-diam flood vapor slope which-juncs
41401 0.0242495,0.0,1.0,1.0,11
*card  Bf       Cf  Br       Cr  junc num
43001  2474.278,1.0,2474.278,1.0,11
*-------pipe 5
*card name component
50000 core_5 pipe
*card #-of-elements
50001 12
*card angle-type option#
50002 sph 3
*card flow-A-vols which-vols
50101 0.330323,12
*card flow-A-int-juncs which-int-juncs
50201 0.330323,11
*card length which-vols
50301 0.18333,12
*card azimuth-angle which-vols
50501 0.0,12
*card vertica-angle which-vols
50601 90.0,12
*card wall-rough,hydroD,which-vols (local x coords)
```

```
50801 0.0,0.0242495,12
*card fwd loss rev loss which-juncs
50901 28.866518 28.866518 11
*card volume-control-flags tlpvbfe,which-vols
51001 0000010,12
*card junction-control-flags efcahs,which-juncs
51101 0,11
*card vols-init-conds-option P, T,
unused,unused,unused,which-vols
51201 0   5213235. 354593.  354593.  0. 0. 1
51202 0   5179300. 371134.  371134.  0. 0. 2
51203 0   5145334. 393189.  393189.  0. 0. 3
51204 0   5111324. 419839.  419839.  0. 0. 4
51205 0   5077262. 448785.  448785.  0. 0. 5
51206 0   5043138. 478650. 478650. 0. 0. 6
51207 0   5008951. 507597. 507597. 0. 0. 7
51208 0   4974700. 534246. 534246. 0. 0. 8
51209 0   4940388. 557679. 557679. 0. 0. 9
51210 0   4906022. 576977. 576977. 0. 0. 10
51211 0   4871610. 591220. 591220. 0. 0. 11
51212 0   4837164. 599950. 599950. 0. 0. 12
*card initial-cond-mass-flow
51300 0
*card juncs-init-conds-cntrl liquid-vel gas-vel which-
juncs
51301 1.017469 1.017469 0. 1 * 666.775
51302 1.01921  1.01921  0. 2 * 666.775
51303 1.021539 1.021539 0. 3 * 666.775
51304 1.024367 1.024367 0. 4 * 666.775
51305 1.027456 1.027456 0. 5 * 666.775
51306 1.030663 1.030663 0. 6 * 666.775
51307 1.03379  1.03379  0. 7 * 666.775
51308 1.036684 1.036684 0. 8 * 666.775
51309 1.039244 1.039244 0. 9 * 666.775
51310 1.041364 1.041364 0. 10 * 666.775
51311 1.04293  1.04293  0. 11 * 666.775
*card juncs-hyd-diam flood vapor slope which-juncs
51401 0.0242495,0.0,1.0,1.0,11
*card  Bf       Cf  Br       Cr  junc num
53001  2474.278,1.0,2474.278,1.0,11
*-------pipe 6
*card name component
60000 core_6 pipe
*card #-of-elements
60001 12
*card angle-type option#
60002 sph 3
*card flow-A-vols which-vols
60101 0.412904,12
*card flow-A-int-juncs which-int-juncs
60201 0.412904,11
*card length which-vols
60301 0.18333,12
*card azimuth-angle which-vols
60501 0.0,12
*card vertica-angle which-vols
60601 90.0,12
*card wall-rough,hydroD,which-vols (local x coords)
60801 0.0,0.0242495,12
*card fwd loss rev loss which-juncs
60901 28.866518 28.866518 11
*card volume-control-flags tlpvbfe,which-vols
61001 0000010,12
*card junction-control-flags efcahs,which-juncs
61101 0,11
*card vols-init-conds-option P, T,
unused,unused,unused,which-vols
61201 0   5213234. 354593.5 354593.5 0. 0. 1
61202 0   5179300. 371134.  371134.  0. 0. 2
61203 0   5145334. 393189.  393189.  0. 0. 3
61204 0   5111324. 419838.  419838.  0. 0. 4
61205 0   5077262. 448785.  448785.  0. 0. 5
61206 0   5043138. 478650.  478650.  0. 0. 6
61207 0   5008951. 507597. 507597. 0. 0. 7
61208 0   4974700. 534246. 534246. 0. 0. 8
61209 0   4940388. 557680. 557680. 0. 0. 9
61210 0   4906022. 576978. 576978. 0. 0. 10
61211 0   4871610. 591221. 591221. 0. 0. 11
61212 0   4837164. 599951. 599951. 0. 0. 12
*card initial-cond-mass-flow
61300 0
*card juncs-init-conds-cntrl liquid-vel gas-vel which-
juncs
61301 1.017468 1.017468 0. 1 * 833.47
61302 1.01921  1.01921  0. 2 * 833.47
61303 1.021538 1.021538 0. 3 * 833.47
61304 1.024366 1.024366 0. 4 * 833.47
61305 1.027455 1.027455 0. 5 * 833.47
61306 1.030663 1.030663 0. 6 * 833.47
61307 1.03379  1.03379  0. 7 * 833.47
```

```
61308 1.036683 1.036683 0. 8 * 833.47
61309 1.039244 1.039244 0. 9 * 833.47
61310 1.041363 1.041363 0. 10 * 833.47
61311 1.04293  1.04293  0. 11 * 833.47
*card juncs-hyd-diam flood vapor slope which-juncs
61401 0.0242495,0.0,1.0,1.0,11
*card  Bf       Cf  Br       Cr  junc num
63001  2474.278,1.0,2474.278,1.0,11
*-------pipe 7
*card name component
70000 core_7 pipe
*card #-of-elements
70001 12
*card angle-type option#
70002 sph 3
*card flow-A-vols which-vols
70101 0.330323,12
*card flow-A-int-juncs which-int-juncs
70201 0.330323,11
*card length which-vols
70301 0.18333,12
*card azimuth-angle which-vols
70501 0.0,12
*card vertica-angle which-vols
70601 90.0,12
*card wall-rough,hydroD,which-vols (local x coords)
70801 0.0,0.0242495,12
*card fwd loss rev loss which-juncs
70901 28.866518 28.866518 11
*card volume-control-flags tlpvbfe,which-vols
71001 0000010,12
*card junction-control-flags efcahs,which-juncs
71101 0,11
*card vols-init-conds-option P, T,
unused,unused,unused,which-vols
71201 0   5213235. 354593.  354593.  0. 0. 1
71202 0   5179300. 371134.  371134.  0. 0. 2
71203 0   5145334. 393189.  393189.  0. 0. 3
71204 0   5111324. 419839.  419839.  0. 0. 4
71205 0   5077262. 448785.  448785.  0. 0. 5
71206 0   5043138. 478650.  478650.  0. 0. 6
71207 0   5008951. 507597. 507597. 0. 0. 7
71208 0   4974700. 534246. 534246. 0. 0. 8
71209 0   4940388. 557679. 557679. 0. 0. 9
71210 0   4906022. 576977. 576977. 0. 0. 10
71211 0   4871610. 591220. 591220. 0. 0. 11
71212 0   4837164. 599950. 599950. 0. 0. 12
*card initial-cond-mass-flow
71300 0
*card juncs-init-conds-cntrl liquid-vel gas-vel which-
juncs
71301 1.017469 1.017469 0. 1 * 666.775
71302 1.01921  1.01921  0. 2 * 666.775
71303 1.021539 1.021539 0. 3 * 666.775
71304 1.024367 1.024367 0. 4 * 666.775
71305 1.027456 1.027456 0. 5 * 666.775
71306 1.030663 1.030663 0. 6 * 666.775
71307 1.03379  1.03379  0. 7 * 666.775
71308 1.036684 1.036684 0. 8 * 666.775
71309 1.039244 1.039244 0. 9 * 666.775
71310 1.041364 1.041364 0. 10 * 666.775
71311 1.04293  1.04293  0. 11 * 666.775
*card juncs-hyd-diam flood vapor slope which-juncs
71401 0.0242495,0.0,1.0,1.0,11
*card  Bf       Cf  Br       Cr  junc num
73001  2474.278,1.0,2474.278,1.0,11
*-------pipe 8
*card name component
80000 core_1 pipe
*card #-of-elements
80001 12
*card angle-type option#
80002 sph 3
*card flow-A-vols which-vols
80101 0.247742,12
*card flow-A-int-juncs which-int-juncs
80201 0.247742,11
*card length which-vols
80301 0.18333,12
*card azimuth-angle which-vols
80501 0.0,12
*card vertica-angle which-vols
80601 90.0,12
*card wall-rough,hydroD,which-vols (local x coords)
80801 0.0,0.0242495,12
*card fwd loss rev loss which-juncs
80901 28.866518 28.866518 11
*card volume-control-flags tlpvbfe,which-vols
81001 0000010,12
*card junction-control-flags efcahs,which-juncs
```

```
81101 0,11
*card vols-init-conds-option P, T,
unused,unused,unused,which-vols
81201 0   5213236. 354594.  354594.  0. 0. 1
81202 0   5179300. 371134.  371134.  0. 0. 2
81203 0   5145334. 393189.  393189.  0. 0. 3
81204 0   5111325. 419839.  419839.  0. 0. 4
81205 0   5077262. 448787.  448787.  0. 0. 5
81206 0   5043139. 478652. 478652. 0. 0. 6
81207 0   5008952. 507600. 507600. 0. 0. 7
81208 0   4974700. 534250. 534250. 0. 0. 8
81209 0   4940388. 557683. 557683. 0. 0. 9
81210 0   4906022. 576982. 576982. 0. 0. 10
81211 0   4871610. 591226. 591226. 0. 0. 11
81212 0   4837164. 599956. 599956. 0. 0. 12
*card initial-cond-mass-flow
81300 0
*card juncs-init-conds-cntrl liquid-vel gas-vel which-
juncs
81301 1.01747  1.01747  0. 1 * 500.081
81302 1.01921  1.01921  0. 2 * 500.081
81303 1.02154  1.02154  0. 3 * 500.081
81304 1.024367 1.024367 0. 4 * 500.081
81305 1.027457 1.027457 0. 5 * 500.081
81306 1.030664 1.030664 0. 6 * 500.081
81307 1.033792 1.033792 0. 7 * 500.081
81308 1.036685 1.036685 0. 8 * 500.081
81309 1.039245 1.039245 0. 9 * 500.081
81310 1.041365 1.041365 0. 10 * 500.081
81311 1.042932 1.042932 0. 11 * 500.081
*card juncs-hyd-diam flood vapor slope which-juncs
81401 0.0242495,0.0,1.0,1.0,11
*card  Bf       Cf  Br       Cr  junc num
83001  2474.278,1.0,2474.278,1.0,11
*-------snglvol 10
*card    name          component
100000   sink          snglvol
*card    Aflow-x-dir   Length-x-dir   Vol      ang-azm
ang-inc   elev
100101   1.74843       0.7           0.0      0.0
90.0      0.7
*card    Roughness-x   Hyd Diam-x     tlpvbfe
100102   0.0000        0.0           0
*card    Aflow-z-dir   Length-z-dir
100191   0.30597525    4.0
*card    Roughness-z   Hyd Diam-z     tlpvbfe  unused
unused    dZz
100192   0.0000        0.0           0        0
0         0.0
*card    ebt           P             T
100200   0             5251060.      344945.  344945.
0.
*-------junction 11
*card    name          component
110000   sngjun        sngljun
*card    from          to            area     fwloss
fwrever   flags
110101   10010000      12000000      1.74843  0.0
0.0       0
*card    init-mflow    liquid        vapor    intercept
110201   0             1.016186      1.016186 0. *
3528.36
*-------branch 12
*card    name          component
120000   inltplnm      branch
*card    num-of-juncs ctrl-specify-massflow
120001   8             0
*card    area          Length-x   Vol
120101   1.74843       1.50       0.0
*card    angl:Azmth    ang:Incl   Elev-chng**************
120102   0.0           90.0000    1.50
*card    Roughness     Hyd Diam   Vol-ctrl-flag
120103   0.0000       0.00000    0
*card    ebt           P          T
120200   0             5229628.   344945.  344945.  0.
*card    from vol      to vol     jun area      fwd loss
rev loss jun flag
121101   12010000      1000000    0.0137672     0.0
0.0      0
122101   12010000      2000000    0.0825808     0.0
0.0      0
123101   12010000      3000000    0.1651616     0.0
0.0      0
124101   12010000      4000000    0.1651616     0.0
0.0      0
125101   12010000      5000000    0.3303230     0.0
0.0      0
126101   12010000      6000000    0.4129040     0.0
0.0      0
```

```
127101   12010000     7000000    0.3303230     0.0
0.0      0
128101   12010000     8000000    0.2477420     0.0
0.0      0
*card    hyd diam     flood      vapor/gas     slope
121110   0.0          0.0        1.0           1.0
122110   0.0          0.0        1.0           1.0
123110   0.0          0.0        1.0           1.0
124110   0.0          0.0        1.0           1.0
125110   0.0          0.0        1.0           1.0
126110   0.0          0.0        1.0           1.0
127110   0.0          0.0        1.0           1.0
128110   0.0          0.0        1.0           1.0
*card    int-flowf    int-flowg  velj
121201   1.01646      1.01646    0. * 27.78993
122201   1.01646      1.01646    0. * 166.6942
123201   1.016459     1.016459   0. * 333.388
124201   1.016459     1.016459   0. * 333.388
125201   1.016458     1.016458   0. * 666.775
126201   1.016457     1.016457   0. * 833.47
127201   1.016458     1.016458   0. * 666.775
128201   1.016458     1.016458   0. * 500.081
*-------branch 13
*card    name         component
130000   oultplnm     branch
*card    num-of-juncs ctrl-specify-massflow
130001   8            0
*card    area         Length-x   Vol
130101   1.74843      0.10       0.0
*card    angl:Azmth   ang:Incl   Elev-chng**************
130102   0.0          90.0000    0.10
*card    Roughness    Hyd Diam   Vol-ctrl-flag
130103   0.0000      0.00000    0
*card    ebt          P          T
130200   0            4834478.   599951. 599951. 0.
*card    from vol     to vol     jun area      fwd loss
rev loss jun flag
131101   1010000      13000000   0.0137672     0.0
0.0      0
132101   2010000      13000000   0.0825808     0.0
0.0      0
133101   3010000      13000000   0.1651616     0.0
0.0      0
134101   4010000      13000000   0.1651616     0.0
0.0      0
```

```
135101   5010000      13000000   0.3303230     0.0
0.0      0
136101   6010000      13000000   0.4129040     0.0
0.0      0
137101   7010000      13000000   0.3303230     0.0
0.0      0
138101   8010000      13000000   0.2477420     0.0
0.0      0
*card    hyd diam     flood      vapor/gas     slope
131110   0.0          0.0        1.0           1.0
132110   0.0          0.0        1.0           1.0
133110   0.0          0.0        1.0           1.0
134110   0.0          0.0        1.0           1.0
135110   0.0          0.0        1.0           1.0
136110   0.0          0.0        1.0           1.0
137110   0.0          0.0        1.0           1.0
138110   0.0          0.0        1.0           1.0
*card    int-flowf    int-flowg  velj
131201   1.0439       1.0439     0. * 27.78993
132201   1.0439       1.0439     0. * 166.6942
133201   1.0439       1.0439     0. * 333.388
134201   1.0439       1.0439     0. * 333.388
135201   1.043898     1.043898   0. * 666.775
136201   1.043898     1.043898   0. * 833.47
137201   1.043898     1.043898   0. * 666.775
138201   1.0439       1.0439     0. * 500.081
*-------junction 14
*card    name          component
140000   sngjun        sngljun
*card    from          to             area     fwloss
fwrever   flags
140101   13010000      15000000       1.74843  0.0
0.0       0
*card    init-mflow    liquid         vapor    intercept
140201   0             1.04362        1.04362  0. *
3528.36
*-------pipe 15
*card name component
150000 upp_ref pipe
*card #-of-elements
150001 10
*card angle-type option#
150002 sph 3
*card flow-A-vols which-vols
150101 0.9352,10
```

```
*card flow-A-int-juncs which-int-juncs
150201 0.9352,9
*card length which-vols
150301 0.0618,10
*card azimuth-angle which-vols
150501 0.0,10
*card vertica-angle which-vols
150601 90.0,10
*card wall-rough,hydroD,which-vols (local x coords)
150801 0.0000,0.015,10
*card fwd loss rev loss which-juncs
150901 0.0 0.0 9
*card volume-control-flags tlpvbfe,which-vols
151001 0,10
*card junction-control-flags efcahs,which-juncs
151101 0,9
*card vols-init-conds-option P, T,
unused,unused,unused,which-vols
151201 0   4830085. 599951. 599951. 0. 0. 1
151202 0   4828453. 599952. 599952. 0. 0. 2
151203 0   4826821. 599952. 599952. 0. 0. 3
151204 0   4825189. 599952. 599952. 0. 0. 4
151205 0   4823557. 599952. 599952. 0. 0. 5
151206 0   4821925. 599953. 599953. 0. 0. 6
151207 0   4820293. 599953. 599953. 0. 0. 7
151208 0   4818661. 599953. 599953. 0. 0. 8
151209 0   4817029. 599953. 599953. 0. 0. 9
151210 0   4815397. 599954. 599954. 0. 0. 10
*card initial-cond-mass-flow
151300 0
*card juncs-init-conds-cntrl liquid-vel gas-vel which-
juncs
151301 1.95113  1.95113  0. 1 * 3528.36
151302 1.95113  1.95113  0. 2 * 3528.36
151303 1.95113  1.95113  0. 3 * 3528.36
151304 1.95113  1.95113  0. 4 * 3528.36
151305 1.95113  1.95113  0. 5 * 3528.36
151306 1.95113  1.95113  0. 6 * 3528.36
151307 1.951132 1.951132 0. 7 * 3528.36
151308 1.951132 1.951132 0. 8 * 3528.36
151309 1.951133 1.951133 0. 9 * 3528.36
*card juncs-hyd-diam flood vapor slope which-juncs
151401 0.015,0.0,1.0,1.0,9
*card  Bf,Cf,Br,Cr,which-juncs
153001  0.0,1.0,0.0,1.0,9
```

```
*-------junction 16
*card    name          component
160000   sngjun        sngljun
*card    from          to             area     fwloss
fwrever   flags
160101   15010000      17000000       1.74843  0.0
0.0       0
*card    init-mflow    liquid         vapor    intercept
160201   0             1.043622       1.043622 0. *
3528.36
*-------snglvol 17
*card    name          component
170000   sink          snglvol
*card    Aflow-x-dir   Length-x-dir   Vol      ang-azm
ang-inc   elev
170101   1.74843       0.7            0.0      0.0
90.0      0.7
*card    Roughness-x   Hyd Diam-x     tlpvbfe
170102   0.0000        0.0            0
*card    Aflow-z-dir   Length-z-dir
170191   0.30597525    4.0
*card    Roughness-z   Hyd Diam-z     tlpvbfe  unused
unused    dZz
170192   0.0000        0.0            0        0
0         0.0
*card    ebt           P              T
170200   0             4810563.       591981. 591981. 0.
*-------valve 18
180000   val_1         valve
*card    from-vol      to-vol         aflow    fwd-loss
rev-loss jefvcahs
180101   13010000      19000000       0.1      0.0
0.0      0
*card    ctrl-mflow    flowf          flowg    velj
180201   0             0.             0.        0. * 0.
*card    valve-type
180300   trpvlv
*card    trip num
180301   18
*-------tmdpvol 19
*card    name          component
190000   source        tmdpvol
*card    Aflow-x-dir   Length-x-dir   Vol      ang-azm
ang-inc   elev
```

```
190101   1000.0        0.0           1.0e6    180.0          *-------pipe 23
0.0       0.0                                                *card name component
*card    Roughness-x   Hyd Diam-x    tlpvbfe                 230000 riser pipe
190102   0.0000       0.0           0                       *card #-of-elements
*card    ebt                                                 230001 15
190200   003                                                 *card angle-type option#
*card    time          P             T                       230002 sph 3
190201   0.000         4.9e6         879.0                   *card flow-A-vols which-vols
190202   100.0         4.9e6         879.0                   230101 0.125664,15
*-------valve 20                                            *card flow-A-int-juncs which-int-juncs
200000   val_2         valve                                 230201 0.125664,14
*card    from-vol      to-vol        aflow    fwd-loss       *card length which-vols
rev-loss jefvcahs                                           230301 0.100,5
200101   21010000      13010000      0.1      0.0            230302 0.505,15
0.0      0                                                  *card azimuth-angle which-vols
*card    ctrl-mflow    flowf         flowg    velj           230501 180.0,5
200201   0             0.            0.       0. * 0.        230502 0.000,15
*card    valve-type                                         *card vertica-angle which-vols
200300   trpvlv                                             230601 0.000,5
*card    trip num                                           230602 90.00,15
200301   20                                                  *card wall-rough,hydroD,which-vols (local x coords)
*-------tmdpvol 21                                         230801 0,0,15
*card    name          component                             *card volume-control-flags tlpvbfe,which-vols
210000   sink          tmdpvol                               231001 0,15
*card    Aflow-x-dir   Length-x-dir  Vol      ang-azm        *card junction-control-flags efcahs,which-juncs
ang-inc   elev                                              231101 0,14
210101   1000.0        0.0           1.0e6    180.0          *card vols-init-conds-option P, T,
0.0       0.0                                               unused,unused,unused,which-vols
*card    Roughness-x   Hyd Diam-x    tlpvbfe                 231201 0 5270088. 344945.  344945.  0. 0. 1
210102   0.0000       0.0           0                       231202 0 5270085. 344945.  344945.  0. 0. 2
*card    ebt                                                 231203 0 5270082. 344945.  344945.  0. 0. 3
210200   003                                                 231204 0 5270079. 344945.  344945.  0. 0. 4
*card    time          P             T                       231205 0 5270076. 344945.  344945.  0. 0. 5
210201   0.000         4.9e6         879.0                   231206 0 5265198. 344945.  344945.  0. 0. 6
210202   100.0         4.9e6         879.0                   231207 0 5255446. 344945.  344945.  0. 0. 7
*-------junction 22                                        231208 0 5245694. 344945.  344945.  0. 0. 8
*card    name          component                             231209 0 5235941. 344945.  344945.  0. 0. 9
220000   jun22         sngljun                               231210 0 5226188. 344945.  344945.  0. 0. 10
*card    from          to            area     fwloss         231211 0 5216436. 344945.  344945.  0. 0. 11
fwrever   flags                                             231212 0 5206684. 344945.  344945.  0. 0. 12
220101   10010006      23010001      0.125664 0.0            231213 0 5196932. 344945.  344945.  0. 0. 13
0.0       0                                                 231214 0 5187179. 344945.  344945.  0. 0. 14
*card    init-mflow    liquid        vapor    intercept      231215 0 5177426. 344945.  344945.  0. 0. 15
220201   0             .651325       .651325  0. *           *card juncs-init-conds-cntrl,liquid-vel,gas-vel,which-
90.5415                                                     juncs
```

```
231301 .651325  .651325  0. 1 * 90.5415
231302 .651325  .651325  0. 2 * 90.5415
231303 .651325  .651325  0. 3 * 90.5415
231304 .651325  .651325  0. 4 * 90.5415
231305 .651325  .651325  0. 5 * 90.5415
231306 .651325  .651325  0. 6 * 90.5415
231307 .651325  .651325  0. 7 * 90.5415
231308 .651326  .651326  0. 8 * 90.5415
231309 .651326  .651326  0. 9 * 90.5415
231310 .651326  .651326  0. 10 * 90.5415
231311 .651326  .651326  0. 11 * 90.5415
231312 .651327  .651327  0. 12 * 90.5415
231313 .651327  .651327  0. 13 * 90.5415
231314 .651327  .651327  0. 14 * 90.5415
*-------junction 24
*card    name          component
240000   fluidic       sngljun
*card    from          to             area       fwloss
fwrever   flags
240101   23010000      25000000       0.0239635  65.0
0.0       0
*card    init-mflow    liquid         vapor
intercept
240201   0             1.302656       1.302656   0. *
90.5415
*-------pipe 25**********************
*card name component
250000 xchger pipe
*card #-of-elements
250001 22
*card angle-type option#
250002 sph 3
*card flow-A-vols which-vols
250101 0.656,10
250102 0.125664,22
*card flow-A-int-juncs which-int-juncs
250201 0.656,10
250202 0.125664,21
*card length which-vols
250301 0.258,10
250302 0.100,14
250303 0.125,18
250304 0.728,22
*card azimuth-angle which-vols
250501 0.0,22
```

```
*card vertica-angle which-vols
250601 90.00,14
250602 0.000,18
250603 -90.0,22
*coordinates capitalized are fixed coords
*card  dXx,dYx,dZx,which-vols (local x coords)
250701 0.0,0.0,0.258,10
250702 0.0,0.0,0.1,14
250703 0.125,0.0,0.0000,18
250704 0.000,0.0,-0.728,22
*card  dXy,dYy,dZy,which-vols (local y coords)
252101 0.0,0.0,0.0,22
*card  dXz,dYz,dZz,which-vols (local z coords)
252201 0.0,0.0,0.0,22
*card  wall-rough,hydroD,which-vols (local x coords)
250801 0.0000,0.0,10
250802 0.0000,0.0,14
250803 0.0000,0.0,18
250804 0.0000,0.0,22
*card fwd loss rev loss which-juncs
250901 10.112,10.112,10
250902 0.00,0.00,21
*card  wall-rough,hydroD,which-vols (local y coords)
252301 0.0000,0.0,22
*card  wall-rough,hydroD,which-vols (local z coords)
252401 0.0000,0.0,22
*card volume-control-flags tlpvbfe,which-vols
251001 0000010,10
251002 0,22
*card junction-control-flags efcahs,which-juncs
251101 0,21
*card vols-init-conds-option P, T,
unused,unused,unused,which-vols
251201 0 4830829. 331778.5 331778.5 0. 0. 1
251202 0 4825666. 320952.  320952.  0. 0. 2
251203 0 4820497. 312043.  312043.  0. 0. 3
251204 0 4815324. 304720.  304720.  0. 0. 4
251205 0 4810148. 298693.5 298693.5 0. 0. 5
251206 0 4804969. 293734.4 293734.4 0. 0. 6
251207 0 4799788. 289659.5 289659.5 0. 0. 7
251208 0 4794604. 286306.3 286306.3 0. 0. 8
251209 0 4789420. 283547.  283547.  0. 0. 9
251210 0 4784234. 281278.4 281278.4 0. 0. 10
251211 0 4780322. 281278.4 281278.4 0. 0. 11
251212 0 4778358. 281278.4 281278.4 0. 0. 12
```

```
251213 0 4776395. 281278.4 281278.4 0. 0. 13
251214 0 4774432. 281278.4 281278.4 0. 0. 14
251215 0 4773448. 281278.4 281278.4 0. 0. 15
251216 0 4773444. 281278.4 281278.4 0. 0. 16
251217 0 4773440. 281278.4 281278.4 0. 0. 17
251218 0 4773436. 281278.4 281278.4 0. 0. 18
251219 0 4780485. 281278.5 281278.5 0. 0. 19
251220 0 4794586. 281278.6 281278.6 0. 0. 20
251221 0 4808688. 281278.6 281278.6 0. 0. 21
251222 0 4822788. 281278.7 281278.7 0. 0. 22
*card juncs-init-conds-cntrl,liquid-vel,gas-vel,which-
juncs
251301 .19107     .19107     0. 1 * 90.5415
251302 .190857    .190857    0. 2 * 90.5415
251303 .1906826   .1906826   0. 3 * 90.5415
251304 .190539    .190539    0. 4 * 90.5415
251305 .1904215   .1904215   0. 5 * 90.5415
251306 .190325    .190325    0. 6 * 90.5415
251307 .1902456   .1902456   0. 7 * 90.5415
251308 .1901804   .1901804   0. 8 * 90.5415
251309 .1901268   .1901268   0. 9 * 90.5415
251310 .647094    .647094    0. 10 * 90.5415
251311 .647094  .647094  0. 11 * 90.5415
251312 .647094  .647094  0. 12 * 90.5415
251313 .647094  .647094  0. 13 * 90.5415
251314 .647094  .647094  0. 14 * 90.5415
251315 .647094  .647094  0. 15 * 90.5415
251316 .647094  .647094  0. 16 * 90.5415
251317 .647094  .647094  0. 17 * 90.5415
251318 .647094  .647094  0. 18 * 90.5415
251319 .647094  .647094  0. 19 * 90.5415
251320 .647094  .647094  0. 20 * 90.5415
251321 .647093  .647093  0. 21 * 90.5415
*-------junction 26
*card    name          component
260000   junc26        sngljun
*card    from          to             area       fwloss
revloss   flags
260101   25010000      17010006       0.125664   0.0
0.0       0
*card    init-mflow    liquid         vapor
intercept
260201   0             .647093        .647093    0. *
90.5415
*************************
```

```
* Auxiliary system
*************************
*-------pipe 30
*card  name component
300000 cooler pipe
*card  #-of-elements
300001 98
*card  angle-type option#
300002 sph 3
*card  flow-A-vols-x-dir which-vols
300101 0.127,5
300102 0.4859,15
300103 0.127,54
300104 0.164,64
300105 0.127,98
*card  flow-A-vols-z-dir which-vols
301701 0.031416,98
*card  flow-A-int-juncs which-int-juncs
300201 0.127,5
300202 0.4859,14
300203 0.127,54
300204 0.164,63
300205 0.127,97
*card  length which-vols
300301 0.1,5
300302 1.860,15
300303 0.06,25
300304 0.75,45
300305 0.055555555,54
300306 0.245,64
300307 0.483928,92
300308 0.1,98
*card  azimuth-angle which-vols
300501 180.0,5
300502 0.000,92
300503 180.0,98
*card  vertica-angle which-vols
300601 0.000,5
300602 -90.0,15
300603 0.000,25
300604 -90.00,45
300605 0.000,54
300606 90.00,92
300607 0.00,98
*coordinates capitalized are fixed coords
```

```
*card  dXx,dYx,dZx,which-vols (local x coords)
300701 -0.1,0.0,0.0,5
300702 0.0,0.0,-0.1,15
300703 0.06,0.0,0.0,25
300704 0.0,0.0,-0.75,45
300705 0.055555555,0.0,0.0,54
300706 0.0,0.0,0.245,64
300707 0.0,0.0,0.483928,92
300708 -0.1,0.0,0.0,98
*card  dXy,dYy,dZy,which-vols (local y coords)
302101 0.0,0.0,0.0,98
*card  dXz,dYz,dZz,which-vols (local z coords)
302201 0.0,0.0,0.0,98
*card  wall-rough,hydroD,which-vols (local x coords)
300801 0.0000,0.0,5
300802 0.0000,0.03,15
300803 0.0000,0.0,54
300804 0.0000,0.006855,64
300805 0.0000,0.0,98
*card  wall-rough,hydroD,which-vols (local y coords)
302301 0,0,98
*card  wall-rough,hydroD,which-vols (local z coords)
302401 0,0,98
*card  volume-control-flags tlpvbfe,which-vols
301001 0,98
*card  junction-control-flags efcahs,which-juncs
301101 0,97
*card  vols-init-conds-option P, T,
unused,unused,unused,which-vols
301201 0 7346932. 207256.4 207256.4 0. 0. 1
301202 0 7346929. 207256.4 207256.4 0. 0. 2
301203 0 7346926. 207256.4 207256.4 0. 0. 3
301204 0 7346924. 207256.4 207256.4 0. 0. 4
301205 0 7346922. 207256.4 207256.4 0. 0. 5
301206 0 7350990. 206927.8 206927.8 0. 0. 6
301207 0 7358475. 206378.6 206378.6 0. 0. 7
301208 0 7365962. 205465.3 205465.3 0. 0. 8
301209 0 7373449. 203951.  203951.  0. 0. 9
301210 0 7380940. 201445.2 201445.2 0. 0. 10
301211 0 7388435. 197295.  197295.  0. 0. 11
301212 0 7395938. 190319.3 190319.3 0. 0. 12
301213 0 7403454. 178597.2 178597.2 0. 0. 13
301214 0 7410990. 158910.  158910.  0. 0. 14
301215 0 7418564. 125581.6 125581.6 0. 0. 15
301216 0 7422040. 125581.6 125581.6 0. 0. 16
301217 0 7422038. 125581.6 125581.6 0. 0. 17
301218 0 7422037. 125581.6 125581.6 0. 0. 18
301219 0 7422036. 125581.6 125581.6 0. 0. 19
301220 0 7422034. 125581.6 125581.6 0. 0. 20
301221 0 7422032. 125581.6 125581.6 0. 0. 21
301222 0 7422031. 125581.6 125581.6 0. 0. 22
301223 0 7422030. 125581.7 125581.7 0. 0. 23
301224 0 7422028. 125581.7 125581.7 0. 0. 24
301225 0 7422026. 125581.7 125581.7 0. 0. 25
301226 0 7426238. 125581.7 125581.7 0. 0. 26
301227 0 7434664. 125581.8 125581.8 0. 0. 27
301228 0 7443089. 125582.  125582.  0. 0. 28
301229 0 7451514. 125582.  125582.  0. 0. 29
301230 0 7459939. 125582.  125582.  0. 0. 30
301231 0 7468364. 125582.  125582.  0. 0. 31
301232 0 7476790. 125582.1 125582.1 0. 0. 32
301233 0 7485214. 125582.2 125582.2 0. 0. 33
301234 0 7493640. 125582.2 125582.2 0. 0. 34
301235 0 7502065. 125582.3 125582.3 0. 0. 35
301236 0 7510490. 125582.4 125582.4 0. 0. 36
301237 0 7518916. 125582.4 125582.4 0. 0. 37
301238 0 7527340. 125582.5 125582.5 0. 0. 38
301239 0 7535766. 125582.6 125582.6 0. 0. 39
301240 0 7544191. 125582.6 125582.6 0. 0. 40
301241 0 7552616. 125582.7 125582.7 0. 0. 41
301242 0 7561042. 125582.8 125582.8 0. 0. 42
301243 0 7569466. 125582.8 125582.8 0. 0. 43
301244 0 7577892. 125583.  125583.  0. 0. 44
301245 0 7586317. 125583.  125583.  0. 0. 45
301246 0 7590529. 125583.  125583.  0. 0. 46
301247 0 7590528. 125583.  125583.  0. 0. 47
301248 0 7590526. 125583.  125583.  0. 0. 48
301249 0 7590524. 125583.  125583.  0. 0. 49
301250 0 7590523. 125583.  125583.  0. 0. 50
301251 0 7590522. 125583.  125583.  0. 0. 51
301252 0 7590520. 125583.  125583.  0. 0. 52
301253 0 7590519. 125583.  125583.  0. 0. 53
301254 0 7590518. 125583.  125583.  0. 0. 54
301255 0 7587954. 142471.4 142471.4 0. 0. 55
301256 0 7582270. 156358.3 156358.3 0. 0. 56
301257 0 7576608. 167786.  167786.  0. 0. 57
301258 0 7570962. 177179.7 177179.7 0. 0. 58
301259 0 7565330. 184909.8 184909.8 0. 0. 59
301260 0 7559710. 191271.  191271.  0. 0. 60
301261 0 7554098. 196498.  196498.  0. 0. 61
```

```
301262 0 7548494. 200799.  200799.  0. 0. 62
301263 0 7542897. 204338.7 204338.7 0. 0. 63
301264 0 7537304. 207249.  207249.  0. 0. 64
301265 0 7530875. 207249.  207249.  0. 0. 65
301266 0 7524186. 207249.  207249.  0. 0. 66
301267 0 7517498. 207249.  207249.  0. 0. 67
301268 0 7510810. 207249.  207249.  0. 0. 68
301269 0 7504122. 207249.  207249.  0. 0. 69
301270 0 7497434. 207249.  207249.  0. 0. 70
301271 0 7490745. 207249.  207249.  0. 0. 71
301272 0 7484057. 207249.  207249.  0. 0. 72
301273 0 7477368. 207249.  207249.  0. 0. 73
301274 0 7470680. 207249.2 207249.2 0. 0. 74
301275 0 7.464+6  207249.2 207249.2 0. 0. 75
301276 0 7457304. 207249.3 207249.3 0. 0. 76
301277 0 7450616. 207249.3 207249.3 0. 0. 77
301278 0 7443927. 207249.3 207249.3 0. 0. 78
301279 0 7437239. 207249.4 207249.4 0. 0. 79
301280 0 7430550. 207249.4 207249.4 0. 0. 80
301281 0 7423862. 207249.4 207249.4 0. 0. 81
301282 0 7417174. 207249.5 207249.5 0. 0. 82
301283 0 7410486. 207249.5 207249.5 0. 0. 83
301284 0 7403798. 207249.5 207249.5 0. 0. 84
301285 0 7397109. 207249.5 207249.5 0. 0. 85
301286 0 7390421. 207249.6 207249.6 0. 0. 86
301287 0 7383732. 207249.6 207249.6 0. 0. 87
301288 0 7377044. 207249.6 207249.6 0. 0. 88
301289 0 7370356. 207249.7 207249.7 0. 0. 89
301290 0 7363668. 207249.7 207249.7 0. 0. 90
301291 0 7356980. 207249.7 207249.7 0. 0. 91
301292 0 7350292. 207249.8 207249.8 0. 0. 92
301293 0 7346946. 207250.  207250.  0. 0. 93
301294 0 7346944. 207250.  207250.  0. 0. 94
301295 0 7346941. 207256.3 207256.3 0. 0. 95
301296 0 7346938. 207256.4 207256.4 0. 0. 96
301297 0 7346936. 207256.4 207256.4 0. 0. 97
301298 0 7346934. 207256.4 207256.4 0. 0. 98
*card  juncs-init-conds-cntrl,liquid-vel,gas-vel,which-
juncs
301301 .555062  .555062  0. 1 * 70.5619
301302 .555062  .555062  0. 2 * 70.5619
301303 .555062  .555062  0. 3 * 70.5619
301304 .555062  .555062  0. 4 * 70.5619
301305 .555062  .555062  0. 5 * 70.5619
301306 .01001854 .01001854 0. 6 * 70.5618
301307 .01001752 .01001752 0. 7 * 70.5616
301308 .01001582 .01001582 0. 8 * 70.5614
301309 .01001303 .01001303 0. 9 * 70.5613
301310 .01000843 .01000843 0. 10 * 70.5611
301311 .01000084 .01000084 0. 11 * 70.5609
301312 .00998803 .00998803 0. 12 * 70.5607
301313 .00996675 .00996675 0. 13 * 70.5605
301314 .00993115 .00993115 0. 14 * 70.5603
301315 .546879  .546879  0. 15 * 70.5601
301316 .546879  .546879  0. 16 * 70.5601
301317 .546879  .546879  0. 17 * 70.5601
301318 .546879  .546879  0. 18 * 70.5601
301319 .546879  .546879  0. 19 * 70.5601
301320 .546879  .546879  0. 20 * 70.5601
301321 .546879  .546879  0. 21 * 70.5601
301322 .546879  .546879  0. 22 * 70.5601
301323 .546879  .546879  0. 23 * 70.5601
301324 .546879  .546879  0. 24 * 70.5601
301325 .546879  .546879  0. 25 * 70.5601
301326 .546879  .546879  0. 26 * 70.5601
301327 .546879  .546879  0. 27 * 70.5601
301328 .546879  .546879  0. 28 * 70.5601
301329 .546878  .546878  0. 29 * 70.5601
301330 .546878  .546878  0. 30 * 70.5601
301331 .546878  .546878  0. 31 * 70.5601
301332 .546878  .546878  0. 32 * 70.5601
301333 .546878  .546878  0. 33 * 70.5601
301334 .546877  .546877  0. 34 * 70.5601
301335 .546877  .546877  0. 35 * 70.5601
301336 .546877  .546877  0. 36 * 70.5601
301337 .546877  .546877  0. 37 * 70.5601
301338 .546877  .546877  0. 38 * 70.5601
301339 .546877  .546877  0. 39 * 70.5601
301340 .546876  .546876  0. 40 * 70.5601
301341 .546876  .546876  0. 41 * 70.5601
301342 .546876  .546876  0. 42 * 70.5601
301343 .546876  .546876  0. 43 * 70.5601
301344 .546876  .546876  0. 44 * 70.5601
301345 .546875  .546875  0. 45 * 70.5601
301346 .546875  .546875  0. 46 * 70.5601
301347 .546875  .546875  0. 47 * 70.5601
301348 .546875  .546875  0. 48 * 70.5601
301349 .546875  .546875  0. 49 * 70.5601
301350 .546875  .546875  0. 50 * 70.5601
301351 .546875  .546875  0. 51 * 70.5601
```

```
301352 .546875  .546875  0. 52 * 70.5601
301353 .546875  .546875  0. 53 * 70.5601
301354 .546875  .546875  0. 54 * 70.5601
301355 .183052   .183052   0. 55 * 70.5601
301356 .183513   .183513   0. 56 * 70.5601
301357 .1838925  .1838925  0. 57 * 70.5601
301358 .184208   .184208   0. 58 * 70.5601
301359 .1844664  .1844664  0. 59 * 70.5601
301360 .1846796  .1846796  0. 60 * 70.5601
301361 .1848575  .1848575  0. 61 * 70.5601
301362 .1850023  .1850023  0. 62 * 70.5601
301363 .1851216  .1851216  0. 63 * 70.5601
301364 .555042  .555042  0. 64 * 70.5601
301365 .555042  .555042  0. 65 * 70.5601
301366 .555042  .555042  0. 66 * 70.5601
301367 .555042  .555042  0. 67 * 70.5601
301368 .555043  .555043  0. 68 * 70.5601
301369 .555043  .555043  0. 69 * 70.5601
301370 .555043  .555043  0. 70 * 70.5601
301371 .555043  .555043  0. 71 * 70.5601
301372 .555043  .555043  0. 72 * 70.5601
301373 .555043  .555043  0. 73 * 70.5601
301374 .555044  .555044  0. 74 * 70.5601
301375 .555044  .555044  0. 75 * 70.5601
301376 .555044  .555044  0. 76 * 70.5601
301377 .555044  .555044  0. 77 * 70.5601
301378 .555044  .555044  0. 78 * 70.5601
301379 .555045  .555045  0. 79 * 70.5601
301380 .555045  .555045  0. 80 * 70.5601
301381 .555045  .555045  0. 81 * 70.5601
301382 .555045  .555045  0. 82 * 70.5601
301383 .555045  .555045  0. 83 * 70.5601
301384 .555045  .555045  0. 84 * 70.5601
301385 .555046  .555046  0. 85 * 70.5601
301386 .555046  .555046  0. 86 * 70.5601
301387 .555046  .555046  0. 87 * 70.5601
301388 .555046  .555046  0. 88 * 70.5601
301389 .555046  .555046  0. 89 * 70.5601
301390 .555046  .555046  0. 90 * 70.5601
301391 .555047  .555047  0. 91 * 70.5601
301392 .555047  .555047  0. 92 * 70.5601
301393 .555047  .555047  0. 93 * 70.5601
301394 .555047  .555047  0. 94 * 70.5601
301395 .555062  .555062  0. 95 * 70.5619
301396 .555062  .555062  0. 96 * 70.5619
301397 .555062  .555062  0. 97 * 70.5619
*-------junction 31
*card name     component
310000 sngjun   sngljun
*card   from    to        area        fwloss   fwrever
flags
310101   30010000 30000000   0.127    0.0      0.0
0
*card  init-mflow liquid   vapor   intercept
310201   0         .555062  .555062  0. * 70.5619
*-------volume 32
*card   name       component
320000   sink      tmdpvol
*card   area     length    vol   hor-ang   ver-ang
elev-change
320101   2.0       0.2     0.0   0.0       -90.0     -
0.2
*card   rough     hydro    flags
320102   0.0       0.0      0000000
*card   init-cond
320200   003
*card   time    Pressure  Temperature
320201   0.0     7.341e6   973.817
320202   100.0   7.341e6   973.817
*-------junction 33
*card   name     component
330000   out-jun   sngljun
*card   from      to        area       fwloss   fwrever
flags
330101   32010000 34000000  0.031416   0.0      0.0
0
*card   init-mflow liquid   vapor   intercept
330201   0          2.84426-5   2.84426-5   0. *
.00180446
*-------pipe 34
*card name component
340000 cooler pipe
*card #-of-elements
340001 3
*card angle-type option#
340002 sph 3
*card flow-A-vols which-vols
340101 0.031416,3
*card flow-A-int-juncs which-int-juncs
340201 0.031416,2
```

```
*card length which-vols
340301 0.1,3
*card azimuth-angle which-vols
340501 0.0,3
*card vertica-angle which-vols
340601 -90.0,3
*card wall-rough,hydroD,which-vols (local x coords)
340801 0,0,3
*card volume-control-flags tlpvbfe,which-vols
341001 0,3
*card junction-control-flags efcahs,which-juncs
341101 0,2
*card vols-init-conds-option P, T,
unused,unused,unused,which-vols
341201 0 7341990. 463544.  463544.  0. 0. 1
341202 0 7343970. 463544.  463544.  0. 0. 2
341203 0 7345951. 463544.  463544.  0. 0. 3
*card juncs-init-conds-cntrl,liquid-vel,gas-vel,which-
juncs
341301 2.84426-5   2.84426-5   0. 1 * .00180446
341302 2.84426-5   2.84426-5   0. 2 * .00180446
*-------junction 35
*card   name     component
350000   out-jun   sngljun
*card   from    to        area          fwloss   fwrever
flags
350101   34030002 30950005   0.031416   0.0      0.0
0
*card   init-mflow liquid   vapor   intercept
350201   0          2.84426-5   2.84426-5   0. *
.00180446
*************************
* Intermediate system
*************************
*-------valve 40
400000   val_1         valve
*card    from-vol      to-vol         aflow    fwd-loss
rev-loss jefvcahs
400101   17010005      41000000       0.19634  0.0
0.0      0
*card    ctrl-mflow    flowf          flowg    velj
400201   0             9.524          9.524    0.
* 3618.904
*card    valve-type
400300   trpvlv
*card    trip num
400301   778
*-------pipe 41
*card name component
410000 cooler pipe
*card #-of-elements
410001 20
*card angle-type option#
410002 sph 3
*card flow-A-vols which-vols
410101 0.19634,20
*card flow-A-int-juncs which-int-juncs
410201 0.19634,19
*card length which-vols
410301 0.5,10
410302 0.45,20
*card azimuth-angle which-vols
410501 0.0,20
*card vertica-angle which-vols
410601 90.0,10
410602 0.00,20
*card wall-rough,hydroD,which-vols (local x coords)
410801 0.0000,0,20
*card volume-control-flags tlpvbfe,which-vols
411001 0,20
*card junction-control-flags efcahs,which-juncs
411101 0,19
*card vols-init-conds-option P, T,
unused,unused,unused,which-vols
411201 0 4736008. 591982. 591982. 0. 0. 1
411202 0 4725584. 591982. 591982. 0. 0. 2
411203 0 4715161. 591983. 591983. 0. 0. 3
411204 0 4704738. 591983. 591983. 0. 0. 4
411205 0 4694315. 591984. 591984. 0. 0. 5
411206 0 4683892. 591984. 591984. 0. 0. 6
411207 0 4673469. 591985. 591985. 0. 0. 7
411208 0 4663046. 591985. 591985. 0. 0. 8
411209 0 4652623. 591986. 591986. 0. 0. 9
411210 0 4642200. 591986. 591986. 0. 0. 10
411211 0 4636568. 591987. 591987. 0. 0. 11
411212 0 4635728. 591987. 591987. 0. 0. 12
411213 0 4634888. 591987. 591987. 0. 0. 13
411214 0 4634048. 591988. 591988. 0. 0. 14
411215 0 4633208. 591988. 591988. 0. 0. 15
411216 0 4632368. 591989. 591989. 0. 0. 16
```

```
411217 0 4631527. 591989. 591989. 0. 0. 17
411218 0 4630687. 591990. 591990. 0. 0. 18
411219 0 4629846. 591990. 591990. 0. 0. 19
411220 0 4629006. 591990. 591990. 0. 0. 20
*card juncs-init-conds-cntrl,liquid-vel,gas-vel,which-
juncs
411301 9.52404 9.52404 0. 1 * 3618.904
411302 9.52405 9.52405 0. 2 * 3618.904
411303 9.52405 9.52405 0. 3 * 3618.904
411304 9.52406 9.52406 0. 4 * 3618.904
411305 9.52407 9.52407 0. 5 * 3618.904
411306 9.52407 9.52407 0. 6 * 3618.904
411307 9.52408 9.52408 0. 7 * 3618.904
411308 9.52409 9.52409 0. 8 * 3618.904
411309 9.5241  9.5241  0. 9 * 3618.904
411310 9.5241  9.5241  0. 10 * 3618.904
411311 9.5241  9.5241  0. 11 * 3618.904
411312 9.5241  9.5241  0. 12 * 3618.904
411313 9.5241  9.5241  0. 13 * 3618.904
411314 9.5241  9.5241  0. 14 * 3618.904
411315 9.5241  9.5241  0. 15 * 3618.904
411316 9.5241  9.5241  0. 16 * 3618.904
411317 9.52411 9.52411 0. 17 * 3618.904
411318 9.52411 9.52411 0. 18 * 3618.904
411319 9.52411 9.52411 0. 19 * 3618.904
*--------- pump 42
*card          name         type
4200000        pripump      pump
*card          Area-flow    Length         Vol   az-
angle inc-angle
*+ aditional   dz           ctrl
4200101        0.19634      1.0            0.0   0.0
0.0
+              0.0          0
*card          ebt          P              T
4200200        0            4870380.       591783.
591783. 0.
*card          from-vol     area           fwd-loss
rev-loss
*+ aditional   efvcahs
4200108        41200002     0.19634        0.0
0.0
+              0
*card          to-vol       area           fwd-loss
rev-loss
*+ aditional   efvcahs
4200109        43010001     0.19634        0.0
0.0
+              0
*card          ctrl         inlet:flowf    inlet:flowg
inlet:velj
4200201        0            9.52411        9.52411
0. * 3618.904
*card          ctrl         outlet:flowf   outlet:flowg
outlet:velj
4200202        0            9.52376        9.52376
0. * 3618.904
*card          1phase       2phase         2pdiff
torque
*+ aditional   pvel         ptrip          rvrse
4200301        -1           -1             -3
-1
+               0            0              0
*card          rpvel        initv          rflow
rhead
*+ aditional   rtork        momi           rdens
4200302        200.000000   .925           2.0000
30.0000
+              1000.00000   5.00000e4      2000.0
*card          rmotk        tf2            tf0
tf1
*+ aditional   tf3
4200303        200.000000   0.000000       0.00000
0.0000
+              0.00000
*card          time       angular-velocity
4206100        0          time
4206101        0.000000   185.00
4206102        100.0000   185.00
4206103        101.2000   0.0000
4206104        5000.000   0.0000
*-------pipe 43
*card  name component
430000 ihx  pipe
*card  #-of-elements
430001 60
*card  angle-type option#
430002 sph 3
*card  flow-A-vols-x-dir which-vols
430101 0.196340,10
```

```
430102 1.419000,20
430103 0.196340,60
*card  flow-A-int-juncs which-int-juncs
430201 0.196340,10
430202 1.419000,19
430203 0.196340,59
*card  length which-vols
430301 0.100,10
430302 0.833,20
430303 0.100,25
430304 0.733,35
430305 0.550,45
430306 0.9118,55
430307 0.100,60
*card  azimuth-angle which-vols
430501 0.0,20
430502 180.0,60
*card  vertica-angle which-vols
430601 0.000,10
430602 -90.0,20
430603 0.000,25
430604 90.00,35
430605 0.000,45
430606 -90.0,55
430607 0.000,60
*coordinates capitalized are fixed coords
*card  dXx,dYx,dZx,which-vols (local x coords)
430701 0.1,0.0,0.0,10
430702 0.0,0.0,-0.833,20
430703 -0.1,0.0,0.0,25
430704 0.0,0.0,0.733,35
430705 -0.55,0.0,0.0,45
430706 0.0,0.0,-0.9118,55
430707 -0.1,0.0,0.0,60
*card  dXy,dYy,dZy,which-vols (local y coords)
432101 0.0,0.0,0.0,60
*card  dXz,dYz,dZz,which-vols (local z coords)
432201 0.0,0.0,0.0,60
*card  wall-rough,hydroD,which-vols (local x coords)
430801 0.0000,0.0,10
430802 0.0000,0.006855,20
430803 0.0000,0.0,60
*card  wall-rough,hydroD,which-vols (local y coords)
432301 0,0,60
*card  wall-rough,hydroD,which-vols (local z coords)
432401 0,0,60
*card  volume-control-flags tlpvbfe,which-vols
431001 0,60
*card  junction-control-flags efcahs,which-juncs
431101 0,59
*card  vols-init-conds-option P, T,
unused,unused,unused,which-vols
431201 0 5112082. 591783. 591783. 0. 0. 1
431202 0 5111896. 591783. 591783. 0. 0. 2
431203 0 5111710. 591783. 591783. 0. 0. 3
431204 0 5111522. 591783. 591783. 0. 0. 4
431205 0 5111336. 591784. 591784. 0. 0. 5
431206 0 5111150. 591784. 591784. 0. 0. 6
431207 0 5110962. 591784. 591784. 0. 0. 7
431208 0 5110776. 591784. 591784. 0. 0. 8
431209 0 5110589. 591784. 591784. 0. 0. 9
431210 0 5110402. 591784. 591784. 0. 0. 10
431211 0 5199968. 575059.  575059.  0. 0. 11
431212 0 5207089. 556819.  556819.  0. 0. 12
431213 0 5214220. 536961.  536961.  0. 0. 13
431214 0 5221556. 515382.  515382.  0. 0. 14
431215 0 5229279. 491984.  491984.  0. 0. 15
431216 0 5237440. 466677.  466677.  0. 0. 16
431217 0 5246104. 439374.  439374.  0. 0. 17
431218 0 5255342. 410011.  410011.  0. 0. 18
431219 0 5265237. 378533.  378533.  0. 0. 19
431220 0 5275393. 344921.3 344921.3 0. 0. 20
431221 0 5196442. 344921.4 344921.4 0. 0. 21
431222 0 5196246. 344921.5 344921.5 0. 0. 22
431223 0 5196049. 344921.6 344921.6 0. 0. 23
431224 0 5195852. 344922.  344922.  0. 0. 24
431225 0 5195656. 344922.  344922.  0. 0. 25
431226 0 5187701. 344922.5 344922.5 0. 0. 26
431227 0 5171987. 344923.  344923.  0. 0. 27
431228 0 5156273. 344924.  344924.  0. 0. 28
431229 0 5140558. 344925.  344925.  0. 0. 29
431230 0 5124844. 344925.4 344925.4 0. 0. 30
431231 0 5109130. 344926.  344926.  0. 0. 31
431232 0 5093416. 344927.  344927.  0. 0. 32
431233 0 5077702. 344927.6 344927.6 0. 0. 33
431234 0 5061988. 344928.  344928.  0. 0. 34
431235 0 5046274. 344929.  344929.  0. 0. 35
431236 0 5037876. 344929.6 344929.6 0. 0. 36
431237 0 5036797. 344930.  344930.  0. 0. 37
431238 0 5035717. 344931.  344931.  0. 0. 38
```

```
431239 0 5034637. 344931.  344931.  0. 0. 39
431240 0 5033558. 344932.  344932.  0. 0. 40
431241 0 5032478. 344932.  344932.  0. 0. 41
431242 0 5031398. 344933.  344933.  0. 0. 42
431243 0 5030318. 344933.4 344933.4 0. 0. 43
431244 0 5029238. 344934.  344934.  0. 0. 44
431245 0 5028158. 344934.5 344934.5 0. 0. 45
431246 0 5035602. 344935.4 344935.4 0. 0. 46
431247 0 5051568. 344936.  344936.  0. 0. 47
431248 0 5067536. 344937.  344937.  0. 0. 48
431249 0 5083502. 344938.  344938.  0. 0. 49
431250 0 5099470. 344939.  344939.  0. 0. 50
431251 0 5115436. 344940.  344940.  0. 0. 51
431252 0 5131404. 344941.  344941.  0. 0. 52
431253 0 5147370. 344942.  344942.  0. 0. 53
431254 0 5163338. 344942.6 344942.6 0. 0. 54
431255 0 5179305. 344943.5 344943.5 0. 0. 55
431256 0 5187190. 344943.6 344943.6 0. 0. 56
431257 0 5186994. 344944.  344944.  0. 0. 57
431258 0 5186798. 344944.  344944.  0. 0. 58
431259 0 5186602. 344944.  344944.  0. 0. 59
431260 0 5186405. 344944.  344944.  0. 0. 60
*card  juncs-init-conds-cntrl,liquid-vel,gas-vel,which-
juncs
431301 9.52368 9.52368 0. 1 * 3618.904
431302 9.52368 9.52368 0. 2 * 3618.904
431303 9.52368 9.52368 0. 3 * 3618.904
431304 9.52368 9.52368 0. 4 * 3618.904
431305 9.52368 9.52368 0. 5 * 3618.904
431306 9.52368 9.52368 0. 6 * 3618.904
431307 9.52368 9.52368 0. 7 * 3618.904
431308 9.52368 9.52368 0. 8 * 3618.904
431309 9.52368 9.52368 0. 9 * 3618.904
431310 9.52368 9.52368 0. 10 * 3618.904
431311 1.315414 1.315414 0. 11 * 3618.904
431312 1.312887 1.312887 0. 12 * 3618.904
431313 1.310146 1.310146 0. 13 * 3618.904
431314 1.30718  1.30718  0. 14 * 3618.904
431315 1.30398  1.30398  0. 15 * 3618.904
431316 1.300538 1.300538 0. 16 * 3618.904
431317 1.296845 1.296845 0. 17 * 3618.904
431318 1.292896 1.292896 0. 18 * 3618.904
431319 1.28869  1.28869  0. 19 * 3618.904
431320 9.28143 9.28143 0. 20 * 3618.904
431321 9.28146 9.28146 0. 21 * 3618.904
431322 9.28146 9.28146 0. 22 * 3618.904
431323 9.28146 9.28146 0. 23 * 3618.904
431324 9.28146 9.28146 0. 24 * 3618.904
431325 9.28147 9.28147 0. 25 * 3618.904
431326 9.28147 9.28147 0. 26 * 3618.904
431327 9.28148 9.28148 0. 27 * 3618.904
431328 9.28149 9.28149 0. 28 * 3618.904
431329 9.2815  9.2815  0. 29 * 3618.904
431330 9.2815  9.2815  0. 30 * 3618.904
431331 9.28151 9.28151 0. 31 * 3618.904
431332 9.28152 9.28152 0. 32 * 3618.904
431333 9.28153 9.28153 0. 33 * 3618.904
431334 9.28154 9.28154 0. 34 * 3618.904
431335 9.28154 9.28154 0. 35 * 3618.904
431336 9.28155 9.28155 0. 36 * 3618.904
431337 9.28155 9.28155 0. 37 * 3618.904
431338 9.28155 9.28155 0. 38 * 3618.904
431339 9.28155 9.28155 0. 39 * 3618.904
431340 9.28155 9.28155 0. 40 * 3618.904
431341 9.28155 9.28155 0. 41 * 3618.904
431342 9.28155 9.28155 0. 42 * 3618.904
431343 9.28155 9.28155 0. 43 * 3618.904
431344 9.28156 9.28156 0. 44 * 3618.904
431345 9.28156 9.28156 0. 45 * 3618.904
431346 9.28155 9.28155 0. 46 * 3618.904
431347 9.28155 9.28155 0. 47 * 3618.904
431348 9.28154 9.28154 0. 48 * 3618.904
431349 9.28153 9.28153 0. 49 * 3618.904
431350 9.28153 9.28153 0. 50 * 3618.904
431351 9.28152 9.28152 0. 51 * 3618.904
431352 9.28151 9.28151 0. 52 * 3618.904
431353 9.2815  9.2815  0. 53 * 3618.904
431354 9.2815  9.2815  0. 54 * 3618.904
431355 9.2815  9.2815  0. 55 * 3618.904
431356 9.28149 9.28149 0. 56 * 3618.904
431357 9.28149 9.28149 0. 57 * 3618.904
431358 9.28149 9.28149 0. 58 * 3618.904
431359 9.28149 9.28149 0. 59 * 3618.904
*-------junction 44
*card   name     component
440000   out-jun   sngljun
*card   from      to         area          fwloss
fwrever   flags
440101   43010000  10010005   0.19634      0.0      0.0
0
```

```
*card   init-mflow liquid   vapor   intercept
440201   0          9.28149  9.28149 0. * 3618.904
*******************************************************
***
* Secondary cooling
*******************************************************
***
*-------volume 50
*card   name       component
500000   source     tmdpvol
*card   area     length    vol   hor-ang   ver-ang
elev-change
500101   2.0       0.2     0.0   180.0       0.0
0.0
*card   rough     hydro    flags
500102   0.0       0.0      0000000
*card   init-cond
500200   003
*card   time    Pressure  Temperature
500201   0.0     5.4e6   808.0
500202   100.0   5.4e6   808.0
*-------junction 51
*card   name      component
510000   in-jun   tmdpjun
*card   from      to        area       flags
510101   50010000 52000000  0.19634    0
*card   init-mass-flow-flag
510200    1
*card   time        liquid   vapor   intercept
510201   0.0000     -3292.0      0.0     0.0
510202   100.00     -3292.0      0.0     0.0
510203   100.05     0.00000      0.0     0.0
510204   5000.0     0.00000      0.0     0.0

*-------pipe 52
*card  name component
520000 ihx  pipe
*card  #-of-elements
520001 40
*card  angle-type option#
520002 sph 3
*card  flow-A-vols-x-dir which-vols
520101 0.196340,10
520102 2.193600,20
520103 0.196340,40
*card  flow-A-int-juncs which-int-juncs
520201 0.196340,10
520202 2.193600,19
520203 0.196340,39
*card  length which-vols
520301 0.100,10
520302 0.833,20
520303 0.100,25
520304 0.733,35
520305 0.100,40
*card  azimuth-angle which-vols
520501 180.0,10
520502 0.000,40
*card  vertica-angle which-vols
520601 0.000,10
520602 -90.0,20
520603 0.000,25
520604 90.00,35
520605 0.000,40
*coordinates capitalized are fixed coords
*card  dXx,dYx,dZx,which-vols (local x coords)
520701 -0.1,0.0,0.0,10
520702 0.0,0.0,-0.833,20
520703 0.1,0.0,0.0,25
520704 0.0,0.0,0.733,35
520705 0.10,0.0,0.0,40
*card  dXy,dYy,dZy,which-vols (local y coords)
522101 0.0,0.0,0.0,40
*card  dXz,dYz,dZz,which-vols (local z coords)
522201 0.0,0.0,0.0,40
*card  wall-rough,hydroD,which-vols (local x coords)
520801 0.0000,0.0,10
520802 0.0000,0.009252,20
520803 0.0000,0.0,40
*card fwd loss rev loss which-juncs
520901 0.000,0.000,10
520902 65.0747,65.0747,20
520903 0.000,0.000,39
*card  wall-rough,hydroD,which-vols (local y coords)
522301 0,0,40
*card  wall-rough,hydroD,which-vols (local z coords)
522401 0,0,40
*card volume-control-flags tlpvbfe,which-vols
521001 0,10
521002 0000010,20
```

```
521003 0,40
*card  junction-control-flags efcahs,which-juncs
521101 0,39
*card  vols-init-conds-option P, T,
unused,unused,unused,which-vols
521201 0 701014.  423304.  2652788. 0. 0. 1
521202 0 701151.  423304.  2652810. 0. 0. 2
521203 0 701288.  423303.5 2652833. 0. 0. 3
521204 0 701425.  423303.4 2652855. 0. 0. 4
521205 0 701563.  423303.  2652877. 0. 0. 5
521206 0 701700.  423303.  2652899. 0. 0. 6
521207 0 701837.  423303.  2652922. 0. 0. 7
521208 0 701974.  423303.  2652944. 0. 0. 8
521209 0 702112.  423303.  2652966. 0. 0. 9
521210 0 702249.  423303.  2652988. 0. 0. 10
521211 0 779165.  423303.  2664886. 0. 0. 11
521212 0 832196.  404908.  2672529. 0. 0. 12
521213 0 885155.  384848.  2679766. 0. 0. 13
521214 0 938033.  363008.3 2686641. 0. 0. 14
521215 0 990825.  339277.  2693190. 0. 0. 15
521216 0 1043525. 313545.  2699444. 0. 0. 16
521217 0 1096128. 285716.  2705430. 0. 0. 17
521218 0 1148629. 255692.5 2711171. 0. 0. 18
521219 0 1201022. 223403.5 2716687. 0. 0. 19
521220 0 1253299. 188790.4 2721996. 0. 0. 20
521221 0 5476510. 151831.1 151831.1 0. 0. 21
521222 0 5476658. 151831.  151831.  0. 0. 22
521223 0 5476806. 151831.  151831.  0. 0. 23
521224 0 5476954. 151831.  151831.  0. 0. 24
521225 0 5477103. 151831.  151831.  0. 0. 25
521226 0 5470028. 151830.8 151830.8 0. 0. 26
521227 0 5455732. 151830.3 151830.3 0. 0. 27
521228 0 5441435. 151829.8 151829.8 0. 0. 28
521229 0 5427138. 151829.3 151829.3 0. 0. 29
521230 0 5412842. 151828.8 151828.8 0. 0. 30
521231 0 5398545. 151828.2 151828.2 0. 0. 31
521232 0 5384248. 151827.8 151827.8 0. 0. 32
521233 0 5369952. 151827.2 151827.2 0. 0. 33
521234 0 5355656. 151826.7 151826.7 0. 0. 34
521235 0 5341359. 151826.2 151826.2 0. 0. 35
521236 0 5334284. 151825.7 151825.7 0. 0. 36
521237 0 5334433. 151825.6 151825.6 0. 0. 37
521238 0 5334581. 151825.6 151825.6 0. 0. 38
521239 0 5334730. 151825.5 151825.5 0. 0. 39
521240 0 5334878. 151825.4 151825.4 0. 0. 40
```

```
*card  juncs-init-conds-cntrl,liquid-vel,gas-vel,which-
juncs
521301 -8.24093 -8.24093 0. 1 * -3292.
521302 -8.24093 -8.24093 0. 2 * -3292.
521303 -8.24093 -8.24093 0. 3 * -3292.
521304 -8.24093 -8.24093 0. 4 * -3292.
521305 -8.24093 -8.24093 0. 5 * -3292.
521306 -8.24093 -8.24093 0. 6 * -3292.
521307 -8.24093 -8.24093 0. 7 * -3292.
521308 -8.24093 -8.24093 0. 8 * -3292.
521309 -8.24093 -8.24093 0. 9 * -3292.
521310 -8.2409  -8.98658 0. 10 * -3292.
521311 -.735033  -.93309   0. 11 * -3292.
521312 -.732243 -.929473 0. 12 * -3292.
521313 -.72923   -.925566  0. 13 * -3292.
521314 -.725984  -.921358  0. 14 * -3292.
521315 -.722499  -.91684   0. 15 * -3292.
521316 -.718764  -.911998  0. 16 * -3292.
521317 -.714781  -.906835  0. 17 * -3292.
521318 -.710546  -.901345  0. 18 * -3292.
521319 -.70606   -.895532  0. 19 * -3292.
521320 -7.83459 -7.83459 0. 20 * -3292.
521321 -7.83459 -7.83459 0. 21 * -3292.
521322 -7.83459 -7.83459 0. 22 * -3292.
521323 -7.83459 -7.83459 0. 23 * -3292.
521324 -7.83459 -7.83459 0. 24 * -3292.
521325 -7.83459 -7.83459 0. 25 * -3292.
521326 -7.8346  -7.8346  0. 26 * -3292.
521327 -7.8346  -7.8346  0. 27 * -3292.
521328 -7.8346  -7.8346  0. 28 * -3292.
521329 -7.83461 -7.83461 0. 29 * -3292.
521330 -7.83461 -7.83461 0. 30 * -3292.
521331 -7.83462 -7.83462 0. 31 * -3292.
521332 -7.83462 -7.83462 0. 32 * -3292.
521333 -7.83463 -7.83463 0. 33 * -3292.
521334 -7.83463 -7.83463 0. 34 * -3292.
521335 -7.83463 -7.83463 0. 35 * -3292.
521336 -7.83463 -7.83463 0. 36 * -3292.
521337 -7.83463 -7.83463 0. 37 * -3292.
521338 -7.83463 -7.83463 0. 38 * -3292.
521339 -7.83463 -7.83463 0. 39 * -3292.
*-------junction 53
*card   name     component
530000   out-jun   sngljun
```

```
*card   from      to        area       fwloss   fwrever
flags
530101   52010000 54000000  0.19634    0.0      0.0
0
*card   init-mflow liquid   vapor   intercept
530201   0          -7.83461 -7.83461 0. * -3292.
*-------volume 54
*card   name       component
540000   sink       tmdpvol
*card   area     length    vol   hor-ang   ver-ang
elev-change
540101   2.0        0.2     0.0   0.0       0.0       0.0
*card   rough     hydro    flags
540102   0.0        0.0      0000000
*card   init-cond
540200   003
*card   time    Pressure  Temperature
540201   0.0     5.4e6   808.1
540202   100.0   5.4e6   808.1

*******************************************************
***
* External cooling
*******************************************************
***
*-------volume 60
*card   name       component
600000   source     tmdpvol
*card   area     length    vol   hor-ang   ver-ang
elev-change
600101   10.00       0.2     0.0   0.0       -90.0     -
0.2
*card   rough     hydro    flags
600102   0.0        0.0      0000000
*card   init-cond
600200   003
*card   time    Pressure  Temperature
600201   0.0     1.01e5   293.0
600202   100.0   1.01e5   293.0

*-------junction 61
*card   name     component
610000   in-jun   sngljun
*card   from      to        area       fwloss   fwrever
flags
610101   60010000 62000000  10.00    0.0      0.0
0
*card   init-mflow liquid   vapor   intercept
610201   0          1.710284 1.710284 0. * 9.93452


*-------valve 61
610000   val_1         valve
*card    from-vol      to-vol         aflow    fwd-loss
rev-loss jefvcahs
610101   60010000 62000000            5.00     0.0
0.0      00000100
*card    ctrl-mflow    flowf          flowg    velj
610201   0             1.71           1.71    0.       *
3618.904
*card    valve-type
610300   mtrvlv
*card    open-trip close-trip vlv-chg-rate init-pos
table-num
610301   780       779        1.0          0.0      911


*-------pipe 62
*card  name component
620000 airloop  pipe
*card  #-of-elements
620001 35
*card  angle-type option#
620002 sph 3
*card  flow-A-vols-x-dir which-vols
620101 10.00,10
620102 10.00,15
620103 32.23,25
620104 10.00,35
*card  flow-A-int-juncs which-int-juncs
620201 10.00,9
620202 10.00,14
620203 32.23,24
620204 10.00,34
*card  length which-vols
620301 0.80,10
620302 0.10,15
620303 0.10,25
620304 0.80,35
*card  azimuth-angle which-vols
```

```
620501 0.0,10
620502 0.0,15
620503 0.0,25
620504 0.0,35
*card  vertica-angle which-vols
620601 -90.0,10
620602 0.000,15
620603 90.00,25
620604 90.00,35
*card  wall-rough,hydroD,which-vols (local x coords)
620801 0.0000,0.000,10
620802 0.0000,0.000,15
620803 0.0000,0.000,25
620804 0.0000,0.000,35
*card fwd loss rev loss which-juncs
620901 0.0000,0.0000,10
620902 0.0000,0.0000,15
620903 1.4000,1.4000,24
620904 0.0000,0.0000,34
*card  volume-control-flags tlpvbfe,which-vols
621001 0000000,10
621002 0000000,15
621003 0000010,25
621004 0000000,35
*card  junction-control-flags efcahs,which-juncs
621101 0,34
*card  ebt P,      T           vols
621201 0   100859.8 27659.66 366825.  1. 0. 1
621202 0   100886.6 27664.24 366841.5 1. 0. 2
621203 0   100913.5 27668.8  366858. 1. 0. 3
621204 0   100940.3 27673.4  366874.5 1. 0. 4
621205 0   100967.2 27678.   366891.  1. 0. 5
621206 0   100994.  27682.55 366907.6 1. 0. 6
621207 0   101021.  27687.13 366924. 1. 0. 7
621208 0   101047.8 27691.7  366941.  1. 0. 8
621209 0   101074.6 27696.3  366957. 1. 0. 9
621210 0   101101.5 27700.87 366974.  1. 0. 10
621211 0   101115.  27703.16 366982. 1. 0. 11
621212 0   101115.  27703.16 366982. 1. 0. 12
621213 0   101115.  27703.16 366982. 1. 0. 13
621214 0   101115.  27703.16 366982. 1. 0. 14
621215 0   101115.  27703.16 366982. 1. 0. 15
621216 0   101115.4 27703.24 536694. 1. 0. 16
621217 0   101112.2 27702.7 638110. 1. 0. 17
621218 0   101109.  27702.13 698962. 1. 0. 18
621219 0   101105.7 27701.6  735211. 1. 0. 19
621220 0   101102.5 27701.03 756811. 1. 0. 20
621221 0   101099.2 27700.5  770057. 1. 0. 21
621222 0   101096.  27699.9  778103. 1. 0. 22
621223 0   101092.7 27699.36 782982. 1. 0. 23
621224 0   101089.4 27698.8  785938. 1. 0. 24
621225 0   101086.1 27698.24 787729. 1. 0. 25
621226 0   101076.6 27696.6  787712. 1. 0. 26
621227 0   101068.5 27695.25 787697. 1. 0. 27
621228 0   101060.5 27693.9  787683. 1. 0. 28
621229 0   101052.4 27692.5  787668. 1. 0. 29
621230 0   101044.3 27691.13 787654. 1. 0. 30
621231 0   101036.3 27689.75 787639. 1. 0. 31
621232 0   101028.2 27688.4  787625. 1. 0. 32
621233 0   101020.2 27687.   787610. 1. 0. 33
621234 0   101012.1 27685.63 787596. 1. 0. 34
621235 0   101004.  27684.26 787581. 1. 0. 35
*card  juncs-init-conds-cntrl,liquid-vel,gas-vel,which-
juncs
621301 1.71198  1.71198  0. 1 * 9.93452
621302 1.711657 1.711657 0. 2 * 9.93452
621303 1.71133  1.71133  0. 3 * 9.93452
621304 1.711007 1.711007 0. 4 * 9.93452
621305 1.710682 1.710682 0. 5 * 9.93452
621306 1.710357 1.710357 0. 6 * 9.93452
621307 1.710033 1.710033 0. 7 * 9.93452
621308 1.709708 1.709708 0. 8 * 9.93452
621309 1.709384 1.709384 0. 9 * 9.93452
621310 1.70906  1.70906  0. 10 * 9.93452
621311 1.708897 1.708897 0. 11 * 9.93452
621312 1.708897 1.708897 0. 12 * 9.93452
621313 1.708897 1.708897 0. 13 * 9.93452
621314 1.708897 1.708897 0. 14 * 9.93452
621315 1.708897 1.708897 0. 15 * 9.93452
621316 .370886  .370886  0. 16 * 9.93452
621317 .463793  .463793  0. 17 * 9.93452
621318 .518129  .518129  0. 18 * 9.93452
621319 .550504  .550504  0. 19 * 9.93452
621320 .569803  .569803  0. 20 * 9.93452
621321 .581072  .581072  0. 21 * 9.93452
621322 .587878  .587878  0. 22 * 9.93452
621323 .592012  .592012  0. 23 * 9.93452
621324 .594525  .594525  0. 24 * 9.93452
621325 4.87099  4.87099  0. 25 * 9.93452
621326 4.87133  4.87133  0. 26 * 9.93452
```

```
621327 4.87162  4.87162  0. 27 * 9.93452
621328 4.87191  4.87191  0. 28 * 9.93451
621329 4.8722   4.8722   0. 29 * 9.93451
621330 4.87249  4.87249  0. 30 * 9.93451
621331 4.87278  4.87278  0. 31 * 9.93451
621332 4.87307  4.87307  0. 32 * 9.93451
621333 4.87335  4.87335  0. 33 * 9.93451
621334 4.87364  4.87364  0. 34 * 9.93451

*-------junction 63
*card   name     component
630000   out-jun   sngljun
*card   from       to        area       fwloss   fwrever
flags
630101   62010000  64000000  10.000    0.0      0.0
0
*card   init-mflow liquid   vapor   intercept
630201   0          4.87393  4.87393  0. * 9.93451
*-------volume 64
*card   name       component
640000   sink      tmdpvol
*card   area     length    vol   hor-ang   ver-ang
elev-change
640101   10.000     0.2     0.0   0.0       90.0
0.2
*card   rough     hydro    flags
640102   0.0       0.0      0000000
*card   init-cond
640200   003
*card   time    Pressure  Temp
640201   0.000   1.01e5   293.0
640202   100.0   1.01e5   293.0

*******************************************************
***
* Heat structures
*******************************************************
***
*------------ core
*card ax-mesh rad-mesh geom-sph sty-init-flg-calc-by-
code lft-bndr
10011000   12       13       3           1
0.0
*card msh-flag-geom-composit&source-distrib-entered-here
deflt-intrvl-format
10011100   0        1
*card num-of-intrvls right-coordinate
10011101   5        0.0099
10011102   5        0.0125
10011103   2        0.0150
*card composit-num intrvl-num
10011201  -1        5
10011202   2        10
10011203  -1        12
*card relative-source-value intrvl-num
10011301   0.0      5
10011302   1.0      10
10011303   0.0      12
*card initial-temp-flag
10011400   0
*card initial-temp mesh-pnt-num
10011401   1000.0   13
*card lft-bnd-vol incr bound-cond-typ-ins surf-area-
code-sph-num sph-num axl-msh
10011501  0       0        0              0
0.00000  12
*card rgt-bnd-vol incr bound-cond-typ-aut surf-area-
code-sph-num sph-num axl-msh
10011601  1010000 10000    134            0
0.50466  12
*card src-typ-kntcs intrnl-mult mod-heting-mult-lft mod-
heting-mult-rgth axl-msh
10011701  900      0.000298    0.0                0.0
1
10011702  900      0.000511    0.0                0.0
2
10011703  900      0.000681    0.0                0.0
3
10011704  900      0.000823    0.0                0.0
4
10011705  900      0.000894    0.0                0.0
5
10011706  900      0.000922    0.0                0.0
6
10011707  900      0.000894    0.0                0.0
7
10011708  900      0.000823    0.0                0.0
8
10011709  900      0.000724    0.0                0.0
9
```

```
10011710  900      0.000596    0.0                 0.0
10
10011711  900      0.000440    0.0                 0.0
11
10011712  900      0.000270    0.0                 0.0
12
*card adtnl-lft-bndry-opt
10011800 1
*card heat-hyD heat-L-fwd grd-spcr-fwd grd-spcr-rev grd-
ls-cf-fwd grd-ls-cf-rev
10011801 0.02492 10.0 10.0 0.0 0.0 0.0 0.0 1.0 0.0 100.0
1.000 12
*card adtnl-rght-bndry-opt
10011900 1
*card heat-hyD heat-L-fwd grd-spcr-fwd grd-spcr-rev grd-
ls-cf-fwd grd-ls-cf-rev
10011901 0.02492 10.0 10.0 0.0 0.0 0.0 0.0 1.0 0.0 100.0
1.972 12
*------------ core
*card ax-mesh rad-mesh geom-sph sty-init-flg-calc-by-
code lft-bndr
10021000   12       13       3           1
0.0
*card msh-flag-geom-composit&source-distrib-entered-here
deflt-intrvl-format
10021100   0        1
*card num-of-intrvls right-coordinate
10021101   5        0.0099
10021102   5        0.0125
10021103   2        0.0150
*card composit-num intrvl-num
10021201  -1        5
10021202   2        10
10021203  -1        12
*card relative-source-value intrvl-num
10021301   0.0      5
10021302   1.0      10
10021303   0.0      12
*card initial-temp-flag
10021400   0
*card initial-temp mesh-pnt-num
10021401   1000.0   13
*card lft-bnd-vol incr bound-cond-typ-ins surf-area-
code-sph-num sph-num axl-msh
10021501  0       0        0              0
0.00000  12
*card rgt-bnd-vol incr bound-cond-typ-aut surf-area-
code-sph-num sph-num axl-msh
10021601  2010000 10000    134            0
3.02796  12
*card src-typ-kntcs intrnl-mult mod-heting-mult-lft mod-
heting-mult-rgth axl-msh
10021701  900      0.001788    0.0                 0.0
1
10021702  900      0.003064    0.0                 0.0
2
10021703  900      0.004086    0.0                 0.0
3
10021704  900      0.004937    0.0                 0.0
4
10021705  900      0.005363    0.0                 0.0
5
10021706  900      0.005533    0.0                 0.0
6
10021707  900      0.005363    0.0                 0.0
7
10021708  900      0.004937    0.0                 0.0
8
10021709  900      0.004341    0.0                 0.0
9
10021710  900      0.003575    0.0                 0.0
10
10021711  900      0.002639    0.0                 0.0
11
10021712  900      0.001617    0.0                 0.0
12
*card adtnl-lft-bndry-opt
10021800 1
*card heat-hyD heat-L-fwd grd-spcr-fwd grd-spcr-rev grd-
ls-cf-fwd grd-ls-cf-rev
10021801 0.02492 10.0 10.0 0.0 0.0 0.0 0.0 1.0 0.0 100.0
1.000 12
*card adtnl-rght-bndry-opt
10021900 1
*card heat-hyD heat-L-fwd grd-spcr-fwd grd-spcr-rev grd-
ls-cf-fwd grd-ls-cf-rev
10021901 0.02492 10.0 10.0 0.0 0.0 0.0 0.0 1.0 0.0 100.0
1.972 12
*------------ core
```

```
*card ax-mesh rad-mesh geom-sph sty-init-flg-calc-by-
code lft-bndr
10031000   12       13       3           1
0.0
*card msh-flag-geom-composit&source-distrib-entered-here
deflt-intrvl-format
10031100   0        1
*card num-of-intrvls right-coordinate
10031101   5        0.0099
10031102   5        0.0125
10031103   2        0.0150
*card composit-num intrvl-num
10031201  -1        5
10031202   2        10
10031203  -1        12
*card relative-source-value intrvl-num
10031301   0.0      5
10031302   1.0      10
10031303   0.0      12
*card initial-temp-flag
10031400   0
*card initial-temp mesh-pnt-num
10031401   1000.0   13
*card lft-bnd-vol incr bound-cond-typ-ins surf-area-
code-sph-num sph-num axl-msh
10031501  0       0        0              0
0.00000  12
*card rgt-bnd-vol incr bound-cond-typ-aut surf-area-
code-sph-num sph-num axl-msh
10031601  3010000 10000    134            0
6.05592  12
*card src-typ-kntcs intrnl-mult mod-heting-mult-lft mod-
heting-mult-rgth axl-msh
10031701  900      0.003575    0.0                0.0
1
10031702  900      0.006129    0.0                0.0
2
10031703  900      0.008172    0.0                0.0
3
10031704  900      0.009874    0.0                0.0
4
10031705  900      0.010726    0.0                0.0
5
10031706  900      0.011066    0.0                0.0
6
10031707  900      0.010726    0.0                0.0
7
10031708  900      0.009874    0.0                0.0
8
10031709  900      0.008683    0.0                0.0
9
10031710  900      0.007150    0.0                0.0
10
10031711  900      0.005278    0.0                0.0
11
10031712  900      0.003235    0.0                0.0
12
*card adtnl-lft-bndry-opt
10031800 1
*card heat-hyD heat-L-fwd grd-spcr-fwd grd-spcr-rev grd-
ls-cf-fwd grd-ls-cf-rev
10031801 0.02492 10.0 10.0 0.0 0.0 0.0 0.0 1.0 0.0 100.0
1.000 12
*card adtnl-rght-bndry-opt
10031900 1
*card heat-hyD heat-L-fwd grd-spcr-fwd grd-spcr-rev grd-
ls-cf-fwd grd-ls-cf-rev
10031901 0.02492 10.0 10.0 0.0 0.0 0.0 0.0 1.0 0.0 100.0
1.972 12
*------------ core
*card ax-mesh rad-mesh geom-sph sty-init-flg-calc-by-
code lft-bndr
10041000   12       13       3           1
0.0
*card msh-flag-geom-composit&source-distrib-entered-here
deflt-intrvl-format
10041100   0        1
*card num-of-intrvls right-coordinate
10041101   5        0.0099
10041102   5        0.0125
10041103   2        0.0150
*card composit-num intrvl-num
10041201  -1        5
10041202   2        10
10041203  -1        12
*card relative-source-value intrvl-num
10041301   0.0      5
10041302   1.0      10
10041303   0.0      12
*card initial-temp-flag
```

```
10041400   0
*card initial-temp mesh-pnt-num
10041401   1000.0   13
*card lft-bnd-vol incr bound-cond-typ-ins surf-area-
code-sph-num sph-num axl-msh
10041501  0       0        0              0
0.00000  12
*card rgt-bnd-vol incr bound-cond-typ-aut surf-area-
code-sph-num sph-num axl-msh
10041601  4010000 10000    134            0
6.05592  12
*card src-typ-kntcs intrnl-mult mod-heting-mult-lft mod-
heting-mult-rgth axl-msh
10041701  900      0.003575    0.0                0.0
1
10041702  900      0.006129    0.0                0.0
2
10041703  900      0.008172    0.0                0.0
3
10041704  900      0.009874    0.0                0.0
4
10041705  900      0.010726    0.0                0.0
5
10041706  900      0.011066    0.0                0.0
6
10041707  900      0.010726    0.0                0.0
7
10041708  900      0.009874    0.0                0.0
8
10041709  900      0.008683    0.0                0.0
9
10041710  900      0.007150    0.0                0.0
10
10041711  900      0.005278    0.0                0.0
11
10041712  900      0.003235    0.0                0.0
12
*card adtnl-lft-bndry-opt
10041800 1
*card heat-hyD heat-L-fwd grd-spcr-fwd grd-spcr-rev grd-
ls-cf-fwd grd-ls-cf-rev
10041801 0.02492 10.0 10.0 0.0 0.0 0.0 0.0 1.0 0.0 100.0
1.000 12
*card adtnl-rght-bndry-opt
10041900 1
*card heat-hyD heat-L-fwd grd-spcr-fwd grd-spcr-rev grd-
ls-cf-fwd grd-ls-cf-rev
10041901 0.02492 10.0 10.0 0.0 0.0 0.0 0.0 1.0 0.0 100.0
1.972 12
*------------ core
*card ax-mesh rad-mesh geom-sph sty-init-flg-calc-by-
code lft-bndr
10051000   12       13       3           1
0.0
*card msh-flag-geom-composit&source-distrib-entered-here
deflt-intrvl-format
10051100   0        1
*card num-of-intrvls right-coordinate
10051101   5        0.0099
10051102   5        0.0125
10051103   2        0.0150
*card composit-num intrvl-num
10051201  -1        5
10051202   2        10
10051203  -1        12
*card relative-source-value intrvl-num
10051301   0.0      5
10051302   1.0      10
10051303   0.0      12
*card initial-temp-flag
10051400   0
*card initial-temp mesh-pnt-num
10051401   1000.0   13
*card lft-bnd-vol incr bound-cond-typ-ins surf-area-
code-sph-num sph-num axl-msh
10051501  0       0        0              0
0.00000  12
*card rgt-bnd-vol incr bound-cond-typ-aut surf-area-
code-sph-num sph-num axl-msh
10051601  5010000 10000    134            0
12.1119  12
*card src-typ-kntcs intrnl-mult mod-heting-mult-lft mod-
heting-mult-rgth axl-msh
10051701  900      0.007150    0.0                0.0
1
10051702  900      0.012258    0.0                0.0
2
10051703  900      0.016344    0.0                0.0
3
```

```
10051704  900      0.019749    0.0                 0.0
4
10051705  900      0.021451    0.0                 0.0
5
10051706  900      0.022132    0.0                 0.0
6
10051707  900      0.021451    0.0                 0.0
7
10051708  900      0.019749    0.0                 0.0
8
10051709  900      0.017365    0.0                 0.0
9
10051710  900      0.014301    0.0                 0.0
10
10051711  900      0.010555    0.0                 0.0
11
10051712  900      0.006469    0.0                 0.0
12
*card adtnl-lft-bndry-opt
10051800 1
*card heat-hyD heat-L-fwd grd-spcr-fwd grd-spcr-rev grd-
ls-cf-fwd grd-ls-cf-rev
10051801 0.02492 10.0 10.0 0.0 0.0 0.0 0.0 1.0 0.0 100.0
1.000 12
*card adtnl-rght-bndry-opt
10051900 1
*card heat-hyD heat-L-fwd grd-spcr-fwd grd-spcr-rev grd-
ls-cf-fwd grd-ls-cf-rev
10051901 0.02492 10.0 10.0 0.0 0.0 0.0 0.0 1.0 0.0 100.0
1.972 12
*------------ core
*card ax-mesh rad-mesh geom-sph sty-init-flg-calc-by-
code lft-bndr
10061000   12       13       3           1
0.0
*card msh-flag-geom-composit&source-distrib-entered-here
deflt-intrvl-format
10061100   0        1
*card num-of-intrvls right-coordinate
10061101   5        0.0099
10061102   5        0.0125
10061103   2        0.0150
*card composit-num intrvl-num
10061201  -1        5
10061202   2        10
10061203  -1        12
*card relative-source-value intrvl-num
10061301   0.0      5
10061302   1.0      10
10061303   0.0      12
*card initial-temp-flag
10061400   0
*card initial-temp mesh-pnt-num
10061401   1000.0   13
*card lft-bnd-vol incr bound-cond-typ-ins surf-area-
code-sph-num sph-num axl-msh
10061501  0       0        0              0
0.00000  12
*card rgt-bnd-vol incr bound-cond-typ-aut surf-area-
code-sph-num sph-num axl-msh
10061601  6010000 10000    134            0
15.1398  12
*card src-typ-kntcs intrnl-mult mod-heting-mult-lft mod-
heting-mult-rgth axl-msh
10061701  900      0.008938    0.0                 0.0
1
10061702  900      0.015322    0.0                 0.0
2
10061703  900      0.020430    0.0                 0.0
3
10061704  900      0.024686    0.0                 0.0
4
10061705  900      0.026814    0.0                 0.0
5
10061706  900      0.027665    0.0                 0.0
6
10061707  900      0.026814    0.0                 0.0
7
10061708  900      0.024686    0.0                 0.0
8
10061709  900      0.021707    0.0                 0.0
9
10061710  900      0.017876    0.0                 0.0
10
10061711  900      0.013194    0.0                 0.0
11
10061712  900      0.008087    0.0                 0.0
12
*card adtnl-lft-bndry-opt
10061800 1
```

```
*card heat-hyD heat-L-fwd grd-spcr-fwd grd-spcr-rev grd-
ls-cf-fwd grd-ls-cf-rev
10061801 0.02492 10.0 10.0 0.0 0.0 0.0 0.0 1.0 0.0 100.0
1.000 12
*card adtnl-rght-bndry-opt
10061900 1
*card heat-hyD heat-L-fwd grd-spcr-fwd grd-spcr-rev grd-
ls-cf-fwd grd-ls-cf-rev
10061901 0.02492 10.0 10.0 0.0 0.0 0.0 0.0 1.0 0.0 100.0
1.972 12
*------------ core
*card ax-mesh rad-mesh geom-sph sty-init-flg-calc-by-
code lft-bndr
10071000   12       13       3           1
0.0
*card msh-flag-geom-composit&source-distrib-entered-here
deflt-intrvl-format
10071100   0        1
*card num-of-intrvls right-coordinate
10071101   5        0.0099
10071102   5        0.0125
10071103   2        0.0150
*card composit-num intrvl-num
10071201  -1        5
10071202   2        10
10071203  -1        12
*card relative-source-value intrvl-num
10071301   0.0      5
10071302   1.0      10
10071303   0.0      12
*card initial-temp-flag
10071400   0
*card initial-temp mesh-pnt-num
10071401   1000.0   13
*card lft-bnd-vol incr bound-cond-typ-ins surf-area-
code-sph-num sph-num axl-msh
10071501  0       0        0              0
0.00000  12
*card rgt-bnd-vol incr bound-cond-typ-aut surf-area-
code-sph-num sph-num axl-msh
10071601  7010000 10000    134            0
12.1119  12
*card src-typ-kntcs intrnl-mult mod-heting-mult-lft mod-
heting-mult-rgth axl-msh
10071701  900      0.007150    0.0                0.0
1
10071702  900      0.012258    0.0                0.0
2
10071703  900      0.016344    0.0                0.0
3
10071704  900      0.019749    0.0                0.0
4
10071705  900      0.021451    0.0                0.0
5
10071706  900      0.022132    0.0                0.0
6
10071707  900      0.021451    0.0                0.0
7
10071708  900      0.019749    0.0                0.0
8
10071709  900      0.017365    0.0                0.0
9
10071710  900      0.014301    0.0                0.0
10
10071711  900      0.010555    0.0                0.0
11
10071712  900      0.006469    0.0                0.0
12
*card adtnl-lft-bndry-opt
10071800 1
*card heat-hyD heat-L-fwd grd-spcr-fwd grd-spcr-rev grd-
ls-cf-fwd grd-ls-cf-rev
10071801 0.02492 10.0 10.0 0.0 0.0 0.0 0.0 1.0 0.0 100.0
1.000 12
*card adtnl-rght-bndry-opt
10071900 1
*card heat-hyD heat-L-fwd grd-spcr-fwd grd-spcr-rev grd-
ls-cf-fwd grd-ls-cf-rev
10071901 0.02492 10.0 10.0 0.0 0.0 0.0 0.0 1.0 0.0 100.0
1.972 12
*------------ core
*card ax-mesh rad-mesh geom-sph sty-init-flg-calc-by-
code lft-bndr
10081000   12       13       3           1
0.0
*card msh-flag-geom-composit&source-distrib-entered-here
deflt-intrvl-format
10081100   0        1
*card num-of-intrvls right-coordinate
```

```
10081101   5        0.0099
10081102   5        0.0125
10081103   2        0.0150
*card composit-num intrvl-num
10081201  -1        5
10081202   2        10
10081203  -1        12
*card relative-source-value intrvl-num
10081301   0.0      5
10081302   1.0      10
10081303   0.0      12
*card initial-temp-flag
10081400   0
*card initial-temp mesh-pnt-num
10081401   1000.0   13
*card lft-bnd-vol incr bound-cond-typ-ins surf-area-
code-sph-num sph-num axl-msh
10081501  0       0        0              0
0.00000  12
*card rgt-bnd-vol incr bound-cond-typ-aut surf-area-
code-sph-num sph-num axl-msh
10081601  8010000 10000    134            0
9.08389  12
*card src-typ-kntcs intrnl-mult mod-heting-mult-lft mod-
heting-mult-rgth axl-msh
10081701  900      0.005363    0.0                0.0
1
10081702  900      0.009193    0.0                0.0
2
10081703  900      0.012258    0.0                0.0
3
10081704  900      0.014812    0.0                0.0
4
10081705  900      0.016089    0.0                0.0
5
10081706  900      0.016599    0.0                0.0
6
10081707  900      0.016089    0.0                0.0
7
10081708  900      0.014812    0.0                0.0
8
10081709  900      0.013024    0.0                0.0
9
10081710  900      0.010726    0.0                0.0
10
10081711  900      0.007917    0.0                0.0
11
10081712  900      0.004852    0.0                0.0
12
*card adtnl-lft-bndry-opt
10081800 1
*card heat-hyD heat-L-fwd grd-spcr-fwd grd-spcr-rev grd-
ls-cf-fwd grd-ls-cf-rev
10081801 0.02492 10.0 10.0 0.0 0.0 0.0 0.0 1.0 0.0 100.0
1.000 12
*card adtnl-rght-bndry-opt
10081900 1
*card heat-hyD heat-L-fwd grd-spcr-fwd grd-spcr-rev grd-
ls-cf-fwd grd-ls-cf-rev
10081901 0.02492 10.0 10.0 0.0 0.0 0.0 0.0 1.0 0.0 100.0
1.972 12

*------------ core reflectors
*card ax-mesh rad-mesh geom-cyl sty-init-flg-calc-by-
code lft-bndr
10012000  12 5 2 1 0.099
*card msh-flag-geom-composit&source-distrib-entered-here
deflt-intrvl-format
10012100  0 1
*card num-of-intrvls right-coordinate
10012101  4 0.1540797
*card composit-num intrvl-num
10012201  1  4
*card relative-source-value intrvl-num
10012301  0.0 4
*card initial-temp-entered-here
10012400  0
*card initial-temp mesh-pnt-num
10012401  1000.0 5
*card lft-bnd-vol incr bound-cond-typ-auto-cnvcv surf-
area-code-cyl-hgt cyl-hgt
10012501  001010000 10000 101  0 0.1140398 12
*card rght-bnd-vol incr bound-cond-typ-tbl-cnvcv surf-
area-code-cyl-hgt cyl-hgt
10012601  002010000 10000 101  0 0.1774892 12
*card src-typ-no-src intrnl-mult mod-heting-mult-lft
mod-heting-mult-rgth axl-ms
10012701  0 0.0 0.0 0.0 12
*card adtnl-lft-bndry-opt
10012800  1
```

```
*card heat-hyD heat-L-fwd heat-L-rev grd-spcr-fwd grd-
spcr-rev grd-ls-cf-fwd grd
10012801  0.198  10.0 10.0 0.0 0.0 0.0 0.0 1.0 0.0 1.1
1.0 12
*card adtnl-rgt-bndry-opt
10012900  1
*card heat-hyD heat-L-fwd grd-spcr-fwd grd-spcr-rev grd-
ls-cf-fwd grd-ls-cf-rev
10012901  0.198  10.0 10.0 0.0 0.0 0.0 0.0 1.0 0.0 1.1
1.0 12
*------------ core reflectors
*card ax-mesh rad-mesh geom-cyl sty-init-flg-calc-by-
code lft-bndr
10022000  12 5 2 1 0.242499
*card msh-flag-geom-composit&source-distrib-entered-here
deflt-intrvl-format
10022100  0 1
*card num-of-intrvls right-coordinate
10022101  4 0.3774166
*card composit-num intrvl-num
10022201  1  4
*card relative-source-value intrvl-num
10022301  0.0 4
*card initial-temp-entered-here
10022400  0
*card initial-temp mesh-pnt-num
10022401  1000.0 5
*card lft-bnd-vol incr bound-cond-typ-auto-cnvcv surf-
area-code-cyl-hgt cyl-hgt
10022501  002010000 10000 101  0 0.6842389 12
*card rght-bnd-vol incr bound-cond-typ-tbl-cnvcv surf-
area-code-cyl-hgt cyl-hgt
10022601  003010000 10000 101  0 1.0649353 12
*card src-typ-no-src intrnl-mult mod-heting-mult-lft
mod-heting-mult-rgth axl-ms
10022701  0 0.0 0.0 0.0 12
*card adtnl-lft-bndry-opt
10022800  1
*card heat-hyD heat-L-fwd heat-L-rev grd-spcr-fwd grd-
spcr-rev grd-ls-cf-fwd grd
10022801  0.198  10.0 10.0 0.0 0.0 0.0 0.0 1.0 0.0 1.1
1.0 12
*card adtnl-rgt-bndry-opt
10022900  1
*card heat-hyD heat-L-fwd grd-spcr-fwd grd-spcr-rev grd-
ls-cf-fwd grd-ls-cf-rev
10022901  0.198 10.0 10.0 0.0 0.0 0.0 0.0 1.0 0.0 1.1
1.0 12
*------------ core reflectors
*card ax-mesh rad-mesh geom-cyl sty-init-flg-calc-by-
code lft-bndr
10032000  12 5 2 1 0.342946
*card msh-flag-geom-composit&source-distrib-entered-here
deflt-intrvl-format
10032100  0 1
*card num-of-intrvls right-coordinate
10032101  4 0.5337507
*card composit-num intrvl-num
10032201  1  4
*card relative-source-value intrvl-num
10032301  0.0 4
*card initial-temp-entered-here
10032400  0
*card initial-temp mesh-pnt-num
10032401  1000.0 5
*card lft-bnd-vol incr bound-cond-typ-auto-cnvcv surf-
area-code-cyl-hgt cyl-hgt
10032501  003010000 10000 101  0 1.3684778 12
*card rght-bnd-vol incr bound-cond-typ-tbl-cnvcv surf-
area-code-cyl-hgt cyl-hgt
10032601  004010000 10000 101  0 2.1298536 12
*card src-typ-no-src intrnl-mult mod-heting-mult-lft
mod-heting-mult-rgth axl-ms
10032701  0 0.0 0.0 0.0 12
*card adtnl-lft-bndry-opt
10032800  1
*card heat-hyD heat-L-fwd heat-L-rev grd-spcr-fwd grd-
spcr-rev grd-ls-cf-fwd grd
10032801  0.198  10.0 10.0 0.0 0.0 0.0 0.0 1.0 0.0 1.1
1.0 12
*card adtnl-rgt-bndry-opt
10032900  1
*card heat-hyD heat-L-fwd grd-spcr-fwd grd-spcr-rev grd-
ls-cf-fwd grd-ls-cf-rev
10032901  0.198 10.0 10.0 0.0 0.0 0.0 0.0 1.0 0.0 1.1
1.0 12

*------------ core reflectors
```

```
*card ax-mesh rad-mesh geom-cyl sty-init-flg-calc-by-
code lft-bndr
10042000  12 5 2 1 0.342946
*card msh-flag-geom-composit&source-distrib-entered-here
deflt-intrvl-format
10042100  0 1
*card num-of-intrvls right-coordinate
10042101  4 0.5337507
*card composit-num intrvl-num
10042201  1  4
*card relative-source-value intrvl-num
10042301  0.0 4
*card initial-temp-entered-here
10042400  0
*card initial-temp mesh-pnt-num
10042401  1000.0 5
*card lft-bnd-vol incr bound-cond-typ-auto-cnvcv surf-
area-code-cyl-hgt cyl-hgt
10042501  004010000 10000 101  0 1.3684778 12
*card rght-bnd-vol incr bound-cond-typ-tbl-cnvcv surf-
area-code-cyl-hgt cyl-hgt
10042601  005010000 10000 101  0 2.1298536 12
*card src-typ-no-src intrnl-mult mod-heting-mult-lft
mod-heting-mult-rgth axl-ms
10042701  0 0.0 0.0 0.0 12
*card adtnl-lft-bndry-opt
10042800  1
*card heat-hyD heat-L-fwd heat-L-rev grd-spcr-fwd grd-
spcr-rev grd-ls-cf-fwd grd
10042801  0.198  10.0 10.0 0.0 0.0 0.0 0.0 1.0 0.0 1.1
1.0 12
*card adtnl-rgt-bndry-opt
10042900  1
*card heat-hyD heat-L-fwd grd-spcr-fwd grd-spcr-rev grd-
ls-cf-fwd grd-ls-cf-rev
10042901  0.198 10.0 10.0 0.0 0.0 0.0 0.0 1.0 0.0 1.1
1.0 12

*------------ core reflectors
*card ax-mesh rad-mesh geom-cyl sty-init-flg-calc-by-
code lft-bndr
10052000  12 5 2 1 0.48499
*card msh-flag-geom-composit&source-distrib-entered-here
deflt-intrvl-format
10052100  0 1
*card num-of-intrvls right-coordinate
10052101  4 0.7548374
*card composit-num intrvl-num
10052201  1  4
*card relative-source-value intrvl-num
10052301  0.0 4
*card initial-temp-entered-here
10052400  0
*card initial-temp mesh-pnt-num
10052401  1000.0 5
*card lft-bnd-vol incr bound-cond-typ-auto-cnvcv surf-
area-code-cyl-hgt cyl-hgt
10052501  005010000 10000 101  0 2.7369555 12
*card rght-bnd-vol incr bound-cond-typ-tbl-cnvcv surf-
area-code-cyl-hgt cyl-hgt
10052601  006010000 10000 101  0 4.2597072 12
*card src-typ-no-src intrnl-mult mod-heting-mult-lft
mod-heting-mult-rgth axl-ms
10052701  0 0.0 0.0 0.0 12
*card adtnl-lft-bndry-opt
10052800  1
*card heat-hyD heat-L-fwd heat-L-rev grd-spcr-fwd grd-
spcr-rev grd-ls-cf-fwd grd
10052801  0.198  10.0 10.0 0.0 0.0 0.0 0.0 1.0 0.0 1.1
1.0 12
*card adtnl-rgt-bndry-opt
10052900  1
*card heat-hyD heat-L-fwd grd-spcr-fwd grd-spcr-rev grd-
ls-cf-fwd grd-ls-cf-rev
10052901  0.198  10.0 10.0 0.0 0.0 0.0 0.0 1.0 0.0 1.1
1.0 12

*------------ core reflectors
*card ax-mesh rad-mesh geom-cyl sty-init-flg-calc-by-
code lft-bndr
10062000  12 5 2 1 0.542245
*card msh-flag-geom-composit&source-distrib-entered-here
deflt-intrvl-format
10062100  0 1
*card num-of-intrvls right-coordinate
10062101  4 0.8439329
*card composit-num intrvl-num
10062201  1  4
*card relative-source-value intrvl-num
10062301  0.0 4
```

```
*card initial-temp-entered-here
10062400  0
*card initial-temp mesh-pnt-num
10062401  1000.0 5
*card lft-bnd-vol incr bound-cond-typ-auto-cnvcv surf-
area-code-cyl-hgt cyl-hgt
10062501  006010000 10000 101  0 3.4211944 12
*card rght-bnd-vol incr bound-cond-typ-tbl-cnvcv surf-
area-code-cyl-hgt cyl-hgt
10062601  007010000 10000 101  0 5.3246425 12
*card src-typ-no-src intrnl-mult mod-heting-mult-lft
mod-heting-mult-rgth axl-ms
10062701  0 0.0 0.0 0.0 12
*card adtnl-lft-bndry-opt
10062800  1
*card heat-hyD heat-L-fwd heat-L-rev grd-spcr-fwd grd-
spcr-rev grd-ls-cf-fwd grd
10062801  0.198  10.0 10.0 0.0 0.0 0.0 0.0 1.0 0.0 1.1
1.0 12
*card adtnl-rgt-bndry-opt
10062900  1
*card heat-hyD heat-L-fwd grd-spcr-fwd grd-spcr-rev grd-
ls-cf-fwd grd-ls-cf-rev
10062901  0.198  10.0 10.0 0.0 0.0 0.0 0.0 1.0 0.0 1.1
1.0 12

*------------ core reflectors
*card ax-mesh rad-mesh geom-cyl sty-init-flg-calc-by-
code lft-bndr
10072000  12 5 2 1 0.484999
*card msh-flag-geom-composit&source-distrib-entered-here
deflt-intrvl-format
10072100  0 1
*card num-of-intrvls right-coordinate
10072101  4 0.7548374
*card composit-num intrvl-num
10072201  1  4
*card relative-source-value intrvl-num
10072301  0.0 4
*card initial-temp-entered-here
10072400  0
*card initial-temp mesh-pnt-num
10072401  1000.0 5
*card lft-bnd-vol incr bound-cond-typ-auto-cnvcv surf-
area-code-cyl-hgt cyl-hgt
10072501  007010000 10000 101  0 2.7369555 12
*card rght-bnd-vol incr bound-cond-typ-tbl-cnvcv surf-
area-code-cyl-hgt cyl-hgt
10072601  008010000 10000 101  0 4.2597072 12
*card src-typ-no-src intrnl-mult mod-heting-mult-lft
mod-heting-mult-rgth axl-ms
10072701  0 0.0 0.0 0.0 12
*card adtnl-lft-bndry-opt
10072800  1
*card heat-hyD heat-L-fwd heat-L-rev grd-spcr-fwd grd-
spcr-rev grd-ls-cf-fwd grd
10072801  0.198  10.0 10.0 0.0 0.0 0.0 0.0 1.0 0.0 1.1
1.0 12
*card adtnl-rgt-bndry-opt
10072900  1
*card heat-hyD heat-L-fwd grd-spcr-fwd grd-spcr-rev grd-
ls-cf-fwd grd-ls-cf-rev
10072901  0.198  10.0 10.0 0.0 0.0 0.0 0.0 1.0 0.0 1.1
1.0 12

*------------ core reflectors
*card ax-mesh rad-mesh geom-cyl sty-init-flg-calc-by-
code lft-bndr
10082000  12 5 2 1 0.420021
*card msh-flag-geom-composit&source-distrib-entered-here
deflt-intrvl-format
10082100  0 1
*card num-of-intrvls right-coordinate
10082101  4 0.6537072
*card composit-num intrvl-num
10082201  1  4
*card relative-source-value intrvl-num
10082301  0.0 4
*card initial-temp-entered-here
10082400  0
*card initial-temp mesh-pnt-num
10082401  1000.0 5
*card lft-bnd-vol incr bound-cond-typ-auto-cnvcv surf-
area-code-cyl-hgt cyl-hgt
10082501  008010000 10000 101  0 2.0527166 12
*card rght-bnd-vol incr bound-cond-typ-tbl-cnvcv surf-
area-code-cyl-hgt cyl-hgt
10082601  0         0     0    0 3.1947889 12
*card src-typ-no-src intrnl-mult mod-heting-mult-lft
mod-heting-mult-rgth axl-ms
```

```
10082701  0 0.0 0.0 0.0 12
*card adtnl-lft-bndry-opt
10082800  1
*card heat-hyD heat-L-fwd heat-L-rev grd-spcr-fwd grd-
spcr-rev grd-ls-cf-fwd grd
10082801  0.198  10.0 10.0 0.0 0.0 0.0 0.0 1.0 0.0 1.1
1.0 12
*card adtnl-rgt-bndry-opt
10082900  1
*card heat-hyD heat-L-fwd grd-spcr-fwd grd-spcr-rev grd-
ls-cf-fwd grd-ls-cf-rev
10082901  0.198  10.0 10.0 0.0 0.0 0.0 0.0 1.0 0.0 1.1
1.0 12

*------------ upper reflector
*card ax-mesh rad-mesh geom-cyl sty-init-flg-calc-by-
code lft-bndr
10151000 10 4 2 1 0.0075
*card msh-flag-geom,composit,source-distrib-entered-here
deflt-intrvl-format
10151100 0 1
*card num-of-intrvls right-coordinate
10151101 3 0.02395
*card composit-num intrvl-num
10151201 1 3
*card relative-source-value intrvl-num
10151301 0.0 3
*card initial-temp mesh-pnt-num
10151401 818.0 4
*card lft-bnd-vol incr bound-cond-typ-auto-cnvcv surf-
area-code-cyl-hgt cyl-hgt
10151501 015010000 10000  101  0  15.41169 10
*card rght-bnd-vol incr bound-cond-typ-tbl-cnvcv surf-
area-code-cyl-hgt cyl-hgt
10151601 0          0     0    0  49.21466 10
*card src-typ-no-src intrnl-mult mod-heting-mult-lft
mod-heting-mult-rgth axl-ms
10151701 0 0.0 0.0 0.0 10
*card adtnl-lft-bndry-opt
10151800 1
*card heat-hyD heat-L-fwd heat-L-rev grd-spcr-fwd grd-
spcr-rev grd-ls-cf-fwd grd
10151801 0.015   10.0 10.0 0.0 0.0 0.0 0.0 1.0 0.0 1.1
1.0 10
*card adtnl-rght-bndry-opt
10151900 1
*card heat-hyD heat-L-fwd grd-spcr-fwd grd-spcr-rev grd-
ls-cf-fwd grd-ls-cf-rev
10151901 0.015   10.0 10.0 0.0 0.0 0.0 0.0 1.0 0.0 1.1
1.0 10

*------------ ihx
*card ax-mesh rad-mesh geom-cyl sty-init-flg-calc-by-
code lft-bndr
10551000 10 4 2 1 0.0034275
*card msh-flag-geom,composit,source-distrib-entered-here
deflt-intrvl-format
10551100 0 1
*card num-of-intrvls right-coordinate
10551101 3 0.0047625
*card composit-num intrvl-num
10551201 3 3
*card relative-source-value intrvl-num
10551301 0.0 3
*card initial-temp mesh-pnt-num
10551401 818.0 4
*card lft-bnd-vol incr bound-cond-typ-auto-cnvcv surf-
area-code-cyl-hgt cyl-hgt
10551501 043110000 10000  101  0 740.270 10
*card rght-bnd-vol incr bound-cond-typ-tbl-cnvcv surf-
area-code-cyl-hgt cyl-hgt
10551601 052110000 10000  134  0 1028.61 10
*card src-typ-no-src intrnl-mult mod-heting-mult-lft
mod-heting-mult-rgth axl-ms
10551701 0 0.0 0.0 0.0 10
*card adtnl-lft-bndry-opt
10551800 1
*card heat-hyD heat-L-fwd grd-spcr-fwd grd-spcr-rev grd-
ls-cf-fwd grd-ls-cf-rev
10551801 0.006855 10.0 10.0 0.0 0.0 0.0 0.0 1.0 0.0
100.0 1.0000  10
*card adtnl-rght-bndry-opt
10551900 1
*card heat-hyD heat-L-fwd grd-spcr-fwd grd-spcr-rev grd-
ls-cf-fwd grd-ls-cf-rev
10551901 0.009525 10.0 10.0 0.0 0.0 0.0 0.0 1.0 0.0
100.0 1.2391  10
*------------ dhx
*card ax-mesh rad-mesh geom-cyl sty-init-flg-calc-by-
code lft-bndr
```

```
10561000 10 4 2 1 0.0034275
*card msh-flag-geom,composit,source-distrib-entered-here
deflt-intrvl-format
10561100 0 1
*card num-of-intrvls right-coordinate
10561101 3 0.0047625
*card composit-num intrvl-num
10561201 3 3
*card relative-source-value intrvl-num
10561301 0.0 3
*card initial-temp mesh-pnt-num
10561401 973.817 4
*card lft-bnd-vol incr bound-cond-typ-auto-cnvcv surf-
area-code-cyl-hgt cyl-hgt
10561501 030550000 10000  101  0 25.1463654 10
*card rght-bnd-vol incr bound-cond-typ-tbl-cnvcv surf-
area-code-cyl-hgt cyl-hgt
10561601 025010000 10000  134  0 34.9407922 10
*card src-typ-no-src intrnl-mult mod-heting-mult-lft
mod-heting-mult-rgth axl-ms
10561701 0 0.0 0.0 0.0 10
*card adtnl-lft-bndry-opt
10561800 1
*card heat-hyD heat-L-fwd grd-spcr-fwd grd-spcr-rev grd-
ls-cf-fwd grd-ls-cf-rev
10561801 0.006855 10.0 10.0 0.0 0.0 0.0 0.0 1.0 0.0
100.0 1.00 10
*card adtnl-rght-bndry-opt
10561900 1
*card heat-hyD heat-L-fwd grd-spcr-fwd grd-spcr-rev grd-
ls-cf-fwd grd-ls-cf-rev
10561901 0.009525 10.0 10.0 0.0 0.0 0.0 0.0 1.0 0.0
100.0 1.2391 10
*--------- ndhx
*card ax-mesh rad-mesh geom-cyl sty-init-flg-calc-by-
code lft-bndr
10571000 10 4 2 1 0.015
*card msh-flag-geom,composit,source-distrib-entered-here
deflt-intrvl-format
10571100 0 1
*card num-of-intrvls right-coordinate
10571101 3 0.018
*card composit-num intrvl-num
10571201 3 3
*card relative-source-value intrvl-num
10571301 0.0 3
*card initial-temp mesh-pnt-num
10571401 873.817 4
*card lft-bnd-vol incr bound-cond-typ-auto-cnvcv surf-
area-code-tot-area tot-are
10571501 030060000  10000 101  0 101.975 10
*card rght-bnd-vol incr bound-cond-typ-auto-cnvcv surf-
area-code-cyl-hgt cyl-hgt
10571601 062250000 -10000 134  0 122.37 10
*card src-typ-no-src intrnl-mult mod-heting-mult-lft
mod-heting-mult-rgth axl-ms
10571701 0 0.0 0.0 0.0 10
*card adtnl-lft-bndry-opt
10571800 1
*card heat-hyD heat-L-fwd grd-spcr-fwd grd-spcr-rev grd-
ls-cf-fwd grd-ls-cf-rev
10571801 0.03 10.0 10.0 0.0 0.0 0.0 0.0 1.0 0.0 100.0
1.00 10
*card adtnl-rght-bndry-opt
10571900 1
*card heat-hyD heat-L-fwd grd-spcr-fwd grd-spcr-rev grd-
ls-cf-fwd grd-ls-cf-rev
10571901 0.03 10.0 10.0 0.0 0.0 0.0 0.0 1.0 0.0 100.0
1.235 10
*******************************************************
*  material properties
*******************************************************
*---------H-451 graphite conductivity
20100100   tbl/fctn  1  1
20100101    250.0  80.00
20100110   3000.0  80.00
*---------H-451 graphite volumetric heat capacity
20100151    250.0  3.000e6
20100179   3000.0  3.000e6

*---------graphite based fuel conductivity
20100200   tbl/fctn  1  1
20100201    250.0  15.00
20100210   3000.0  15.00
*---------graphite based fuel volumetric heat capacity
20100251    250.0  3.000e6
20100279   3000.0  3.000e6


*---------stainless steel conductivity
```

```
20100300   tbl/fctn  1  1
20100301    250.0   40.00
20100302   3000.0   40.00
*---------stainless steel volumetric heat capacity
20100351    250.0   3.50e6
20100352   3000.0   3.50e6

*******************************************************
*  general tables
*******************************************************
*---------time dependent table for core power
* ANS 79 heat decay power
20290000   power  777  1.0  900.0e6
20290001 -1. 1.0
20290002 0. 0.070378
20290003 0.01 0.060267
20290004 1. 0.056023
20290005 10. 0.0442
20290006 100. 0.030097
20290007 300. 0.024553
20290008 600. 0.021438
20290009 1000. 0.019068
20290010 3600. 0.013091
20290011 7200. 0.010493
20290012 10800. 0.0092643
20290013 14400. 0.0085067
20290014 18000. 0.0079773
20290015 21600. 0.0075778
20290016 25200. 0.007259
20290017 28800. 0.0069943
20290018 32400. 0.006768
20290019 36000. 0.0065705
20290020 39600. 0.0063955
20290021 43200. 0.0062387
20290022 46800. 0.0060968
20290023 50400. 0.0059678
20290024 54000. 0.0058495
20290025 57600. 0.0057405
20290026 61200. 0.0056397
20290027 64800. 0.0055458
20290028 68400. 0.0054583
20290029 72000. 0.0053765
20290030 75600. 0.0052995
20290031 79200. 0.005227
20290032 82800. 0.0051585
20290033 86400. 0.0050937
20290034 90000. 0.005032
20290035 93600. 0.0049735
20290036 97200. 0.0049175
20290037 100800. 0.0048642
20290038 104400. 0.004813
20290039 108000. 0.0047642
20290040 111600. 0.004717
20290041 115200. 0.0046718
20290042 118800. 0.0046283
20290043 122400. 0.0045865
20290044 126000. 0.004546
20290045 129600. 0.0045068
20290046 133200. 0.0044692
20290047 136800. 0.0044325
20290048 140400. 0.004397
20290049 144000. 0.0043627
20290050 147600. 0.0043293
20290051 151200. 0.004297
20290052 154800. 0.0042655
20290053 158400. 0.004235
20290054 162000. 0.0042052
20290055 165600. 0.0041762
20290056 169200. 0.004148
20290057 172800. 0.0041205
20290058 180000. 0.0040673
20290059 187200. 0.0040167
20290060 194400. 0.0039683
20290061 201600. 0.0039222
20290062 208800. 0.0038777
20290063 216000. 0.0038352
20290064 223200. 0.0037942
20290065 230400. 0.0037547
20290066 237600. 0.0037167
20290067 244800. 0.0036798
20290068 252000. 0.0036443
20290069 259200. 0.00361
20290070 266400. 0.0035767
20290071 273600. 0.0035445
20290072 280800. 0.0035132
20290073 288000. 0.0034827
20290074 295200. 0.0034532
20290075 302400. 0.0034243
20290076 309600. 0.0033963
20290077 316800. 0.0033692
```

```
20290078 324000. 0.0033425
20290079 331200. 0.0033167
20290080 338400. 0.0032913
20290081 345600. 0.0032667
20290082 352800. 0.0032427
20290083 360000. 0.003219
20290084 378000. 0.0031623
20290085 396000. 0.0031087
20290086 414000. 0.0030577
20290087 432000. 0.0030092
20290088 450000. 0.0029628
20290089 468000. 0.0029187
20290090 486000. 0.0028763
20290091 504000. 0.0028358
20290092 522000. 0.002797
20290093 540000. 0.0027597
20290094 558000. 0.0027238
20290095 576000. 0.0026893
20290096 594000. 0.0026562
20290097 612000. 0.002624
20290098 630000. 0.0025932
20290099 648000. 0.0025632
```

```
*********************************************************
* derived parameters
*********************************************************
20500000  999

*-------temperature difference on the AIR loop fluid
*card    name     operator  coef    init-guess calc-
init-val
20515400 press    sum       1.00    541.574  1
*card    coef      variable  volume
20515401  0.0 1.0  tempg  062250000
20515402  -1.0  tempg     062140000
*-------temperature difference on the DRACS loop fluid
*card    name     operator  coef    init-guess calc-
init-val
20516000 press    sum       1.00    43.3652    1
*card    coef      variable  volume
20516001  0.0 1.0  tempf  030930000
20516002  -1.0  tempf  030430000
*-------temperature difference on the DCS loop fluid
*card    name     operator  coef    init-guess calc-
init-val
20516300 press    sum       -1.00    -26.71354 1
*card    coef      variable  volume
20516301  0.0 1.0  tempf  023100000
20516302  -1.0  tempf  025150000



*-------pressure drop on each segment of heater
*card    name     operator  coef   init-guess calc-init-
val
20512100 mul001   mult      1.0    450.019    1
*card    variable volume
20512101 fwalfj   030550000
20512102 rhof     030550000
20512103 velfj    030550000
20512104 velfj    030550000
*card    name     operator  coef   init-guess calc-init-
val
20512200 mul001   mult      1.0    432.1475   1
*card    variable volume
20512201 fwalfj   030560000
20512202 rhof     030560000
20512203 velfj    030560000
20512204 velfj    030560000
*card    name     operator  coef   init-guess calc-init-
val
20512300 mul001   mult      1.0    418.258    1
*card    variable volume
20512301 fwalfj   030570000
20512302 rhof     030570000
20512303 velfj    030570000
20512304 velfj    030570000
*card    name     operator  coef   init-guess calc-init-
val
20512400 mul001   mult      1.0    407.278    1
*card    variable volume
20512401 fwalfj   030580000
20512402 rhof     030580000
```

```
20512403 velfj    030580000
20512404 velfj    030580000
*card    name     operator  coef   init-guess calc-init-
val
20512500 mul001   mult      1.0    398.557    1
*card    variable volume
20512501 fwalfj   030590000
20512502 rhof     030590000
20512503 velfj    030590000
20512504 velfj    030590000
*card    name     operator  coef   init-guess calc-init-
val
20512600 mul001   mult      1.0    391.522    1
*card    variable volume
20512601 fwalfj   030600000
20512602 rhof     030600000
20512603 velfj    030600000
20512604 velfj    030600000
*card    name     operator  coef   init-guess calc-init-
val
20512700 mul001   mult      1.0    385.984    1
*card    variable volume
20512701 fwalfj   030610000
20512702 rhof     030610000
20512703 velfj    030610000
20512704 velfj    030610000
*card    name     operator  coef   init-guess calc-init-
val
20512800 mul001   mult      1.0    381.522    1
*card    variable volume
20512801 fwalfj   030620000
20512802 rhof     030620000
20512803 velfj    030620000
20512804 velfj    030620000
*card    name     operator  coef   init-guess calc-init-
val
20512900 mul001   mult      1.0    377.846    1
*card    variable volume
20512901 fwalfj   030630000
20512902 rhof     030630000
20512903 velfj    030630000
20512904 velfj    030630000
*card    name     operator  coef   init-guess calc-init-
val
20513000 mul001   mult      1.0    195.837    1
```

```
*card    variable volume
20513001 fwalfj   030640000
20513002 rhof     030640000
20513003 velfj    030640000
20513004 velfj    030640000
*-------sum of pressure drop of all heater segments show
above
*card    name     operator  coef    init-guess calc-
init-val
20500200 press    sum       0.50    1919.484   1 * (1/2)
from rho*v^2/2
*card    coef      variable  volume
20500201  0.0 1.0  cntrlvar  121
20500202  1.0  cntrlvar  122
20500203  1.0  cntrlvar  123
20500204  1.0  cntrlvar  124
20500205  1.0  cntrlvar  125
20500206  1.0  cntrlvar  126
20500207  1.0  cntrlvar  127
20500208  1.0  cntrlvar  128
20500209  1.0  cntrlvar  129
20500210  1.0  cntrlvar  130



*-------pressure drop (1-5)
*card    name     operator  coef   init-guess calc-init-
val
 $pygmsg: data not found on rstplt
20514800 mul001   mult      2.5    12.0428    1* 5 elems
x (1/2)
*card    variable volume
20514801 fwalfj   030030000
20514802 rhof     030030000
20514803 velfj    030030000
20514804 velfj    030030000
*-------pressure drop (16-25)
*card    name     operator  coef   init-guess calc-init-
val
 $pygmsg: data not found on rstplt
20514900 mul001   mult      5.0    15.1307    1* 10
elems x (1/2)
*card    variable volume
20514901 fwalfj   030200000
20514902 rhof     030200000
```

```
20514903 velfj    030200000
20514904 velfj    030200000
*-------pressure drop vertical segment below the cooler
(26-45)
*card    name     operator  coef   init-guess calc-init-
val
20515000 mul001   mult      10.0    201.7417   1* 20
elems x (1/2)
*card    variable volume
20515001 fwalfj   030300000
20515002 rhof     030300000
20515003 velfj    030300000
20515004 velfj    030300000
*-------pressure drop bottom horizontal pipe and upward
elbow (46-54)
*card    name     operator  coef   init-guess calc-init-
val
20515100 mul001   mult      4.5    12.6087    1* 9 elems
x (1/2)
*card    variable volume
20515101 fwalfj   030480000
20515102 rhof     030480000
20515103 velfj    030480000
20515104 velfj    030480000
*-------pressure drop vertical segment above the heater
(65-92)
*card    name     operator  coef   init-guess calc-init-
val
20515200 mul001   mult      14.0    216.823    1* 28
elems x (1/2)
*card    variable volume
20515201 fwalfj   030780000
20515202 rhof     030780000
20515203 velfj    030780000
20515204 velfj    030780000
*-------pressure drop top horizontal pipe and downward
elbow (93-98)
*card    name     operator  coef   init-guess calc-init-
val
20515300 mul001   mult      3.0    14.45135   1* 6 elems
x (1/2)
*card    variable volume
20515301 fwalfj   030970000
20515302 rhof     030970000
20515303 velfj    030970000
20515304 velfj    030970000
*-------sum of pressure drop everywhere else in loop
*card    name     operator  coef    init-guess calc-
init-val
20500300 press    sum       1.00    472.798    1
*card    coef      variable  volume
20500301  0.0 1.0  cntrlvar  150
20500302  1.0  cntrlvar  151
20500303  1.0  cntrlvar  152
20500304  1.0  cntrlvar  153
20500305  1.0  cntrlvar  148
20500306  1.0  cntrlvar  149

*-------pressure drop vertical segment inlet chimeny
*card    name     operator  coef   init-guess calc-init-
val
20515500 mul001   mult      5.0    .2324445   1* 10
elems x (1/2)
*card    variable volume
20515501 fwalgj   062050000
20515502 rhog     062050000
20515503 velgj    062050000
20515504 velgj    062050000
*-------pressure drop horizontal segment inlet
*card    name     operator  coef   init-guess calc-init-
val
20515600 mul001   mult      2.5    .00491927  1* 5 elems
x (1/2)
*card    variable volume
20515601 fwalgj   062120000
20515602 rhog     062120000
20515603 velgj    062120000
20515604 velgj    062120000
*-------sum of pressure drop inlet chiney
*card    name     operator  coef    init-guess calc-
init-val
20515700 press    sum       1.00    .237364    1
*card    coef      variable  volume
20515701  0.0 1.0  cntrlvar  155
20515702  1.0  cntrlvar  156


*-------pressure drop vertical segment outlet chimeny
*card    name     operator  coef   init-guess calc-init-
val
```

```
20515800 mul001   mult      5.0    .64849     1* 10
elems x (1/2)
*card    variable volume
20515801 fwalgj   062300000
20515802 rhog     062300000
20515803 velgj    062300000
20515804 velgj    062300000


*-------pressure drop vertical segment core fluid path
*card    name     operator  coef   init-guess calc-init-
val
20517000 mul001   mult      2.5    15.0483    1* 5 elems
x (1/2)
*card    variable volume
20517001 fwalfj   023030000
20517002 rhof     023030000
20517003 velfj    023030000
20517004 velfj    023030000
*-------pressure drop vertical segment core fluid path
*card    name     operator  coef   init-guess calc-init-
val
20517100 mul001   mult      5.0    150.4835   1* 10
elems x (1/2)
*card    variable volume
20517101 fwalfj   023100000
20517102 rhof     023100000
20517103 velfj    023100000
20517104 velfj    023100000
*-------pressure drop vertical segment core fluid path
*card    name     operator  coef   init-guess calc-init-
val
20517200 mul001   mult      2.0    12.33037   1* 4 elems
x (1/2)
*card    variable volume
20517201 fwalfj   025120000
20517202 rhof     025120000
20517203 velfj    025120000
20517204 velfj    025120000
*-------pressure drop vertical segment core fluid path
*card    name     operator  coef   init-guess calc-init-
val
20517300 mul001   mult      2.0    15.41297   1* 4 elems
x (1/2)
*card    variable volume
20517301 fwalfj   025160000
20517302 rhof     025160000
20517303 velfj    025160000
20517304 velfj    025160000
*-------pressure drop vertical segment core fluid path
*card    name     operator  coef   init-guess calc-init-
val
20517400 mul001   mult      2.0    88.8402    1* 4 elems
x (1/2)
*card    variable volume
20517401 fwalfj   025200000
20517402 rhof     025200000
20517403 velfj    025200000
20517404 velfj    025200000
*-------sum of pressure drop everywhere in core loop
*card    name     operator  coef    init-guess calc-
init-val
20517500 press    sum       1.00    103.8885   1
*card    coef      variable  volume
20517501  0.0 1.0  cntrlvar  170
20517502  1.0  cntrlvar  171
20517502  1.0  cntrlvar  172
20517502  1.0  cntrlvar  173
20517502  1.0  cntrlvar  174


*-------pressure drop air heater
*card    name     operator  coef   init-guess calc-init-
val
20517600 mul001   mult      1.0    2.258855   1
*card    variable volume
20517601 fjunft   062160000
20517602 rhog     062160000
20517603 velgj    062160000
20517604 velgj    062160000
*-------pressure drop air heater
*card    name     operator  coef   init-guess calc-init-
val
20517700 mul001   mult      1.0    2.8247     1
*card    variable volume
20517701 fjunft   062170000
20517702 rhog     062170000
20517703 velgj    062170000
20517704 velgj    062170000
*-------pressure drop air heater
```

```
*card    name     operator  coef   init-guess calc-init-
val
20517800 mul001   mult      1.0    3.15563    1
*card    variable volume
20517801 fjunft   062180000
20517802 rhog     062180000
20517803 velgj    062180000
20517804 velgj    062180000
*-------pressure drop air heater
*card    name     operator  coef   init-guess calc-init-
val
20517900 mul001   mult      1.0    3.3528     1
*card    variable volume
20517901 fjunft   062190000
20517902 rhog     062190000
20517903 velgj    062190000
20517904 velgj    062190000
*-------pressure drop air heater
*card    name     operator  coef   init-guess calc-init-
val
20518000 mul001   mult      1.0    3.470346   1
*card    variable volume
20518001 fjunft   062200000
20518002 rhog     062200000
20518003 velgj    062200000
20518004 velgj    062200000
*-------pressure drop air heater
*card    name     operator  coef   init-guess calc-init-
val
20518100 mul001   mult      1.0    3.538974   1
*card    variable volume
20518101 fjunft   062210000
20518102 rhog     062210000
20518103 velgj    062210000
20518104 velgj    062210000
*-------pressure drop air heater
*card    name     operator  coef   init-guess calc-init-
val
20518200 mul001   mult      1.0    3.580426   1
*card    variable volume
20518201 fjunft   062220000
20518202 rhog     062220000
20518203 velgj    062220000
20518204 velgj    062220000
*-------pressure drop air heater
```

```
*card    name     operator  coef   init-guess calc-init-
val
20518300 mul001   mult      1.0    3.6056     1
*card    variable volume
20518301 fjunft   062230000
20518302 rhog     062230000
20518303 velgj    062230000
20518304 velgj    062230000
*-------pressure drop air heater
*card    name     operator  coef   init-guess calc-init-
val
20518400 mul001   mult      1.0    3.62091    1
*card    variable volume
20518401 fjunft   062240000
20518402 rhog     062240000
20518403 velgj    062240000
20518404 velgj    062240000
*-------sum of pressure drop air heater
*card    name     operator  coef    init-guess calc-
init-val
20518600 press    sum       1.00    29.40824   1
*card    coef      variable  volume
20518601  0.0 1.0  cntrlvar  176
20518602  1.0  cntrlvar  177
20518603  1.0  cntrlvar  178
20518604  1.0  cntrlvar  179
20518605  1.0  cntrlvar  180
20518606  1.0  cntrlvar  181
20518607  1.0  cntrlvar  182
20518608  1.0  cntrlvar  183
20518609  1.0  cntrlvar  184

*-------pressure drop coil segment ndhx
*card    name     operator  coef   init-guess calc-init-
val
20518700 mul001   mult      4.5    4.7224     1* 9 juncs
x (1/2)
*card    variable volume
20518701 fjunft   030080000
20518702 rhof     030080000
20518703 velfj    030080000
20518704 velfj    030080000

*-------pressure drop crossflow bundle segment dhx
```

```
*card    name     operator  coef   init-guess calc-init-
val
20518800 mul001   mult      4.5    771.973    1* 9 elems
x (1/2)
*card    variable volume
20518801 fjunft   025050000
20518802 rhof     025050000
20518803 velfj    025050000
20518804 velfj    025050000

*-------pressure drop core pebble bed
*card    name     operator  coef   init-guess calc-init-
val
20518900 mul001   mult      6.0    364448.4   1* 12
elems x (1/2)
*card    variable volume
20518901 fjunft   001060000
20518902 rhof     001060000
20518903 velfj    001060000
20518904 velfj    001060000

*-------division 1
*card    name     operator  coef   init-guess calc-init-
val
20520100 div001   div       1.0    .00341432  1
*card    variable volume
20520101 tempg   062350000
20520101 tempg   062010000
*-------division 2
*card    name     operator  coef   init-guess calc-init-
val
20520200 div001   div       1.0    .00184647  1
*card    variable volume
20520201 cntrlvar 154
*-------natural logarithm
*card    name     operator  coef   init-guess calc-init-
val
20520300 log001   stdfnctn  1.0    -5.67978   1
*card    operat variable  volume
20520301 log    cntrlvar   201
*-------multiplying logarithm with dT inverse
*card    name     operator  coef   init-guess calc-init-
val
20520400 mul001   mult      1.0    -.01048753 1
*card    variable volume
20520401 cntrlvar 203
20520402 cntrlvar 202
*-------sum of buoyant contributions: air
*card    name     operator  coef    init-guess calc-
init-val
20520700 press    sum       9.81    573.474    1*
gravity
*card    coef      variable  volume
20520701  0.0 3.1  rhog  062010000  *ndhx height
20520702      3.1  cntrlvar    204
20520703     35.0  rhog  062010000  *chimney height
20520704     35.0  rhog  062300000

*-------buoyancy cooling loop
*card    name     operator  coef   init-guess calc-init-
val
20520900 mul001   mult      81.66    2580.37    1
*9.81*Lthermal=8.325
*card    variable volume
20520901 betaff 030100000*beta-mid temp
20520902 cntrlvar 160 *dT
20520903 rhof 030010000*rho-cold-reference


*-------buoyancy safety loop
*card    name     operator  coef   init-guess calc-init-
val
20521000 mul001   mult      21.33    -277.1226  1
*9.81*Lthermal=2.175
*card    variable volume
20521001 betaff 025050000*beta-mid temp
20521002 cntrlvar 163 *dT
20521003 rhof 025010000*rho-cold-reference

*-------reynolds air mult
*card    name     operator  coef   init-guess calc-init-
val
20521500 mul001   mult      0.0267    .00637984  1
*dhydro
*card    variable volume
20521501 rhog 062200000*rho mid
20521502 velg 062200000*vel mid
*-------reynolds air div
*card    name     operator  coef   init-guess calc-init-
val
```

```
20521600 div001   div       1.0    178.327    1
*card    variable volume
20521601 viscg    062200000
20521602 cntrlvar 215

*-------reynolds coil mult
*card    name     operator  coef   init-guess calc-init-
val
20521700 mul001   mult      0.05    1.061632   1 *dhydro
*card    variable volume
20521701 rhof 030100000*rho mid
20521702 velf 030100000*vel mid
*-------reynolds coil div
*card    name     operator  coef   init-guess calc-init-
val
20521800 div001   div       1.0    179.3363   1
*card    variable volume
20521801 viscf    030100000
20521802 cntrlvar 217

*-------reynolds tube mult
*card    name     operator  coef   init-guess calc-init-
val
20521900 mul001   mult      0.0069    2.70625    1
*dhydro
*card    variable volume
20521901 rhof 030600000*rho mid
20521902 velf 030600000*vel mid
*-------reynolds tube div
*card    name     operator  coef   init-guess calc-init-
val
20522000 div001   div       1.0    442.661    1
*card    variable volume
20522001 viscf    030600000
20522002 cntrlvar 219

*-------reynolds dhx shell mult
*card    name     operator  coef   init-guess calc-init-
val
20522100 mul001   mult      -0.0095    -3.61062   1
*dhydro (negative velocity)
*card    variable volume
20522101 rhof 025050000*rho mid
20522102 velf 025050000*vel mid
*-------reynolds dhx shell div
```

```
*card    name     operator  coef   init-guess calc-init-
val
20522200 div001   div       1.0    -388.144   1
*card    variable volume
20522201 viscf    025050000
20522202 cntrlvar 221


*-------euler air mult
*card    name     operator  coef   init-guess calc-init-
val
20522300 mul001   mult      0.5    .0669031   1 *(1/2)
*card    variable volume
20522301 rhog 062200000*rho mid
20522302 velg 062200000*vel mid
20522303 velg 062200000*vel mid
*-------euler air div
*card    name     operator  coef   init-guess calc-init-
val
20522400 div001   div       1.0    439.5645   1
*card    variable volume
20522401 cntrlvar 223
20522402 cntrlvar 186

*-------euler coil mult
*card    name     operator  coef   init-guess calc-init-
val
20522500 mul001   mult      0.5    .1062771   1 *(1/2)
*card    variable volume
20522501 rhof 030100000*rho mid
20522502 velf 030100000*vel mid
20522503 velf 030100000*vel mid
*-------euler coil div
*card    name     operator  coef   init-guess calc-init-
val
20522600 div001   div       1.0    44.4348    1
*card    variable volume
20522601 cntrlvar 225
20522602 cntrlvar 187

*-------euler tube mult
*card    name     operator  coef   init-guess calc-init-
val
20522700 mul001   mult      0.5    36.19566   1 *(1/2)
*card    variable volume
```

```
20522701 rhof 030600000*rho mid
20522702 velf 030600000*vel mid
20522703 velf 030600000*vel mid
*-------euler tube div
*card    name     operator  coef   init-guess calc-init-
val
20522800 div001   div       1.0    53.0308    1
*card    variable volume
20522801 cntrlvar 227
20522802 cntrlvar 002

*-------euler dhx crossflow mult
*card    name     operator  coef   init-guess calc-init-
val
20522900 mul001   mult      0.5    36.1974    1 *(1/2)
*card    variable volume
20522901 rhof 025050000*rho mid
20522902 velf 025050000*vel mid
20522903 velf 025050000*vel mid
*-------euler dhx crossflow div
*card    name     operator  coef   init-guess calc-init-
val
20523000 div001   div       1.0    21.32674   1
*card    variable volume
20523001 cntrlvar 229
20523002 cntrlvar 188

*-------Average heat transfer coeficient DHX shellside
*card    name     operator  coef    init-guess calc-
init-val
20501300 HTavDHSH  sum       0.10    5295.    1
*card    coef      variable  volume
20501301  0.0 1.0  hthtc 056100101
20501302  1.0  hthtc 056100201
20501303  1.0  hthtc 056100301
20501304  1.0  hthtc 056100401
20501305  1.0  hthtc 056100501
20501306  1.0  hthtc 056100601
20501307  1.0  hthtc 056100701
20501308  1.0  hthtc 056100801
20501309  1.0  hthtc 056100901
20501310  1.0  hthtc 056101001
*-------Average heat transfer coeficient DHX tubeside
*card    name     operator  coef    init-guess calc-
init-val
```

```
20501400 HTavDHSH  sum       0.10    608.3    1
*card    coef      variable  volume
20501401  0.0 1.0  hthtc 056100100
20501402  1.0  hthtc 056100200
20501403  1.0  hthtc 056100300
20501404  1.0  hthtc 056100400
20501405  1.0  hthtc 056100500
20501406  1.0  hthtc 056100600
20501407  1.0  hthtc 056100700
20501408  1.0  hthtc 056100800
20501409  1.0  hthtc 056100900
20501410  1.0  hthtc 056101000


*-------Average heat transfer coeficient NDHX shellside
*card    name     operator  coef    init-guess calc-
init-val
20501500 HTavNDSH  sum       0.10    19.69    1
*card    coef      variable  volume
20501501  0.0 1.0  hthtc 057100101
20501502  1.0  hthtc 057100201
20501503  1.0  hthtc 057100301
20501504  1.0  hthtc 057100401
20501505  1.0  hthtc 057100501
20501506  1.0  hthtc 057100601
20501507  1.0  hthtc 057100701
20501508  1.0  hthtc 057100801
20501509  1.0  hthtc 057100901
20501510  1.0  hthtc 057101001
*-------Average heat transfer coeficient NDHX tubeside
*card    name     operator  coef    init-guess calc-
init-val
20501600 HTavNDSH  sum       0.10    82.82    1
*card    coef      variable  volume
20501601  0.0 1.0  hthtc 057100100
20501602  1.0  hthtc 057100200
20501603  1.0  hthtc 057100300
20501604  1.0  hthtc 057100400
20501605  1.0  hthtc 057100500
20501606  1.0  hthtc 057100600
20501607  1.0  hthtc 057100700
20501608  1.0  hthtc 057100800
20501609  1.0  hthtc 057100900
20501610  1.0  hthtc 057101000
```

```
*******************************************************
*  trips
*******************************************************
20600000  expanded
*-------- Presurizer trips
20600180  p  13010000   ge   null    0     5.000e6   n
*sink
20600200  p  13010000   le   null    0     4.800e6   n
*source
20607770  time      0   gt   null    0     100.000   l
*scram
20607780  time      0   lt   null    0     102.00    n
*close IHX valve
20607790  time      0   lt   null    0     100.000   n
20607800  time      0   ge   null    0     100.000   n

*******************************************************
* special variables
*******************************************************

*20800000     none
20800002     fwalfj 030300000
20800003     fwalfj 030480000
20800004     fwalfj 030780000
20800005     fwalfj 030970000

20800006     fwalfj 030060000
20800007     fwalfj 030070000
20800008     fwalfj 030080000
20800009     fwalfj 030090000
20800010     fwalfj 030100000
20800011     fwalfj 030110000
20800012     fwalfj 030120000
20800013     fwalfj 030130000
20800014     fwalfj 030140000
20800015     fwalfj 030150000

20800016     fwalfj 030550000
20800017     fwalfj 030560000
20800018     fwalfj 030570000
20800019     fwalfj 030580000
20800020     fwalfj 030590000
20800021     fwalfj 030600000
20800022     fwalfj 030610000
20800023     fwalfj 030620000
20800024     fwalfj 030630000
20800025     fwalfj 030640000

20800026     fwalgj 062050000
20800027     fwalgj 062120000
20800028     fwalgj 062300000

20800029     fwalfj 023030000
20800030     fwalfj 023100000
20800031     fwalfj 025120000
20800032     fwalfj 025160000
20800033     fwalfj 025200000

20800034     fjunft 062160000
20800035     fjunft 062170000
20800036     fjunft 062180000
20800037     fjunft 062190000
20800038     fjunft 062200000
20800039     fjunft 062210000
20800040     fjunft 062220000
20800041     fjunft 062230000
20800042     fjunft 062240000
20800043     fjunft 062250000

20800045     fjunft 030080000
20800046     fjunft 025050000
20800047     fjunft 001060000

20800048     betaff 030100000
20800049     betaff 025050000

20800050     viscg  062200000
20800051     viscf  030100000
20800052     viscf  030600000
20800053     viscf  025050000

20800060     httemp 001100602
20800061     httemp 001100603
20800062     httemp 001100604
```

```
20800063     httemp 001100605
20800064     httemp 001100606
20800065     httemp 001100607
20800066     httemp 001100608
20800067     httemp 001100609
20800068     httemp 001100610
20800069     httemp 001100611
20800070     httemp 001100612

20800071     fwalfj   030030000
20800072     fwalfj   030200000

*******************************
***********replacement cards
*******************************


220101   10010006 23010001 0.0700 0.000 0.00 0
240101   23010000 25000000 0.0350 200.0 0.00 0
260101   25010000 17010006 0.0700 0.000 0.00 0
310101   30010000 30000000 0.0600 0.000 0.00 0
*610101   60010000 62000000 5.0000 90.000 0.00 0
630101   62010000 64000000 5.0000 0.000 0.00 0
640101   5.0000 0.20000000 0.0 0.0  90.00 0.20
600101   5.0000 0.20000000 0.0 0.0  -90.0 -0.2
10561000 10 4 2 1                0.0034500
10561101 3                       0.0047500
10561501 030550000  10000 3995  0 32.118991579 10
10561601 025010000  10000 3996  0 44.221800000 10
10561801 0.0069000 10.0 10.0 0.0 0.0 0.0 0.0 1.0 0.0
1.000 0.36 10
10561901 0.0095000 10.0 10.0 0.0 0.0 0.0 0.0 1.0 0.0
100.0 1.55 10
10571000 10 4 2 1                0.0250000
10571101 3                       0.0280000
10571501 030060000  10000 3997 0 492.582218638 10
10571601 062250000 -10000 3998 0 551.692084874 10
10571801 0.0500000 10.0 10.0 0.0 0.0 0.0 0.0 1.0 0.0
1.000 0.700 10
10571901 0.0266823 10.0 10.0 0.0 0.0 0.0 0.0 1.0 0.0
100.0 2.500 10
*Heat transfer number
20299500  htc-t
20299501 0.0  608.300
20299600  htc-t
20299601 0.0  5295.000
20299700  htc-t
20299701 0.0  82.820
20299800  htc-t
20299801 0.0  19.6900
230101 0.0700 15
230201 0.0700 14
230301 0.1000 5
230302 0.5000 15
250101 0.2383 10
250102 0.0700 22
250201 0.2383 9
250202 0.0700 21
250301 0.2600 10
250302 0.1000 14
250303 0.1250 18
250304 0.7205 22
250701 0.0000 0.0  0.2600 10
250702 0.0000 0.0  0.1000 14
250703 0.1250 0.0  0.0000 18
250704 0.0000 0.0 -0.7205 22
250801 0.0000 0.0095 10
250802 0.0000 0.00000 14
250803 0.0000 0.00000 18
250804 0.0000 0.00000 22
250901 2.3711 2.3711 9
250902 0.00000 0.00000 21
251001 0000010 10
251002 0000000 22
251401 0.0095 0 1.0 1.0 9
251402 0.0000 0 1.0 1.0 21
253001 0.0 0.0 0.0 0.0 10
253002 0.0 0.0 0.0 0.0 21
300101 0.0600 5
300102 3.3240 15
300103 0.0600 54
300104 0.1798 64
300105 0.0600 98
300201 0.0600 5
300202 3.3240 14
300203 0.0600 54
300204 0.1798 63
300205 0.0600 97
300302 1.852360474 15
300304 0.4000 45
```

```
300306 0.2600 64
300307 0.321522242 92
300702 0.0 0.0 -0.360262277 15
300704 0.0 0.0 -0.4000 45
300706 0.0 0.0  0.2600 64
300707 0.0 0.0  0.321522242 92
300802 0.0000 0.0500 15
300804 0.0000 0.0069 64
300901 0.0 0.0 5
300902 4.9358 4.9358 14
300903 0.0 0.0 97
301001 0000000 5
301002 0000010 15
301003 0000000 98
301401 0.0000 0 1.0 1.0 5
301402 0.0500 0 1.0 1.0 15
301403 0.0000 0 1.0 1.0 97
303001 0.0000 0.0 0.0000 0.0 5
303002 0.0000 0.50 0.0000 0.50 14
303003 0.0000 0.0 0.0000 0.0 97
620101 5.0000 10
620102 5.0000 15
620103 40.8603 25
620104 5.0000 35
620201 5.0000 9
620202 5.0000 15
620203 40.8603 24
620204 5.0000 34
620301 2.3603 10
620302 0.1000 15
620303 0.3603 25
620304 2.0000 35
620701 0.0 0.0 -2.3603 10
620702 0.1000 0.0 0.0 15
620703 0.0 0.0 0.3603 25
620704 0.0 0.0 2.0000 35
620801 0.0000 0.0000 10
620802 0.0000 0.0000 15
620803 0.0000 0.0267 25
620804 0.0000 0.0000 35
620901 0.0 0.0 10
620902 0.0 0.0 15
620903 25.0497 25.0497 24
620904 0.0 0.0 34
621001 0000000 10
621002 0000000 15
621003 0000010 25
621004 0000000 35
621401 0.0000 0 1.0 1.0 10
621402 0.0000 0 1.0 1.0 15
621403 0.0267 0 1.0 1.0 24
621404 0.0000 0 1.0 1.0 34
623001 0.0000 0.0 0.0000 0.0 10
623002 0.0000 0.0 0.0000 0.0 15
623003 0.0000 0.15 0.0000 0.15 24
623004 0.0000 0.0 0.0000 0.0 34


**********NEW VARIABLES 4/9/11
*-------Core power
*card    name     operator  coef    init-guess calc-
init-val
20560000 corePow sum 127.0 900.0e6 1
*card    coef      variable  volume
20560001  0.0 1.0  htpowg    0011001
20560002  1.0  htpowg 0011002
20560003  1.0  htpowg 0011003
20560004  1.0  htpowg 0011004
20560005  1.0  htpowg 0011005
20560006  1.0  htpowg 0011006
20560007  1.0  htpowg 0011007
20560008  1.0  htpowg 0011008
20560009  1.0  htpowg 0011009
20560010  1.0  htpowg 0011010
20560011  1.0  htpowg 0011011
20560012  1.0  htpowg 0011012


*-------pressure drop diode
*card    name     operator  coef   init-guess calc-init-
val
20529900 diod   mult        0.5    4.7224     1* 1 juncs
x (1/2)
*card    variable volume
20529901 fjunrt   024000000
20529902 rhof     023140000
20529903 velfj    023140000
20529904 velfj    023140000

*-------pressure drop diode
```

```
*card    name     operator  coef   init-guess calc-init-
val
20530000 diod   mult        0.5    4.7224     1* 1 juncs
x (1/2)
*card    variable volume
20530001 fjunft   024000000
20530002 rhof     025010000
20530003 velfj    025010000
20530004 velfj    025010000


*-------pressure drop air vent
*card    name     operator  coef   init-guess calc-init-
val
20530100 diod   mult        0.5    4.7224     1* 1 juncs
x (1/2)
*card    variable volume
20530101 fjunft   061000000
20530102 rhog     062010000
20530103 velgj    062010000
20530104 velgj    062010000

*-------power transferred in the cooling loop
*card    name     operator  coef   init-guess calc-init-
val
20500400 coopow   mult      1.0    5972536.   1
*card    variable volume
20500401 mflowfj  030480000
20500402 csubpf   030480000
20500403 cntrlvar 160  *temp difference dT of fluid on
loop


*-------power transferred in the air loop part1
*card    name     operator  coef   init-guess calc-init-
val
20500800 mul001   mult      1.0    5972536.   1
*card    variable volume
20500801 mflowj   062010000
20500802 csubpg   062010000
20500803 tempg    062010000  *temp air inlet
*-------power transferred in the air loop part2
*card    name     operator  coef   init-guess calc-init-
val
20500900 mul001   mult      1.0    5972536.   1
*card    variable volume
20500901 mflowj   062300000
20500902 csubpg   062350000
20500903 tempg    062350000  *temp air outlet
*-------power transferred in the air loop part3
*card    name     operator  coef   init-guess calc-init-
val
20501000 airpow   sum       1.0    5972536.   1
*card    coef variable volume
20501001 0.0 1.0 cntrlvar  009
20501002 -1.0 cntrlvar   008


*card    name     operator  coef    init-guess calc-
init-val
20560000 corePow sum 127.0 900.0e6 1
*card    coef      variable  volume
20560001  0.0 1.0  htpowg    0011001
20560002  1.0  htpowg 0011002
20560003  1.0  htpowg 0011003
20560004  1.0  htpowg 0011004

*-------power transferred in the safety loop
*card    name     operator  coef   init-guess calc-init-
val
20500700 mul001   mult      -1.0    5975730.   1
*card    variable volume
20500701 mflowfj  025050000
20500702 csubpf   025050000
20500703 cntrlvar 163  *temp difference dT of fluid on
loop


*-------power transferred to NDHX metallic structure
*card    name     operator  coef   init-guess calc-init-
val
20543100 dT/dt1   diffrend  4.895e6    -47.04 1
*card    variable volume
20543101 htvat    0571001
*card    name     operator  coef   init-guess calc-init-
val
20543200 dT/dt1   diffrend  4.895e6    -41.9012 1
*card    variable volume
20543201 htvat    0571002
```

```
*card    name     operator  coef   init-guess calc-init-
val
20543300 dT/dt1   diffrend  4.895e6    -38.0657 1
*card    variable volume
20543301 htvat    0571003
*card    name     operator  coef   init-guess calc-init-
val
20543400 dT/dt1   diffrend  4.895e6    -35.21866 1
*card    variable volume
20543401 htvat    0571004
*card    name     operator  coef   init-guess calc-init-
val
20543500 dT/dt1   diffrend  4.895e6    -32.9173 1
*card    variable volume
20543501 htvat    0571005
*card    name     operator  coef   init-guess calc-init-
val
20543600 dT/dt1   diffrend  4.895e6    -30.7994 1
*card    variable volume
20543601 htvat    0571006
*card    name     operator  coef   init-guess calc-init-
val
20543700 dT/dt1   diffrend  4.895e6    -28.3504 1
*card    variable volume
20543701 htvat    0571007
*card    name     operator  coef   init-guess calc-init-
val
20543800 dT/dt1   diffrend  4.895e6    -25.15223 1
*card    variable volume
20543801 htvat    0571008
*card    name     operator  coef   init-guess calc-init-
val
20543900 dT/dt1   diffrend  4.895e6    -20.7111 1
*card    variable volume
20543901 htvat    0571009
*card    name     operator  coef   init-guess calc-init-
val
20544000 dT/dt1   diffrend  4.895e6    -10.4084 1
*card    variable volume
20544001 htvat    0571010
*card    name     operator  coef    init-guess calc-
init-val
*-------power transferred to NDHX transient
20544100 press    sum       1.00    -310.5643 1
*card    coef      variable  volume
20544101  0.0 1.0  cntrlvar  431
20544102  1.0  cntrlvar  432
20544103  1.0  cntrlvar  433
20544104  1.0  cntrlvar  434
20544105  1.0  cntrlvar  435
20544106  1.0  cntrlvar  436
20544107  1.0  cntrlvar  437
20544108  1.0  cntrlvar  438
20544109  1.0  cntrlvar  439
20544110  1.0  cntrlvar  440

*-------power transferred to DHX metallic structure
*card    name     operator  coef   init-guess calc-init-
val
20545100 dT/dt1   diffrend  1.7366e5    -47.04 1
*card    variable volume
20545101 htvat    0571001
*card    name     operator  coef   init-guess calc-init-
val
20545200 dT/dt1   diffrend  1.7366e5   -41.9012 1
*card    variable volume
20545201 htvat    0571002
*card    name     operator  coef   init-guess calc-init-
val
20545300 dT/dt1   diffrend  1.7366e5   -38.0657 1
*card    variable volume
20545301 htvat    0571003
*card    name     operator  coef   init-guess calc-init-
val
20545400 dT/dt1   diffrend  1.7366e5   -35.21866 1
*card    variable volume
20545401 htvat    0571004
*card    name     operator  coef   init-guess calc-init-
val
20545500 dT/dt1   diffrend  1.7366e5   -32.9173 1
*card    variable volume
20545501 htvat    0571005
*card    name     operator  coef   init-guess calc-init-
val
20545600 dT/dt1   diffrend  1.7366e5   -30.7994 1
*card    variable volume
20545601 htvat    0571006
*card    name     operator  coef   init-guess calc-init-
val
20545700 dT/dt1   diffrend  1.7366e5   -28.3504 1
```

```
*card    variable volume
20545701 htvat    0571007
*card    name     operator  coef   init-guess calc-init-
val
20545800 dT/dt1   diffrend  1.7366e5   -25.15223 1
*card    variable volume
20545801 htvat    0571008
*card    name     operator  coef   init-guess calc-init-
val
20545900 dT/dt1   diffrend  1.7366e5   -20.7111 1
*card    variable volume
20545901 htvat    0571009
*card    name     operator  coef   init-guess calc-init-
val
20546000 dT/dt1   diffrend  1.7366e5   -10.4084 1
*card    variable volume
20546001 htvat    0571010
*card    name     operator  coef    init-guess calc-
init-val
*-------power transferred to dHX transient
20546100 press    sum       1.00    -310.5643 1
*card    coef      variable  volume
20546101  0.0 1.0  cntrlvar  451
20546102  1.0  cntrlvar  452
20546103  1.0  cntrlvar  453
20546104  1.0  cntrlvar  454
20546105  1.0  cntrlvar  455
20546106  1.0  cntrlvar  456
20546107  1.0  cntrlvar  457
20546108  1.0  cntrlvar  458
20546109  1.0  cntrlvar  459
20546110  1.0  cntrlvar  460



*-------power transferred to pebbles center
*card    name     operator  coef   init-guess calc-init-
val
20550100 mul001   diffrend  9372.83    -.0660115  1
*card    variable volume
20550101 htvat    0011001
*card    name     operator  coef   init-guess calc-init-
val
20550200 mul001   diffrend  9372.83    -.03672396 1
*card    variable volume
20550201 htvat    0011002
*card    name     operator  coef   init-guess calc-init-
val
20550300 mul001   diffrend  9372.83    -.0373053  1
*card    variable volume
20550301 htvat    0011003
*card    name     operator  coef   init-guess calc-init-
val
20550400 mul001   diffrend  9372.83    -.0312658  1
*card    variable volume
20550401 htvat    0011004
*card    name     operator  coef   init-guess calc-init-
val
20550500 mul001   diffrend  9372.83    -.02252067 1
*card    variable volume
20550501 htvat    0011005
*card    name     operator  coef   init-guess calc-init-
val
20550600 mul001   diffrend  9372.83    -.0492372  1
*card    variable volume
20550601 htvat    0011006
*card    name     operator  coef   init-guess calc-init-
val
20550700 mul001   diffrend  9372.83    -.0413135  1
*card    variable volume
20550701 htvat    0011007
*card    name     operator  coef   init-guess calc-init-
val
20550800 mul001   diffrend  9372.83    -.0371734  1
*card    variable volume
20550801 htvat    0011008
*card    name     operator  coef   init-guess calc-init-
val
20550900 mul001   diffrend  9372.83    -.0383667  1
*card    variable volume
20550901 htvat    0011009
*card    name     operator  coef   init-guess calc-init-
val
20551000 mul001   diffrend  9372.83    -.0470571  1
*card    variable volume
20551001 htvat    0011010
*card    name     operator  coef   init-guess calc-init-
val
20551100 mul001   diffrend  9372.83    -.02293255 1
*card    variable volume
```

```
20551101 htvat    0011011
*card    name     operator  coef   init-guess calc-init-
val
20551200 mul001   diffrend  9372.83    -.0513792  1
*card    variable volume
20551201 htvat    0011012
*-------total transient power deposited to pebbles
*card    name     operator  coef    init-guess calc-
init-val
20551300 press    sum       127.00    -17.45805  1
*card    coef      variable  volume
20551301  0.0 1.0  cntrlvar  501
20551302  1.0  cntrlvar  502
20551303  1.0  cntrlvar  503
20551304  1.0  cntrlvar  504
20551305  1.0  cntrlvar  505
20551306  1.0  cntrlvar  506
20551307  1.0  cntrlvar  507
20551308  1.0  cntrlvar  508
20551309  1.0  cntrlvar  509
20551310  1.0  cntrlvar  510
20551311  1.0  cntrlvar  511
20551312  1.0  cntrlvar  512


*-------power transferred to reflector center
*card    name     operator  coef   init-guess calc-init-
val
20552100 mul001   diffrend  24043.0    -.0660115  1
*card    variable volume
20552101 htvat    0012001
*card    name     operator  coef   init-guess calc-init-
val
20552200 mul001   diffrend  24043.0    -.03672396 1
*card    variable volume
20552201 htvat    0012002
*card    name     operator  coef   init-guess calc-init-
val
20552300 mul001   diffrend  24043.0    -.0373053  1
*card    variable volume
20552301 htvat    0012003
*card    name     operator  coef   init-guess calc-init-
val
20552400 mul001   diffrend  24043.0    -.0312658  1
*card    variable volume
20552401 htvat    0012004
*card    name     operator  coef   init-guess calc-init-
val
20552500 mul001   diffrend  24043.0    -.02252067 1
*card    variable volume
20552501 htvat    0012005
*card    name     operator  coef   init-guess calc-init-
val
20552600 mul001   diffrend  24043.0    -.0492372  1
*card    variable volume
20552601 htvat    0012006
*card    name     operator  coef   init-guess calc-init-
val
20552700 mul001   diffrend  24043.0    -.0413135  1
*card    variable volume
20552701 htvat    0012007
*card    name     operator  coef   init-guess calc-init-
val
20552800 mul001   diffrend  24043.0    -.0371734  1
*card    variable volume
20552801 htvat    0012008
*card    name     operator  coef   init-guess calc-init-
val
20552900 mul001   diffrend  24043.0    -.0383667  1
*card    variable volume
20552901 htvat    0012009
*card    name     operator  coef   init-guess calc-init-
val
20553000 mul001   diffrend  24043.0    -.0470571  1
*card    variable volume
20553001 htvat    0012010
*card    name     operator  coef   init-guess calc-init-
val
20553100 mul001   diffrend  24043.0    -.02293255 1
*card    variable volume
20553101 htvat    0012011
*card    name     operator  coef   init-guess calc-init-
val
20553200 mul001   diffrend  24043.0    -.0513792  1
*card    variable volume
20553201 htvat    0012012
*-------total transient power deposited to pebbles
*card    name     operator  coef    init-guess calc-
init-val
20553300 press    sum       127.00    -17.45805  1
```

```
*card    coef      variable  volume
20553301  0.0 1.0  cntrlvar  521
20553302  1.0  cntrlvar  522
20553303  1.0  cntrlvar  523
20553304  1.0  cntrlvar  524
20553305  1.0  cntrlvar  525
20553306  1.0  cntrlvar  526
20553307  1.0  cntrlvar  527
20553308  1.0  cntrlvar  528
20553309  1.0  cntrlvar  529
20553310  1.0  cntrlvar  530
20553311  1.0  cntrlvar  531
20553312  1.0  cntrlvar  532

*-------power transferred to upper reflector
*card    name     operator  coef   init-guess calc-init-
val
20554100 mul001   diffrend  1594655.3    -.0660115  1
*card    variable volume
20554101 htvat    0151001
*card    name     operator  coef   init-guess calc-init-
val
20554200 mul001   diffrend  1594655.3    -.03672396 1
*card    variable volume
20554201 htvat    0151002
*card    name     operator  coef   init-guess calc-init-
val
20554300 mul001   diffrend  1594655.3    -.0373053  1
*card    variable volume
20554301 htvat    0151003
*card    name     operator  coef   init-guess calc-init-
val
20554400 mul001   diffrend  1594655.3    -.0312658  1
*card    variable volume
20554401 htvat    0151004
*card    name     operator  coef   init-guess calc-init-
val
20554500 mul001   diffrend  1594655.3    -.02252067 1
*card    variable volume
20554501 htvat    0151005
*card    name     operator  coef   init-guess calc-init-
val
20554600 mul001   diffrend  1594655.3    -.0492372  1
*card    variable volume
20554601 htvat    0151006
```

```
*card    name     operator  coef   init-guess calc-init-
val
20554700 mul001   diffrend  1594655.3    -.0413135  1
*card    variable volume
20554701 htvat    0151007
*card    name     operator  coef   init-guess calc-init-
val
20554800 mul001   diffrend  1594655.3    -.0371734  1
*card    variable volume
20554801 htvat    0151008
*card    name     operator  coef   init-guess calc-init-
val
20554900 mul001   diffrend  1594655.3    -.0383667  1
*card    variable volume
20554901 htvat    0151009
*card    name     operator  coef   init-guess calc-init-
val
20555000 mul001   diffrend  1594655.3    -.0470571  1
*card    variable volume
20555001 htvat    0011010
*-------total transient power deposited to pebbles
*card    name     operator  coef    init-guess calc-
init-val
20555100 press    sum       1.00    -17.45805  1
*card    coef      variable  volume
20555101  0.0 1.0  cntrlvar  541
20555102  1.0  cntrlvar  542
20555103  1.0  cntrlvar  543
20555104  1.0  cntrlvar  544
20555105  1.0  cntrlvar  545
20555106  1.0  cntrlvar  546
20555107  1.0  cntrlvar  547
20555108  1.0  cntrlvar  548
20555109  1.0  cntrlvar  549
20555110  1.0  cntrlvar  550


*-------safety fluid loop volume weighted temperature
sum
*card    name     operator  coef   init-guess calc-init-
val
20555500 mul001   mult  1.2239    -.0660115  1
*card    variable volume
20555501 tempf    010010000
```

```
*card    name     operator  coef   init-guess calc-init-
val
20555600 mul001   mult  2.6226    -.0660115  1
*card    variable volume
20555601 tempf    012010000
*card    name     operator  coef   init-guess calc-init-
val
20555700 mul001   sum  0.32032    -.0660115  1
*card    variable volume
20555701 0.0 1.0 tempf    001010000
20555702 1.0 tempf    001020000
20555703 1.0 tempf    001030000
20555704 1.0 tempf    001040000
20555705 1.0 tempf    001050000
20555706 1.0 tempf    001060000
20555707 1.0 tempf    001070000
20555708 1.0 tempf    001080000
20555709 1.0 tempf    001090000
20555710 1.0 tempf    001100000
20555711 1.0 tempf    001110000
20555712 1.0 tempf    001120000
*card    name     operator  coef   init-guess calc-init-
val
20555800 mul001   sum  0.0578    -.0660115  1
*card    variable volume
20555801 0.0 1.0 tempf    015010000
20555802 1.0 tempf    015020000
20555803 1.0 tempf    015030000
20555804 1.0 tempf    015040000
20555805 1.0 tempf    015050000
20555806 1.0 tempf    015060000
20555807 1.0 tempf    015070000
20555808 1.0 tempf    015080000
20555809 1.0 tempf    015090000
20555810 1.0 tempf    015100000
*card    name     operator  coef   init-guess calc-init-
val
20555900 mul001   mult  1.2239    -.0660115  1
*card    variable volume
20555901 tempf    017010000
*card    name     operator  coef   init-guess calc-init-
val
20556000 mul001   mult  0.2646    -.0660115  1
*card    variable volume
20556001 tempf    025200000
```

```
*card    name     operator  coef   init-guess calc-init-
val
20556100 mul001   sum  0.06495    -.0660115  1
*card    variable volume
20556101 0.0 1.0 tempf    025010000
20556102 1.0 tempf    025020000
20556103 1.0 tempf    025030000
20556104 1.0 tempf    025040000
20556105 1.0 tempf    025050000
20556106 1.0 tempf    025060000
20556107 1.0 tempf    025070000
20556108 1.0 tempf    025080000
20556109 1.0 tempf    025090000
20556110 1.0 tempf    025100000
*card    name     operator  coef   init-guess calc-init-
val
20556200 mul001   mult  0.385    -.0660115  1
*card    variable volume
20556201 tempf    023120000
*-------average temperature
*card    name     operator  coef    init-guess calc-
init-val
20556300 press    sum       0.0929    -17.45805  1
*card    coef      variable  volume
20556301  0.0 1.0  cntrlvar  555
20556302  1.0  cntrlvar  556
20556303  1.0  cntrlvar  557
20556304  1.0  cntrlvar  558
20556305  1.0  cntrlvar  559
20556306  1.0  cntrlvar  560
20556307  1.0  cntrlvar  561
20556308  1.0  cntrlvar  562
*-------power transferred safety coolant
*card    name     operator  coef   init-guess calc-init-
val
20556400 mul001   diffrend  5.0711e7    -.0660115  1
*card    variable volume
20556401 cntrlvar    563


*-------cooling fluid loop volume weighted temperature
sum
*card    name     operator  coef   init-guess calc-init-
val
20556500 mul001   sum  6.156    -.0660115  1
```

```
*card    variable volume
20556501 0.0 1.0 tempf    030150000
20556502 1.0 tempf    030060000
20556503 1.0 tempf    030070000
20556504 1.0 tempf    030080000
20556505 1.0 tempf    030090000
20556506 1.0 tempf    030100000
20556507 1.0 tempf    030110000
20556508 1.0 tempf    030120000
20556509 1.0 tempf    030130000
20556510 1.0 tempf    030140000
*card    name     operator  coef   init-guess calc-init-
val
20556600 mul001   sum  0.0467    -.0660115  1
*card    variable volume
20556601 0.0 1.0 tempf    030550000
20556602 1.0 tempf    030560000
20556603 1.0 tempf    030570000
20556604 1.0 tempf    030580000
20556605 1.0 tempf    030590000
20556606 1.0 tempf    030600000
20556607 1.0 tempf    030610000
20556608 1.0 tempf    030620000
20556609 1.0 tempf    030630000
20556610 1.0 tempf    030640000
*card    name     operator  coef   init-guess calc-init-
val
20556700 mul001   mult  0.546    -.0660115  1
*card    variable volume
20556701 tempf    030200000
*card    name     operator  coef   init-guess calc-init-
val
20556800 mul001   mult  0.6036    -.0660115  1
*card    variable volume
20556801 tempf    030700000
*-------average temperature
*card    name     operator  coef    init-guess calc-
init-val
20556900 press    sum       0.0158    -17.45805  1
*card    coef      variable  volume
20556901  0.0 1.0  cntrlvar  565
20556902  1.0  cntrlvar  566
20556903  1.0  cntrlvar  567
20556904  1.0  cntrlvar  568
*-------power transferred safety coolant
```

```
*card    name     operator  coef   init-guess calc-init-
val
20557000 mul001   diffrend  2.374e8    -.0660115  1
*card    variable volume
20557001 cntrlvar    569



**********************************
*steady instead of tran calc
**********************************
*510203   100.05     -3292.00000      0.0     0.0
*510204   5000.0     -3292.00000      0.0     0.0

*4206103        101.2000   185.0000
*4206104        5000.000   185.0000

*20607770  time      0   gt   null    0     11000.000
l *scram
*20607780  time      0   lt   null    0     11000.00   n
*close IHX valve

*20607790  time      0   lt   null    0     100.000   n
*20607800  time      0   ge   null    0     100.000   n


*table 911 vlv area tbl
20291100  normarea
20291101  0.0  0.15
20291102  1.0  1.00


.---------end of cass
```